جامعة سيدي محمد بن عبد الله بفاس
UNIVERSITÉ SIDI MOHAMED BEN ABDELLAH DE FES

كلية العلوم والتقنيات فاس
FACULTÉ DES SCIENCES ET TECHNIQUES DE FÈS

N° d'ordre : 29/2024

Centre des Etudes Doctorales : Sciences et Techniques et Sciences Médicales
Formation Doctorale : Sciences de l'Ingénieur, Sciences Physiques, Mathématiques et Informatique.
Discipline : Physique.
Spécialité : Electronique et Télécommunications.
Laboratoire : Signaux, Systèmes et Composants (LSSC).

Thèse pour l'obtention de DOCTORAT

Design and Production of Directional, Broadband, Circularly-Polarized and Multi-Beam Planar Antennas for ISM and Terahertz Bands

Préparée par : Mr. ABDELAAZIZ EL ANSARI

Soutenue le 11/06/2024 devant le jury :

Nom et Prénom	Grade	Etablissement	Qualité
Pr.Mhammed LAHBABI	PES	FST de Fès, USMBA	Président
Pr.Abdelwahed TRIBAK	PES	INPT-Rabat	Rapporteur
Pr.Nawfal JEBBOR	PH	FST ERRACHIDIA, UMI	Rapporteur
Pr.Jamal BELKDID	PES	EST- USMBA	Rapporteur
Pr.Ali EL ALAMI	PH	FST ERRACHIDIA, UMI	Examinateur
Pr. Najiba El AMRANI El IDRISSI	PES	FST de Fès, USMBA	Directeur de thèse

Dedication

To my father Allah rest his soul,

To my mother Allah prolong her age

To my brother

To my sisters

To my wife and my sweet kids,

Hiba and Ahmed Omar

Acknowledgements

In the beginning, my thanks go to **ALLAH** (الله) the Almighty for giving me the courage, the will and the patience to complete this work.

I would like to thank my supervisor **Pr. Najiba El Amrani El Idrissi** for agreeing to guide this research work during the years of completion of this thesis. His ideas and help have been a significant factor for success in my thesis. His advice and constructive remarks have been very beneficial for my work. His constant support as well as his availability for the completion of this thesis have been very favorable to me.

I would like to thank our collaborator **Dr. Sudipta Das**, from ‘’**Department of Electronics & Communication Engineering, IMPS College of Engineering & Technology, Malda, West Bengal, India**’’ for his cooperation that allowed us carry out measurements on the designed antenna in order to validate the results obtained by the simulations. For his significant help I have gotten from him.

I extend my sincere thanks to **Pr Mhammed LAHBABI,** Professor at Faculty of Sciences and Technologies Fes- Sidi Mohamed Ben ABDELLAH University, Morocco, for agreeing to chair my thesis jury. I would like to express my deep gratitude to him for his availability and attention.

I would also like to express my sincere thanks to:

***Pr.AbdelwahedTRIBAK:** Professor at the National Institute of Posts and Telecommunications Rabat-Morrocco.

***Pr.Nawfal JEBBOR:** Professor at the Faculty of Sciences and Technologies Errachidia-Moulay Ismail University, Morocco.

***Pr.Jamal BELKDID:** Professor at National school of Technology Fes- Sidi Mohamed Ben ABDELLAH University, Morocco.

For being the reporters for their interest in my research work, the time they have devoted to reading my manuscript, and his precious Remarks.

I would also like to express my sincere thanks to **Pr. Ali EL ALAMI** Professor at the Faculty of Sciences and Technologies Errachidia-Moulay Ismail University, Morocco, for having done me the honor of evaluating, examining and enriching our modest work.

My heartiest thanks and most profound appreciation are due to my mother, my sisters, my brother, my wife and my friends (especially **Dr. Abdelhak Bendali**) for standing beside me, encouraging and supporting me all the time I have been working on this thesis. Thanks to all those who assisted me in all terms and helped me to bring out this work.

Abstract

An antenna is an impedance adapter between free space and communication devices, without which no data exchange is possible. Nowadays, most popular antennas are planar, directional, broadband, multi-beam and circularly polarized, mainly for applications such as base stations, radars, satellites and so on. Directional antennas are essential for applications requiring targeted transmission or reception. These antennas are generally built using massive antenna arrays. The wideband multi-beam antennas are crucial for achieving broad coverage and high data rates. They are realized by feeding an antenna array through a beamformer circuit. Circularly polarized antennas offer advantages in terms of signal robustness and interference mitigation. They can be achieved by exciting two resonance modes via dual or single feeding methods, or by modifying the antenna's geometry.

Although planar antennas offer some advantages, they are still limited in terms of flexibility, low gain, linear polarization, omnidirectional radiation pattern and narrow bandwidth. So, this thesis topic addresses all these limitations of patch antennas and deals with design and realization of directional, multibeam, wideband, and circularly polarized planar array antennas for ISM and THz bands.

The ISM (Industrial, Scientific, and Medical) bands are portions of microwave bands. One of the most significant aspects of the ISM bands, is that they enable the operation of license-free devices in many countries. This has led to their widespread use in a variety of modern applications especially around the 2.4-2.5 GHz band, such as: Wireless medical devices, RFID (radio frequency identification) technology, GPS (Global Positioning Systems), WI-FI (wireless-fidelity), Bluetooth WLAN and Wi-Max etc...

The Terahertz band is the frequency range between the microwave and the optical bands, with a range from 0.1 THz to 10 THz. Due to the availability of enormous unallocated bandwidth, the Terahertz band supports significant high-speed communication for the next 6th and 7th generations. Moroever, it has a tremendous application potential in many fields, including outdoor and indoor communications, manufacturing, agriculture, materials characterization, spectroscopic imaging and security.

Keywords: array antenna, directional antenna, broadband antenna; planar antenna, circular polarization, LHCP, RHCP, Rotman lens, Lüneburg lens, Butler matrix.

Résumé

Une antenne est un adaptateur d'impédance entre l'espace libre et les appareils de communication, qui sans elle, aucun échange de données n'est possible. De nos jours, les antennes les plus demandées sont les antennes planaires directionnelles, large bande, multifaisceaux et à polarisation circulaire, principalement pour des applications telles que les stations de base, les radars, les satellites, etc. Les antennes directionnelles sont essentielles pour les applications nécessitant une transmission ou une réception focalisée. Elles sont généralement réalisées à l'aide de réseaux d'antennes massifs. Les antennes multifaisceaux à large bande passante sont cruciales pour obtenir une large couverture et un débit élevé. Elles sont réalisées en alimentant un réseau d'antennes à travers un circuit de formation de faisceaux. Les antennes à polarisation circulaire offrent des avantages en termes de robustesse du signal et d'atténuation des interférences. Elles peuvent être obtenues en excitant deux modes de résonance soit par alimentation double ou simple en modifiant la géométrie de l'antenne.

Bien que les antennes planaires présentent certains avantages, elles restent limitées en termes de flexibilité, faible gain, polarisation linéaire, diagramme de rayonnement omnidirectionnel et bande passante étroite. Ainsi, ce sujet de thèse aborde ces limitations des antennes patch et traite la conception et réalisation d'antennes réseaux planaires directionnelles, multifaisceaux, large bande et à polarisation circulaire adaptées aux bandes ISM et THz.

Les bandes ISM sont des bandes micro-ondes réservées aux utilisations Industrielles, Scientifiques et Médicales. L'un des aspects les plus importants des bandes ISM est qu'elles permettent l'exploitation d'appareils sans avoir besoin d'une licence. Il existe de nombreuses bandes ISM mais la plus populaire est la bande 2,4-2,5 GHz. Autour de ces fréquences, il existe de nombreuses applications telles que : dispositifs médicaux sans fil, RFID (radio frequency identification), GPS (Global Positioning Systems), WI-FI , Bluetooth etc…

La bande Térahertz est la gamme de fréquences située entre la bande micro-onde et la bande optique, son spectre s'étend de 0,1 THz à 10 THz. En raison de la disponibilité d'une énorme bande passante non allouée, la bande térahertz prend en charge un énorme potentiel d'applications dans de nombreux domaines, y compris les communications extérieures et intérieures, la fabrication, l'agriculture, la caractérisation des matériaux, l'imagerie spectroscopique et la sécurité, communication à haut débit etc.

Mots clés : antenne réseau, antenne directionnelle, antenne large bande ; antenne à bande étroite, polarisation circulaire, LHCP, RHCP, lentille de Rotman, lentille de Lüneburg, matrice de Butler.

Outline :

General Introduction 1
Chapter I: Overview of Fundamental Characteristics of Antennas,Planar Antennas and Beamforming Techniques 4
1. Introduction 4
2. Characteristics Parameters of Antenna Adaptation 5
2.1. Reflection Coefficient S_{11} 5
2.2. Impedance Bandwidth 5
2.3. The Voltage Standing Wave Ratio (VSWR) 6
2.4. Input Impedance 7
3. Antenna Polarization 8
3.1. Linear Polarization (LP) 8
3.2. Circular Polarization (CP) 9
3.3. Elliptical Polarization (EP) 9
3.4. Axial Ratio (AR) 10
3.5. polarization diversity 11
4. Antenna Radiation Characteristic parameters 11
4.1 Antenna directivity 11
4.2 Antenna gain 12
4.3. Antenna radiation efficiency 13
4.5. Antenna radiation pattern 14
4.6. Polarization patterns: co-polarization and cross-polarization 15
5. Planar antennas 16
5.1. Feeding techniques 17
5.1.1. Coaxial cable Feeding 17
5.1.2. Coplanar Line Feeding 18
5.1.3. Proximity Coupling 18
5.1.4. Aperture Coupling 19
5.1.5. Mutual Coupling Feeding 19
5.1.6. Feeding via microstrip line 20
5.2. Circular polarization 21
5.2.1. CP via dual feed 21
5.2.2. CP via single feed 22
5.3. Microstrip Antenna array 22
6. Beamforming Techniques 25
6.1. Digital beamformers: 26
6.2 Switched beamformers 27
6.2.1. Microwave Lens based Beamformer 28

6.2.1.1. Luneburg gradient-index lens 29
6.2.1.2. Rotman lens 30
6.2.2.Hybrid coupler based beamformer 31
6.2.2.1. Blass matrix configuration 32
6.2.2.2. Nolen Matrix 33
6.2.2.3. Butler Matrix 33
6.2.2.3.1. 2x2 Butler Matrix 34
6.2.2.3.2. 4x4 Butler Matrix 36
6.2.2.3.3. 8x8 Butler Matrix 37
7. Conclusion 39
8. Specification Sheet 40
References 41
Chapter II: A High-Gain Directional 1×8 Planar Array antenna for 2.4 GHz RFID Reader Applications 45
1. Introduction 45
2. The Suggested Advanced 1×8 Power Divider 46
2.1 Analysis and Design Methodology 47
2.1.1. Study and Design of the Basic 1×2 Power Divider (3 dB): 47
2.1.2. Study and Design of a 1×4 T Power Divider (6 dB): 50
2.1.3. Design of the Proposed T 1×8 Power Divider (TPD 9dB): 52
2.2. Simulation Results 53
3. Optimization Process of The Basic Planar Antenna 56
3.1. Analytical Equations 56
3.2. Design Steps 57
3.3. Simulation results of the Optimized Planar Antenna 58
4. The Proposed Directional 1×8 Antenna Array 60
4.1 Theoretical study 60
4.2. Design of the suggested 1×8 Planar Antenna Array 62
4.3. Results and Discussion 63
5. Performance Comparison with State-of-the-Art 64
6. Conclusion 65
References 66
Chapter III: Design And Realization of a Broadband Switched Phased Array Antenna Based on Hybrid Coupler For ISM Band 2.45 Ghz RFID Reader Applications 69
1. Introduction 69
2. Design and miniaturization of the basic patch antenna 70
2.1. Design steps of the miniaturized basic element 70
2.2. Simulation results and discussion 72
3. Design and simulation of the basic 3dB 90° hybrid coupler 74
3.1. Theoretical study 74

3.2. Design and Simulation Results 75
4. Design, realization and measurement of the proposed beam switchable broadband 1×2 array antenna 77
4.1. Concept of the switched beam antenna 78
4.2. Design and realization of the switched beam antenna 79
4.3. Simulated results versus measured results 80
4.4. Performance comparison analysis 83
5. Hybrid Coupler Integrated 1×4 Printed Array Antenna 83
5.1. Design and simulation results of the miniaturized 1×2 array antenna 83
5.2. Geometry and simulation of the hybrid coupler fed 1x4 array antenna 87
5.2.1. Simulation versus measurement results 88
5.2.2. Comparative analysis with some other published works 91
6. Conclusion 92
Chapter IV: A Four-Beams Array antenna Based on a New Beamformer Circuit For ISM Band Aplications 95
1.Introduction 95
2. Switched-beam antenna concept 96
3. The 4x4 Butler Matrix and its vulnerability 97
3.1. Presentation of the 4x4 Butler Matrix 97
3.2. The vulnerability of Butler's matrix 98
4. Design process for the new 4x4 Beamformer 100
4.1. The proposed 3dB 90°/-90° hybrid couplers 100
4.2. The proposed 3dB hybrid couplers 45°/-135° and 135°/-45° 102
5. Four-beams antenna based the proposed 4x4 beamformer circuit 106
5.1. Design 106
5.2. Simulation versus measurements results of the Proposed Four-Beams antenna 107
6. Reconfigurable ultra-wideband, microstrip crossover for ISM band applications 111
6.1. The 0 dB hybrid coupler-based Crossover 111
6.2. The proposed Reconfigurable Crossover 113
7. Conclusion 116
References 117
Chapter V: A Circularly Polarized Graphene based Wideband 1×2 Array Antenna for Terahertz Spectrum Applications 120
1. Introduction 120
2. Basic Radiating Element Design Methodology 122
2.1 Effect of Truncated Corners 122
2.2 Effect of Flower Slots 124
3. Proposed 1×2 Array Antenna 128
4. Performance comparison with other terahertz antennas and Discussion 131
5. Conclusion 132
References 133

General Conclusion and Perspective 137

Figures liste :

Figure I. 1 Antenna with adapter circuit and power source. 5
Figure I. 2 Example of the Reflection Coefficient vs. Frequency. (a) narrow band antenna (b) wideband antenna, (c): Ultra-wideband antenna [13-14]. 6
Figure I. 3 Example of VSWR against Frequency. (a) narrow band antenna (b) wideband antenna [13]. 7
Figure I. 4 Load powered by a 50 Ohm impedance generator [15] 7
Figure I. 5 Input impedance patch antenna. (a) its real part against frequency; (b) its imaginary part 8
Figure I. 6 state of linearly polarized electrical field vector; (a) vertical linear polarization, (b) horizontal linear polarization, (c) oblique linear polarization. 9
Figure I. 7 Electrical field vector in the case of circular polarization; (a): LHCP, (b): RHCP. 9
Figure I. 8 Electrical field vector in the case of elliptical polarization; (a): LHEP, (b): RHEP. 10
Figure I. 9 Minor and major axes of elliptical polarization [17]. 10
Figure I. 10 Axial-ratio versus frequency of CP antenna [18] 11
Figure I. 11 Equivalent diagram of an antenna. Rr: radiation resistance, RP: loss resistance, Xp: antenna reactance. 12
Figure I. 12 gain and directivity in dB versus frequency in GHz [19]. 13
Figure I. 13 gain and directivity versus frequency [19] 13
Figure I. 14 3D radiation pattern in terms of : (a) gain; (b) directivity [4]. 14
Figure I. 15 E and H plane radiation patterns: (a) 3D; (b): 2D. [19] 15
Figure I. 16 Different radiation pattern types (a): omnidirectional; (b): directional radiation pattern; (c): Beamforming radiation pattern. [5,21]. 15
Figure I. 17 Co versus Cross polarization. (a): as function of frequency;(b):in the plan E [22,23]. 16
Figure I. 18 The most typical patch antenna shapes [20] 17
Figure I. 19 planar antenna with Coaxial line feed [24]. 17
Figure I. 20 planar antenna with coplanar feed line [24-25]. 18
Figure I. 21 Electromagnetic Coupling feed 19
Figure I. 22 patch antenna fed via aperture coupling. 19
Figure I. 23 Mutual Coupling Feedline 20
Figure I. 24 Feeding via Microstrip line technique 20
Figure I. 25 Dual orthogonal feed circularly polarized Microstrip antenna (a) fed via a power splitter (b) fed through a 90° 3dB directional coupler [17]. 21
Figure I. 26 configurations of singly fed circularly polarized microstrip antennas [17] 22
Figure I. 27 Microstrip patch array antenna configuration, (a): 1D, (b): 2D, (c): 3D[27] 23
Figure I. 28 Array factor versus angle θ (b) d = λ and N = 10; (c) d = λ/2 and N = 10 [20]. 24
Figure I. 29 2D radiation pattern. 24
Figure I. 30 Structure of a switched multi-beam antenna. 25
Figure I. 31 Structure of an adaptive antenna system [8]. 27
Figure I. 32 diode PIN and its equivalent models, a: Structure, b: Symbol, c: equivalent model of diode on state, d: equivalent model of off state [30]. 28
Figure I. 33 Varactor diode and its equivalent models, a: Symbol, b: equivalent model of diode on, c: equivalent model of off [30] 28
Figure I. 34 Diagram of a microwave lens powering an antenna array [42] 29
Figure I. 35 (a). Propagation in a Lüneburg lens; (b), (c). printed Lüneburg lens [40-41]. 30
Figure I. 36 Diagram of a trifocal Rotman lens 31
Figure I. 37 Romane lens having 5 input ports and 8 output ports (a) Design, (b): fabricated prototype in PCB technology; (c). Maximum beam directions corresponding to output ports [44]. 31
Figure I. 38 Microstrip hybrid directional coupler. 32
Figure I. 39 Blass matrix configuration [47] 32
Figure I. 40 Nolen matrix configuration fed a phased array antennas [49]. 33

Figure I. 41 2x2 Butler matrix configuration feed a phased array antenna: a, b, c designs; d: fabrication in microtip technology [52-53]..... 35
Figure I. 42 two directions provided by 2x2 Butler matrix; a:+30°, b: -30° [53]..... 36
Figure I. 43 4x4 Butler matrix configuration fed a phased array antenna, a: schematic diagram; b fabrication in microtip technology [54-56]..... 36
Figure I. 44 four directions of 4x4 Butler matrix; a:-15°,b: 45°, c:-45°, d:15°[57]..... 37
Figure I. 45 8x8 Butler matrix, a: schematic diagram, b: its fabrication in in microtip technology [58]..... 38
Figure I. 46 eight directions provided by 8x8 Butler matrix[59]. 39

Figure II. 1 (a) Power divider. (b) Powers combiner [29] 46
Figure II. 2 Design steps of the proposed advanced TPD. (a): 1×2 TPD, (b): 1×4 TPD, (c): 1×8 TPD. 47
Figure II. 3 Port layout of 1×.2 T power splitter. 47
Figure II. 4 Design of the proposed 1×2 TPD. 48
Figure II. 5 S11, S12 and S13 (dB) vs. frequency, (b): phases of S12 and S13 vs. frequency of the proposed 1×2 TPD..... 50
Figure II. 6 Structure of the proposed 1×4 TPD. 51
Figure II. 7 (a): S parameters versus frequency, (b): phases of S12, S13, S14 and S15 versus frequency of the proposed 1×4 TPD. 52
Figure II. 8 Structure of the proposed 1×8 power divider 53
Figure II. 9 (a) S11, S21, S31 parameters vs. frequency; (b) S11, S41, S51 parameters vs. frequency; 54
Figure II. 10 Angle of transmission parameters against frequency, (a): S12 vs S13, (b): S14 vs S15 55
Figure II. 11 Design steps of the basic antenna 58
Figure II. 12 Reflection coefficients for different optimization steps of the basic antenna 58
Figure II. 13 HFSS versus CST simulation results: (a): S11 return loss, (b): VSWR, (c): Gain of antenna, (d): antenna's efficiency, (e): E-plane radiation pattern; (f): H-plane radiation pattern..... 60
Figure II. 14 Two-element array antenna 61
Figure II. 15 Structure of the suggested directional high gain 1x8 antenna array. 63
Figure II. 16 HFSS versus CST simulation results of the proposed planar 1x8 antenna array; (a): S11 return loss, (b): VSWR, (c): Gain of antenna, (d): antenna efficiency, (e): Electric Field (E) Plane radiation pattern and (f): Magnetic Field (H) Plane radiation pattern 64

Figure III. 1 Flowchart of the RFID System with the multi-beam antenna 70
Figure III. 2 Design and optimization steps of the elementary patch antenna 71
Figure III. 3 S11 versus frequency of various design cases..... 71
Figure III. 4 Simulation results by HFSS and CST for the proposed basic element antenna. (a): S11 (b): VSWR (c): Efficiency (d): Gain (e): E plane radiation patterns, and (f): H plane radiation patterns., (g) maximum beam direction. 73
Figure III. 5 Design of microstrip line hybrid directional coupler 76
Figure III. 6 Magnitude of S11, S12, S13, and S14 parameters (b): phase variations of S12 and S13for the designed hybrid coupler..... 77
Figure III. 7 Diagram of a phased array antenna comprising two elements 78
Figure III. 8 The topology of the proposed switched beam antenna: (a) front view, (b) back view, (c) front view of fabricated prototype, and (d) back view of fabricated prototype 80
Figure III. 9 Simulated and measured results of the proposed antenna for input port 1 (a): S11Vs. frequency, (b): Gain versus frequency, (c): Radiation efficiency versus frequency, (d): Beam direction 82
Figure III. 10 Simulated and measured results of the proposed antenna for input port 2 (a): S11 vs. frequency, (b): Gain versus frequency, (c): Radiation efficiency versus frequency, (d): Beam direction, and (e): Radiation pattern. 82
Figure III. 11 design of T power divider 83
Figure III. 12 Scattering parameters S11, S12 and S13. (a): magnitude versus frequency (b): angles in degrees versus frequency. 84
Figure III. 13 Proposed miniaturized 1×2 array antenna. 84
Figure III. 14 Characteristic parameters of the 1×2 array antenna fed by T power divider (a): S11, (b): VSWR, (c): Efficiency, (d): Gain and Directivity, (e): E and H plane radiation patterns, (f): maximum beam direction 86

Figure III. 15 3dB hybrid coupler integrated 1x4 array antenna. 87
Figure III. 16 Simulated results of the proposed antenna for excitation at input port 1 (a): VSWR (b): Gain (c) Directivity (d): Radiation efficiency (e): Maximum beam direction 89
Figure III. 17 Simulated results of the proposed antenna for excitation at input port 1 (a): VSWR (b): Gain (c) Directivity (d): Radiation efficiency (e): Maximum beam direction. 90

Figure IV. 1 Structure of a switched multi-beam antenna. 96
Figure IV. 2 Structure of switched four beams array antenna feed by the 4x4 Butler matrix. 97
Figure IV. 3 Microstrip crossover 98
Figure IV. 4 Different configurations have been used to avoid crossings in the 4x4 Butler Matrix PCB circuit. . 99
Figure IV. 5 Structure of the proposed 3dB beamformer circuit 100
Figure IV. 6 Designed 3 dB 90°/-90° hybrid couplers 101
Figure IV. 7 Simulation results for the 3dB ±90° proposed hybrid coupler; (a) module of the scatring parameters versus frequency; (b): angles of the transmission coefficients versus frequency. 102
Figure IV. 8 phase delay line 103
Figure IV. 9 Enhanced 3 dB hybrid couplers: a: 45°/-135°; b:135°/-45°. 103
Figure IV. 10 Simulation results of the proposed 3dB hybrid coupler; (a) module of the scattering parameters versus frequency; (b): angles of the transmission coefficients versus frequency. 105
Figure IV. 11 Simulation results of the proposed 3dB 135°/-45° hybrid coupler; (a) module of the scattering parameters versus frequency; (b): angles of the transmission coefficients versus frequency. 106
Figure IV. 12 design of the proposed 4x4 beamformer feeding an array antenna (a): front view, (b): back view. 107
Figure IV. 13 Réflexion coefficient associated with Port 1, Port 2, Port 3 and port 4. 108
Figure IV. 14 Gain in dB associated with Port 1, Port 2, Port 3 and port 4. 109
Figure IV. 15 Radiation efficiency associated with Port 1, Port 2, Port 3 and port 4. 109
Figure IV. 16 Maximum beam direction in 2D radiation pattern associated with port 1, port 2, port 3 and port4. 110
Figure IV. 17 Maximum beam direction in 3D radiation patterns for Port 1, Port 2, Port 3 and port 4. 110
Figure IV. 18 Two cascaded 3dB hybrid. 112
Figure IV. 19 The designed 0dB hybrid coupler 112
Figure IV. 20 Simulation results of designed 0dB coupler in terms of scattring parameters, (a): their magnitudes, (b): their angles. 113
Figure IV. 21 Simulation results of the proposed crossover in terms of scattering parameters, (a): their magnitudes, (b): their angles 114

Figure V. 1 (a) The basic element fed by a folded quarter wave impedance transformer. (b) The basic element with two truncated corners 123
Figure V. 2 Simulation results of case 1 versus case 2. (a): S11 versus frequency (b): The axial ratio versus frequency. 123
Figure V. 3 Flower shaped slots loaded design cases (a) one flower slot (b) two (c) three (d) four flower slots 124
Figure V. 4 Simulation results of Case 2, 3, 4, 5, and 6. (a): S11 versus frequency (b): Axial ratio versus frequency 125
Figure V. 5 Proposed Flower- shaped and circular slots-based CP antenna 126
Figure V. 6 Simulation results of the proposed single fed circularly polarized basic element antenna. (a): reflection coefficient bandwidth. (b): Axial ratio bandwidth. (c): Gain. (d): Radiation efficiency 126
Figure V. 7 surface current distribution 2.45 THz with the phase of (a) 0° (b) 90° (c) 180° (d) 270° 127
Figure V. 8 Variations in operating bandwidth as a function of circular slot radius ‘r’ (a) S11 (dB) (b) Axial Ratio (dB) 128
Figure V. 9 Proposed single fed circular polarized 1×2 array antenna 128
Figure V. 10 Simulation results of the proposed single fed circularly polarized 1×2 array antenna. (a): S11 (dB) (b): Axial ratio bandwidth. (c): Gain (d): Radiation efficiency versus frequency 129
Figure V. 11 Radiation patterns representing Co-pol and Cross-pol at 2.45 THz (a) E plane (b) H-plane 130
Figure V. 12 surface current distribution of the proposed 1×2 array antenna at 2.45 THz with phases of :(a) 0° (b) 90° (c) 180° (d) 270° 130

Tables liste :

Table II. 1 Summary of values and angles of the eight-transmission coefficient 55
Table II. 2 Recap of HFSS versus CST simulation results 59
Table II. 3 Summary of simulation results of 1×8 antenna array 64
Table II. 4 Comparison of our directional planar antenna array To state of the Art 65

Table III. 1 Dimensions summary of the elementary patch antenna 71
Table III. 2 Summary of simulation results of the proposed antenna. 74
Table III. 3 Performance comparison of the proposed miniaturized antenna with state-of-the-art 74
Table III. 4 parameters of the proposed miniaturized 1×2 array antenna 85
Table III. 5 Summary of simulation results of proposed the miniaturized 1×2 array antenna 86
Table III. 6 Comparison of the proposed 1×2-array antenna with other works 86
Table III. 7 Summary of simulation results of proposed switched antenna. 91
Table III. 8 Comparison of the proposed dual-beam array antenna with previous reported works. 91

Table IV. 1 Summary of the simulation results obtained for the proposed 3 dB 90° hybrid coupler at 2.45 GHz operating. 102
Table IV. 2 Summary of the obtained simulation for the proposed 45°/-135° 3 dB hybrid coupler at 2.45 GHz the operating frequency. 104
Table IV. 3 Summary of the simulation for the proposed 135°/-45°3 dB hybrid coupler at 2.45GHz operating frequency. 105
Table IV. 4 Summary of simulation resultes obtained from the proposed four beam antenna associated with Port1, Port 2, and Port 3 and port 4 110
Table IV. 5 The PIN diode based crossover versus the 0dB coupler based crossover. 115
Table IV. 6 Table 6 The proposed PIN diode based crossover versus others published crossovers 115

Table V. 1 The final geometrical parameters of the basic antenna 126
Table V. 2 Performance comparison of the proposed array antenna with other previous references 132

General Introduction:

An antenna is a sensor capable of converting electrical energy into electromagnetic waves and vice versa. It plays an essential role in all wireless communication systems, without it, no data exchange is possible. The importance of antennas lies in their ability to transmit, receive, and shape electromagnetic waves to optimize the range, quality and reliability of communications. There are many kinds of antennas. However, the most popular are planar antennas, due to their affordability, compactness, lightweight, ease of fabrication and easy integration with PCB (Printed Circuit Boards) devices. Nowadays, the most requested planar antennas are the directional, multi-beam and circular polarized ones which are most in-demand for satellites, base stations, radars etc.

Directional antenna is an antenna that radiate energy in a specific direction. It plays a crucial role in enabling concentration of signals in specific directions, thereby reducing interference and improving communications security, leading to a significant improvement in the range, quality, and efficiency of communications. A directional antenna can be obtained by combining a set of antennas to form an antenna array, whether linear or circular.

A multibeam antenna is a reconfigurable antenna that can radiate energy in many directions to increase area coverage. To obtain a multibeam antenna, a switched network beamformer must feed an array antenna. These antennas revolutionize the way electromagnetic signals are transmitted and received by enabling the simultaneous formation of multiple directional beams. This targeted transmit and receive capability provides significant advantages in terms of spectral efficiency, wide coverage, and interference management.

High-speed data transmission over a wide frequency range requires high-bandwidth antennas; the importance of which lies in their ability to cover a wide frequency spectrum with a single structure. These antennas are essential for wireless networks, satellite communications, radar, surveillance systems and many other applications. Their ability to support high data rates, quickly adapt frequencies and meet the diverse needs of modern communications make them a key element in meeting today's technological challenges.

Circularly polarized antennas are a crucial component of advanced wireless communications systems. Their importance lies in their unique ability to manipulate the orientation of electromagnetic waves to achieve circular polarization, offering considerable benefits in terms of reducing signal degradation effects in complex and multi-reflective environments.

These antennas play a vital role in applications such as satellite communication, mobile telephony, global positioning systems (GPS), remote sensing and long-distance wireless links. Their ability

to minimize interference and improve the quality of communications in a variety of conditions makes them essential components for reliable, high-performance communications.

Although planar antennas offer certain advantages, they have some limitation such as: low gain, linear polarization, omnidirectional radiation pattern, narrow bandwidth and inflexibility. So, this thesis addresses all these limitations of patch antennas in the ISM band (industrial and medical band), and in the THz band [0.1 THz to 10 THz].

Thus, after this introduction, this thesis report is organized into five chapters as follows:

Chapter I:

This chapter provides an overview of the fundamental characteristics of antennas, planar antennas and beamforming techniques. Within this artic, we are going to highlight the essential characteristics of an antenna in terms of the polarization types (linear, elliptical and circular polarization (LHCP & RHCP)), Matching characteristics parameters (reflection coefficient, impedance bandwidth at -10dB, VSWR, and input impedance), radiation characteristic parameters (gain, directivity, radiation efficiency and radiation patterns). Subsequently, it describes planar antennas, their feeding mechanisms, the antennas array and the methodologies employed to achieve their circular polarization. Finally, this chapter examines Beamforming Techniques, including digital and switched beamformers.

Chapter II:

This chapter presents a high gain directional 1×8 planar array antenna for ISM 2.4 GHz band uses. To achieve this antenna, a well-matched broadband power splitter is developed and implemented for the design of the suggested antenna array. Then eight identical patch elements with good reflection coefficient, high gain and excellent radiation efficiency are connected to the eight-output port of the 1×8-power divider to obtain an eight-element array antenna. A quarter-wave impedance adapter is used to achieve a perfect impedance matching between the patches and the power divider. The suggested directional antenna resonates at 2.4 GHz and offers good performance. This printed antenna array is a potential candidate for all applications operating around 2.4 GHz, such as: Wi-Fi Networks, Bluetooth technology, Wireless medical devices and RFID readers, due to its outstanding impedance and radiation characteristics.

Chapter III:

This chapter presents the design and analysis of a switchable beam planar array antenna fed by a hybrid coupler for applications in the 2.45 GHz ISM band. The proposed switchable-beam patch array antenna consists of an array antenna, a pleated quarter-wavelength impedance transformer (PQWIT), and a hybrid coupler. The PQWIT concept was used to reduce the overall implementation area of the patch elements. The overall surface area of the patch element is

miniaturized by 50% due to the implementation of a pleated quarter-wavelength impedance transformer. This miniaturized antenna is used as a radiating element to design a 1×2 switchable-beam array antenna and a 1x4 array antenna fed by a hybrid coupler. They offer a broad bandwidth with two switchable beams in two directions −30° & + 30°.

Chapter IV:

The most in-demand beamformer is the Butler Matrix, thanks to its use of parallel feeding. However, it sufers from the weak spot of crossovers, particularly in microstript technology. So, in this this chapter we are going to suggest a new 4x4 beamformer circuit without using crossovers. The proposed beamformer is used to obtain a switched multibeam microstript antenna that radiates energy in four different directions 15°, -45°. +45° and -15° by swiching its four input ports. Moreover, in this chapter, we will suggest another solution of the weak spot microstript crossover. The proposed solution is an ultra-wideband, reconfigurable microstrip crossover. Thanks to the incredible and significant results it presents and its flexibilty, the proposed crossover could be used not only for Butler matrix for beamforming purposes, but it is also dedecated for phased array antennas, reconfigurable antennas, MIMO antenna, reconfigurable filters…etc to control the power feed throughout the desired port(s).

Chapter V:

This chapter presents a graphene-based 1×2 microstrip array antenna with circular polarization for terahertz applications. The opposite corners of the patches have been truncated, and structural modifications are performed with the insertion of four flower-shaped slots in addition to a circular slot. The aim is to achieve an improved reflection coefficient and better impedance bandwidth. It also shows much wider 3dB axial ratio bandwidth, confirming circular polarization due to the suggested modifications in its geometry. Next, an array antenna was formed to provide better gain. The proposed 1×2 array antenna could be used for high-speed data transmission, material characterization, terahertz spectroscopy and terahertz imaging, and more applications.

Finally, this report will be finished by general conclusion and perspective.

Chapter I: Overview of Fundamental Characteristics of Antennas,Planar Antennas and Beamforming Techniques

1. Introduction

The postulates of electromagnetism (also called the four Maxwell equations) were introduced by James Clerk Maxwell in 1876. Then, in 1877, Hertz Heinrich demonstrated the presence of electromagnetic waves expected by J.C.Maxwell using his famous experiment and he founded the field of telecommunications. Next, in 1899, Nicolas Tesla also contributed to the understanding of electromagnetic waves. He conducted experiments on the production and detection of electromagnetic waves. These experiences laid the foundation for the development of wireless communication technologies. This wireless communication can only be achieved with a transmitting or receiving antenna [1].

An antenna is a sensor that converts the electrical energy into electromagnetic wave and vice versa. It performs a crucial function in all radio communication systems. As vital interfaces between the electromagnetic and electrical domains, it ensures the efficient transmission of signals between transmitters and receivers. The importance of antennas lies in their ability to transmit, receive, catch and shape electromagnetic waves to optimize the range, quality, and reliability of communications [2-3].

Generally, antennas are classified into five categories which are: wire antennas (dipole, monopole, and Yagi antenna), Aperture Antennas (horn antenna), Reflector Antennas (parabolic antenna), Lens and Planar Antennas [4]. The last type is also called patch or microstrip antennas. They are the most popular ones due to their strengths e.g: the ease of integration with printed circuit boards, low weight and low cost. These advantages have attracted many researchers and scientists around the world to do research for developing this type of antenna.

Currently, there is a wide range of planar antennas, depending on their function, design, and technology. Additionally, ongoing research aims to enhance these antennas even further such as: directional antennas [5], circular polarization antennas [6], antennas with a wide bandwidth [7], smart antennas [8-9], reconfigurable antennas [10], rectifier antennas (rectenna) [11], and multibeam antennas [12-13]. These types of antennas are crucial in the field of communications and advanced wireless systems.

After this introduction, this chapter will be outlined in seven sections: section II clarifies the characteristics parameters of antenna adaptation. Section III elaborate antenna polarization types. Section IV explains the characteristic radiation parameters. Section V presents the Planar antenna. Section VI shows the beamforming techniques. The last section will be the conclusion.

2. Characteristics Parameters of Antenna Adaptation

Matching an antenna (see figure I.1) is an important process to ensure the optimal transfer of energy between the transmitter and receiver. A proper adaptation ensures that the antenna operates optimally while minimizing energy losses. For this, the adaptation of an antenna is the first feature to be checked after the design. The key matching parameters are: input impedance, reflection coefficient S_{11}, the impedance bandwidth at -10dB and VSWR (Voltage Standing Wave Ratio).

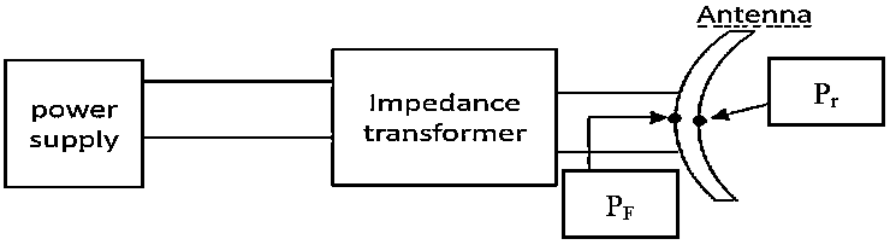

Figure I. 1 Antenna with adapter circuit and power source.

Pf: Power Fed

Pr : Antenna Radiated Power

An ideal case where the antenna is perfect (no losses) we have Pf=Pr.

2.1. Reflection Coefficient S_{11}

The reflection coefficient S_{11} is an S parameter of the scattering matrix that measures the amount of reflected signal Pr relative to the incident signal Pi. S_{11} is often used to evaluate the antenna insertion loss [3].

$$|S_{11}|^2 = \frac{Pr}{Pi} \qquad (1)$$

$$|S_{11}|_{dB} = 20\,log|S_{11}| \qquad (2)$$

2.2. Impedance Bandwidth

The IB (impedance bandwidth) is the impedance frequency interval over which the adaptation between the antenna and the source is considered acceptable.

At a resonant frequency fr we define the impedance bandwidth at -10 dB of the reflection coefficient by [4]:

$$IB = f_{max}(-10dB) - f_{min}(-10dB) \qquad (3)$$

As a percentage, the impedance bandwidth (IB) is defined as follows:

$$IB(\%) = \frac{f_{max}(-10dB) - f_{min}(-10dB)}{f_r} \qquad (4)$$

Depending on reflection coefficient impedance bandwidth at -10dB (see figure I.2), three types of antennas are defined:

*Narrowband antenna: when IB< 500Mhz

*Wideband antennas: when 500Mhz <IB<2GHz

*Ultra-wideband antenna: when IB>2GHz

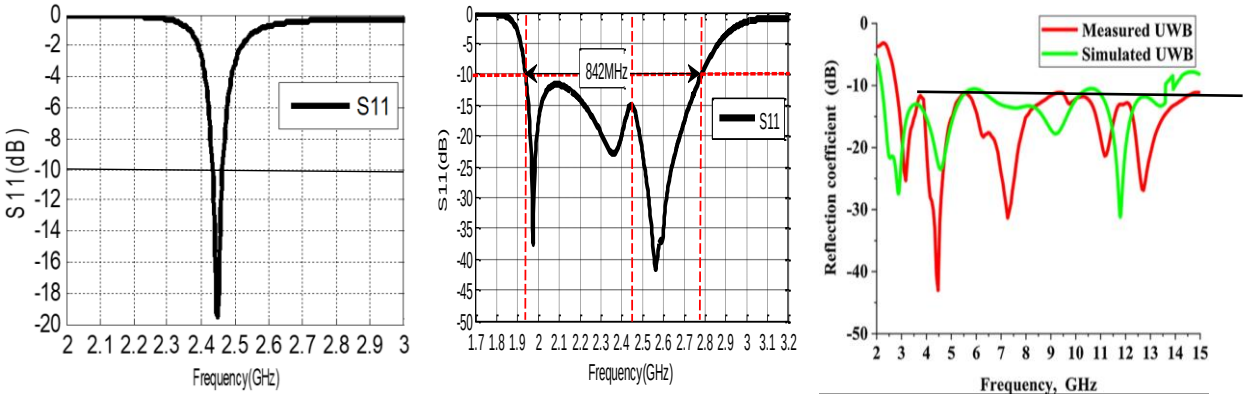

(a) (b) (c)

Figure I. 2 Example of the Reflection Coefficient vs. Frequency. (a) narrow band antenna (b) wideband antenna, (c): Ultra-wideband antenna [13-14].

2.3. The Voltage Standing Wave Ratio (VSWR)

The VSWR is another criterion commonly utilized for evaluating the impedance adaptation of an antenna. The VSWR can be expressed as a function of the reflection coefficient S_{11} as described by the following equation:

$$VSWR = \frac{V_{max}}{V_{min}} = \frac{1+|S_{11}|}{1-|S_{11}|} \qquad (5)$$

Where,

V_{max} is the maximum voltage along the transmission line.

V_{min} is the minimum voltage along the transmission line.

A low VSWR (close to 1) indicates a lossless antenna. However, a VSWR of less than 2 (see figure I.3) indicates a good impedance matching.

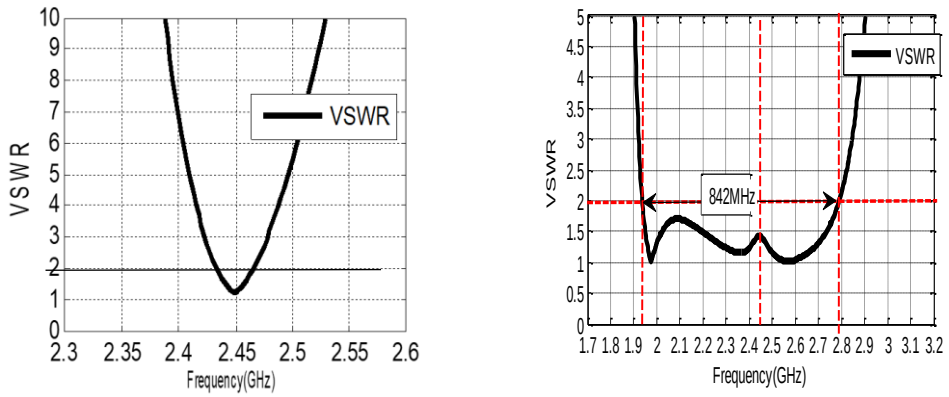

(a) **(b)**

Figure I. 3 Example of VSWR against Frequency. (a) narrow band antenna (b) wideband antenna [13].

2.4. Input Impedance

The antenna input impedance must match the circuit characteristic impedance to which it is connected. Most of power circuits have a $50\,\Omega$ input impedance. A mismatched impedance can lead to energy reflections consequently a loss of efficiency.

Let's consider a power supply line having the characteristic impedance ZC and length L, fed at one extremity by a generator and terminated at the other with antenna as a load of impedance Zr (see Figure I.4).

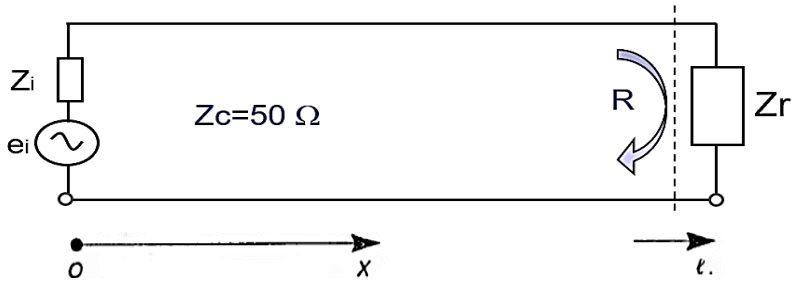

Figure I. 4 Load powered by a 50 Ohm impedance generator [15]

When the transmission line is lossless, the input impedance is given by the following relation [15]:

$$Z_{in} = \frac{Z_r + jZ_C.\tan(\beta l)}{Z_C + jZ_r.\tan(\beta l)} = R + jX \qquad (6)$$

With:

$$\beta = \frac{2\pi}{\lambda}$$

R: is the real part which is the responsible of the antenna radiating power in free space.

X: the imaginary part related to reactive power.

When the real portion is near to $50\,\Omega$ and the imaginary portion is near to zero, the antenna is well matched [3,16] (see figure I.5).

Z_{in} can be expressed as a function of the reflection coefficient S_{11} as described below [3]:

$$Z_{in} = \frac{1+S_{11}}{1-S_{11}} \qquad (7)$$

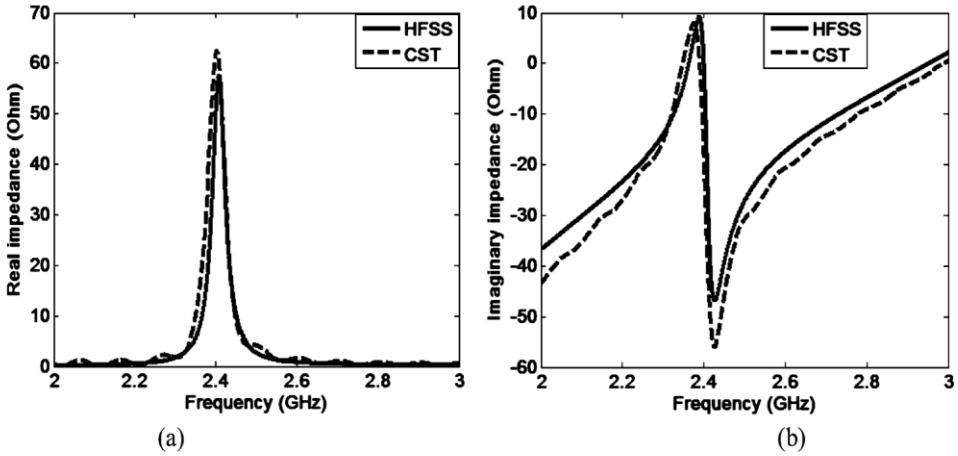

Figure I. 5 Input impedance patch antenna. (a) its real part against frequency; (b) its imaginary part Against s frequency o [16].

3. Antenna Polarization

The antenna polarization refers to state of the antenna-transmitted wave in a specific direction. It is defined by the electric field vector orientation and its variation over time. The polarization can be elliptical, linear, left hand (LHCP) or right-hand (RHCP). In these cases, the electric field vector does not describe any trajectory [17].

For a planar electromagnetic wave, spreading in the Z direction, the electrical field vector is composed of two orthogonal components which are E_x and E_y :

$$\overrightarrow{\mathrm{E}(z,t)} = E_{\mathrm{x}}(z,t).\overrightarrow{\mathrm{e_x}} + E_{\mathrm{y}}(z,t).\overrightarrow{\mathrm{e_y}} \quad (8)$$

With,

$$E_{\mathrm{x}}(z,t) = \mathrm{Re}(E_{0\mathrm{x}}.e^{j(\omega t - k.\mathrm{z} + \varphi x)}) = E_{0\mathrm{x}}.\cos(\omega t - k.\mathrm{z} + \varphi x) \qquad (9)$$

$$E_{\mathrm{y}}(z,t) = \mathrm{Re}(E_{0\mathrm{y}}.e^{j(\omega t - k.\mathrm{z} + \varphi y)}) = E_{0\mathrm{y}}.\cos(\omega t - k.\mathrm{z} + \varphi y) \qquad (10)$$

Where, E_{0x} is the maximum amplitudes of the Ex and E_{0y} is the maximum amplitudes of the Ey. φx and φy are, respectively, their phases.

3.1. Linear Polarization (LP)

A wave plane is linear polarized when the direction of electric field vector does not change over time. It can be vertical, horizontal or oblique (see figure I.6). In this case, phase shift $\Delta\varphi$ between Ex and Ey is defined as: $\Delta\varphi = \varphi y - \varphi x = n\pi$, where, n = 0, 1, 2, 3, . . .

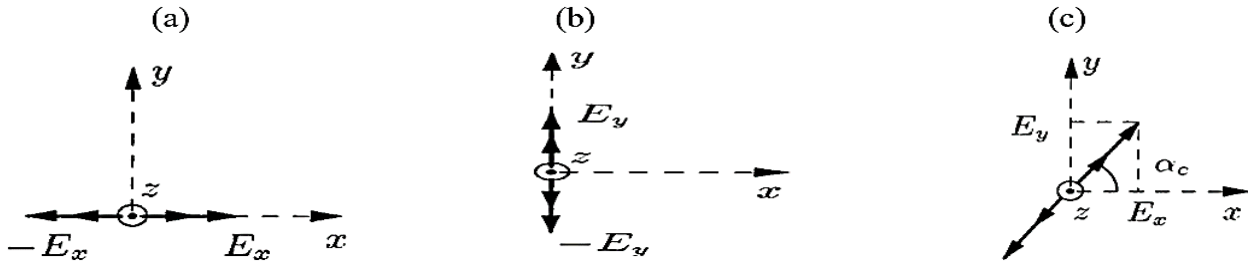

Figure I. 6 state of linearly polarized electrical field vector; (a) vertical linear polarization, (b) horizontal linear polarization, (c) oblique linear polarization.

3.2. Circular Polarization (CP)

A planar wave is circularly polarized when the direction of the electrical field changes its direction and describe a circle over time. In this case, The two electric components have equal amplitudes (E_{0x}=E_{0y}) *and* the phase shift between them is odd multiples of *90°[17]*.

$$\Delta\varphi = \varphi y - \varphi x = \pm(\frac{1}{2}+2n)\pi \quad \textit{where, } n = 0, 1, 2, 3, \ldots \quad (11)$$

When the $\Delta\varphi$ is positive, the electrical field vector turns clockwise sense, in this case the circular polarization is called LHCP (Left Hand Circular Polarization), as shown in figure I.7 (b). When the $\Delta\varphi$ is negative, the electrical field vector turns counterclockwise sense, in this case, the circular polarization is called RHCP (Right Hand Circular Polarization) as presented in figure I.7 (a).

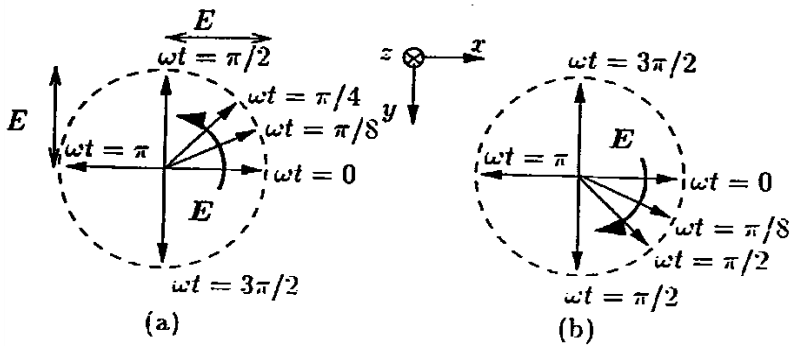

Figure I. 7 Electrical field vector in the case of circular polarization; (a): LHCP, (b): RHCP.

3.3. Elliptical Polarization (EP)

A wave plane is elliptical polarized when electric field vector direction changes its direction over time and describes an ellipsoid (with a major axis B and minor axe A) as depicted in figure I.8. The EP can be obtained in these two cases:

i. When the phase shift between is odd multiples of 90° and the two electric components possess distinct amplitudes ($E_{0x}\neq E_{0y}$) [17]:

$$\Delta\varphi = \varphi y - \varphi x = \pm(\frac{1}{2}+2n)\pi \quad \textit{where, } n = 0, 1, 2, 3, \ldots \quad (12)$$

ii. When the phase shift between Ex and Ey is different to multiples of 90°, whatever the magnitudes of two the electric components:

$$\Delta\varphi = \varphi y - \varphi x \neq \pm\frac{1}{2}n\pi \quad \textit{where, } n = 0, 1, 2, 3, \ldots \quad (13)$$

According to the phase shift Δφ, the EP could be either left hand elliptical polarization (LHEP) when Δφ is negative or left-hand elliptical polarization (LHEP) when Δφ is positive (see figure 8).

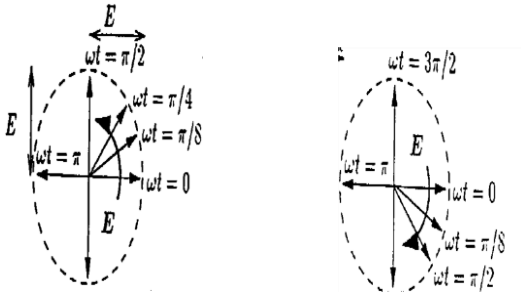

(a) **(b)**

Figure I. 8 Electrical field vector in the case of elliptical polarization; (a): LHEP, (b): RHEP.

3.4. Axial Ratio (AR)

The linear and circular polarization are particular examples of elliptical polarization. The parameter that characterizes the type of elliptical polarization is the AR (axial ratio), which is the rate between the major axis OA and the minor axis OB, as shown in Figure I.9:

$$AR = \frac{major\ axis}{minor\ axis} = \frac{OA}{OB} \qquad 0 \leq AR \leq \infty \quad (14)$$

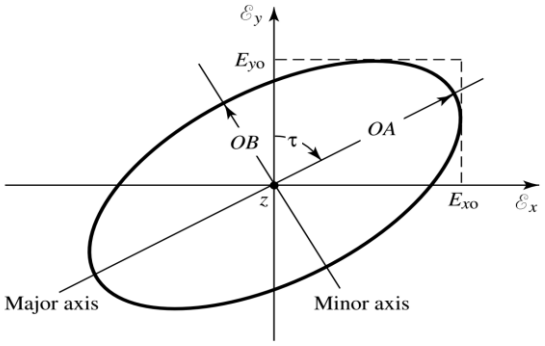

Figure I. 9 Minor and major axes of elliptical polarization [17].

The axial ratio can be expressed as a function of E_{0x}, E_{0y}. and Δφ as described in the following equation [17]:

$$AR = \frac{OA}{OB} = \sqrt{\frac{(E_{0x}/E_{0y})^2 + 1 + \sqrt{(E_{0x}/E_{0y})^4 + 1 + 2.(E_{0x}/E_{0y})^2.\cos(2\Delta\varphi)}}{(E_{0x}/E_{0y})^2 + 1 - \sqrt{(E_{0x}/E_{0y})^4 + 1 + 2.(E_{0x}/E_{0y})^2.\cos(2\Delta\varphi)}}} \quad (15)$$

- For vertical linear polarization, where E_{0x}=0, the axial ratio is AR=0.

-For horizontal linear polarization, where E_{0y}=0, the axial ratio is AR=∞.

-For circular polarization, where OA= OB, the axial ratio is AR=1, indicating ideal circular polarization. However, nearly circular polarization is considered when 1 ≤ AR ≤ 2(AR ≤ -3dB).

The AR could be plotted versus frequency as shown in figure I.10

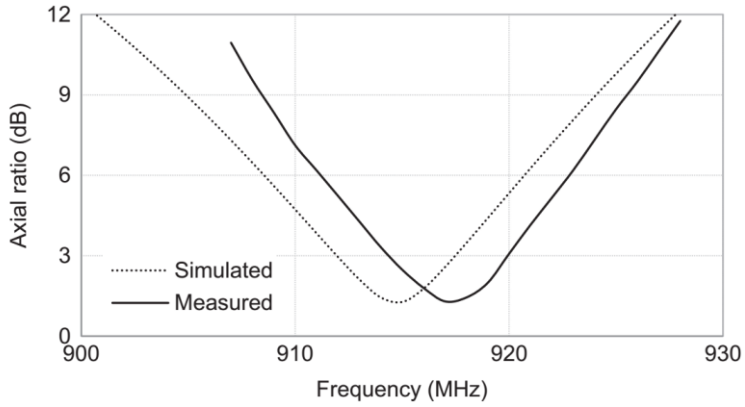

Figure I. 10 Axial-ratio versus frequency of CP antenna [18]

3.5. polarization diversity

And antenna with polarization diversity may be obtained using at least two elements antenna array, one possesses LHCP and the other one possesses RHCP. In this case the total antenna catches the EM wave in whatever its electrical vector (clockwise or counterclockwise sense).

4. Antenna Radiation Characteristic parameters

The radiation parameters that must be evaluated while designing an antenna, include gain, directivity, radiation efficiency, and radiation patterns. These parameters are essential as they determine how effectively the antenna communicates with other devices.

4.1 Antenna directivity

The directivity of antenna, typically expressed in dB (decibels), is a measure of an antenna's ability to direct and concentrate energy in a specific direction. Mathematically, it is defined as the rate of its radiated intensity U in a given direction to the radiated intensity in the space of an isotropic antenna U_0 [17] as expressed by the following equation:

$$D(\theta,\varphi) = \frac{U(\theta,\varphi)}{U_0} = \frac{U(\theta,\varphi)}{\frac{Pr}{4\pi}} \qquad (16)$$

Where, Pr: is the total radiated power (see Figure I.11).

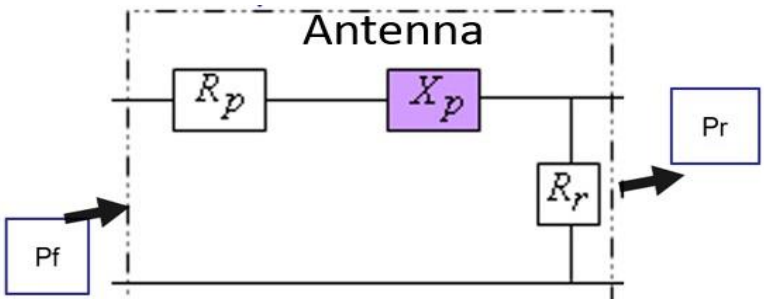

Figure I. 11 Equivalent diagram of an antenna. Rr: radiation resistance, RP: loss resistance, Xp: antenna reactance.

The directivity of an antenna can be influenced by various factors such as its design, size, geometry and other technical characteristics. Generally, a higher directivity is sought; indicating that the antenna is more directive in a specific direction. A directive antenna is Widely applicable in wireless communications, radars, and satellites. The antenna directivity can be plotted versus frequency as shown in figure I.12.

4.2 Antenna gain

The antenna gain is the rate between the radiation intensity in a specific direction and the radiation intensity that would be received if the antenna's power were radiated equally in all directions. The radiation intensity associated with isotropic radiation power equals the supplied power P_f to the antenna splitted by 4π (see figure I.11).

The expression of gain for a radiation direction (θ, φ) is given by the following equation [17]:

$$G(\theta,\varphi) = \frac{U(\theta,\varphi)}{\frac{P_f}{4\pi}} \qquad (17)$$

Where,

$U(\theta,\varphi)$: is the power density transmitted to the antenna.

P_f: is the total power delivered to the antenna (see Figure I.11).

Typically, a higher gain is desirable, as it indicates that the transmitted or received power is concentrated in a specific direction.

The antenna gain can be plotted versus frequency as shown in figure I.12.

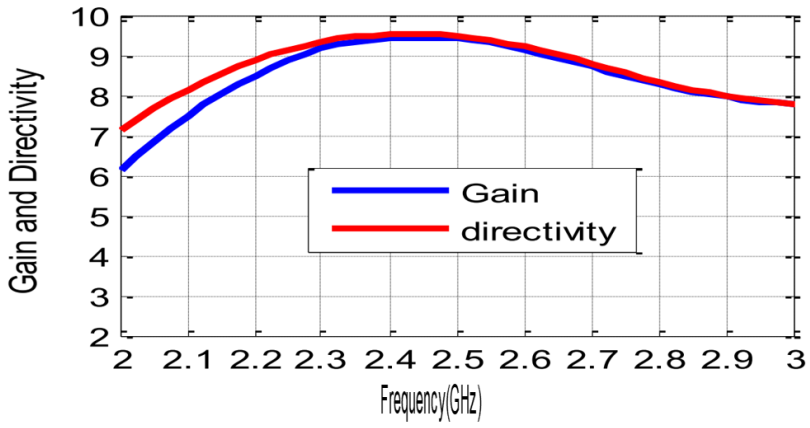

Figure I. 12 gain and directivity in dB versus frequency in GHz [19].

4.3. Antenna radiation efficiency

The radiation efficiency of antenna is the rate between the total radiated power Pr and the power delivered P_f to the radiating element. its expression is given as follow:

$$\eta = \frac{P_r}{P_f} = \frac{R_r}{R_r + R_P} \qquad (18)$$

With:

Rr: radiation resistance,

RP: loss resistance

Xp: antenna reactance

In the case of a lossless antenna (Rp=0) the radiation efficiency would be $\eta = 1$.

The expression of radiation efficiency can be obtained from the expressions of gain and directivity as described below:

$$\eta = \frac{G(\theta,\varphi)}{D(\theta,\varphi)} \qquad (19)$$

Typically, the radiation efficiency is expressed in % and plotted versus frequency as shown in figure I.13.

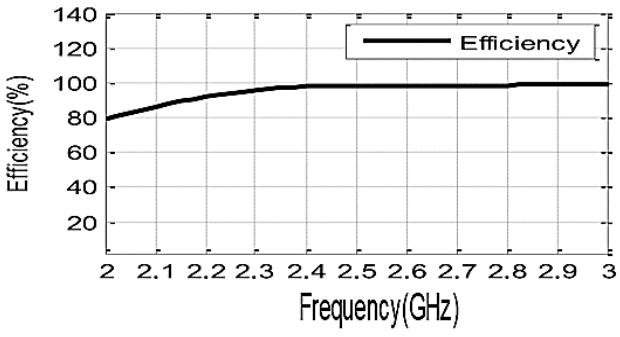

Figure I. 13 gain and directivity versus frequency [19]

4.5. Antenna radiation pattern

The antenna radiation diagram is a graphical representation of how emitted power is distributed spatially. This representation can be plotted in 3D (see Figure I.14). However, 2D graphs are usually used (in the E and H planes see Figure I.15). These radiation patterns are essential for the antenna performance evaluation and can be plotted either in terms of gain or directivity.

The radiation pattern form depends on the design and geometry of antenna. The 3D radiation pattern is plotted in spherical coordinates (r, θ, φ).

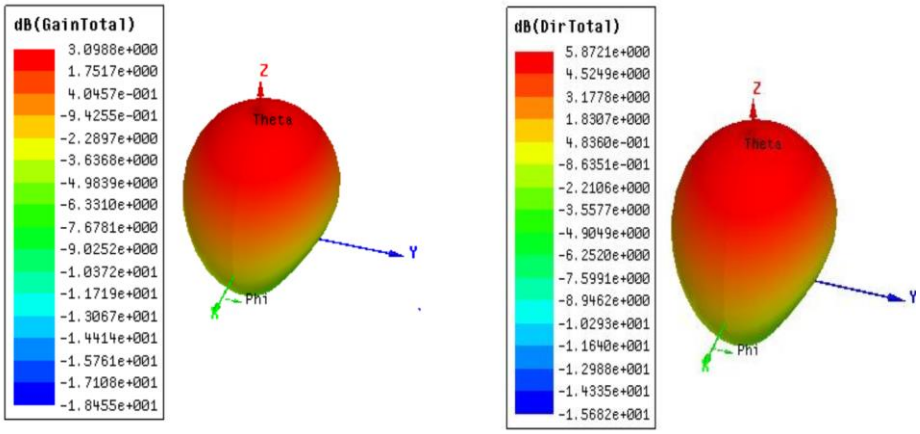

Figure I. 14 3D radiation pattern in terms of : (a) gain; (b) directivity [4].

For practical reasons, the radiation pattern is represented in 2 dimensions (2D) in two separated planes E and H where the power intensity is maximal:

i) **Plane E** (φ = 0°): This plane contains the electromagnetic wave's E-field vector. It is perpendicular to the antenna axis and commonly corresponds to the **vertical plane** in many antenna configurations.

ii) **Plane H** (φ = 90°): This plane contains electromagnetic wave's H-field vector. It is also perpendicular to the antenna axis and often corresponds to the horizontal plane in antenna configurations.

It is important to note that the horizontal plane measures E-field not the H-field. In addition, the radiation pattern always refers the power which is proportional to the E-field squared [20].

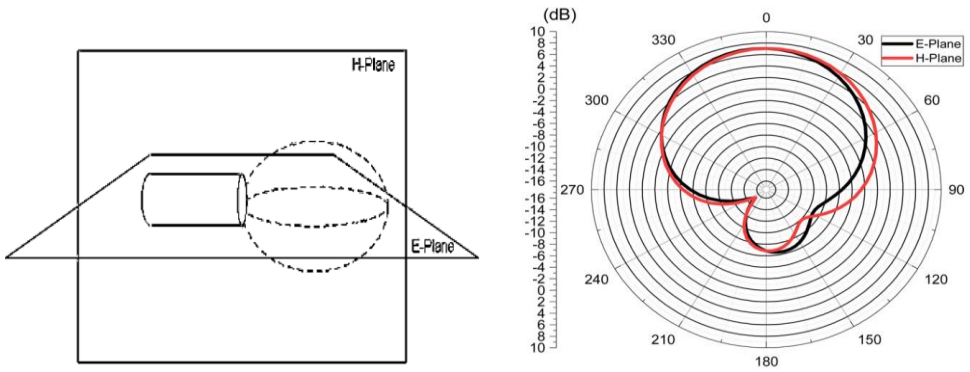

(a) (b)

Figure I. 15 E and H plane radiation patterns: (a) 3D; (b): 2D. [19]

The radiation diagram of antenna could be categorized into 4 main types: Isotropic, Omnidirectional, Directional or Beamforming radiation pattern (see figure I.16).

- **i.** Isotropic radiation pattern: is specific for a hypothetical antenna that radiates in all directions in a uniform manner.
- **ii.** Omnidirectional Radiation Pattern: This pattern occurs when the radiation energy is distributed equally in all directions from the antenna.
- **iii.** Directional radiation pattern: This pattern is observed when the radiated energy is maximal in a specific direction.
- **iv.** Beamforming radiation pattern: this radiating pattern is exhibited when the antenna is multi-beam. in this case the radiation pattern can steer in different directions with a maximum beam in a specific direction.

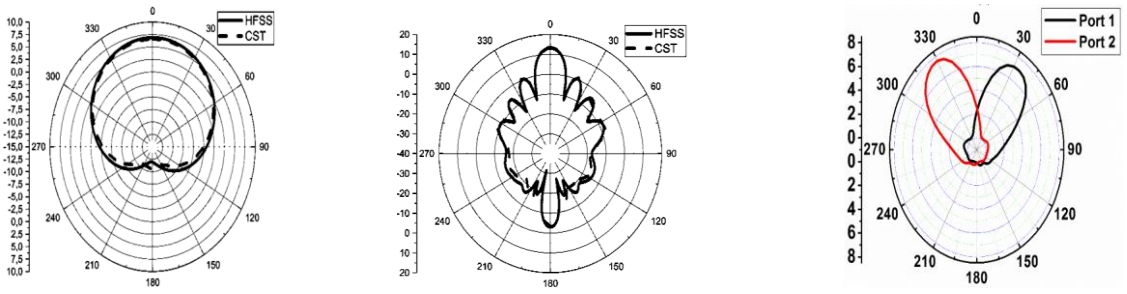

(a) (b) (c)

Figure I. 16 Different radiation pattern types (a): omnidirectional; (b): directional radiation pattern; (c): Beamforming radiation pattern. [5,21].

4.6. Polarization patterns: co-polarization and cross-polarization

The H-plane and E-plane are used as reference planes for a linearly polarized antenna. However, for a circularly polarized antenna the cross-polarization and co-polarization must be presented in

both H and E planes. The co-polarization is E-field vector direction whereas the cross-polarization direction is the H-field direction. Typically, the received power for a co-polarization-oriented antenna is maximum whereas the received power is minimum for the cross-polarization orientation.

The radiation pattern may exhibit different polarizations. Nevertheless, when the polarization is not specified, the polarization type is supposed to be oriented with the direction of the peak gain direction [17].

The co-polarization compared to the cross-polarization is defined for the radiating planes E and H in terms of gain or directivity. It can be plotted as function of frequency (see figure I.17.a) or in spherical coordinates in E and H planes (see figure I.17.b).

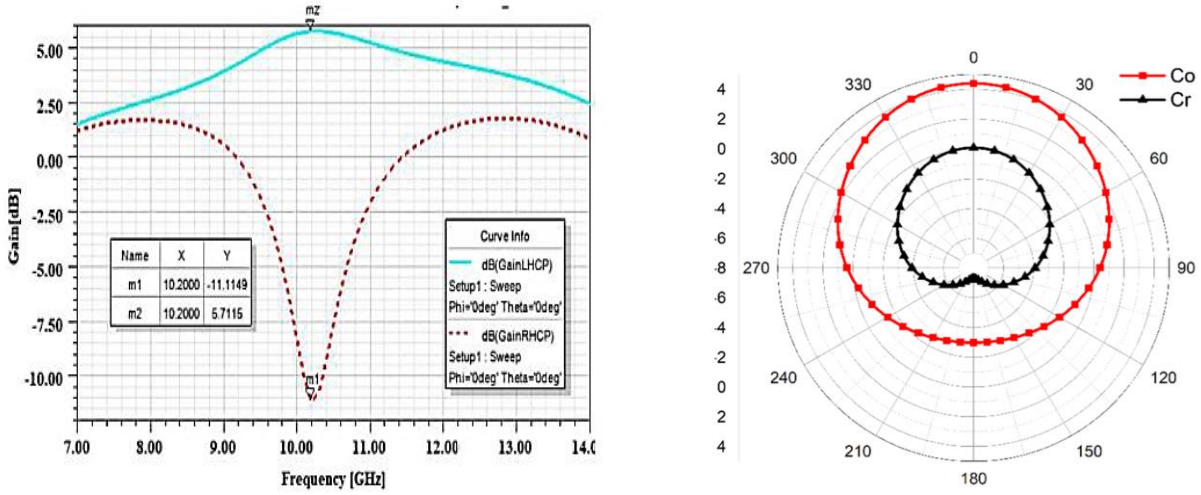

Figure I. 17 Co versus Cross polarization. (a): as function of frequency;(b):in the plan E [22,23].

5. Planar antennas

Typically In general, antennas are classified into five types : wire antennas (dipole, monopole, and Yagi antenna), Aperture Antennas (horn antenna), Reflector Antennas (parabolic antenna), Lens Antennas and Planar Antennas) [4]. The latest type, also called patch or microstrip antennas, is the most commonly used one thanks to its benefits e.g low weight, affordable and simplicity of integration with PCB (printed circuit boards) technology. These advantages have attracted many researchers and scientists around the world to conduct research for developing this antenna type.

The most prevalent shapes planar antennas are square, circular, and rectangular patches, some of which are depicted in figure I.18 [17,20]:

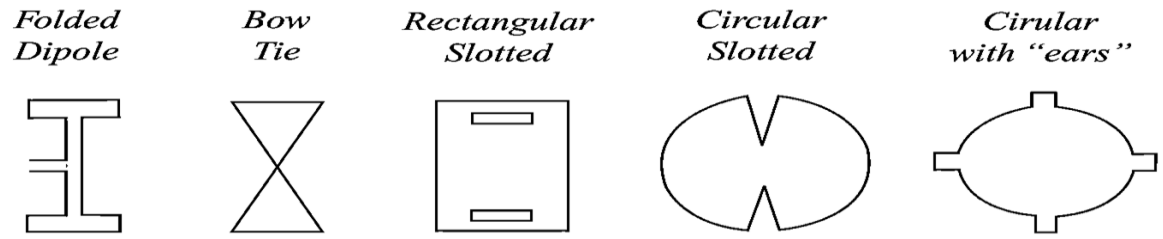

Figure I. 18 The most typical patch antenna shapes [20]

The key components of a patch antenna include: **radiating element** (which is often made of copper or another conductive substance), **dielectric substrate** (which is made of a non-conductive and the radiating element is mounted on it) and **ground plane** (it is conductive substance that is often placed on the opposite face of the substrate from the metal patch) as shown in figure I.19-20.

5.1. Feeding techniques

Planar antennas utilize various feeding techniques such as: coaxial cable, Coplanar Line, Mutual Coupling Feeding and microstrip line. The feeding mechanism significantly impacts the antenna's performance parameters.

5.1.1. Coaxial cable Feeding

Coaxial feeding involves using a coaxial cable to connect the antenna to the transmission line or source. The external conducting of the coaxial cable is usually connected to the ground plane of the antenna, while the center conductor is connected to the feed point on the patch. Coaxial feeding is versatile and is used in various antenna types, including planar antennas. The most commonly used coaxial cable is the 50 Ω one with an N-type coaxial connection. As illustrated in figure I.19, the N-coaxial connection is linked to the ground plane (back side) of the microstrip antenna. The coaxial's center connector is then soldered to the patch after being passed through the substrate [24].

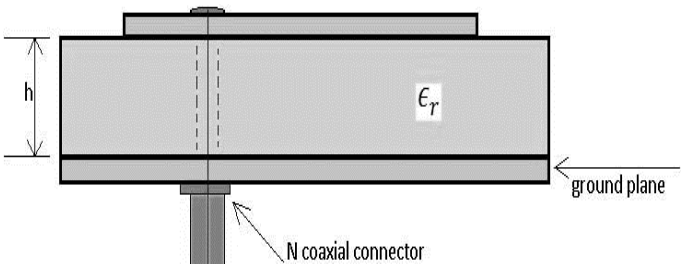

Figure I. 19 planar antenna with Coaxial line feed [24].

5.1.2. **Coplanar Line Feeding**

In coplanar line feeding, both the transmission line and the ground plane are printed into the same plane as the radiating elements (see figure I.20). It could be seen as a form derived from a coaxial cable structure where the internal conductor is isolated from two ground planes [20-24-25]. This feeding technique is particularly advantageous for planar antennas as it simplifies the overall structure. Coplanar feeding line offers a useful and adaptable way to supply electromagnetic energy to the radiating element in planar antennas.

The CPW offers many advantages, including the ease of fabrication and integration in to PCB circuits, the capability to operate at extremely high frequencies (exceeding 100 GHz), and the potential to achieve good circuit isolation. However, it's worth noting that CPW circuits may exhibit higher losses compared to other microstrip circuits, particularly when a compact layout is necessary [20].

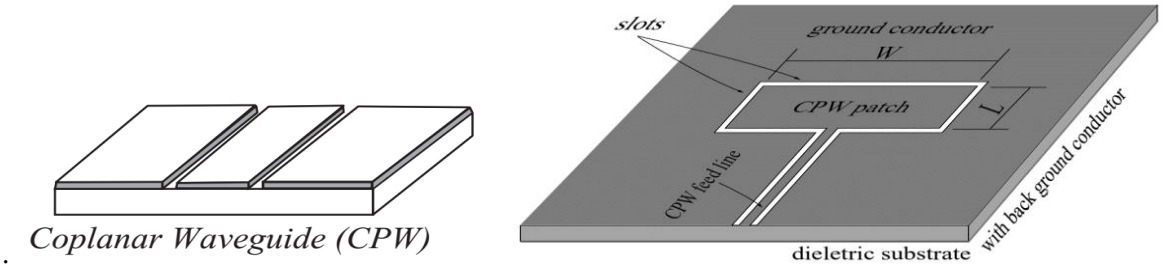

Figure I. 20 planar antenna with coplanar feed line [24-25].

5.1.3. **Proximity Coupling**

This technique uses electromagnetic coupling for feeding, where there is no physical contact between the radiating element and the feeder. The feed line is inserted between two overlapping dielectric substrates, the patch is on the top and the ground plan is on the bottom as shown in figure I.21. The main advantages of this feeding technique include the potential for high bandwidth due to greater spacing between the ground plane and the radiating element, as well as the ability to achieve adaptation by controlling the depth of the feeder under the patch and the width of the patch. However, it's worth noting that this technique is somewhat more complex in terms of fabrication compared to the other methods presented previously [26].

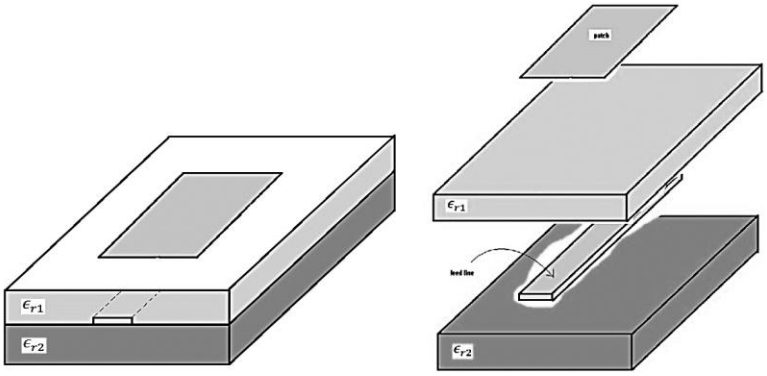

Figure I. 21 Electromagnetic Coupling feed

5.1.4. Aperture Coupling

In this method, two dielectric substrates are used with the ground plane is inserted between them as shown in figure I.22. The upper substrate contains the patch on it, while the lower substrate houses the feeder below it. The coupling between the feeder and the patch is achieved through a slot inserted in the ground plane. This slot is usually centered underneath the patch. Typically, in order to optimize the patch radiation, a high dielectric constant and low thickness are used for the lower substrate, while a larger thickness and a smaller dielectric constant are used for the upper substrate. This type of coupling gives wider bandwidth [20,24]. However, a significant limitation of this method is the complexity of fabrication.

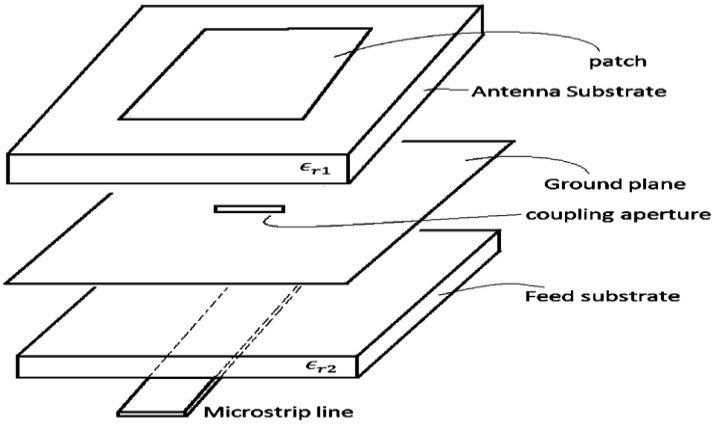

Figure I. 22 patch antenna fed via aperture coupling.

5.1.5. Mutual Coupling Feeding

Mutual coupling occurs when the radiation fields of two antennas placed in close proximity affect each other's performance. Therefore, this feeding technique is another technique where multiple radiating elements are closely spaced, influencing each other's electromagnetic fields (see figure

I.23). This feeding approach plays a significant role in the planar antenna arrays design, affecting

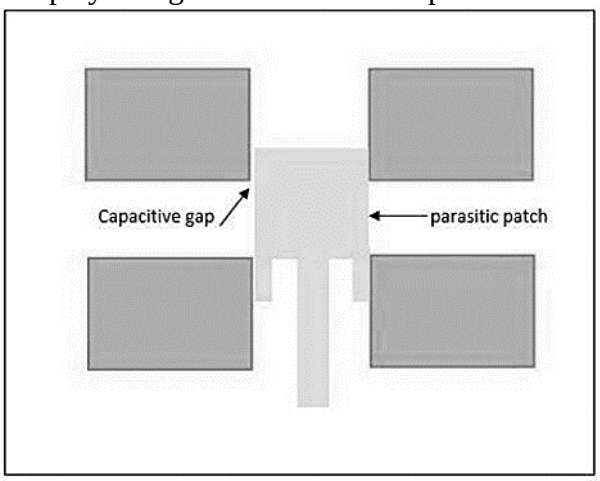

Figure I. 23 Mutual Coupling Feedline

their performance characteristics. However mutual coupling can have negative effects such as crosstalk, distortion of the radiation pattern if an optimal physical separation between antennas is not respected. Including decoupling networks or structures (EBG) between adjacent antennas can minimize the impact of mutual coupling|[26].

5.1.6. **Feeding via microstrip line**

The most popular planar transmission line is 50 Ohm microstrip line. Feeding planar antennas via microstrip lines involves integrating a microstrip transmission line directly into the antenna structure as shown in figure I.24. This method is known for its compactness and suitability for integration with other components on the same substrate.

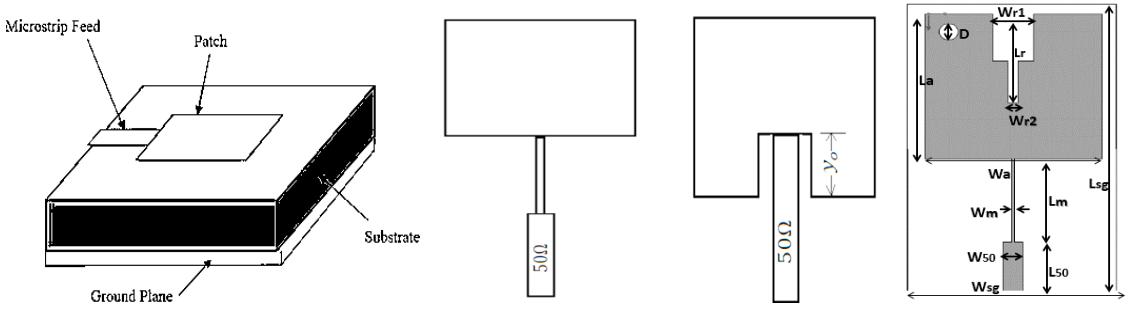

(a) (b) (c) (d)

Figure I. 24 Feeding via Microstrip line technique

Although this method is easy on fabrication, it encounters a poor impedance matching between the patch and feeder. To avoid this problem many techniques have been used to achieve a good adaptation such as:

i. Inserting a quarter wave impedance transformer between the radiation element and the feeder [5] as shown in figure I.24 (b).
ii. Inserting slots in contact with the feeder and the radiating element [3] as shown in figure I.24 (c).
iii. Inserting slots on the patch [3,4].
iv. Utilization of defected ground plane [3].

5.2. Circular polarization

This section will explain the circular polarization concept within the context of planar antennas, outlining the techniques employed to achieve it. Two methods are used to achieve CP either dual feed (see figure I.25) or single feed (see figure I.26).

5.2.1. CP via dual feed

Planar antennas employing dual-feed arrangements can achieve circular polarization. A dual-feed configuration produces circular polarization via excitation of the antenna through two feeding mechanisms that produce a 90-degree phase shift between the perpendicular components of the electrical field [20]. The dual orthogonal feed arrangement offers a wider bandwidth for axial ratio. It can be achieved using either hybrid coupler or a power divider to feed a patch antenna as shown in figure I.25.

When two orthogonal modes are simultaneously induced with identical amplitude and 90°-degree out of phase difference, with the sign controlling the sense of rotation, a single patch antenna can be made to emit circular polarization.

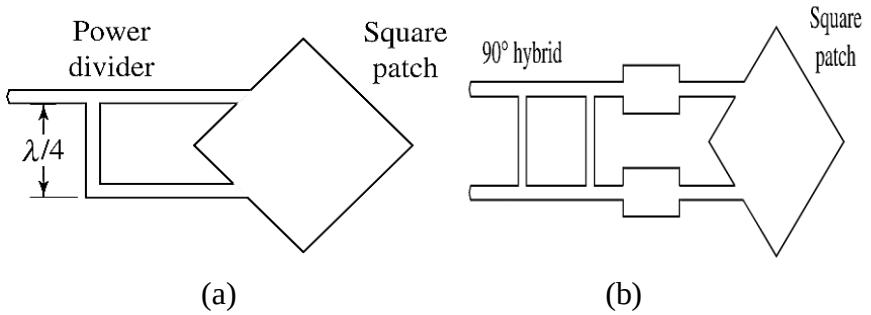

Figure I. 25 Dual orthogonal feed circularly polarized Microstrip antenna (a) fed via a power splitter (b) fed through a 90° 3dB directional coupler [17].

5.2.2. CP via single feed

A patch antenna with a single feed (see figure I.26) often emits linear polarization. However, two orthogonal patch modes with identical magnitude and in phase quadrature must be provided to radiate CP. This can be achieved by feeding the patch at a specific single point or using perturbation segments to detune the degenerate modes of a symmetrical patch antenna [17].

In a single fed configuration, a single point is used without need of an external power divider. When using a power divider network to support dual orthogonal feeds is not feasible, a single point feed patch that can produce CP radiation is highly preferred.

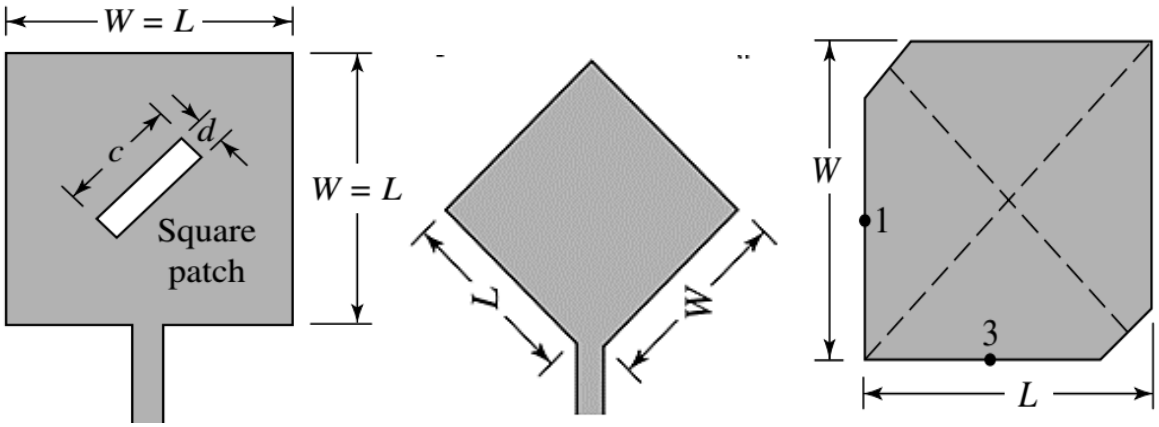

Figure I. 26 configurations of singly fed circularly polarized microstrip antennas [17]

5.3. Microstrip Antenna array

In some applications, a single antenna element may lack the necessary flexibility and usually exhibits limited directivity and gain to transmitting/receiving data, especially over long distances [20]. Actually, to increase the single element performence, several microstrip antennas are arranged systematically to form an array. This array antenna is commonly used in numerous applications i.e: beamforming, beam steering, radar, satellite communication and massive MIMO for 5G or 6G Array antennas are capable of generating a directional radiation pattern with high gain and directivity. In practice, Microstrip antenna arrays are organized in various configurations where the patches are arranged in a specific manner to create a precisely managed 1D, 2D, or 3D arrangement [20,27] as shown in figure I.27

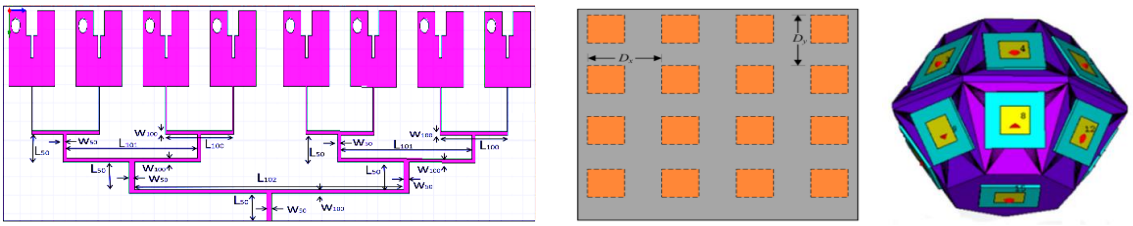

(a) (b) (c)

Figure I. 27 Microstrip patch array antenna configuration, (a): 1D, (b): 2D, (c): 3D[27]

An array antenna comprises multiple radiating elements strategically positioned in space to create an array with specific desired traits. These characteristics are attained by modifying the amplitude and phase of the power feed and relative placement of elements [20].

The primary advantages of an array antenna include its high directivity and gain, as well as its adaptability to create a desired beam, enabling the generation of an electrically scanned beam without the need for mechanical rotation.

However, there are several drawbacks such as the bandwidth limitation, the poor impedance matching due to the complexity of the required feeding network, the mutual coupling and the overall dimensions of an array antenna are substantial [24].

The radiation diagram of the microstrip antenna array is influenced by the array factor, which is the sum of the single element patterns [17]. The array factor (AF) takes into account the phase and amplitude relationships between the elements.

the total field E_T for a linear array antenna with uniform spacing of N elements is given by the equation below [17,20,24]:

$$|E_T| = \mathrm{E(single\ element)}.AF_N \qquad (19)$$

Where, AF_N is the array factor of N elements is expressed as follow:

$$AF_N = 1 + e^{j(\mathrm{k.d}\cos(\alpha)+\beta)} + e^{j2(\mathrm{k.d}\cos(\alpha)+\beta)} \dots\dots\dots\dots\dots + e^{jN(\mathrm{k.d}\cos(\alpha)+\beta)} \qquad (20)$$

Thus, $$AF_N = \sum_{n=1}^{N} e^{j(n-1)\psi} \qquad (21)$$

Where $\psi = k.d\cos(\alpha) + \beta$

The normalized AF of an array antenna with uniform spacing is described as follow:

$$AF_N = \frac{1}{N}\left[\frac{\sin(N.\psi/2)}{sin(\psi/2)}\right] \qquad (22)$$

Figure I.28 shows the normalized *AFn* in dB versus θ in degrees; for $d = \lambda$, $N = 10$ and for $d = \lambda/2$, $N = 10$.

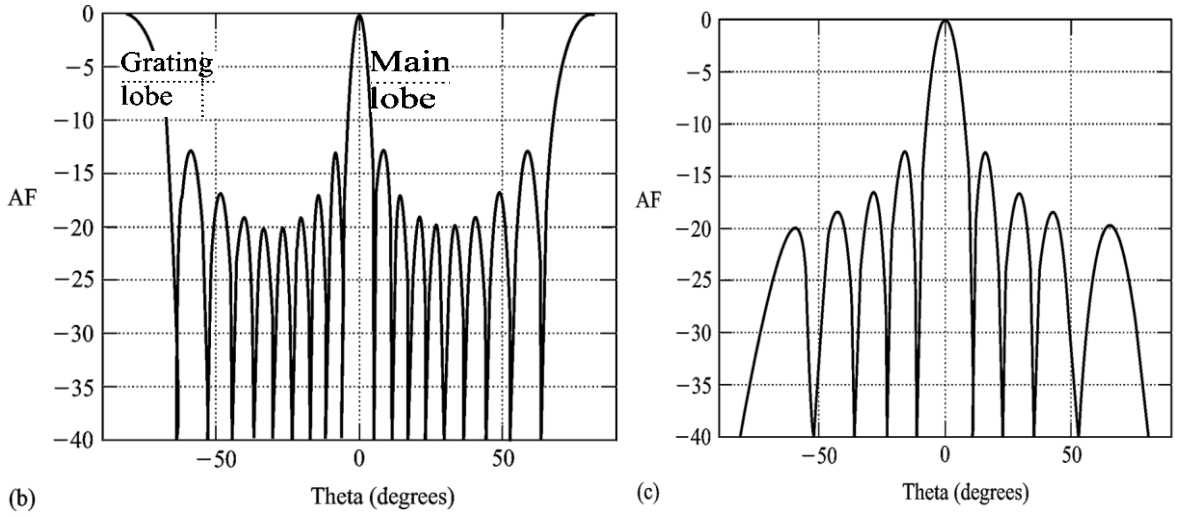

Figure I. 28 Array factor versus angle θ (b) d = λ and N = 10; (c) d = λ/2 and N = 10 [20].

Any radiation pattern contains essential information (refer to Figure I.29) such as:

i. **The HPBW**: is the beamwidth at half power, also known as the main lobe width at -3 dB.
ii. **The 10 dB BW**: is the 10 dB beamwidth providing insight into the main beam's shape.
iii. **The level of the initial side lobe**: is the side-lobe peak relative to the main beam peak
iv. **The front-to-rear ratio**: is the peak of the main lobe over the peak of the back lobe.

Between the main and first grating lobes, there exist (N - 2) side lobes. Typically, grating lobes are undesirable, especially in some applications like radars where a single focused beam is preferred [20].

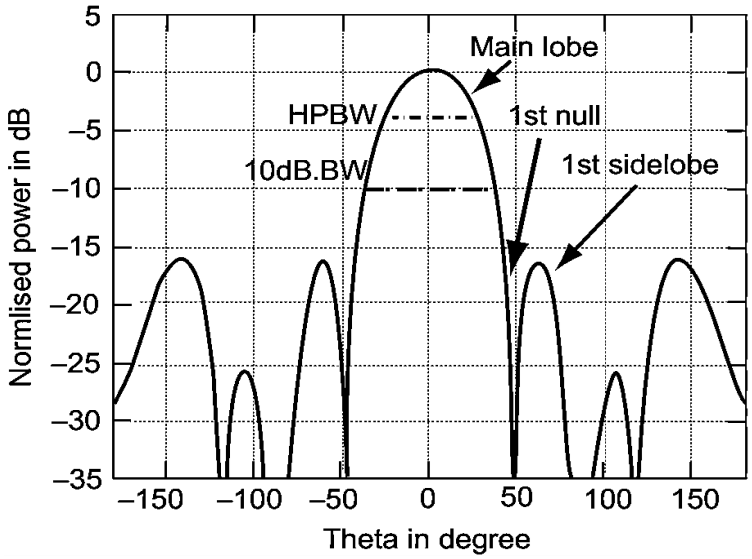

Figure I. 29 2D radiation pattern

The mutual coupling is interaction between adjacent elements in the array antenna. It may have an impact on the array's overall performance and radiation pattern . Additional lobes in

the radiation pattern known as grating lobes might be appeared from improperly managed spacing between array elements. Mutual coupling effects and grating lobes could be reduced by the use of appropriate spacing d between elements in the design strategies (d between patches should respect $\boldsymbol{\lambda/4 \leq\ d \leq \lambda/2}$) [28].

6. Beamforming Techniques

Beamforming is a signal processing technique widely used in telecommunication systems such as: radar, satellite and base stations in order to increase space coverage both in transmission and reception,

Although an array antenna increases gain and directivity of a single element, it still limited in terms of flexibility due to the use of Power divider for feeding. To resolve the flexibility problem, a beamformer circuit (see figure I.30) should be used as feeder of array antennas. In this case, the antenna array will be able to steer electronically its radiation pattern which could be directed towards a desired direction by modifying the phase and magnitude of the signals delivered to each antenna.

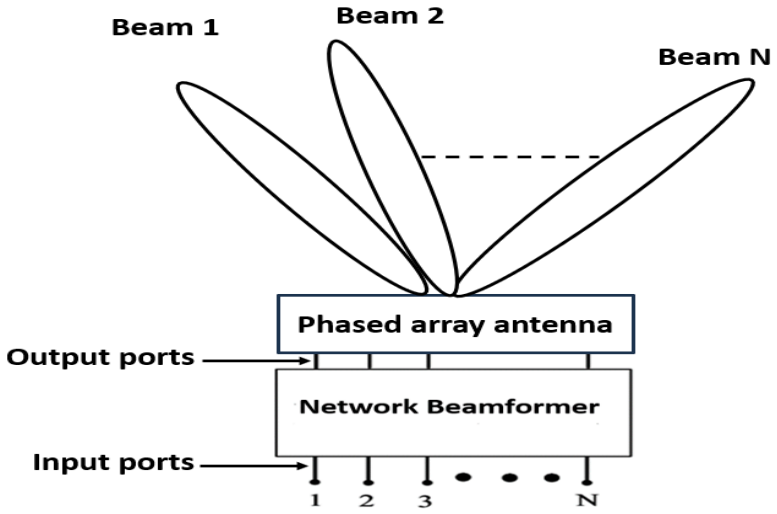

Figure I. 30 Structure of a switched multi-beam antenna.

In particular applications like object tracking, adjusting the antenna's radiation pattern is necessary. To address this requirement, a switched beam antenna (refer to figure I.30) is employed, offering several advantages as outlined below:

i) It focuses the radiation on the target.
ii) It has the capability to choose from a diverse set of predefined radiation patterns to enhance network coverage.

iii) It enhances the directivity and gain depending on the position of the target.

iv) It provides adaptability in the orientation of the radiation beam.

The principle operational of a multibeam antenna that is agile in term of radiation pattern is to make a narrower main lobe and steer it towards an object using a beamformer circuit to feed an array antenna. Actually, there are two different categories of the beamformer circuit: digital beamformer (adaptative beamformer) [8-9] and analog beamformer (switched beamformer) [29-54].

6.1. Digital beamformers:

Typically, a digital beamformer consists of a set of radiation elements and a digital signal processor either the Digital Signal Processor (DSP) or the Field-Programmable Gate Array (FPGA) in which adaptive algorithms are implemented steer beam pattern in real time. These algorithms use a complex diagonal weighting matrix modify the phase and magnitude of the signals received from each radiating element (see Figure I.31). Thanks to these adaptive algorithms, the system estimates the directions of arrival (DOA) then directs the beam towards those directions. Thus, this system performs two main tasks: DOA (Directions Of Arrival) estimation and beam formation along these estimated directions [8-9]. This type of beamformer requires complex signal processing devices (adaptive filters,...) to configure the radiation pattern.

The adaptive algorithms have been designed to adjust and adapt dynamically based on changing environmental conditions. . They usually use feedback mechanisms to adjust its parameters or behavior in real-time. The goal is to optimize performance or find the optimal solution based on the available data.

These adaptive algorithms can be used in various fields, such as signal processing, optimization, machine learning and MIMO systems etc. The most widely used algorithms are: Bartlett, Prony, Capon, MEM, MMSE, MUSIC and Min-Norm, for DOA estimation. Additionally, for beamforming purposes, algorithms such as Null-steering, MVDR, LMS, RLS, DMI, and CMA are extensively employed [8,9].

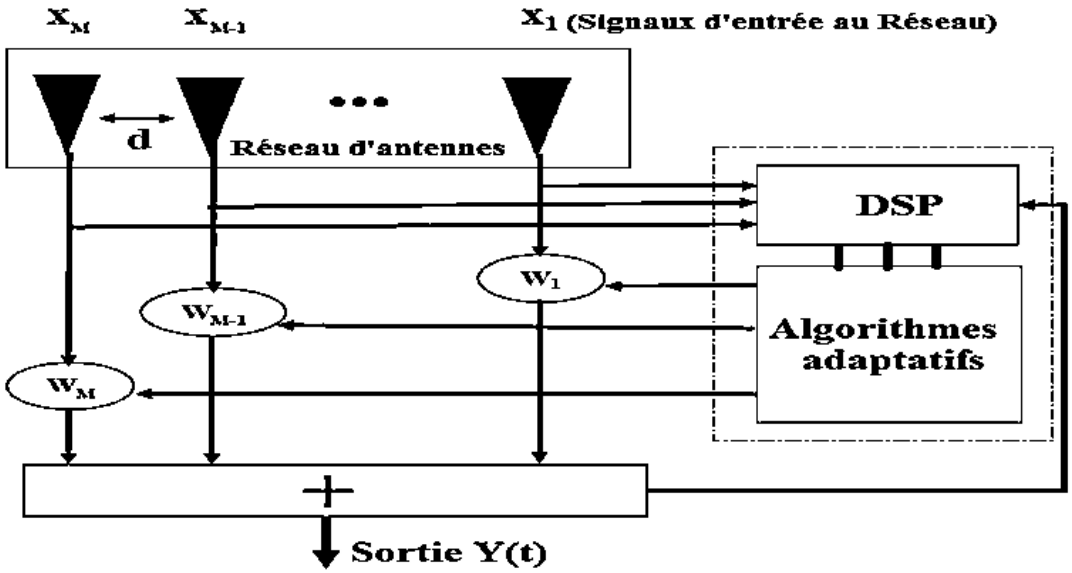

Figure I. 31 Structure of an adaptive antenna system [8].

The output of this system is given in [8] as described below:

$$Y(t) = \sum_{i=1}^{M} W_i . X(t)_i \qquad (23)$$

Where, M: is the number of elementary antennas.

Wi: weighting coefficients

$X(t)_i$: are the signals at the input of each antenna.

6.2 Switched beamformers

A switched beam antenna typically consists of array antenna connected to N output terminals of a beamformer network, whose input ports are linked to a switching circuit that controls the beamformer circuit. Various types of switching circuits may be employed, comprising switches of mechanical, electronic, optical or physical nature. However, the widely switches used are the electronic ones [10,29-30]. Actually, electrical adjustment involving active components is preferable such as RFMEMS (radiofrequency micro-electromechanical system) switches, PIN (Positif-Intrinsic- negative) and varactor diodes whose model are shown in figures I.32 and I.33

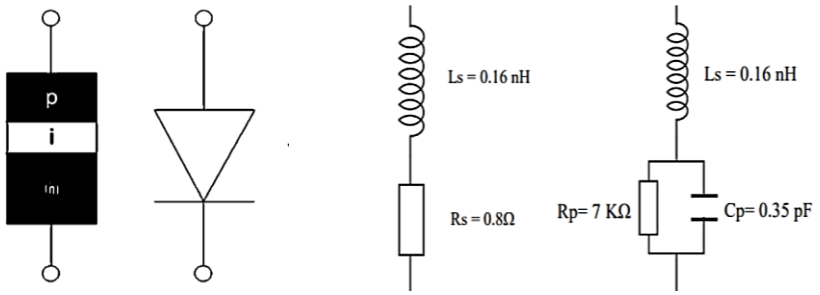

a **b** **c** **d**

Figure I. 32 diode PIN and its equivalent models, a: Structure, b: Symbol, c: equivalent model of diode on state, d: equivalent model of off state [30].

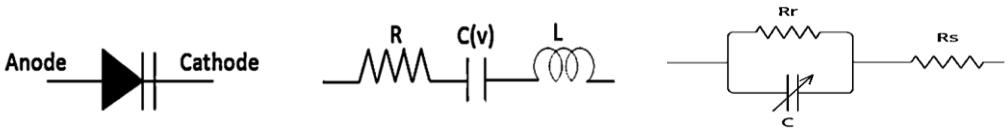

a **b** **c**

Figure I. 33 Varactor diode and its equivalent models, a: Symbol, b: equivalent model of diode on, c: equivalent model of off [30].

Actually, switched network beamformers fall into two primary types such as: Microwave Lens based beamformers and Hybrid Coupler based beamformers.

6.2.1. Microwave Lens based Beamformer

Microwave Lens based Beamformer are microwave circuits having metal lens shape with a parallel plate configuration. They serve to power a set of antennas (see Figure I.34) to obtain a switched beam antenna. The augmentation of the lens input and output ports leads the increasing of number of beams [31]. There are several types of Microwave Lens based Beamformer such as: R-KR lens [32-34], Ruze lens [34-35], Rotman lens [35-37], Bootlace lens [37-39] and Luneburg lens [40.41]. Nevertheless, the most common ones are Luneburg and Rotman lenses which will be presented in the next sections.

The operational principle of these beamformer networks is relies on the geometric optics laws (Law of Rectilinear Propagation of light, Fermat's principle, the reflection and refraction laws) to form beams in different directions (see figure I.34).

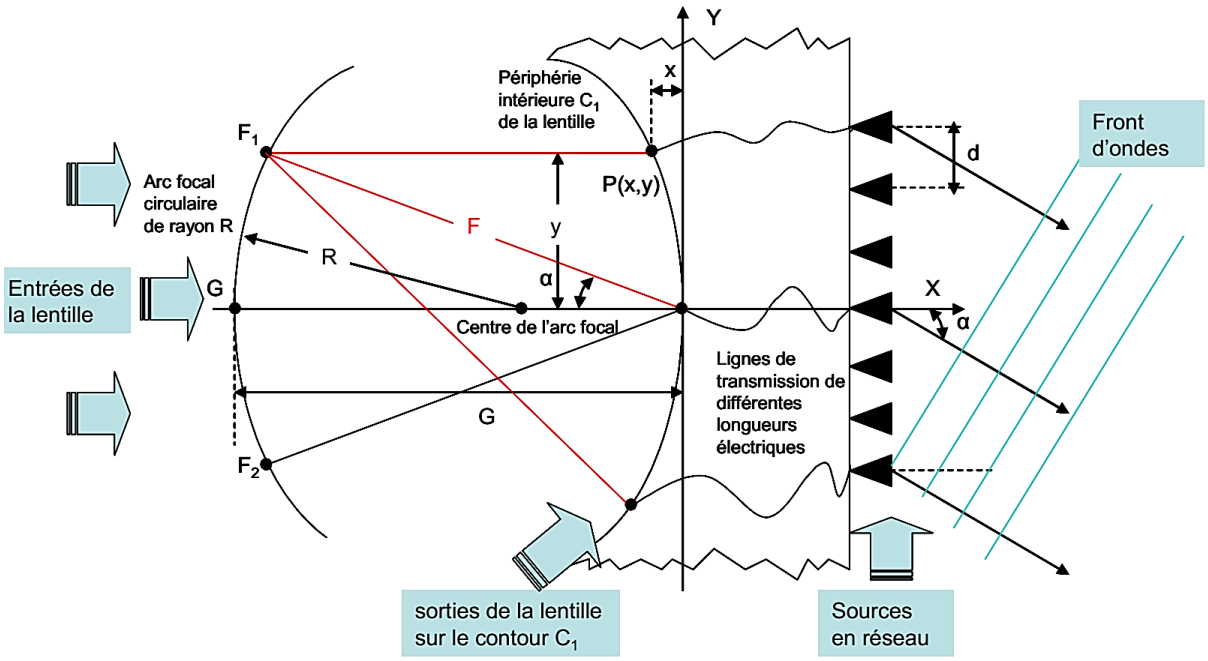

Figure I. 34 Diagram of a microwave lens powering an antenna array [42]

6.2.1.1. **Luneburg gradient-index lens**

The Luneburg lens utilizes gradient refractive index properties and focuses radio waves into a focal point at the edge of the lens, as shown in Figure I.35 a. Within these lenses, the refractive index changes in a radial manner based on the normalized radius r of the lens, as described by the subsequent equation [40-41]:

$$n(r) = \sqrt{2 - r^2} \quad (24)$$

Indeed, the refractive index n varies from $n_{max} = \sqrt{2}$ at the lens's center to $n_{min} = 1$ at the lens's edge. And its total variation is $\Delta n = n_{max} - n_{min} = \sqrt{2} - 1 = 0.414$.

Traditionally, the Luneburg lens has been made using waveguide technology with parallel plates. Between these plates, several multilayer materials with different permittivities are employed; or by modifying the thickness of a parallel-plate guide [41]. Additionnally, the refractive index could also be controlled via introducing small holes through the depth of the substrate existing between the two parallel plates [40]. Therefore, these holes reduce the substrate's effective permittivity by decreasing the amount of dielectric material per unit volume. However, these manufacturing methods are expensive and complicated. Currently, and with the technology advancements, several works are carried out in PCB (Printed Circuit Board) technology (Figure I.35 (b) et (c)) which is economical and seamlessly compatible with electronic circuits.

Etching small, shaped holes on one side of the printed circuit alters the substrate's effective dielectric constant, resulting in a change of the refractive index. The Luneburg lens can operate in either TE10 mode [40] or quasi-TEM mode which maintains a wide bandwidth [41]

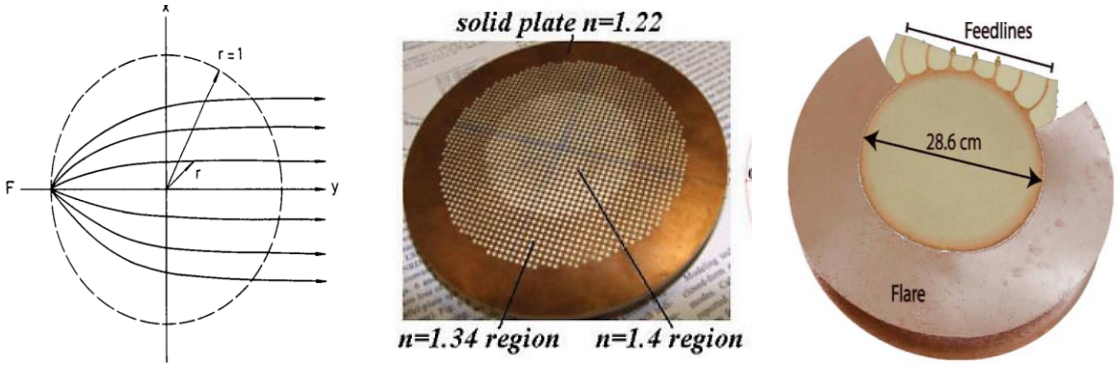

a **b** **c**

Figure I. 35 (a). Propagation in a Lüneburg lens; (b), (c). printed Lüneburg lens [40-41].

6.2.1.2. **Rotman lens**

The Rotman lens stands as one of the most extensively utilized microwave lenses for beamforming applications. It comprises multiples input ports connected by waveguides to a matrix of output ports that excites an antenna array (see Figures I.36-37). In addition, Dummied ports, are incorporated in the Rotman lenses design for sidelobe repression [36]. When power is applied to an input port, it is evenly distributed across all output ports with a phase difference between them. This phase disparity primarily arises from the varying distances traveled between output and input ports, resulting in phase delays. This phase shift imparts flexibility to the array antenna, allowing numerous beams extending in diverse directions.

The design of the Rotman lens should consider the geometrical aspects and the interaction between ports [43]. Indeed, the design of the geometrical optics must be carried out first; followed by adjustments for reducing mutual coupling effects between the input/output ports.

The Rotman lens features seven fundamental design parameters that contribute to its elliptical shape instead of the circular shape. These parameters include the focal angle α, focal ratio $\beta = \frac{F_2}{F_1}$, maximum beam angle ψ, $\gamma = \frac{sin\psi}{sin\alpha}$, the ratio of beam angle ψ to focal angle α, ellipticity of the beam port curve, spacing d of the elements of the array, and focal length f_0 [43].

Figure I.36 shows the flowchart of a trifocal Rotman lens feeding an array of antennas. F_0, F_1 and F_2 are 3 focal points positioned on a curved focal path known as beam contour B. F1 and F2 are symmetrical respecting the focal angle α from origin. Every one of these focal points generates a

phase difference so that the antenna-array orients the radiation diagram in a scan angle direction ψ respecting the Y axis.

$\beta = \frac{F_2}{F_1}$ is called the focal ratio.

T_L represents the Transmission line electrical path length, that can be obtained by fundamental relations introduced by Romane in the reference [44]. For a specific application, the values of α, β, and ψ can be fine-tuned to manage the shapes and overall configuration of the Rotman lens.

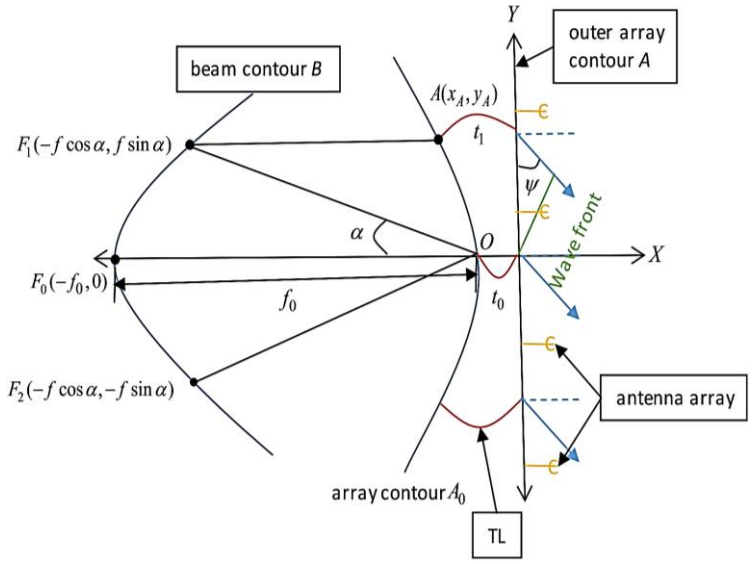

Figure I. 36 Diagram of a trifocal Rotman lens

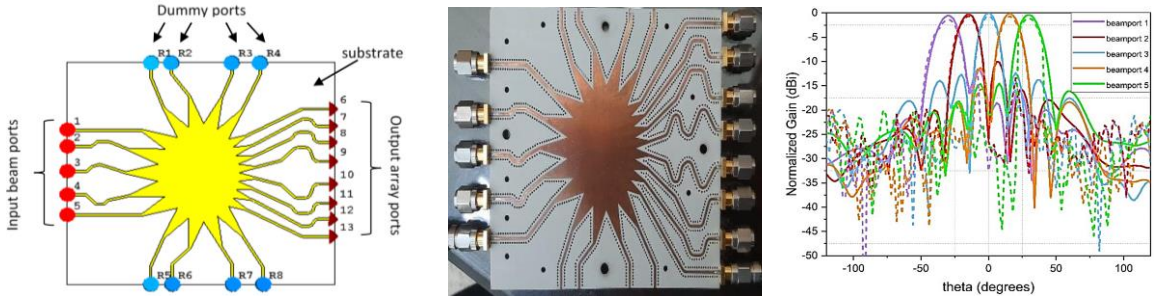

(a) (b) (c)

Figure I. 37 Romane lens having 5 input ports and 8 output ports (a) Design, (b): fabricated prototype in PCB technology; (c). Maximum beam directions corresponding to output ports [44].

6.2.2. Hybrid coupler based beamformer

This beamformer type is based on microwave components such as: couplers, phase shifters and transmission line. A hybrid coupler is a four-ports passive microwave component (see figure I.38) that can be used as a device for splitting or combining power. The most popular ones are the 3dB directional couplers either 90° or180° which providing two output signals with identical amplitudes and a phase difference of 90° or 180° between them..

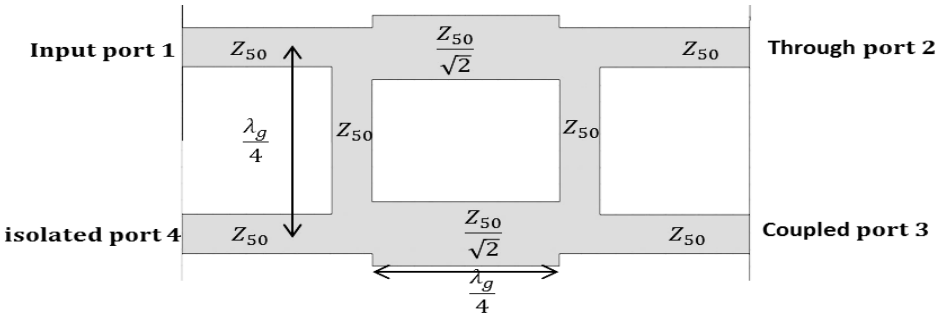

Figure I. 38 Microstrip hybrid directional coupler

Due to the phase shift provided by a hybrid coupler; it can be used to build a beamformer for feeding a phased array antenna.

Actually, three main classifications of Hybrid coupler based beamformer exist, namely the Blass Matrix [45-47], Nolen Matrix [48-50] which provide a serial feeding. In addition to the Butler Matrix [50-54] which provides a parallel feeding.

6.2.2.1. Blass matrix configuration

Blass matrix is a beamformer circuit that was proposed by Judd Blass in 1960 [45] for beam scanning purposes. It consists of transmission lines linked to an antenna-array through additional lines, connected by directional couplers as shown in figure I.39. When a signal is introduced at an input port (beam port), it travels along the feed line, exciting radiating elements at crossover points to generate multiple beams. Although, the Blass matrix enables a phased array antenna to generate arbitrary beams at various directions. It tends to suffer from higher losses because of the presence of numerous termination points [46-47]. The primary limitations of the Blass matrix lie in its complicated design due the huge number of directional couplers used and the interaction between each feed line. Furthermore, its serial feeding mechanism provides unequal distribution of power amplitude among the radiating elements. Consequently, the power could be decreased sequentially from through line into branch line

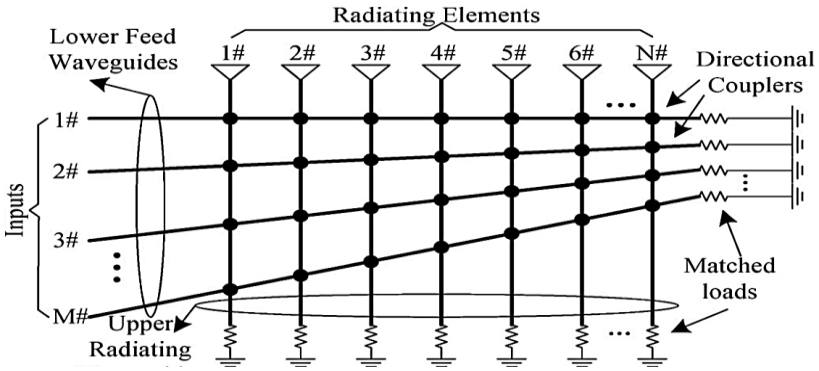

Figure I.39 Blass matrix configuration [47].

6.2.2.2. **Nolen Matrix**

The Nolen matrix was proposed by J.Nolen in 1965 [48] for beamforming applications. It provides a serial feeding approach like the Blass matrix with reduced complexity. Notably, the number of the matched loads and hybrid couplers are reduced (Whole directional couplers beyond the diagonal have been simplified; see figure I.40). Nolen matrix contains N input ports and N output ports linked by the transmit coefficients matrix M as shown in the following equation [49]:

$$\begin{bmatrix} b_1 \\ \vdots \\ b_j \\ \vdots \\ b_N \end{bmatrix}_{\substack{(N,1) \\ 1 \le j \le N}} = [M]_{(N,M)} \cdot \begin{bmatrix} a_1 \\ \vdots \\ a_i \\ \vdots \\ a_M \end{bmatrix}_{\substack{(M,1) \\ 1 \le i \le M}} \quad (23)$$

The typical layout of the Nolen matrix is depicted in figure I.40. In this figure, at each crossover point within the matrix, there is a combination of phase shifters, transmission lines and couplers.

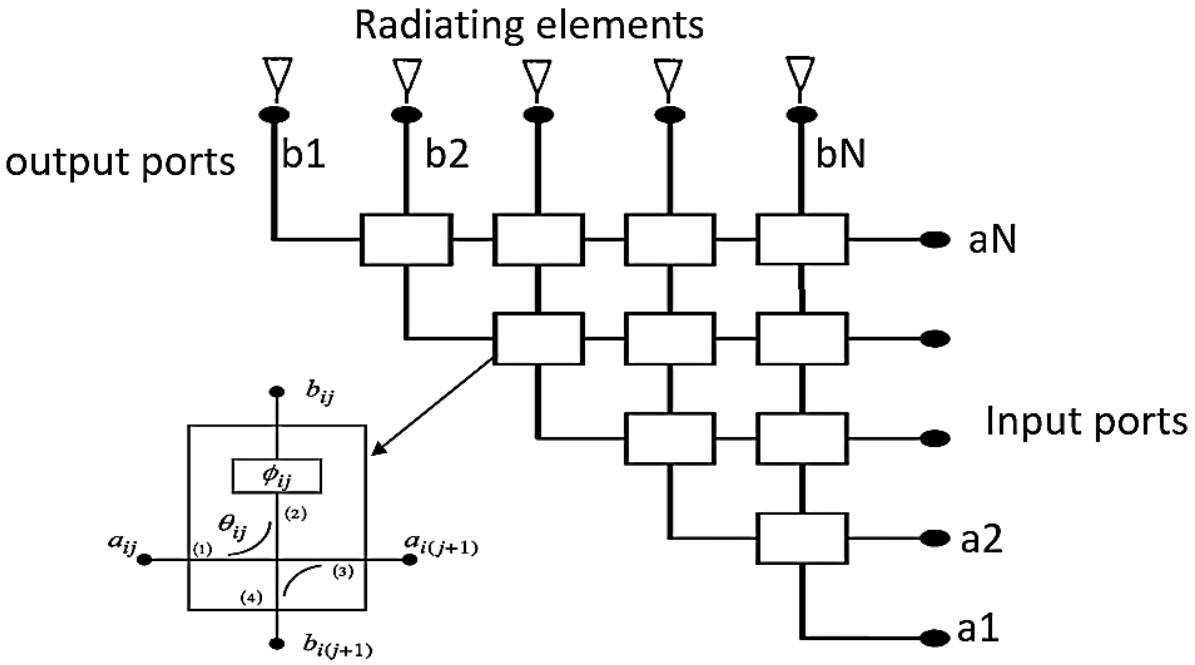

Figure I. 40 Nolen matrix configuration fed a phased array antennas [49].

The Nolen matrix is actually lossy due to the presence of many couplers and transmission lines.

6.2.2.3. **Butler Matrix**

Nolen and Blass matrices are seldom discussed in the literature due to their serial feeding and the huge number of hybrid couplers used.. Consequently, there is limited information available regarding these matrices. Moreover, they still suitable for some narrow band applications.

However, to address these limitations, Butler introduced a new beamformer matrix in 1966 [50] which provides a parallel feeding and wide band applications. This beamformer type is based on microwave components such as: couplers, phase shifters and transmission lines. It has been widely employed to convert the traditional array antenna into a switchable beam system due to its numerous advantages [50-57]:

*A less mismatch loss because of the parallel feeding network of the antenna.

*The input signal is splitted without any loss before reaching the output ports.

*Simplified design due to the symmetry of its topology.

*It allows transforming a classical antenna into a broad-bandwidth, beam-reconfigurable antenna.

Butler matrix is a beamforming circuit utilized for supplying a set of antennas, it consists of N input/output ports driving N antennas generating N orthogonal beams. It contains of crossovers, phase shifters, and couplers whose number augments according to the required number of beams. Typically, the Butler matrix is symmetrical input and output ports. Yet, an asymmetric one is possible [54].

6.2.2.3.1. **2x2 Butler Matrix**

The fundamental Butler matrix is the 2x2 arrangement consisting of a hybrid coupler that feeds two radiating elements or two set of elements. Consequently, switching between the two input ports of the coupler generates two beams in different directions (see figure I.41). This version does not involve crossovers or phase shifters.

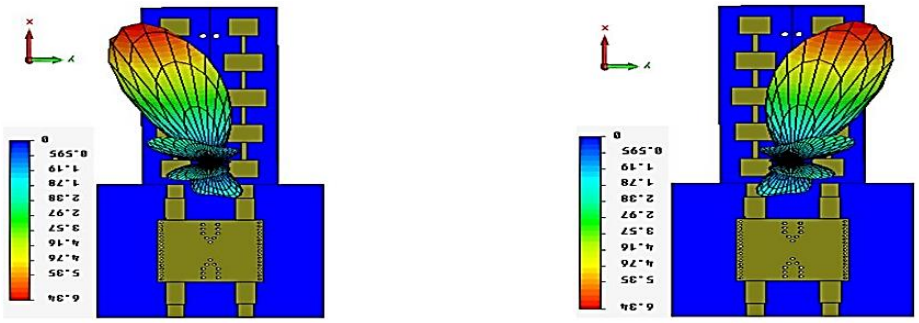

a b

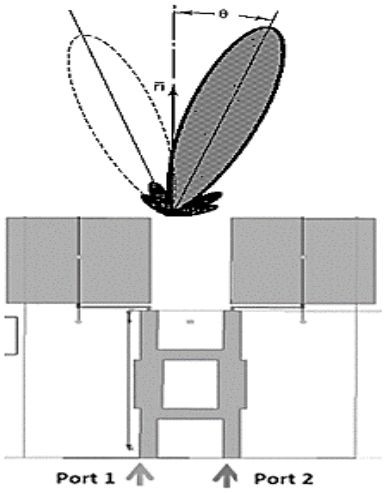

c

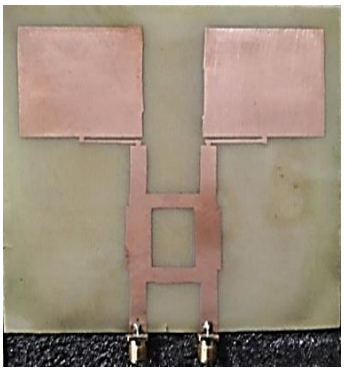

d

Figure I. 391 2x2 Butler matrix configuration feed a phased array antenna: a, b, c designs; d: fabrication in microtip technology [52-53].

The transmit coefficients of the fundamental Butler matrix that contains 3dB coupler of 90° are shown in the following equation [42]:

$$MB_{2x2} = \frac{1}{\sqrt{2}}\begin{bmatrix} e^{j0^\circ} & e^{-j90^\circ} \\ e^{j90^\circ} & e^{j0^\circ} \end{bmatrix} \qquad (24)$$

Therefore, the outputs ports (S_1, S_2) are given by the following equation:

$$\begin{pmatrix} S_1 \\ S_2 \end{pmatrix} = MB_{2x2}.\begin{pmatrix} e_1 \\ e_2 \end{pmatrix} \qquad (25)$$

When the power feed P is at the input port 1 e1, the output ports are given by the following equation:

$$\begin{pmatrix} S_1 \\ S_2 \end{pmatrix} = \frac{1}{\sqrt{2}}\begin{bmatrix} e^{j0^\circ} & e^{-j90^\circ} \\ e^{j90^\circ} & e^{j0^\circ} \end{bmatrix}.\begin{pmatrix} P \\ 0 \end{pmatrix} \qquad (26)$$

$$\begin{pmatrix} S_1 \\ S_2 \end{pmatrix} = \frac{P}{\sqrt{2}}.\begin{pmatrix} e^{j0^\circ} \\ e^{j90^\circ} \end{pmatrix} \qquad (27)$$

When the power feed P is at the input port 2 (e2) the output port are given by as follow:

$$\begin{pmatrix} S_1 \\ S_2 \end{pmatrix} = \frac{1}{\sqrt{2}}\begin{bmatrix} e^{j0^\circ} & e^{-j90^\circ} \\ e^{j90^\circ} & e^{j0^\circ} \end{bmatrix}.\begin{pmatrix} 0 \\ P \end{pmatrix} \qquad (28)$$

$$\begin{pmatrix} S_1 \\ S_2 \end{pmatrix} = \frac{P}{\sqrt{2}}.\begin{pmatrix} e^{-j90^\circ} \\ e^{j0^\circ} \end{pmatrix} \qquad (29)$$

Hence, phase shifts of β = -90° or β = +90° are produced at the output ports of the 2x2 Butler matrix when input port 1 or port 2 is respectively supplied. Thanks to the phase gradient, the beam can be directed into two different directions $\theta = \mp 30^\circ$ (see figure I.42) according to the following equation [53]:

$$\theta = \mathrm{Arcsin}\left(\frac{\lambda.\beta}{2\pi d}\right) \qquad (30)$$

Where:

θ : The angle formed by the maximum beam and the perpendicular axis to the antenna.

d : The spacing among elements.

λ : wave length in free space.

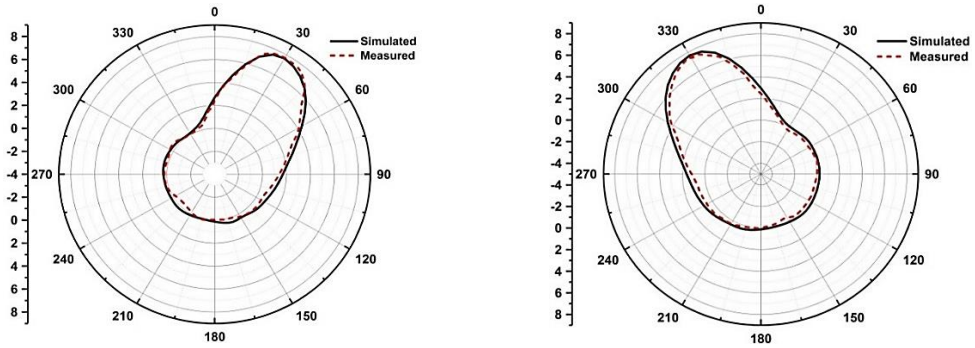

a b

Figure I. 402 two directions provided by 2x2 Butler matrix; a:+30°, b: -30° [53].

6.2.2.3.2. 4x4 Butler Matrix

The Butler matrix with a 4x4 configuration, often regarded as the standard configuration within the Butler matrix family, it comprises 2 crossovers, 2 phase shifters and 4 couplers as illustrated in Figure I.43 [55]. It has 4 symmetric input/output ports, facilitating its use in powering phased array antennas by providing four beams in four distinct direction by swishing between the four input ports [55-57]. Its structure is more complicated than the previous one due to the existence of the crossovers.

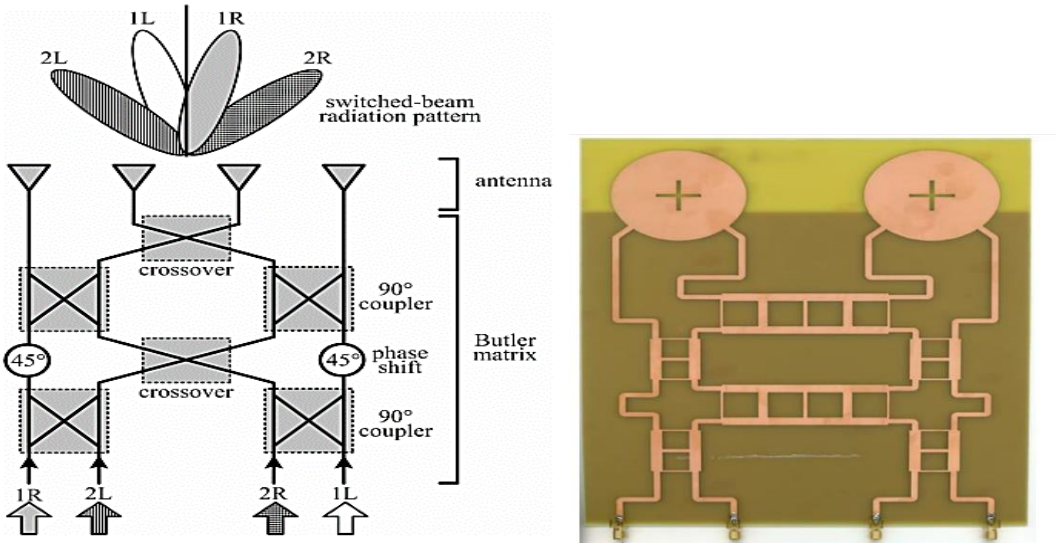

a b

Figure I. 413 4x4 Butler matrix configuration fed a phased array antenna, a: schematic diagram; b fabrication in microtip technology [54-56].

The transmit coefficients of the 4x4 Butler matrix based on 3dB coupler of 90° is as shown in the following equation [42]:

$$MB_{4x4} = \frac{1}{2}\begin{bmatrix} e^{-j45^\circ} & e^{-j135^\circ} & e^{-j90^\circ} & e^{-j180^\circ} \\ e^{-j90^\circ} & e^{j0^\circ} & e^{-j225^\circ} & e^{-j135^\circ} \\ e^{-j135^\circ} & e^{-j225^\circ} & e^{j0^\circ} & e^{-j90^\circ} \\ e^{-j180^\circ} & e^{-j90^\circ} & e^{-j135^\circ} & e^{-j45^\circ} \end{bmatrix} \quad (31)$$

Therefore, the phase gradient β at the four output ports of the 4x4 Butler matrix, corresponding its four input ports 1,2,3 and 4 are +45°, -135°, +135°, -45° respectively. Thanks to the phase gradient, using equation 30, the maximum beam could be oriented into 4 directions: 15°, -45°. +45°, -15° respectively (see figure I.44).

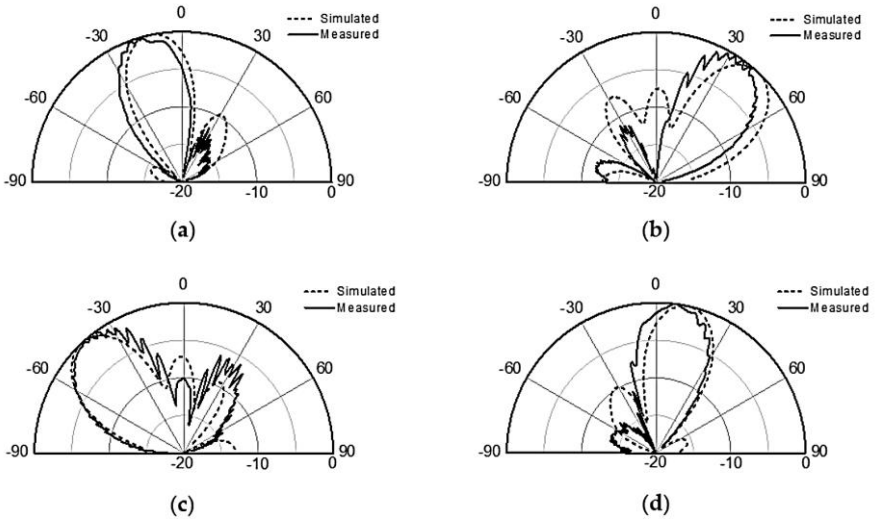

Figure I. 424 four directions of 4x4 Butler matrix; a:-15°,b: 45°, c:-45°, d:15°[57].

6.2.2.3.3. 8x8 Butler Matrix

The 8x8 Butler matrix is a beamformer circuit featuring eight input ports and eight output ports and provides eight beams in eight distinct directions. It is seldom used in the literature due to its huge size and it complicated design. Additionally, its complexity exceeds that of its counterparts due to the larger number of couplers and crossovers. Specifically, it comprises 12 couplers, 16 crossovers, and 8 phase shifters (refer to Figure I.45).

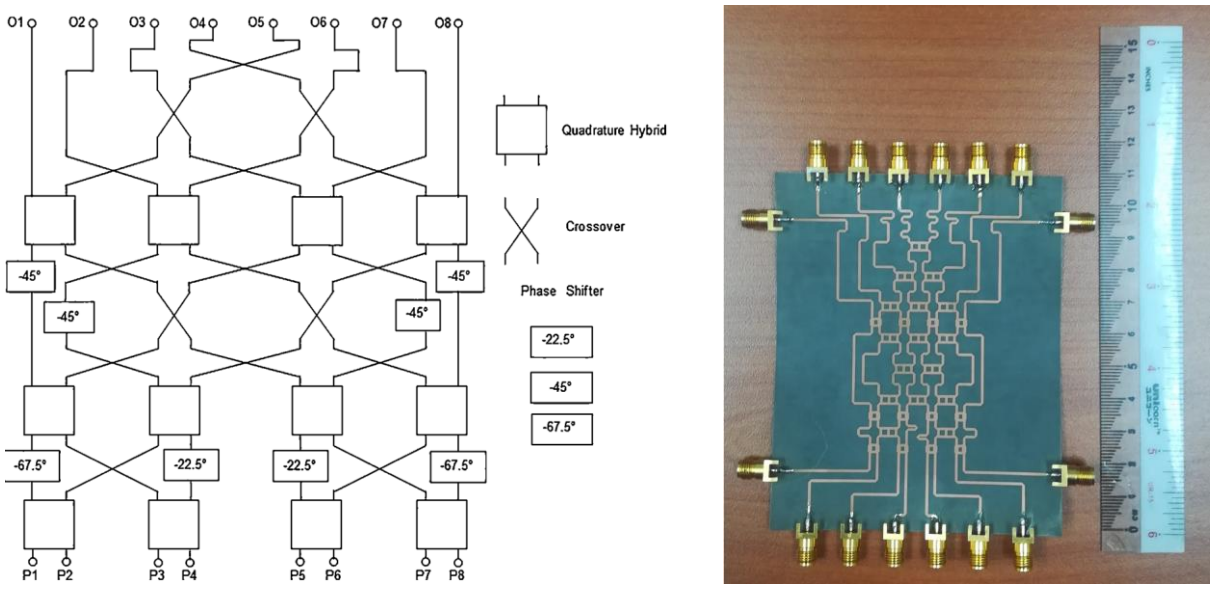

a b

Figure I. 435 8x8 Butler matrix, a: schematic diagram, b: its fabrication in in microtip technology [58].

The transmit coefficients of the 8x8 Butler matrix based on 3dB coupler of 90° is described in the following equation [42]:

$$MB_{8x8} = \frac{1}{2\sqrt{2}} \begin{bmatrix} e^{-j112.5^\circ} & e^{-j202.5^\circ} & e^{-j135^\circ} & e^{-j225^\circ} & e^{-j112.5^\circ} & e^{-j202.5^\circ} & e^{-j1802^\circ} & e^{-j270^\circ} \\ e^{-j135^\circ} & e^{-j45^\circ} & e^{-j247.5^\circ} & e^{-j157.5^\circ} & e^{-j180^\circ} & e^{-j90^\circ} & e^{-j337.5^\circ} & e^{-j247.5^\circ} \\ e^{-j157.5^\circ} & e^{-j247.5^\circ} & e^{-j0^\circ} & e^{-j90^\circ} & e^{-j247.5^\circ} & e^{-j337.5^\circ} & e^{-j135^\circ} & e^{-j225^\circ} \\ e^{-j180^\circ} & e^{-j90^\circ} & e^{-j112.5^\circ} & e^{-j22.5^\circ} & e^{-j315^\circ} & e^{-j225^\circ} & e^{-j292.5^\circ} & e^{-j202.5^\circ} \\ e^{-j202.5^\circ} & e^{-j292.5^\circ} & e^{-j225^\circ} & e^{-j315^\circ} & e^{-j22.5^\circ} & e^{-j112.5^\circ} & e^{-j90^\circ} & e^{-j180^\circ} \\ e^{-j225^\circ} & e^{-j135^\circ} & e^{-j337.5^\circ} & e^{-j247.5^\circ} & e^{-j90^\circ} & e^{-j0^\circ} & e^{-j247.5^\circ} & e^{-j157.5^\circ} \\ e^{-j247.5^\circ} & e^{-j337.5^\circ} & e^{-j90^\circ} & e^{-j180^\circ} & e^{-j157.5^\circ} & e^{-j247.5^\circ} & e^{-j45^\circ} & e^{-j135^\circ} \\ e^{-j270^\circ} & e^{-j180^\circ} & e^{-j202.5^\circ} & e^{-j112.5^\circ} & e^{-j225^\circ} & e^{-j135^\circ} & e^{-j202.5^\circ} & e^{-j112.5^\circ} \end{bmatrix}$$

In this case, the phase gradient β at the eight output ports of the 8x8 Butler matrix corresponding to its eight input ports 1,2,3,4,5,6,7 and 8 resulting in angles of +22.5°, -157.5°, +112.5°, -67.5°, +67.5°, -112.5°, +157.5°, -22.5° respectively. Thanks to the phase gradient, using equation 30, the maximum beam can be oriented into eight distinct directions: 7.5°, -52.5°. -37.5°, -22.5°, +22.5°, -+37.5°. +52.5°, -7.5° respectively (see figure I.46).

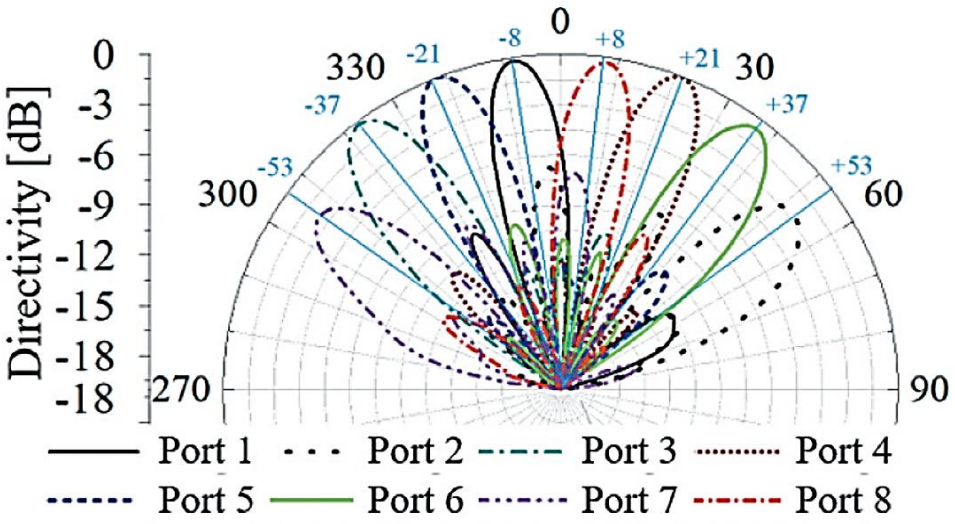

Figure I. 446 eight directions provided by 8x8 Butler matrix[59].

Deduction: Based on the characteristics provided by the different Butler matrix configurations presented earlier, we can deduce the most appropriate choice. The 2x2 Butler matrix offers simplicity but limited coverage from -30° to 30°. On the other hand, the 8x8 matrix, while comprehensive, is overly complex and covers a wider range from -52° to 52°. Positioned between these extremes, the 4x4 Butler matrix strikes a balance, offering moderate complexity and sufficient coverage from -45° to 45°. Therefore, considering these factors, the 4x4 Butler matrix emerges as the most suitable option for our application.

7. Conclusion

In summary, this chapter has covered important concepts related to antennas, planar antennas, and beamforming techniques. We discussed various aspects such as polarization, radiation parameters, feeding methods, and circular polarization specific to planar antennas. Additionally, we explored different types of beamformer circuits, including digital and switched beamformers, and discussed their categories like lens-based and hybrid coupler-based beamformers. Moreover, we compared different Butler matrices based on their complexity and coverage angles. After careful analysis, we found that the 4x4 Butler matrix is the optimal beamformer circuit because of its moderate complexity and appropriate coverage angle range from -45° to 45°. This conclusion was drawn after considering the practical aspects and capabilities of each Butler matrix configuration.

8. Specification Sheet

After this antenna overview chapter, we have realized that the most requested antennas are directional, wideband multi-beam antennas and circular polarization planar antennas primarily for applications such as base stations, radars, and satellites.

***Directional antenna:** Directional antennas are essential for applications requiring focused transmission or reception. These antennas are typically realized through massive antenna arrays, which will be elaborated upon in the upcoming second chapter.

***Wideband multi-beam antenna:** Wideband multi-beam antennas are crucial for achieving broad coverage and high data rates. They are realized by feeding an antenna array through a beamformer circuit. In this study, the Butler matrix has been selected as the beamformer circuit, and its detailed exploration will be presented in Chapters 3 and 4

***Circular polarization antenna:** Circularly polarized antennas offer advantages in terms of signal robustness and interference mitigation. They can be achieved by exciting two resonance modes through dual or single feeding methods or by altering the antenna's geometry. Detailed discussion on circular polarization planar antennas will be provided in the final chapter.

So, as a requirement for this thesis is: the study, design and realization of directional, wideband, multibeam and circular polarization planar antennas in the ISM band and the Terahertz band.

References

1. PÉREZ, José-Philippe, CARLES, Robert, et FLECKINGER, Robert. Electromagnétisme fondements et applications avec 300 exercices et problèmes résolus. Masson, 1996.
2. NACHOUANE, Hamza. Contribution à la conception et à la réalisation d'antennes reconfigurables large bande à diversité pour les systèmes de communication radio cognitive de la quatrième génération. 2017. Thèse de doctorat. Institut National des Postes et Télécommunications.
3. TABAKH, Ikram. Conception et réalisation d'une antenne patch pour la technologie RFID. 2019. Thèse de doctorat. Faculté des Sciences et Techniques de Fès.
4. BENDALI Abdelhak. Conception de circuits micro-ondes en vue de la réalisation d'une chaîne de transmission RFID dans la bande 2.45 GHz. 2019. Thèse de doctorat. Université Ibn Tofail Faculté des Sciences Kénitra.
5. Ansari, A. E., Das, S., Islam, T., Asha, S., El Idrissi, N. E. A., & Madhav, B. T. P. (2024). A High-Gain Directional 1x8 Planar Antenna Array for 2.4 GHz RFID Reader Applications. Journal of Circuits, Systems and Computers.
6. ALMORABETI, Soumaya, RIFI, Mounir, TERCHOUNE, Hanae, et al. 2X2 Circular Polarized Antenna Array for RF Energy Harvesting System to a UAV. International Journal of Microwave & Optical Technology, 2018, vol. 13, no 6.
7. LAKRIT, Soufian, AMMOR, Hassan, MATAH, Soufiane, et al. Study and design of single and double layer square patch antennas for UWB applications. Journal of Circuits, Systems and Computers, 2019, vol. 28, no 14, p. 1950233.
8. BOUSTANI, Btissam, BAGHDAD, Abdennaceur, SAHEL, Aicha, et al. Performance analysis of direction of arrival algorithms for smart antenna. International Journal of Electrical and Computer Engineering, 2019, vol. 9, no 6, p. 4873.
9. S. KEPCHABE and E. TONYE, "Optimisation des performances des antennes intelligentes par synthèse au moyen de réseaux de neurones," Researchgate.Net, no. November, 2015, [Online]. Available: https://www.researchgate.net/profile/Emmanuel_Tonye/publication/285235999
10. OJAROUDI PARCHIN, Naser, JAHANBAKHSH BASHERLOU, Haleh, AL-YASIR, Yasir IA, et al. Reconfigurable antennas: Switching techniques—A survey. Electronics, 2020, vol. 9, no 2, p. 336.
11. ITOH, Kenji, SAKAI, Naoki, et NOGUCHI, Keisuke. Highly efficient high-power rectenna with the diode on antenna (DoA) topology. IEICE Transactions on Electronics, 2022, vol. 105, no 10, p. 483-491.
12. Li, W. R., Chu, C. Y., Lin, K. H., & Chang, S. F. (2004). Switched-beam antenna based on modified Butler matrix with low sidelobe level. Electronics Letters, 40(5), 1.
13. MA, Wenyan, ZHU, Lipeng, et ZHANG, Rui. Multi-beam forming with movable-antenna array. IEEE Communications Letters, 2024.
14. Lakrit, S., Das, S., El Alami, A., Barad, D., & Mohapatra, S. (2019). A compact UWB monopole patch antenna with reconfigurable Band-notched characteristics for Wi-MAX and WLAN applications. AEU-International Journal of Electronics and Communications, 105, 106-115.
15. Combes, Paul F. "Micro-ondes." 1st, Lignes, Guides et cavités. 1997. 71-79.
16. El Alami, A., Ghazaoui, Y., Das, S., Bennani, S. D., & El Ghzaoui, M. (2019). Design and simulation of RFID array antenna 2x1 for detection system of objects or living things in motion. Procedia Computer Science, 151, 1010-1015.

17. BALANIS, Constantine A. Antenna theory: analysis and design. John wiley & sons, 2016.
18. Bhaskar, S., & Singh, A. K. (2019). Meandered cross-shaped slot circularly polarised antenna for handheld UHF RFID reader. AEU-International Journal of Electronics and Communications, 100, 106-113.
19. EL ANSARI, Abdelaaziz, DAS, Sudipta, EL-ARROUCH, Tarik, et al. A Hybrid Coupler Integrated 1× 4 Printed Array Antenna with Broadband and High Performance For Beamforming RFID Reader. In : 2022 9th International Conference on Wireless Networks and Mobile Communications (WINCOM). IEEE, 2022. p. 1-6.
20. Huang, Yi, and Kevin Boyle. Antennas: from theory to practice. UK: John Wiley & Sons, 2008.
21. Ansari, A. E., Jayaprakasan, V., Duraisamy, K., Das, S., El-Arrouch, T., & Idrissi, N. E. A. E. (2023). A Wideband Microstrip 1 x 2 Array Antenna Fed by Coupler for Beam Steering Terahertz (THz) Band Applications.
22. El Hammoumi, M., El Idrissi, N. E. A., Raad, R., Theoharis, P. I., Tubbal, F., & Abulgasem, S. (2022, October). Ultra Wideband dual circularly polarized patch antenna for 5G and CubeSat applications. In 2022 9th International Conference on Wireless Networks and Mobile Communications (WINCOM) (pp. 1-6). IEEE.
23. Shamim, S. M., Uddin, M. S., Hasan, M. R., & Samad, M. (2021). Design and implementation of miniaturized wideband microstrip patch antenna for high-speed terahertz applications. Journal of Computational Electronics, 20, 604-610.
24. ALSAGER, Ahmed Fatthi. Design and analysis of microstrip patch antenna arrays. Unpublished Masters Thesis, University College of Boras, Sweden, 2011, vol. 1, p. 1-80.
25. LI, K., CHENG, Chong Hu, MATSUI, T., et al. Study on coplanar fed cpw patch antennas. In : PROCEEDINGS OF THE INTERNATIONAL SYMPOSIUM ON ANTENNAS AND PROPAGATION JAPAN. 2000. p. 1111-1114.
26. B. Belentepe, "Modeling and design of electromagnetically coupled microstrip patch antennas and antenna arrays", IEEE Antennas and Propagation Magazine, vol. 37, no. 1, 31–39, 1995.
27. Jordão, M., Pires, D., Belo, D., Pinho, P., & Carvalho, N. B. (2021). 3D Antenna Characterization for WPT Applications. Sensors, 21(13), 4461.
28. A. Slimani, S. D. Bennani and A. Alami, E®ect of inter-elements distance and phase shift excitation on radiation performance of linear, planar and circular arrays antennas, 2017 Int. Conf. Wireless Technologies, Embedded and Intelligent Systems (WITS), Fez, Morocco, 19–20 April 2017, pp. 1–7
29. Saha R, Maity S, Bhunia CT. Design and characterization of a tunable patch antenna loaded with capacitive MEMS switch using CSRRs structure on the patch. Alexandria Eng J. 2016;55(3):2621-2630. doi: 10.1016/j.aej.2016.05.002
30. Clemente, A.; Dussopt, L.; Sauleau, R.; Potier, P.; Pouliguen, P. 1-bit reconfigurable unit cell based on PIN diodes for transmit-array applications in x-band. IEEE Trans. Antennas Propag. 2012, 60, 2260–2269
31. J. Dong and A. I. Zaghloul, “Extremely high-frequency beam steerable lens-fed antenna for vehicular sensor applications,” IET Microwaves, Antennas Propag., vol. 4, no. 10, pp. 1549–1558, 2010, doi: 10.1049/iet-map.2009.0271.
32. Cheng, Y. J., Hong, W., & Wu, K. (2010). Design of a substrate integrated waveguide modified R-KR lens for millimetre-wave application. IET microwaves, antennas & propagation, 4(4), 484-491.
33. CHENG, Yu Jian, HONG, Wei, et WU, Ke. Millimeter-wave substrate integrated waveguide multibeam antenna based on the modified R-KR lens. In : 2008 IEEE MTT-S International Microwave Symposium Digest. IEEE, 2008. p. 703-706.

34. Hall, P. S., & Vetterlein, S. J. (1990, October). Review of radio frequency beamforming techniques for scanned and multiple beam antennas. In IEE Proceedings H (Microwaves, Antennas and Propagation) (Vol. 137, No. 5, pp. 293-303). IET Digital Library.
35. SMITH, M. S. et FONG, A. K. S. Amplitude performance of Ruze and Rotman lenses. Radio and Electronic Engineer, 1983, vol. 53, no 9, p. 329-336.
36. A. Eid, J. G. D. Hester, and M. M. Tentzeris, "Rotman Lens-Based Wide Angular Coverage and High-Gain Semipassive Architecture for Ultralong Range mm-Wave RFIDs," IEEE Antennas Wirel. Propag. Lett., vol. 19, no. 11, pp. 1943–1947, 2020, doi: 10.1109/LAWP.2020.3002924.
37. SINGHAL, P. K., KUSHWAH, Ravi Pratap Singh, et SHARMA, P. C. Design of Rotman type bootlace lens for wide area scanning. In : 2009 6th International Conference on Electrical Engineering/Electronics, Computer, Telecommunications and Information Technology. IEEE, 2009. p. 762-765.
38. KUSHWAH, Ravi Pratap Singh, SINGHAL, Pramod Kumar, et SHARMA, P. C. Design of symmetric bootlace lens with gain analysis at UHF band. Progress In Electromagnetics Research Letters, 2009, vol. 6, p. 83-89.
39. RAPPAPORT, Carey M. et ZAGHLOUL, Amir I. Multifocal bootlace lens design concepts: a review. In : 2005 IEEE Antennas and Propagation Society International Symposium. IEEE, 2005. p. 39-42.
40. XUE, L. et FUSCO, V. F. Printed holey plate Luneburg lens. Microwave and Optical Technology Letters, 2008, vol. 50, no 2, p. 378-380.
41. Pfeiffer, C., & Grbic, A. (2010). A printed, broadband Luneburg lens antenna. IEEE Transactions on Antennas and Propagation, 58(9), 3055-3059.
42. Dall'omo, C. (2003). Contribution à l'étude d'antennes à pointage électronique en millimétrique: Conception et réalisation de différentes topologies de Matrices de Butler (Doctoral dissertation, Limoges).
43. R. C. Hansen, "Design Trades for Rotman Lenses," IEEE Trans. Antennas Propag., vol. 39, no. 4, pp. 464–472, 1991, doi: 10.1109/8.81458.
44. M. S. Ali, H. Naveed, M. A. Babar Abbasi, N. Shoaib, and V. F. Fusco, "Substrate-Integrated Coaxial Line (SICL) Rotman Lens Beamformer for 5G/B5G Applications," Electron., vol. 12, no. 1, pp. 0–13, 2023, doi: 10.3390/electronics12010069.
45. J. Blass, "The multidirectional antenna: A new approach to stacked beams," IRE National Convention Rec., New York, NY, pp. 48–50, Mar. 1960.
46. HALL, P. S. et VETTERLEIN, S. J. Review of radio frequency beamforming techniques for scanned and multiple beam antennas. In: IEE Proceedings H (Microwaves, Antennas and Propagation). IET Digital Library, 1990. p. 293-303.
47. CHEN, Peng, HONG, Wei, KUAI, Zhenqi, et al. A double layer substrate integrated waveguide Blass matrix for beamforming applications. IEEE Microwave and Wireless Components Letters, 2009, vol. 19, no 6, p. 374-376.
48. J. Nolen, "Synthesis of multiple beam networks for arbitrary illuminations," PhD Thesis, Bendix Corporation, Radio Division, Baltimore, Apr. 1965
49. FONSECA, Nelson JG. Printed S-Band 4$\times $4 Nolen Matrix for Multiple Beam Antenna Applications. IEEE transactions on antennas and propagation, 2009, vol. 57, no 6, p. 1673-1678.
50. HANSEN, Robert C. Phased array antennas. John Wiley & Sons, 2009.
51. J. Butler and R. Lowe, "Beam-forming matrix simplifies design of electronically scanned antennas," Electronic Design, vol. 9, pp. 170–173, Apr. 1961.

52. Jizat, NoorlindawatyMd, et al. "5G beam-steering 2×2 butler matrix with slotted waveguide antenna array." Telkomnika 17.4 (2019): 1656-1662.
53. Ansari, A. E., Das, S., Tabakh, I., Madhav, B. T. P., Bendali, A., & Idrissi, N. E. A. E. (2022). Design and Realization of a broadband multi-beam 1× 2 array antenna based on 2× 2 Butler Matrix for 2.45 GHz RFID Reader Applications. Journal of Circuits, Systems and Computers, 31(17), 2250305.
54. H. Nachouane, A. Najid, A. Tribak, F. Riouch, "Wideband 3×4 Butler matrix using Wilkinson divider for MIMO applications," Fifth International Conference on Next Generation Networks and Services (NGNS), 28–30 May 2014, Casablanca, Morocco
55. Nachouane, H., Najid, A., Tribak, A., &Riouch, F. (2016). Beamforming Antenna Array Combining Pattern and Polarization Diversity for Cognitive Radio Applications. Wireless Personal Communications, 91(2), 957-973.
56. Tseng, C. H., Chen, C. J., & Chu, T. H. (2008). A low-cost 60-GHz switched-beam patch antenna array with Butler matrix network. IEEE Antennas and Wireless Propagation Letters, 7, 432-435.
57. KIM, Soyeon, YOON, Seongjo, LEE, Yongho, et al. A miniaturized Butler matrix based switched beamforming antenna system in a two-layer hybrid stackup substrate for 5G applications. Electronics, 2019, vol. 8, no 11, p. 1232.
58. IDRUS, Intan Izafina, ABDUL LATEF, Tarik, ARIDAS, Narendra Kumar, et al. A low-loss and compact single-layer butler matrix for a 5G base station antenna. Plos one, 2019, vol. 14, no 12, p. e0226499.
59. DUYEN, Bui Thi, PHUONG THAO, Hoang Thi, MINH THUY, Le, et al. Design of a beam steering antenna array using 8x8 butter matrix for indoor positioning system. Electromagnetics, 2020, vol. 40, no 7, p. 500-514.

Chapter II: A High-Gain Directional 1×8 Planar Array antenna for 2.4 GHz RFID Reader Applications

1. Introduction

During the last decades, wireless technology has created a crucial development, playing a pivotal role in the evolution of industries and communication systems. An antenna stands out as an indispensable component in the transmission and reception chain [1]. Due to the giant growth of wireless systems, the design of an advanced antennas with a high radiation characteristic is essential. During the last decades, wireless technology has created a crucial development, playing a pivotal role in the evolution of industries and communication systems. An antenna stands out as an indispensable component in the transmission and reception chain [1] . Nevertheless, this antenna type has a few drawbacks like low gain, low directivity and low efficiency [7-11]. Several scientists and researchers on global scale have sought to overcome these drawbacks. A method employed to address the issues of low directivity and gain involves feeding a set of antennas together (antenna array). 12-16]. Wireless communication has proven to be the most popular solution for identification of things, like cars, books and person. The oldest identification technology used to identify objects is bar-code technology. However, the remote identification has changed with the introduction of a new contactless identification technology called RFID (Radio Frequency Identification) [17].

The RFID employs radio waves for data swapping between tag and RIFD reader without the need of physical contact. In an RFID reader, the antenna, due to its low gain, has been a significant problem for long-range thing identification [17-18]. To enhance the performance of antennas in terms of gain and directivity, numerous configurations of microstrip array antennas have been proposed by researchers for RFID applications. The configuration of 1×2-array antenna with maximum gain of 4.73 dB is reported in [19], and 6.6 dB is achieved in [20], then 9.36 dB is reported by the researchers in [21]. Various array antenna structures with a 1×4 configuration for RFID applications have been proposed to enhance gain: The peak gain equals to 7.75dB was reached in reference [22], the maximum gain of about 9.22dB is reported in [23], finally, a maximum gain of about 12.6 dB is reported by the authors in reference [24].

The design of an efficient antenna array requires a high precision when designing the power divider, to correctly distribute power to the radiating elements of the array. The T power dividers [25] and Wilkinson power dividers [26-27] are the most commonly used in array

antenna design. However, the Wilkinson power dividers exhibit Some limitations, including narrow bandwidth and large physical dimensions attributed to the employment of quarter-wave length branch lines [28-29]. Hence, the T power dividers are mostly preferred due to their simple configuration. In this chapter, we have designed an advanced T power divider with wideband characteristics to divide the power between the radiating elements of the prescribed 1×8 Antenna array.

This essential requirement of high gain antenna for long distance communication motivates us to propose a higher gain antenna array with high radiation efficiency and directional radiation patterns. Hence, the aim of this chapter is to suggest a new configuration of eight element array antenna in 1×8 aiming to achieve optimal efficiency and maximum gain. The proposed directional high gain antenna is dedicated to RFID readers that operates at 2.4 GHz with impedance bandwidth of 39 MHz (from 2.4225 to 2.4615 GHz) to identify things in motion existing at a great distance.

Following this introduction section, the chapter will be organized into five additional key sections as outlined below: Part II: Analysis of the Proposed Advanced 1×8 Power Splitter. Part III: Design of the Basic Antenna Element. Part IV: Structure of the Proposed Directional 1×8 Antenna Array. Part V: Comparison of Results with Other Published Research. Conclusion: The concluding part of this chapter.

2. The Suggested Advanced 1×8 Power Divider

A power divider is a linear and passive electronic component that obeys the Ohm's law. It can be used for power division or power combination as shown in Figure II.1. Generally, this component provides in-phase output signals with an equal power division ratio (3 dB, 6dB or 9dB…). However, an unequal power division ratio is possible as well. This component is an inevitable element for designing an array antenna.

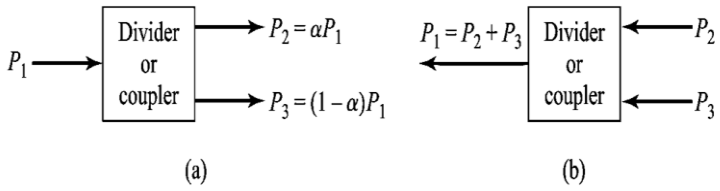

Figure II. 1 (a) Power divider. (b) Powers combiner [29]

The design methodology of the proposed advanced 1×8 T power divider (TPD) includes three stages of structural evolution as shown in Figure II.2. The design has been started with the execution 1×2 TPD. Then, two identical 1×2 T power dividers are used to design a 1×4 TPD. Finally, two identical 1×4 TPD geometries are implemented for designing the proposed advanced 1×8 T power divider (TPD).

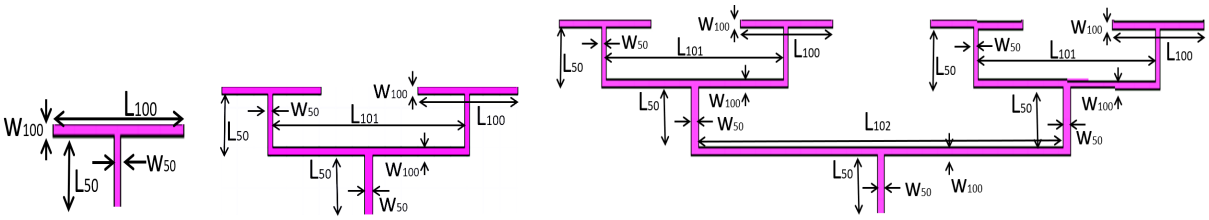

Figure II. 2 Design steps of the proposed advanced TPD. (a): 1×2 TPD, (b): 1×4 TPD, (c): 1×8 TPD.

2.1 Analysis and Design Methodology

2.1.1. Study and Design of the Basic 1×2 Power Divider (3 dB):

The most popular power splitter is the 1×2 configured T power splitter. It is made of three T-shaped waveguide lines (see figure II.3).

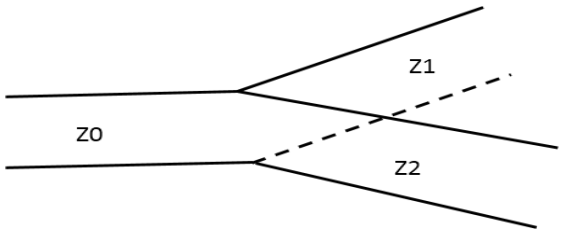

Figure II. 3 Port layout of 1×.2 T power splitter.

For a lossless T-junction, the impedances Z0, Z1, and Z2 must satisfy the following equation [29]:

$$\frac{1}{Z_0} = \frac{1}{Z_1} + \frac{1}{Z_2} \qquad (1)$$

Generally, the scattering matrix [S] of a 1×2 power divider consists of 9 independent parameters as demonstrated in equation below:

$$[S] = \begin{bmatrix} S_{11} & S_{12} & S_{13} \\ S_{21} & S_{22} & S_{23} \\ S_{31} & S_{32} & S_{33} \end{bmatrix} \quad (2)$$

A power divider that does not contain any anisotropic materials is reciprocal. Therefore, its [S] matrix becomes symmetric ($S_{ij} = S_{ji}$) as follow:

$$[S] = \begin{bmatrix} S_{11} & S_{12} & S_{13} \\ S_{12} & S_{22} & S_{23} \\ S_{13} & S_{23} & S_{33} \end{bmatrix} \quad (3)$$

If this structure is lossless with Matched ports $(S_{11} = S_{22} = S_{33} = 0)$ the [S] matrix becomes as follows:

$$[S] = \begin{bmatrix} 0 & S_{12} & S_{13} \\ S_{12} & 0 & S_{23} \\ S_{13} & S_{23} & 0 \end{bmatrix} \quad (4)$$

Unfortunately, a completely lossless structure may not be achievable, but it is acceptable when S_{11}, S_{22}, S_{33} are less than -10dB, the structure is considered as a low-loss structure.

In microstrip technology, the design of a power divider should take into account equations (5) and (6) as outlined in references [29-30]. These equations allow to switch between the characteristic impedance and the width of each branch line.

The most widely used feed line in microstrip technology is the one whose characteristic impedance is equals to 50Ω. Equation (5) can be used to calculate the characteristic impedance of Z_{50} knowing its width W_{50}:

$$Z_{50} = \frac{120\pi}{\sqrt{\varepsilon_r}\left(\frac{W_{50}}{h}+1.393+0.0667\ln\left(\frac{W_{50}}{h}+1.44\right)\right)} =< \frac{126}{\sqrt{\varepsilon_r}} \qquad (5)$$

$$\text{with} \qquad W_{50} > h$$

Conversely, equation (6) can be used to calculate the width W_{50} knowing the impedance Z_{50} [29][30]:

$$\frac{W_{50}}{h} = \frac{2}{\pi}\left[B - 1 - \ln(2B-1) + \frac{\varepsilon_{r-1}}{2\varepsilon_r}\left(\ln(B-1) + 0.39 - \frac{0.61}{\varepsilon_r}\right)\right] \qquad (6)$$

With: $B = \frac{377\pi}{2Z_{50}\sqrt{\varepsilon_r}}$, $\frac{W_{50}}{h} > 2$, h: the thickness of the substrate, and ε_r its relative permittivity. Z_{50}, W_{50} represent impedance and width, respectively, when the line has a characteristic impedance of 50 Ω.

The design of the proposed basic 1×2 T power divider (TPD) is shown in Figure II.4.

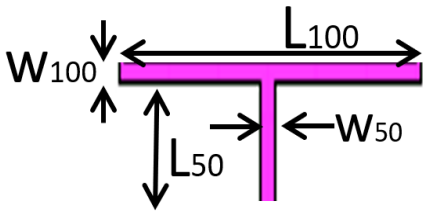

Figure II. 4 Design of the proposed 1×2 TPD.

The calculation of the different parameters of this structure were carried out by using the following approach:

i) Knowing that the input impedance $Z_0 = Z_{50} = 50\Omega$, we found out the output impedances $Z_1 = Z_{100} = 100\ \Omega$ using equation (1),

ii) Equation (6) is used to calculate the width W_{50} and W_{100} of each branch line from their impedances Z_{50} and Z_1 (= Z_2) respectively.

iii) The length of the impedance line 100 Ω is initially chosen $L_{100} \leq \frac{\lambda}{2}$.

iv) A parametric study on lengths L_{50} and L_{100} was performed to obtain a low loss structure (S_{11} lower −10dB) capable of dividing the power feed into two equal parts (S_{12} = S_{13} = -3dB) in phase.

The final optimal dimensions obtained of this structure are: $W_{100} = 2.78mm$, $W_f = 4.48mm$, $L_{100} = 60.7mm$ and $L_{50} = 15mm$.

The simulation results obtained by HFSS, in terms of reflection coefficient S_{11} and transmission coefficients S_{12} and S_{13} are shown in Figure II.5. In Figure II.5. (a) the modules of the parameters S_{11}, S_{12} and S_{13} in dB are represented versus frequency. It can be noted that the bandwidth is wide, approximately 1.4 GHz (ranging from 1.3 to 2.7 GHz). At the operating frequency of 2.4 GHz, S_{11} is -11 dB (indicating a low-loss structure as it is <-10dB), while S_{12} is -3.27 dB and S_{13} is -3.26 dB, closely approaching the ideal value of -3dB. Consequently, the input power was effectively divided into two parts, both with equal magnitudes.

Figure II.5. (b) shows the phases of S_{12} and S_{13} versus frequency. It can be seen that their phases are respectively equals to −175.86° and −174.88°, resulting in a phase shift between them of 0.98°, indicating that the two signals are in phase.

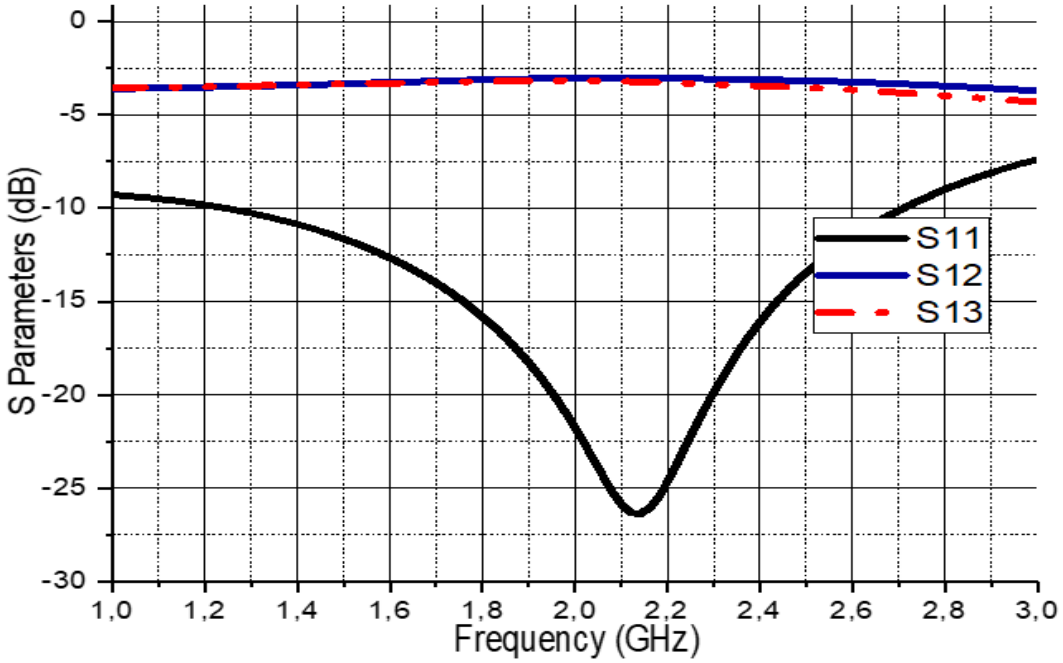

(a)

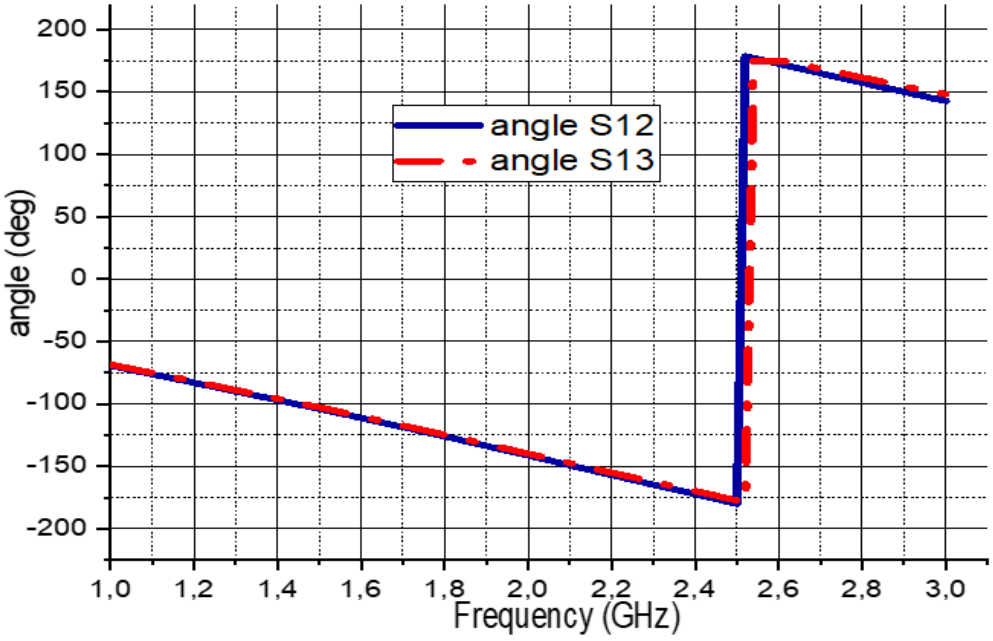

(b)

Figure II. 5 S11, S12 and S13 (dB) vs. frequency, (b): phases of S12 and S13 vs. frequency of the proposed 1×2 TPD

2.1.2. Study and Design of a 1×4 T Power Divider (6 dB):

The proposed 1×4 divider is a T junction having one input port and 4 output ports. It divides the input power into 4 equal quantities (6dB) in phase. This type of divider will be able to feed an array antenna of 4 elements.

For a reciprocal, lossless, symmetric, and isotropic T-junction in a 1×4 configuration, the S matrix is expressed

by the following equation:

$$[S] = \begin{bmatrix} 0 & S_{12} & S_{13} & S_{14} & S_{15} \\ S_{12} & 0 & S_{13} & S_{24} & S_{25} \\ S_{13} & S_{32} & 0 & S_{34} & S_{35} \\ S_{14} & S_{42} & S_{43} & 0 & S_{45} \\ S_{15} & S_{52} & S_{53} & S_{54} & 0 \end{bmatrix} \quad (7)$$

Based on the 1×2 TPD proposed in the previous paragraph, the design process has been extended to T 1×4 power divider as shown in Figure II.6. It has one input port and four output ports and consists of two identical 1×2 TPD which feeds another 1×2 TPD.

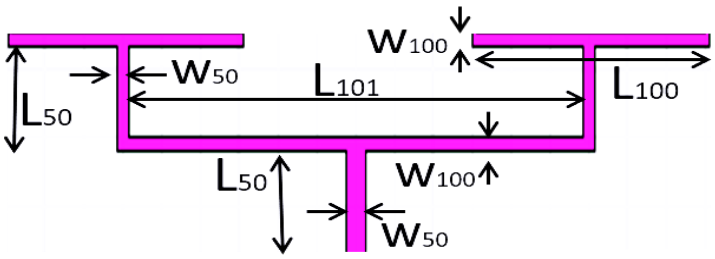

Figure II. 6 Structure of the proposed 1×4 TPD.

The parameters of this optimized structure are given as follows: $W_{100} = 2.78mm$, $W_{50} = 4.48mm$, $L_{100} = 60.7mm$, $L_{50} = 15mm$, $L_{101} = 123mm$.

The simulation results of this structure in terms of S parameters are shown in Figure II.7. Figure II.7/ (a) represents modules of the parameters S_{11}, S_{12}, S_{13}, S_{14} and S_{15} in dB versus frequency. It can be noted that the structure exhibits a wide bandwidth of 900 MHz (ranging from 1.75 to 2.65 GHz), demonstrating very low loss at the operating frequency of 2.4 GHz with S_{11} = -40 dB. Additionally, the transfer parameters, with values of S_{12} = -6.42 dB, S_{13} = -6.36 dB, S_{14} = -6.51 dB and S_{15} = -6.47 dB, are nearly equal and closely approach the desired ideal value of -6 dB. Therefore, the input power was divided into 4 equal quantities.

Figure II.7: (b) shows the phases of S_{12}, S_{13}, S_{14} and S_{15} versus frequency. According to this figure it is clear that these parameters are in good agreement. Indeed, at the operating frequency the phases of the parameters S_{12}, S_{13}, S_{14} and S_{15} are -104.86 °, -106.72 °, -102.63 °, -105.46 ° respectively.

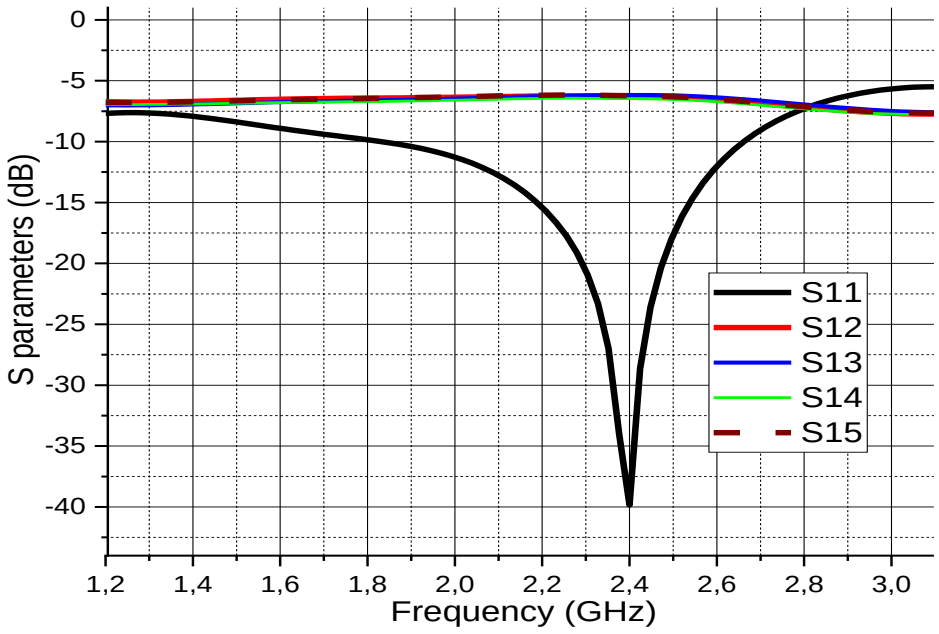

(a)

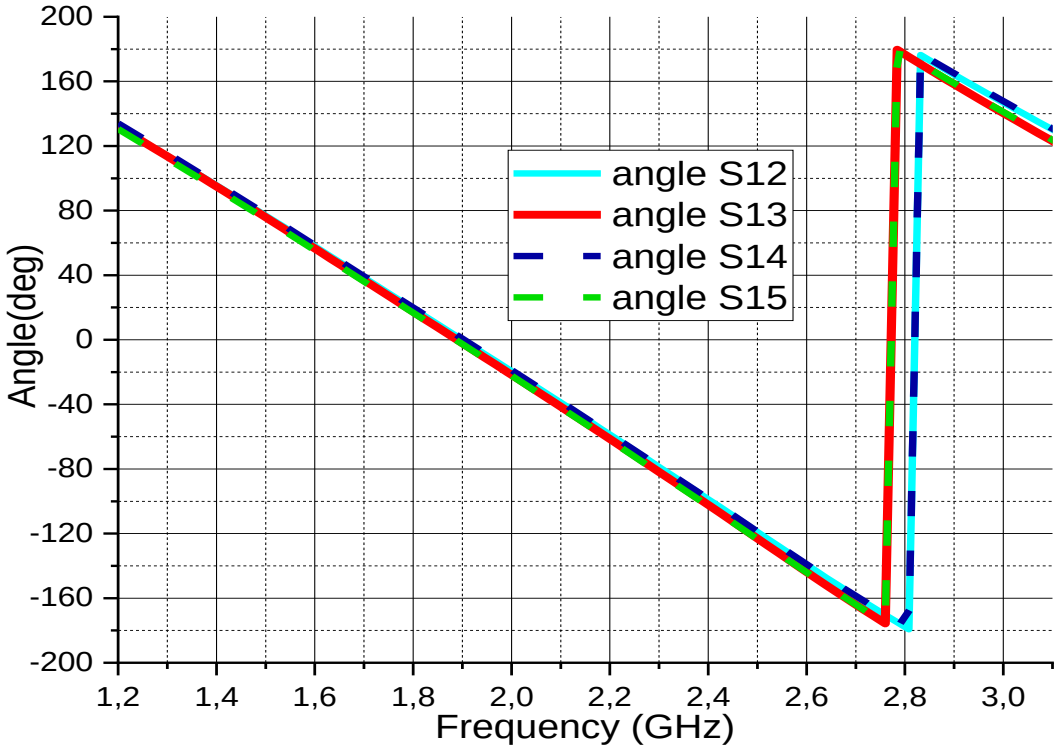

(b)

Figure II. 7 (a): S parameters versus frequency, (b): phases of S12, S13, S14 and S15 versus frequency of the proposed 1×4 TPD.

2.1.3. Design of the Proposed T 1×8 Power Divider (TPD 9dB):

Based on the previously designed 1×2 and 1×4 TPD, the design can be extended to an advanced 1×8 power splitter. It consists of four identical 1×2 TPD which are fed by two others identical TPD as shown in Figure II.8. The proposed 1×8 TPD divide the input signal power into eight equal quantities (a power division ratio equals to 9 dB) in phase agreement. This 1x8 TPD is intended for feeding an antenna array of eight elements to enhance gain and achieve a directional radiation pattern.

The extended scattering matrix of a symmetrical, reciprocal ($S_{ij} = S_{ji}$) and loss less ($S_{ii} = 0$) 1x8 power divider is written as follow [25]:

$$[S] = \begin{bmatrix} 0 & S_{21} & S_{31} & S_{44} & S_{51} & S_{66} & S_{71} & S_{81} & S_{91} \\ S_{21} & 0 & S_{32} & S_{42} & S_{52} & S_{62} & S_{72} & S_{82} & S_{92} \\ S_{31} & S_{32} & 0 & S_{43} & S_{53} & S_{63} & S_{73} & S_{38} & S_{39} \\ S_{41} & S_{42} & S_{43} & 0 & S_{54} & S_{64} & S_{74} & S_{84} & S_{94} \\ S_{51} & S_{52} & S_{53} & S_{54} & 0 & S_{65} & S_{75} & S_{85} & S_{95} \\ S_{61} & S_{62} & S_{63} & S_{64} & S_{65} & 0 & S_{76} & S_{86} & S_{96} \\ S_{71} & S_{72} & S_{73} & S_{74} & S_{75} & S_{76} & 0 & S_{87} & S_{97} \\ S_{81} & S_{82} & S_{83} & S_{84} & S_{85} & S_{86} & S_{87} & 0 & S_{98} \\ S_{91} & S_{92} & S_{93} & S_{94} & S_{95} & S_{96} & S_{97} & S_{98} & 0 \end{bmatrix} \quad (8)$$

The suggested 1×8-power splitter is a T-junction consisting of microstrip lines. It could be used for energy combining or energy splitting purposes. In power division, it can divide the input signal into eight output signals without any phase shift between them. Conversely, in power combining, it can accept eight input signals and combines them at the output port.

The designed 1×8-power divider is shown in Figure II.8, where a T-junction that has a nine-port network consisting of a 50Ω input line and eight 100Ω output lines. The power divider, delivers eight synchronized output signals with a 9dB power division ratio. To switch between the width W and the impedance Z of each arm port of the suggested 1×8 power splitter, the analytical equations (5) and (6) were used [26]. The equation (5) allows to calculate Z_{50} from W_{50} (when $W_{50} > h$) [26-29].

W_{50}, Z_{50} indicate respectively width and impedance of a 50 Ohm of arm.

The final dimensions of the proposed 1×8 power divider are given as follow: L_{50} = 15mm, W_{50} = 4.84mm, W_{100} = 2.78mm, L_{100} = 60.7mm, L_{101} = 123mm, L_{102} = 240.7mm.

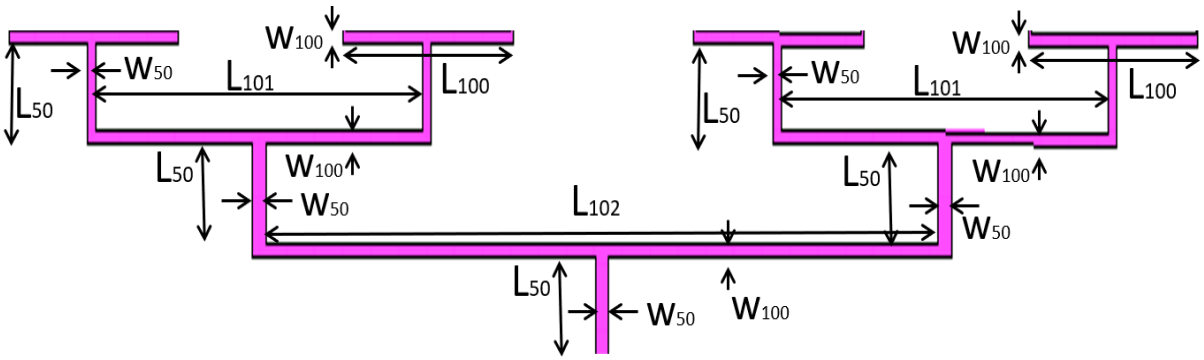

Figure II. 8 Structure of the proposed 1×8 power divider

2.2. Simulation Results

The analysis results of the suggested 1×8 power splitter in terms of scattering parameters are shown in Figure II.9. Figures II.9: (a), (b), (c), and (d) exhibit S_{11} return loss magnitude against two transmittance coefficients corresponding to two output ports with an identical feed. All these figures illustrate that the reflection coefficient S_{11} reached its minimal value of -19.13 dB at the desired frequency 2.4 GHz exhibiting a -10dB impedance bandwidth of 506 MHz (2.022-2.528 GHz). At this band, the S_{11} is less than -10dB which means that approximately 90% of the power feed is transferred to eight output ports. Furthermore, the values of the all-transmission coefficients equal about -9 dB throughout this band (2.022-2.528 GHz). The amplitude of -9 dB confirm that the incoming power is equal splatted at each output port. Hence, we can deduce that the designed power splitter exhibits a broad frequency range of 506 MHz (2.022-2.528 GHz) with an equal power splitting ratio of 9dB.

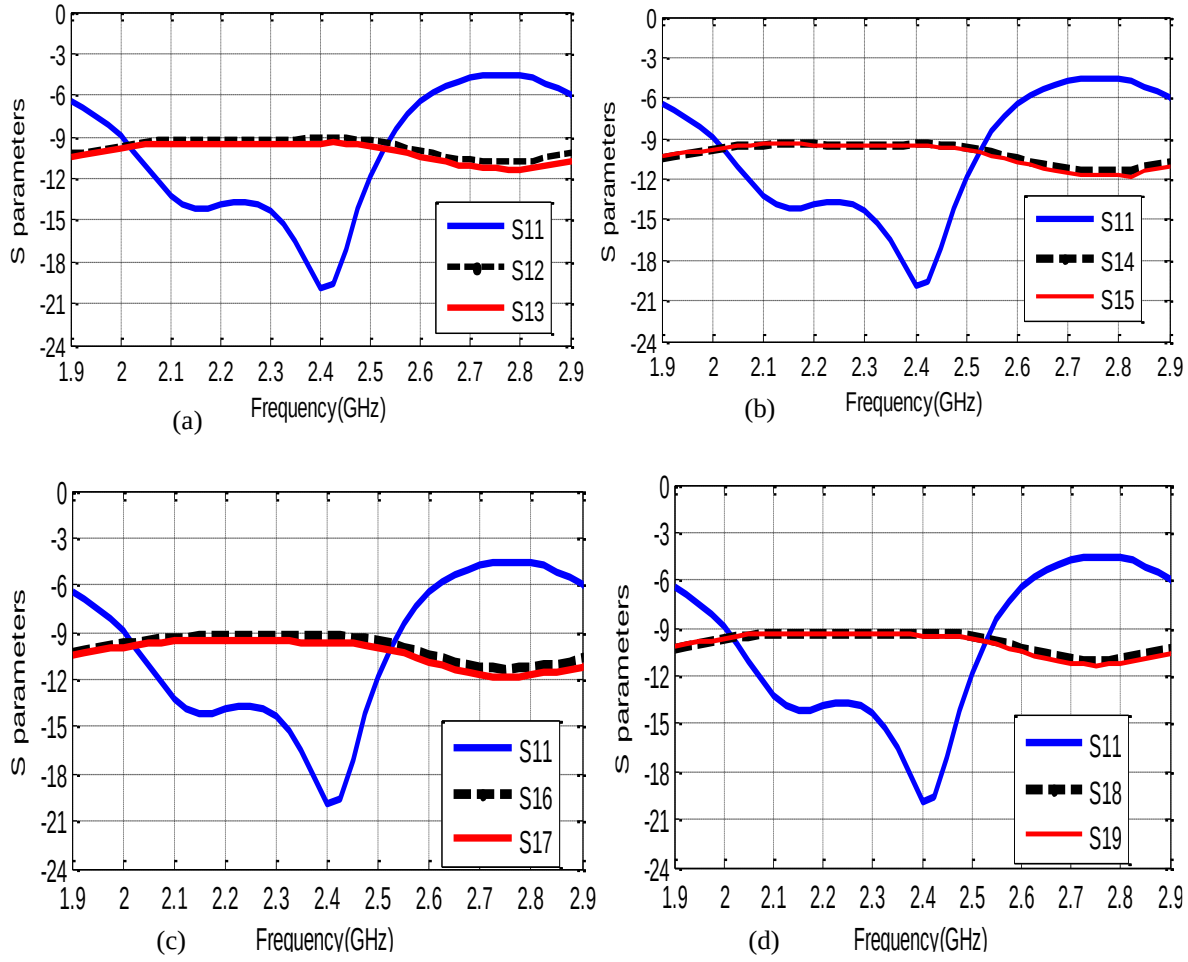

Figure II. 9 (a) S11, S21, S31 parameters vs. frequency; (b) S11, S41, S51 parameters vs. frequency; (c) S11, S61, S71 parameters vs. frequency; (d) S11, S81, S91 parameters vs. frequency

Figure II.10 presents angles of transmission coefficients versus frequency. It shows a comparison of two angles of transmission parameters for two output ports with a common feed and all these curves are in good agreement.

Table II.1 shows a summary of the magnitude and angles of transmittance coefficients; and the phase shift between two transmission coefficients corresponding to two output ports with an identical feed at the operating frequency 2.4GHz. According to this table, we conclude that all transmission coefficients are around –9.2dB and the phase shift between them does not exceed 3 degrees. Therefore, the power feed is splatted into eight equal parts with about 2.6 degrees phase shift between them.

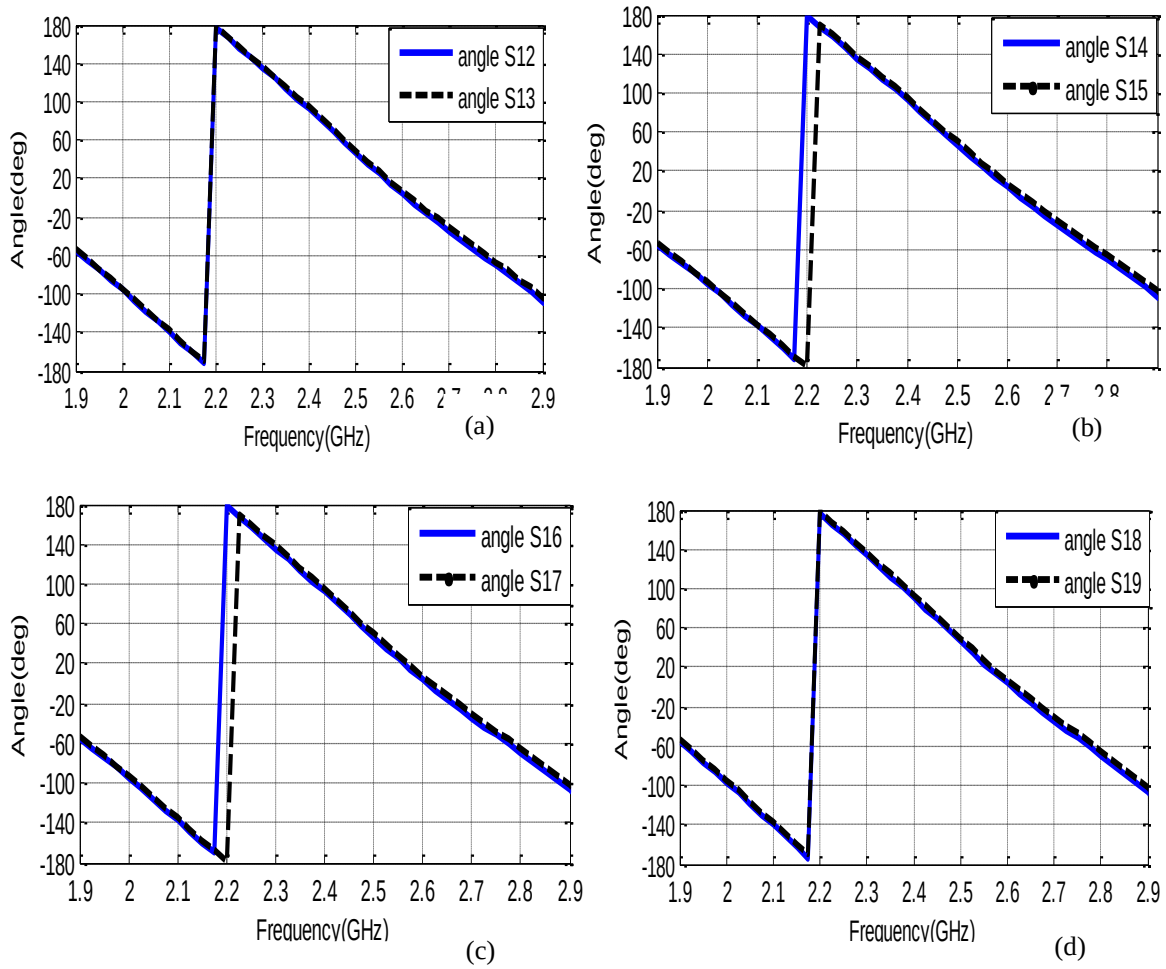

Figure II. 10 Angle of transmission parameters against frequency, (a): S12 vs S13, (b): S14 vs S15 (c): S16 vs S17, (d): S18 vs S19

Table II. 1 Summary of values and angles of the eight-transmission coefficient

S-Parameters	Magnitude(dB)	Angle(degree)	Phase shift (degree)
S_{12}	-9.14	91.92	2.23
S_{13}	-9.45	94.15	
S_{14}	-9.43	92.45	2.67
S_{15}	-9.53	95.12	
S_{16}	-9.27	92.12	2.84
S_{17}	-9.62	95.06	
S_{18}	-9.33	90.99	2.83
S_{19}	-9.45	90.83	

3. Optimization Process of The Basic Planar Antenna

3.1. Analytical Equations

The analytical equations to find out the parameters of a rectangular planar antenna (its length L_p, then its width W_p) and a quarter-wave impedance transformer (its impedance Z_{qw} and width W_{qw}) are presented as follows [29-32]:

$$W_p = \frac{c}{2fr\sqrt{\frac{2}{\varepsilon_r+1}}} \quad (9)$$

Where, fr : The resonant frequency

C: Celerity

ε_r : Substrate's relative electrical permittivity

$$L_p = L_{eff} - 2\Delta L \quad (10)$$

With L_{eff}: The effective width determined via equation (11).

ΔL: The length extension because of edge effects is determined using the following equation (12).

$$L_{eff} = \frac{c}{2fr\sqrt{\varepsilon_{re}}} \quad (11)$$

$$\Delta L = 0.412\left(\frac{\varepsilon_r+0.3}{\varepsilon_r-0.258}\right)\left(\frac{\frac{wp}{h}+0.264}{\frac{wp}{h}+0.813}\right) \quad (12)$$

Where:

ε_{re}: The relative effective permittivity when W/h>1, determined using the equation as described below:

$$\varepsilon_{re} = \frac{\varepsilon_r+1}{2} + \frac{\varepsilon_r-1}{2}\left(\frac{1}{\sqrt{1+12\frac{h}{wp}}}\right) \quad (13)$$

Most of microstrip antennas are fed by the 50Ω microstrip feed line which has its characteristic impedance Z_{50} that can be deduced by its width W_{50} using equation (5). Conversely, knowing the impedance Z_{50} and the permittivity ε_r, the W_{50} can be deduced using equation (6).

The impedance matching of λ/4 transformer Z_{qw} can be calculated through equation 14 [29]:

$$Z_{qw} = \sqrt{Z_p.Z_{50}} \quad (14)$$

Where, $Z_{50} = 50\Omega$ is the feed line's characteristic impedance, Z_p is the patch element's impedance. By using equation (5), a value of Zp = 254 Ω is obtained.

Then $Z_{qw} = \sqrt{Z_p . Z_{50}} = 112\ \Omega.$ (15)

The characteristic impedance of quarter-wavelength impedance transformer may also be calculated from its width W_{qw} using the folowing equation:

$$Z_{qw} = \frac{60}{\sqrt{\varepsilon_r}} ln\left(\frac{8h}{W_{qw}} + \frac{W_{qw}}{4h}\right) > \frac{126}{\sqrt{\varepsilon_r}} \text{When } \frac{W_{qw}}{h} < 1 \quad (16)$$

Conversely, the width W_{qw} can be obtained from its characteristic impedance Z_{qw} using the subsequent equation [5]:

$$\frac{W_{qw}}{h} = \frac{8e^A}{e^{2A}-2} \text{ when } \quad \frac{W_{qw}}{h} < 2 \quad (17)$$

$$\text{With } A = \frac{Z_{qw}}{60}\sqrt{\frac{\varepsilon_r+1}{2}} + \frac{\varepsilon_r-1}{\varepsilon_r+1}\left(0.23 + \frac{0.11}{\varepsilon_r}\right) \quad (18)$$

The length L_{qw} of the quarter-wavelength impedance transformer is odd multiple of $\frac{\lambda_g}{4}$:

$$L_{qw} = (2k+1)\frac{\lambda_g}{4} \quad (19)$$

In the next, the first odd multiple $L_{qw} = \frac{\lambda_g}{4} = 24.13mm$ will be considered.

3.2. Design Steps

Using HFSS simulator, the structure and optimization of the basic radiating element was done on RT/duroid 5880 dielectric substrate ($\boldsymbol{\varepsilon_r}$=2.2, loss tangent = 0.0009, deep = 1.56mm). The proposed single element optimized antenna is obtained after 3 design stages (see Figure II.11). The reflections coefficients of these steps are plotted in Figure II.12. For case I, there is a conventional rectangular patch antenna fed through a 50 Ω microstrip feed line. The return Loss for this case has confirmed that there is no impedance matching between the patch and the fed line. To address this issue, a quarter-wave impedance transformer has been inserted between them. In this case, the minimal value of reflection coefficient S_{11} equal about –24.57dB around the resonant frequency 2.36GHz. To achieve the targeted resonance frequency of 2.4 GHz, circular and rectangular slots have been strategically inserted on the patch. Consequently, the reflection coefficient S_{11} reached its minimum value of -24.34 dB at the specified operating frequency.

The circular and rectangular slots are used to shift the operating frequency to 2.4GHz and to improve the overall antenna characteristics. At first, a wide rectangular slot is inserted then a narrow regular slot has been connected with it. Subsequently, a circular slot is incorporated within the surface of the patch element. The geometrical dimensions of the

incorporated slots are determined through simulation studies in order to precisely shift the resonant frequency to 2.4 GHz.

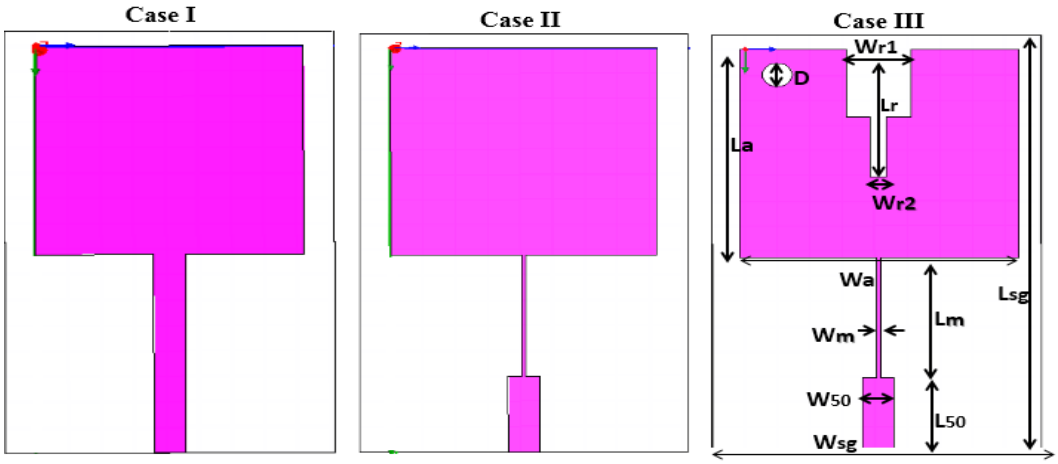

Figure II. 11 Design steps of the basic antenna

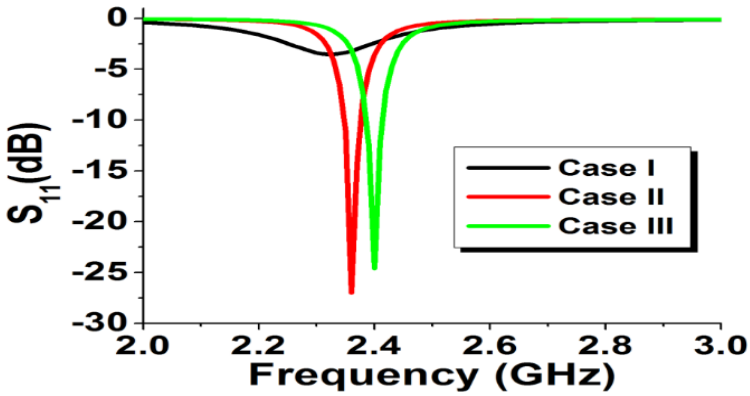

Figure II. 12 Reflection coefficients for different optimization steps of the basic antenna

The final dimensions of the optimized structure are: L_{sg} = 85 mm, W_{sg} = 52 mm, L_a = 42.78 mm, W_a = 41.32 mm, L_m=23.54 mm, W_m = 0.84 mm, L_{50} = 14 mm, W_{50} = 4.84 mm, D = 4.6 mm, L_r = 25.3 mm, W_{r1} = 10 mm, W_{r2} = 2.5 mm.

3.3. Simulation results of the Optimized Planar Antenna

To carry out the design of the suggested basic element antenna, the HFSS EM simulation tools have been employed. The accomplished simulation analyses were validated using the CST-EM simulator to confirm the design results. As shown in Figure II.13, a good agreement has been acheived for results of both EM simulators (HFSS & CST). Figure II.13 (a) presents the insertion loss S_{11} against frequency, it can be noticed that S_{11} =−24.57dB by HFSS and S_{11}=−18dB by CST at the operating frequency. Despite these values show difference, they are both less than −10dB which confirm that both results are satisfactory. Afterward, the VSWR ratio (voltage standing wave) is plotted versus frequency in Figure II.13(b). The reached value by HFSS equals 1.2

exhibiting a narrow operational frequency range of 31MHz, using CST, the obtained value is 1.26 with a restricted bandwidth of 36MHz. Both achieved findings values are under 2 which validates that matching impedance is almost ideal. Figure II.13(c) illustrates the radiating efficiency as a function of frequency, its peak reached value of 97.19% using HFSS, and then 98.2% using CST. Thus, both values confirm that the radiating element exhibits excellent efficiency. The antenna's gain against frequency is shown in Figure II.13 (d), we note that at the operating frequency 2.4GHz, the antenna's maximum gain attained is 7.09dB and 7.3dB, respectively by using HFSS and CST. Therefore, the single planar antenna exhibits a significant gain. The H, E-planes radiation patterns are depicted in Figures II.13(e), (f) respectively, both planes show an omnidirectional radiation with the main beam along the broadside direction.

Table II.2 shows a summary of the HFSS versus CST results of the optimized planar radiating element. According to this Table, we can confirm that the basic element offers notably good performance in terms impedance matching characteristics (S_{11} and VSWR) and radiation traits (antenna's gain and radiating efficiency).

Table II. 2 Recap of HFSS versus CST simulation results

EM Simulator	Return loss	VSWR	Bandwidth	Peak Efficiency	Peak Gain
CST Studio	−18 dB	1.26	36 MHz	98.2%	7.3 dB
Ansys HFSS	−24.57 dB	1.2	31 MHz	97.19%	7.09 dB

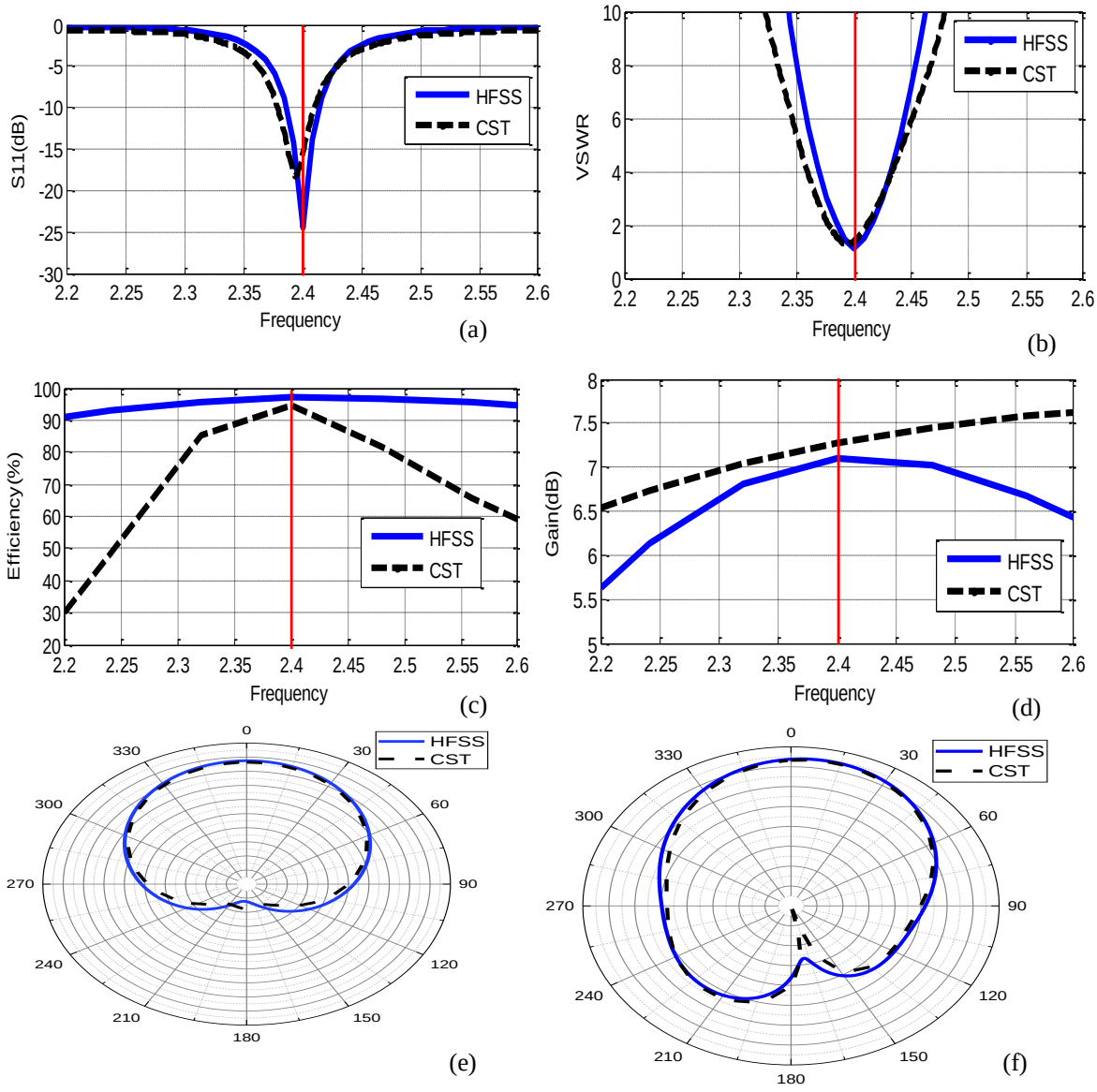

Figure II. 13 HFSS versus CST simulation results: (a): S11 return loss, (b): VSWR, (c): Gain of antenna, (d): antenna's efficiency, (e): E-plane radiation pattern; (f): H-plane radiation pattern.

4. The Proposed Directional 1×8 Antenna Array

4.1 Theoretical study

Let's consider a uniform antenna array consisting of two identical radiating elements separated by a distance d ($d \leq \lambda/2$) and have the same excitation amplitude with a phase difference β between them. These two elements are placed in the plane (xoy) on the axis (oy) as shown in Figure II.14.

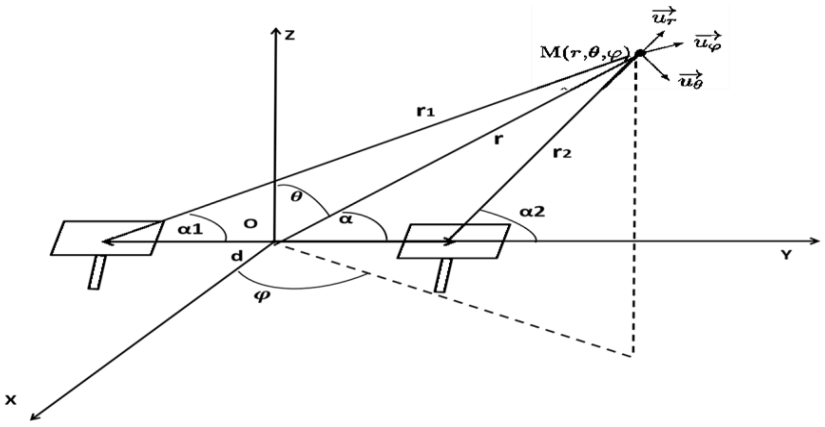

Figure II. 14 Two-element array antenna

In the far-field approximation ($r >> \lambda$), the fields E_1 and E_2 radiated by these two elements at a point M situated at a long-distance r are given by:

$$\underset{E_1}{\rightarrow} = E_{01}.e^{j(\omega t - k.r_1)} \underset{e_\theta}{\rightarrow} \quad (20)$$

$$\underset{E_2}{\rightarrow} = E_{02}.e^{j(\omega t - (k.r_2 - \beta))} \underset{e_\theta}{\rightarrow} \quad (21)$$

Where, $E_{01} = E_{02} = E_0 = \text{j}\eta \frac{\text{K.I}_0.\text{d}}{4\pi.r}.\cos(\alpha)$, with η is the intrinsic impedance of the vacuum

According to the principle of superposition (using the approximation (r1=r2=r)), the total field E_T radiated by the two elements is expressed as follow:

$$E_T = E_1 + E_2 = E_0(e^{j(\omega t - k.r_1)} + e^{j(\omega t - (k.r_2 - \beta))}) \quad (22)$$

$$= E_0.e^{j(\omega t)}(e^{-j(k.r_1)} + e^{-j(k.r_2 - \beta)}) \quad (23)$$

To simplify phase terms, we will use these approximations:

$r_1 = r + \frac{d}{2}\cos(\alpha)$ and $r_2 = r - \frac{d}{2}\cos(\alpha)$

Thus, the E_T field becomes:

$$E_T = E_0.e^{j(\omega t)}(e^{-j\left(k.\left(r+\frac{d}{2}\cos(\alpha)\right)\right)} + e^{-j\left(k.(r-\frac{d}{2}\cos(\alpha)-\beta\right)}) \quad (24)$$

$$= E_0.e^{j(\omega t - k.r)}.(e^{-j\left(\frac{k.d}{2}\cos(\alpha)\right)} + e^{j\left(\frac{k.d}{2}\cos(\alpha)+\beta\right)}) \quad (25)$$

$$E_T = E_0.e^{j(\omega t - k.r)}.e^{-j\left(\frac{k.d}{2}\cos(\alpha)\right)}(1 + e^{j(\text{k.d}\cos(\alpha)+\beta)}) \quad (26)$$

$$= E_0.e^{j\left(\omega t - k.r - \frac{k.d}{2}\cos(\alpha)\right)}.2.\cos(\frac{k.d}{2}\cos(\alpha) + \frac{\beta}{2}) \quad (27)$$

Let E_T be in modulus: $|E_T| = E_0..2.\cos(\frac{k.d}{2}\cos(\alpha) + \frac{\beta}{2})$ (28)

So, $|E_T| = \text{E(single element)}.AF$ (29)

With, $\text{AF} = 2.\cos(\frac{k.d}{2}\cos(\alpha) + \frac{\beta}{2})$ called the array factor of two elements.

And $\text{E(single element)} = E_0 = \text{j}\eta \frac{\text{K.I}_0.\text{d}}{4\pi.r}.\cos(\alpha)$

Consequently, the total field of the 1x2 array antenna equals to the field of a single element multiplied by the array factor of two elements.

Let's generate the total field E_T for array antenna of N elements. In this case the E_T will be:

$$|E_T| = \mathrm{E(single\ element)}.AF_N \qquad (30)$$

Where, AF_N is the array factor of N elements. Using equation (26) it can be expressed as follow:

$$AF_N = 1 + e^{j(\mathrm{k.d}\cos(\alpha)+\beta)} + e^{j2(\mathrm{k.d}\cos(\alpha)+\beta)} \dots\dots\dots\dots\dots + e^{jN(\mathrm{k.d}\cos(\alpha)+\beta)} \qquad (31)$$

Thus,

$$AF_N = \sum_{n=1}^{N} e^{j(n-1)\psi} \qquad (32)$$

Where $\psi = k.d\cos(\alpha) + \beta$

The proposed array antenna is a uniform array composed of eight identical elements (N=8). So, the total field E_T of the proposed 1x8 array antenna is:

$$|E_T| = E_0.\sum_{n=1}^{8} e^{j(n-1)\psi} \quad (33)$$

The radiation pattern of the proposed 1x8 array antenna is the radiation pattern of single element multiplied by the array factor AF_8 of 8-elements which will make the array antenna more directional in a specific direction. The simulation results will prove that in the next section.

4.2. Design of the suggested 1×8 Planar Antenna Array

This part exhibits the designed 1×8 planar antenna array by employing both optimized basic element and the 1×8-power divider. In this eight-element array configuration, the patch elements are connected with the 8 output terminals of the power splitter. The structure of the proposed planar 1×8 array antenna is depicted within figure II.15. The design has been done on RT/duroid 5880 dielectric substrate with the following characteristics: ($\boldsymbol{\varepsilon_r}$=2.2, loss tangent=0.0009, deep=1.56mm) with the total dimension of: Lg×Wg=117×475mm^2.

To reach a high gain, high directivity and avoid the mutual coupling between patches and the grating lobes, the *d;* distance between elements falls within the range of $\boldsymbol{\lambda/4 \leq\ d \leq \lambda/2}$

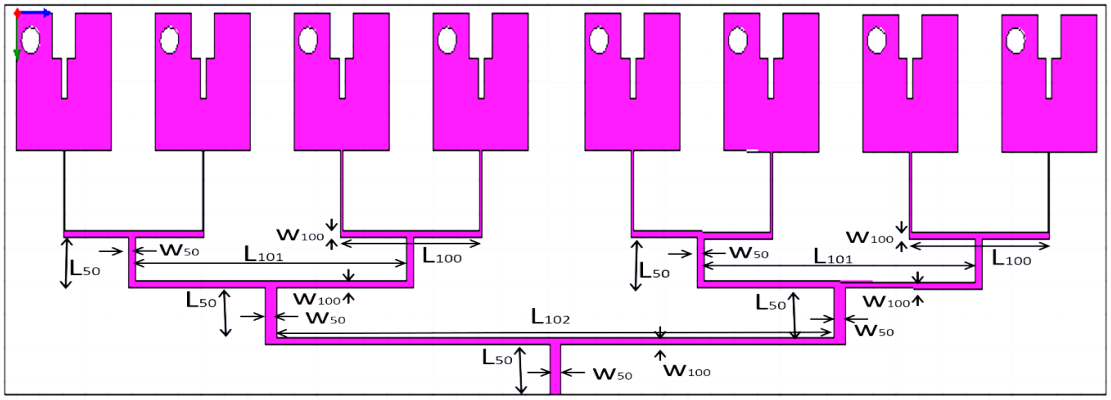

Figure II. 15 Structure of the suggested directional high gain 1x8 antenna array.

4.3. Results and Discussion

Initially, the design of the suggested directional antenna was carried out by HFSS software. The reached results were verified with CST EM simulator. As shown in Figure II.16, both results are in good agreement. Figure II.16 (a) indicates the variation of reflection coefficient S_{11} versus frequency.; We note that its minimum value gets down to −13.14dB at 2.4GHz (operating frequency) with a narrow bandwidth of about 31MHz (2.385 GHz-2.415 GHz) using HFSS. Then its value gets down to −24.34dB with narrow bandwidth of 33MHz (2.383 GHz-2.416 GHz) using CST. According to Figure II.16(b), the VSWR at the aimed frequency 2.4 GHz is 1.45 as obtained from HFSS simulator while as per CST simulation results, it is equal to 1.16. The achieved VSWR values demonstrate effective impedance matching and minimal mismatch losses for the proposed 1×8 antenna array.

Figures II.16 (c) and (d) shows variations of the radiation efficiency and antenna's gain respectively, at the operating resonant frequency 2.4GHz. Maximum gain gets up to 14.61dB using HFSS and 14.76dB using CST. The peak radiation efficiency reaches a value of 98.3% in HFSS and 98.86% in CST. Figures II.16 (e) and (f) depict the E and H-plane radiation patterns, respectively. In the E-plane, the antenna array exhibits a purely broadside radiation pattern, with the principal lobe focused at 0 degrees. In contrast, the H-plane results indicate that the principal lobe is directed towards 0 degrees, achieving a maximum gain of 14.6dB. While there are secondary lobes with gains less than 0 dB, their values are negligible compared to the main lobe. Consequently, the radiation pattern is directional with high gain.

Table II.3 compares the results from CST and HFSS simulators of our structure 1×8 antenna array. According to this table, we note our proposed structure plana antenna array provides good results in terms of S_{11}, VSWR, antenna gain and Efficiency at 2.4GHz frequency.

Table II. 3 Summary of simulation results of 1×8 antenna array

Solvers	Reflection coefficient	Bandwidth	VSWR	Highest gain	Height efficiency
CST Studio	−24.34 dB	41 MHz	1.16	14.76 dB	98.85%
Ansys HFSS	−13.14 dB	36 MHz	1.46	14.6 dB	98.31%

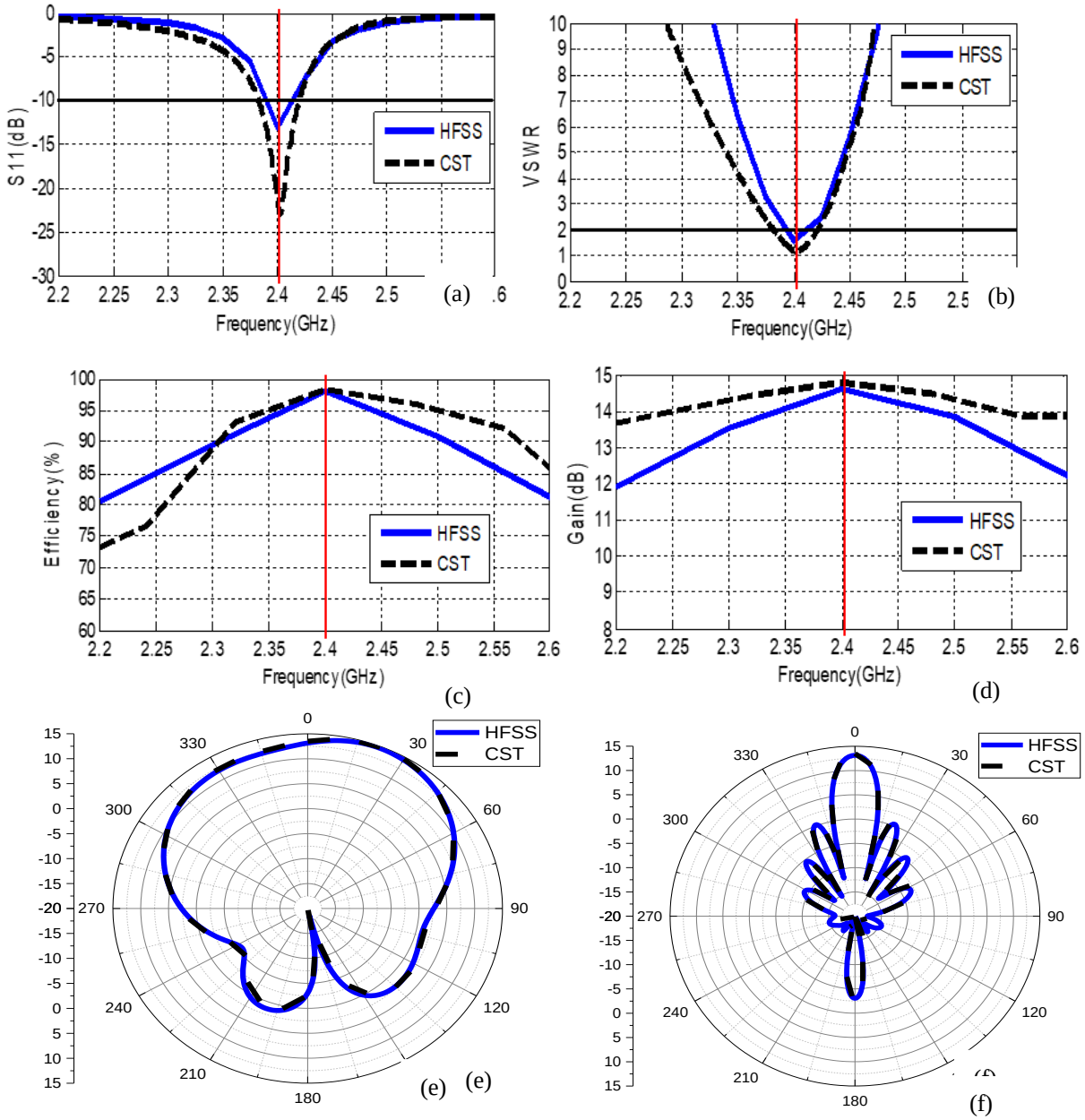

Figure II. 16 HFSS versus CST simulation results of the proposed planar 1x8 antenna array; (a): S11 return loss, (b): VSWR, (c): Gain of antenna, (d): antenna efficiency, (e): Electric Field (E) Plane radiation pattern and (f): Magnetic Field (H) Plane radiation pattern

5. Performance Comparison with State-of-the-Art

Table II.4 exhibits a comparative performance analysis of the suggested planar antenna array with other research works. According to this table, the suggested antenna array offers the highest gain

and good efficiency. Consequently, this printed antenna array emerges as a promising candidate for operation around 2.4 GHz, attributing its notable impedance and radiation characteristics.

Table II. 4 Comparison of our directional planar antenna array to state of the Art

References	fr in GHz	Dimensions in mm^2	Highest gain in dB	Highest Radiation Efficiency	Directional radiation pattern
[19]	2.45	75×95	4.73	55.05%	No
[20]	2.45	135×114	9.65	99.8%	No
[21]	2.40	83×110.5	9.22	-	No
[22]	2.45	95.9×227	7.75	-	No
[23]	2.45	91×161	6.6	60%	No
[24]	2.40	98×223.9	12.6	-	No
This work	**2.40**	**117×475**	**14.61**	**98.3%**	**Yes**

6. Conclusion

In summary, in this chapter we examined and discussed a directional high-gain microstrip 1×8 antenna array designed for 2.4GHz RFID Reader applications. The analysis highlights its excellent impedance matching and high radiation characteristics. To achieve this objective, a methodology was employed, starting with the presentation of an advanced 1x8 power divider design. Subsequently, a detailed analysis and optimization of a single-element antenna were conducted, followed by the completion of the 1×8 array antenna. Simulation analysis were performed using both HFSS and CST EM solvers. The suggested planar 1×8 antenna array configuration resonates at 2.4GHz offering S_{11} and VSWR within acceptable limits that confirms its excellent impedance matching. Also, it has a maximum antenna gain equals to 14.61dB and excellent efficiency of 98.31%. Moreover, it provides a directional radiation diagram.

Although the designed antenna array has a high gain and directional radiation pattern, it presents limitations in terms of impedance bandwidth, hindering its compatibility with other applications in the ISM band. Furthermore, it has relatively large size poses challenges in practical realization. Additionally, the antenna lacks flexibility, particularly in scenarios where the ability to control the radiation pattern is crucial, such as in tracking applications. In the upcoming chapter, we will introduce new methods to address these issues of flexibility, narrow bandwidth, and size, offering potential solutions and improvements.

References

1. Aarti G. Ambekar, Amit A. Deshmukh, « Antenne microbande rectangulaire chargée de plusieurs emplacements pour une réponse multibande polarisée double », International Journal of Microwave and Optical Technology, vol.15, n ° 3, p. 279-288, 2020.
2. Badisa, A., Madhav, B. T. P., & Nadh, B. P. (2022). A circularly polarized, flexible and compact quad-band wearable antenna for off-body communication applications. Journal of Circuits, Systems and Computers, 31(03), 2250057.
3. B. Gowrish, A.Basu. "Analysis and design of a dual-band stepped impedance PCB monopole antenna," IETE J Educat, Vol. 58, pp. 29-38, 2017.
4. H. Medkour, M. Cheniti, A. Narbudowicz, S. Das, E. Vandelle, T.P. Vuong, "Coplanar waveguide-based ultra-wide band antenna with switchable filtering of WiMAX 3.5 GHz and WLAN 5 GHz signals," Microwave and Optical Technology Letters, Vol. 62, No. 6, pp. 2398-240, 2019.
5. S Ghosh, I Sarkar, S Chowdhury, S Dutta, P Dey, S Majumdar, A Ghosh, PP Sarkar, DC Sarkar, Design and Realization of low profile compact wideband monopole printed antenna for C and X band application, Journal of Physics: Conference Series, Vol. 1797, 012030, 2021.
6. S. Das, P.P. Sarkar, S.K. Chowdhury, "Modified π shaped slot loaded multifrequency microstrip antenna, Progress In Electromagnetics Research B, 64, 103-117, 2015.
7. EL ANSARI, Abdelaaziz, DAS, Sudipta, EL-ARROUCH, Tarik, et al. A Hybrid Coupler Integrated 1× 4 Printed Array Antenna with Broadband and High Performance For Beamforming RFID Reader. In : 2022 9th International Conference on Wireless Networks and Mobile Communications (WINCOM). IEEE, 2022. p. 1-6..
8. S. Chatterjee, K. Ghosh, J. Paul, SK Chowdhury, D. Chanda, PP Sarkar, Compact microstrip antenna for mobile communication, Microwave and Opt. Technol. Letts.55, 954-957, 2013.
9. A. Roy, S. Bhunia, D. C. Sarkar, P. P. Sarkar, S. K. Chowdhury, Compact multi frequency strip loaded microstrip patch antenna with spur-lines, International Journal of Microwave and Wireless Technologies, 9, 1111-1121, 2017.
10. S. Maity, T. Tewary, S. Mukherjee, A. Roy, PP Sarkar, S. Bhunia, Super wideband high gain hybrid microstrip patch antenna, AEU-International Journal of Electronics and Communications, 153, 154264, 2022.
11. A. Roy, S. Bhunia, D. C. Sarkar, P. P. Sarkar, Slot loaded compact microstrip patch antenna for dual band operation, Progress In Electromagnetics Research C, 73, 145-156, 2017.
12. EL ARROUCH, Tarik, EL IDRISSI, Najiba El Amrani, et EL ANSARI, Abdelaaziz. Microstrip Patch Antenna using a Parasitic Mushroom for 5GApplication at 28GHz. In: 2022 9th International Conference on Wireless Networks and Mobile Communications (WINCOM). IEEE, 2022. p. 1-6.
13. EL ANSARI, Abdelaaziz, DAS, Sudipta, EL IDRISSI, Najiba El Amrani, et al. Slot incorporated high gain Printed RFID Reader Array antenna for 2.4 GHz ISM band applications. In: E3S Web of Conferences. EDP Sciences, 2022. p. 01056.
14. J.N.Lin, N.N.Wang, T.Y.Du, "A Near-Field focused planar microstrip array for 2.4 GHz RFID readers", Proceedings of ISAP, Okinawa, Japan, pp. 758-759, October 24-28, 2016.

15. S. Lakrit, H. Medkour, S. Das, B.T.P. Madhav, W.A.E. Ali, R.P. Dwivedi, “Design and Analysis of Integrated Wilkinson Power Divider-Fed Conformal High-Gain UWB Array Antenna with Band Rejection Characteristics for WLAN Applications,” Journal of Circuits, Systems and Computers, Vol. 30, No. 8, 2150133, 2021.

16. Ansari, A. E., Jayaprakasan, V., Duraisamy, K., Das, S., El-Arrouch, T., & Idrissi, N. E. A. E. "A Wideband Microstrip 1 x 2 Array Antenna Fed by Coupler for Beam Steering Terahertz (THz) Band Applications." 2023. J. Nano- Electron. Phys, Vol. 15, No. 3, 03028, 2023

17. P. Turalchuk, I. Munina, M. Derkach, O. Vendik, I. Vendik, “Electrically Small Loop Antennas for RFID Applications”, IEEE Antennas and Wireless Propagation Letters, Vol. 14, pp. 1786 – 1789, 2015.

18. M. Abu, N. Masrom, E.E. Hussin, A.R. Othman, N.M. Yatim, F.M. Johar, “2.45 GHz RFID reader array antenna with hexagonal geometry arrangement”, proceedings of IEEE Asia-Pacific Conference on Applied Electromagnetics (APACE), Melaka, Malaysia, pp. 338–341, December 11-13, 2012.

19. T. Ikram, M. Jorio, N. El Amrani El Idrissi, “1x2 RFID reader array antenna for narrowband indoor positioning applications," Journal of Engineering Science and Technology Review, Vol. 12, No. 3, pp.167-172, 2019.

20. T. Ikram, N. El Amrani El Idrissi, M. Jorio, A. Slimani, « A high gain 1* 2 array RFID reader MPA for indoor localization applications. International Conference on Wireless Technologies, Embedded and Intelligent Systems (WITS), IEEE, PP.1-6, 2017.

21. A. El Alami, Y. Ghazaoui, S. Das, S.D. Bennani, M. El Ghzaoui, “Design and simulation of RFID array antenna 2×1 for detection system of objects or living things in motion. Procedia Computer Science, Vol. 151, pp. 1010-1015, 2019.

22. I. Tabakh, S. Das, M. Jorio, N. El Amrani El Idrissi, S. Mohapatra, D. Barad, “Defected Ground Structure (DGS) Incorporated RFID Reader Antenna Array for Indoor Positioning Systems at 2.45 GHz,” International journal of microwave and optical technology, Vol.15, No.6, pp. 517-524, 2020.

23. A. Bendali, A. El Fellahi, M.N,Srifi, S. Bri, M. Habibi, “A Novel Adaptive Array Antenna for a RFID Applications,” International Symposium on Advanced Electrical and Communication Technologies (ISAECT), IEEE, pp. 1-5, 2018.

24. A. El Alami et al. “Design, optimization and realization of high gain RFID array antenna 4×1 for detection system of objects in motion. Journal of Instrumentation,” Vol. 14, No. 05, P05002, 2019.

25. ALTAF, Ahsan, SAJJAD, Hassan, KHAN, Sana, et al. ISM band 1: 16 wilkinson power divider. In : 2018 IEEE 21st International Multi-Topic Conference (INMIC). IEEE, 2018. p. 1-5.

26. YOUNESIRAAD, Hemn, BEMANI, Mohammad, et FOZI, Mahdi. A novel fully planar quad band Wilkinson power divider. AEU-International Journal of Electronics and Communications, 2017, vol. 74, p. 75-82.

27. BARBADEKAR, Aparna B. et PATIL, Pradeep M. Reconfigurable 1: 4 Wilkinson Power Divider Used in ISM Band Applications. In : Sustainable Communication Networks and Application: Proceedings of ICSCN 2021. Singapore : Springer Nature Singapore, 2022. p. 603-620.

28. Ansari, A., Islam, T., Rama Rao, S. V., Saravanan, A., Das, S., & Idrissi, N. A. (2023). "A Broadband Microstrip 1 × 8 Magic-T Power Divider for ISM Band Array Antenna Applications," J. Nano- Electron. Phys, Vol. 15, No. 3, 03003, 2023.

29. D. M Pozar, "Microwave engineering," John wiley & sons, New York: John Wiley & Sons, 2011.

30. Huang, Yi, and Kevin Boyle. Antennas: from theory to practice. UK: John Wiley & Sons, 2008.

31. BALANIS, Constantine A. Antenna theory: analysis and design. New York: John wiley& sons, 2015

32. Ahmed Fatthi Alsager, "Design and Analysis of Microstrip Patch Antenna Arrays", University College of Boras School of Engineering, SE501 90 BORÅ.

Chapter III: Design And Realization of a Broadband Switched Phased Array Antenna Based on Hybrid Coupler For ISM Band 2.45 Ghz RFID Reader Applications

1. Introduction

In the last few decades, the identification of things has existed in numerous forms like paper, card, and others. Recently, the RFID (Radio frequency identification) technology has revolutionized the world of the identification and real-time monitoring of objects. RFID technology is a contactless identification technology based on the exchange of information between the reader and tag antennas through radio waves. This contactless identification can be performed by an optical vision, LF and HF link, UHF, SHF link and infrared link [1]. RFID technology is currently developed in a wide range of applications in various fields, such as: automotive systems, industrial applications, contactless smart cards, monitoring and tracking, personal data and official documents, remote payment of road tolls, and real-time location (RTL) systems etc. Most of these applications are operating in the ultra-high frequency and super high frequency [1-2].

Knowing the significant role that antennas play in various wireless communication applications [3-4], this study focuses on the design of an RFID Reader antenna operating in the 2.45 GHz SHF band .The targeted frequency (2.45 GHz) band supports many modern wireless applications such as wireless fidelity (Wi-Fi), wireless local area network (WLAN), and Bluetooth. In RFID systems, likewise the tag antenna, the RFID reader antenna is also very important. The Reader is also called interrogator or base station and can request or control the tag's reading or writing by using radio frequency communication. It generally consists of a control unit, an interface for transmitting data to a terminal and an antenna.

So far, Most of RFID reader's antennas are narrow band and have a single beam [5-18]. In these references authors solved some weaknesses of the patch antennas like gain and directivity, but they couldn't solve the problem of flexibility and narrow bandwidth due to the use of a T power splitter to power an antenna array.

Therefore, in this chapter, instead of using the T power divider to feed an array antenna, we propose a power arrangement with a 3dB hybrid coupler in order to obtain a wideband, flexible and multibeam antenna (see Figure III.1 below) for ISM band, RFID reader application.

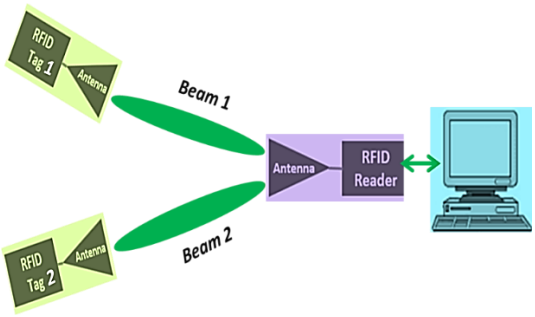

Figure III. 1 Flowchart of the RFID System with the multi-beam antenna

This chapter is organized into six sections as follows: Section 2 delves into the design and miniaturization of the basic element. Section 3 is dedicated to design and simulation of the basic 3dB 90° hybrid coupler, section 4 showcases the design, realization and measurement of the proposed beam switchable broadband 1×2 array antenna. Section 5 discusses the hybrid coupler integrated 1×4 printed array antenna. The final section provides the conclusion for this chapter.

2. Design and miniaturization of the basic patch antenna

2.1. Design steps of the miniaturized basic element

The theoretical equations enabling the calculation of dimensions for a rectangular planar antenna, its feed line, and the quarter-wavelength impedance transformer have been presented in the previous chapter. As shown in Figure III.2, the miniaturized basic patch antenna went through four stages.

The geometrical parameters of the basic antenna are summarized in case 1 of Table III.1. The corresponding simulated S_{11} parameter of this case is presented in Figure III.3 which indicates a poor impedance matching between the basic patch antenna and 50 Ω feed line. To solve this matching issue, a parametric study on the antenna parameters Lp and Wp have been conducted and a quarter-wavelength impedance transformer between the patch antenna and the fed line have been added (Figure III.2, case 2). As presented in case 2 of Figure III.2, a reflection coefficient S_{11} of −13.82 dB is obtained at a resonant frequency of 2.5 GHz. Therefore, the resonant frequency has been shifted by adjusting the lengths L_{qw} and L_{50} as shown in case 3 of Figure III.2. In this scenario, S_{11} reaches a value of −29.2 dB at 2.46 GHz. Finally, the overall size of the antenna has been miniaturized effectively by conceptualizing and introducing a “Pleated Quarter-Wavelength Impedance Transformer (PQWIT)” as demonstrated in case 4 of Figure III.2. Consequently, the overall area occupied by the patch antenna has been miniaturized by 50% due to the implementation of suggested PQWIT. In this design case, the antenna resonates exactly at 2.45

GHz with a reflection coefficient (S_{11}) of −19.86 dB. The final parameters of this miniaturized antenna are summarized in case 4 of Table III.1.

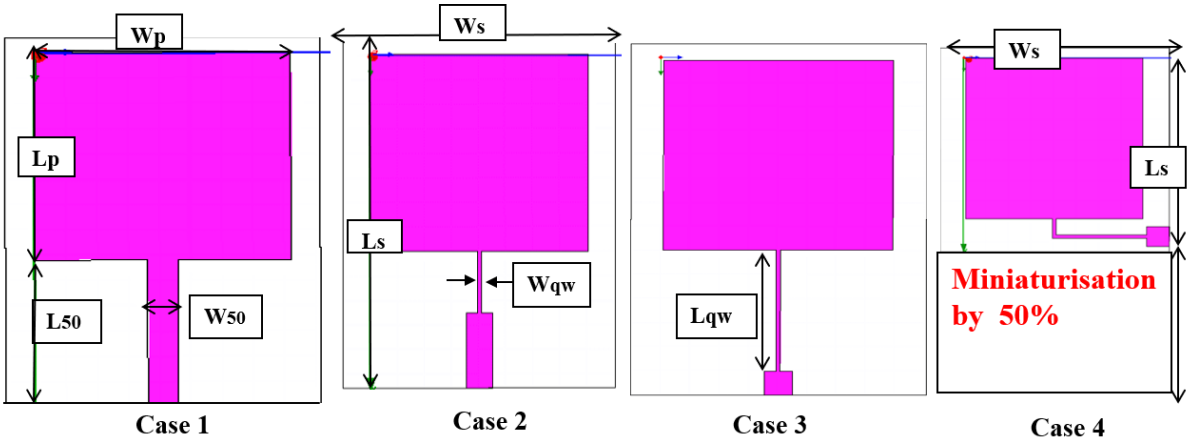

Figure III. 2 Design and optimization steps of the elementary patch antenna

Table III. 1 Dimensions summary of the elementary patch antenna

Parameters	L_s (mm)	W_s (mm)	L_p (mm)	W_p (mm)	L50 (mm)	W50 (mm)	Lqw (mm)	Wqw (mm)
Case1	65.09	60.05	40.48	48.37	22.24	4.84	-	-
Case2	83	56	39.42	39.28	15.24	4.84	10.13	0.75
Case3	83	52	39.42	39.28	5	4.84	22.24	0.75
Case4	**51**	**50**	**39.42**	**39.28**	**5**	**4.84**	**24.13**	**0.75**

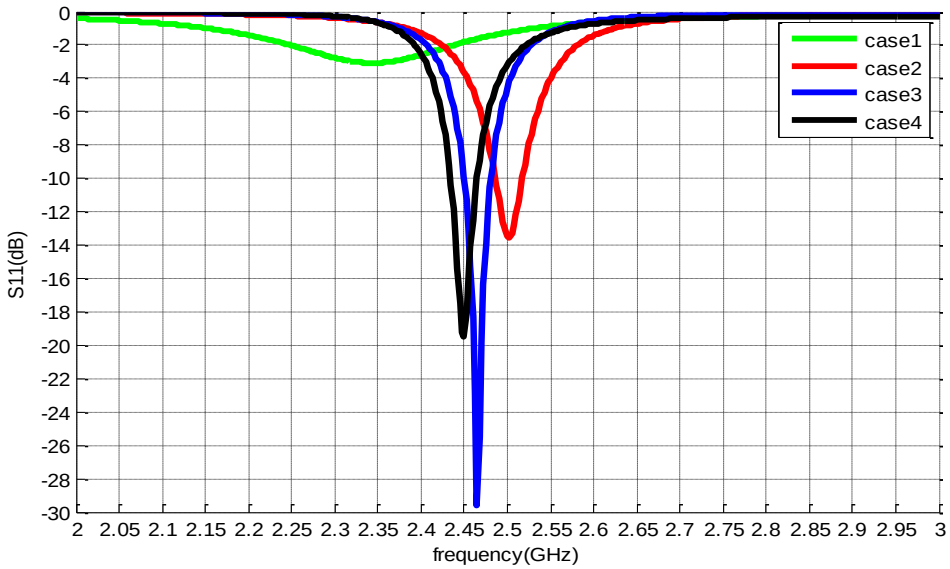

Figure III. 3 S11 versus frequency of various design cases

2.2. Simulation results and discussion

Initially, the design and simulation studies of the proposed basic element has been carried out using HFSS (High Frequency Structure Simulator), then the obtained simulations results are re-validated by CST simulator. The simulation results of the miniaturized single element patch antenna in terms of S_{11}, Voltage Standing Wave Ratio (VSWR), radiation efficiency, gain, directivity, E & H plane radiation patterns, and maximum beam direction are depicted in figure III.4. Figure III.4 (a) shows the S_{11} variation versus frequency. The value obtained by HFSS equals to -18.43 dB with a limited operating bandwidth of 33 MHz, then by CST equals -19.21 dB with a narrow impedance bandwidth of 35 MHz. Although these values are different, they are both less than -10 dB, confirming that both results are good. Figure III.4 (b) illustrates the VSWR versus frequency, the achieved value by using HFSS equals 1.27 whereas by CST, the reported value is 1.21. Both obtained results are less than 2, which confirms that impedance matching is good with minimum mismatch losses. Figure III.4 (c) illustrates the efficiency variation versus frequency. The radiation efficiency achieved via HFSS stands at 98.33%, closely followed by a 98.42% efficiency reported by CST. They are nearly equal, indicating that the basic patch antenna element has high radiation efficiency. Figure III.4 (d) illustrates the gain in dB versus frequency. At the target frequency of 2.4 GHz, the peak gain obtained by HFSS is 7.13 dB, while by CST it is 7.15 dB. Both values are almost identical, confirming consistency. Thus, the basic element offers acceptable gain. Finally, Figures III.4 (e) and (f) depict the radiation patterns in the E and H planes, respectively. Figure III.4 (g) indicates the maximum beam direction, revealing a single fixed beam oriented normal to the antenna's plane. Hence, this antenna is a conventional antenna characterized by a single fixed beam.

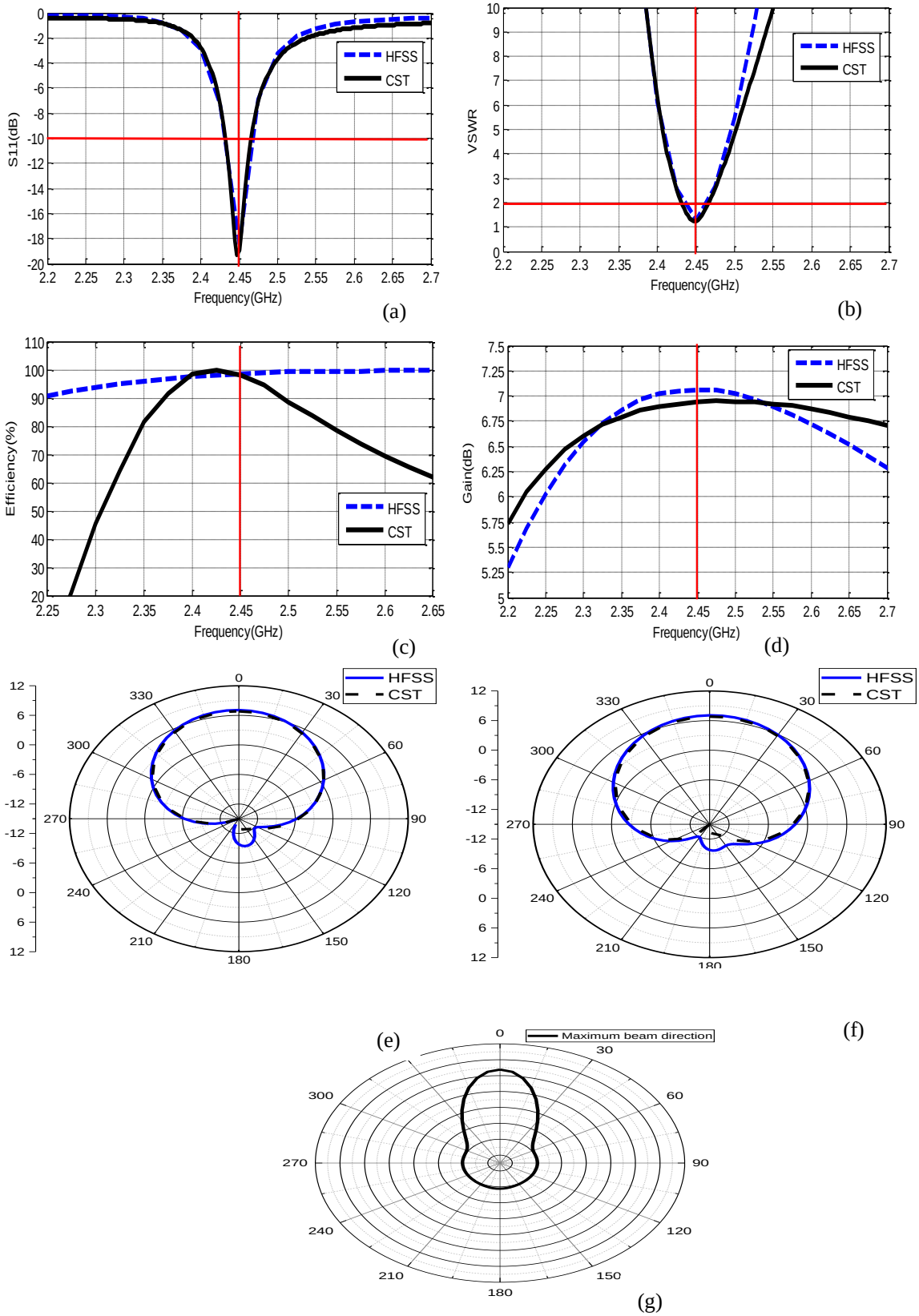

Figure III. 4 Simulation results by HFSS and CST for the proposed basic element antenna. (a): S11 (b): VSWR (c): Efficiency (d): Gain (e): E plane radiation patterns, and (f): H plane radiation patterns., (g) maximum beam direction.

Table III.2 provides a comparison of the simulation results obtained by HFSS and CST of the suggested basic element antenna. As presented in this table, a good radiation performance in terms of reflection coefficient S_{11}, gain, radiation efficiency and a narrow bandwidth has been obtained by using both simulators.

Table III. 2 Summary of simulation results of the proposed antenna.

Simulators	S11 (dB)	Bandwidth (MHz)	VSWR	Gain (dB)	Efficiency (%)
HFSS	−18.43	33	1.27	7.13	98.33
CST	−19.21	35	1.21	7.15	98.42

The performance of the proposed miniaturized antenna has been compared with previous works recommended for ISM band RFID applications, the comparative results are summarized in Table III.3. The presented results clarify that the proposed antenna exhibits a compact size, good gain, and high efficiency. However, it features a single beam, narrow bandwidth, and lacks flexibility. In the next section, we are going to challenge these problems using a 3dB 90° hybrid coupler to fed two identical basic element .

Table III. 3 Performance comparison of the proposed miniaturized antenna with state-of-the-art

Ref.	Frequency (GHz)	Substrate	Size: L×W (mm^2)	Peak gain (dB)	Efficiency (%)
[6]	2.45	Rogers TR5880	82.8×60	7.21	98
[7]	2.4	Rogers TR5880	83×50.5	6.3	-
[10]	2.4	Rogers TR5880	83×50.5	6.32	-
[11]	2.4-2.5	FR4	90×65	5	-
This work	**2.45**	**Rogers TR5880**	**51×50**	**7.11**	**98**

3. Design and simulation of the basic 3dB 90° hybrid coupler

3.1. Theoretical study

The coupler is a four-port passive microwave component that can be used as a power divider or a power combiner. In the case of a lossless symmetric isotropic reciprocal structure, its matrix S is given as follow [5]:

$$[S] = \begin{bmatrix} 0 & S_{12} & S_{13} & 0 \\ S_{12} & 0 & 0 & S_{24} \\ S_{13} & 0 & 0 & S_{34} \\ 0 & S_{24} & S_{34} & 0 \end{bmatrix} \qquad (1)$$

To characterize the performance of a coupler, four main parameters are typically considered: insertion loss (L), isolation (I), coupling factor (C), and directivity (D). These parameters are deduced from the S-matrix, and their expressions are provided by equations 2, 3, 3, and 4, respectively [19].:

$$L = 10log\frac{P_1}{P_2} = -20log|S_{12}|\ dB = -S_{12}\ dB \quad (2)$$

$$C = 10log\frac{P_1}{P_3} = -20log|S_{13}|\ dB = -S_{13}dB \quad (3)$$

$$I = 10log\frac{P_1}{P_4} = -20log|S_{14}|\ dB = -S_{14}\ dB \quad (4)$$

$$D = 10log\frac{P_3}{P_4} = 20log\frac{|S_{13}|}{|S_{14}|}\ dB = S_{13}dB - S_{14}\ dB \quad (5)$$

An ideal coupler has infinite directivity and isolation i.e $S_{14} = 0dB$, indicating that no power is delivered to the isolated port (port 4)

The most popular directional couplers in the literature are 90° and 180° hybrid couplers that provide two outputs with equal amplitude and phase shifted by (90° and 180° respectively). This section is dedicated to the 90° hybrid coupler, for which the scattering matrix is provided in [19][20].

$$[S] = \frac{1}{\sqrt{2}}\begin{bmatrix} 0 & 1 & e^{j\frac{\pi}{2}} & 0 \\ 1 & 0 & 0 & e^{j\frac{\pi}{2}} \\ e^{j\frac{\pi}{2}} & 0 & 0 & 1 \\ 0 & e^{j\frac{\pi}{2}} & 1 & 0 \end{bmatrix} \quad (5)$$

3.2. Design and Simulation Results

The designed microstrip hybrid coupler using High Frequency Simulation Software (HFSS) is shown in Figure III.5. The coupler has a source impedance of $Z_{50} = 50\Omega$ at its shunt arm, and impedance, $\frac{Z_{50}}{\sqrt{2}} = 35.35\ \Omega$ at the series arm.

The numerical equations used to determine the widths and lengths of the parallel and series lines of the coupler are described as follows [21-22]:

$$\frac{W_{50}}{h} = \frac{2}{\pi}\left[B - 1 - \ln(2B-1) + \frac{\varepsilon_{r-1}}{2\varepsilon_r}\left(\ln(B-1) + 0.39 - \frac{0.61}{\varepsilon_r}\right)\right] \quad (6)$$

$$L_{50} = \frac{\lambda_g}{4} \quad (7)$$

where λ_g is the effective wavelength.

As shown in Figure III.5, the structure exhibits symmetry, as indicated by the scattering matrix being equal to its transpose.

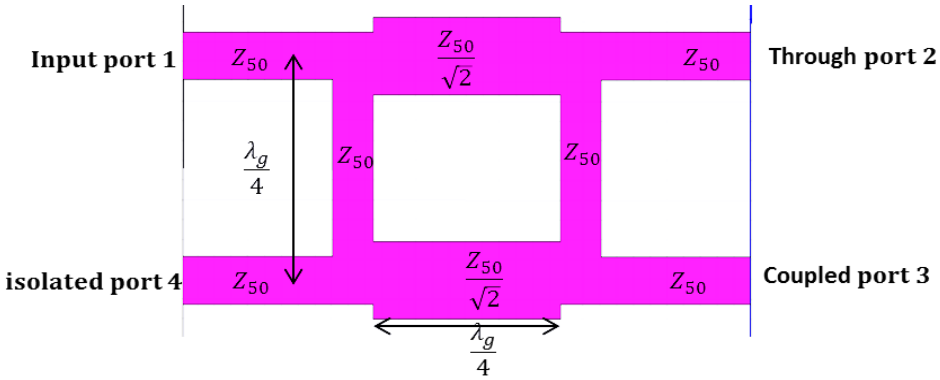

Figure III. 5 Design of microstrip line hybrid directional coupler

The simulated S-parameters of the hybrid directional coupler is shown in Figure III.6. Figure III.6 (a) presents the amplitudes of the parameters S_{11}, S_{12} ,S_{13} and S_{14} versus frequency. $S_{11} = -44.6$ dB, $S_{12} = -3.11$dB, $S_{13} = -3.1$dB, and S_{14} =-37.1 dB values are attained at the operating frequency 2.45 GHz.With these obtained values,the following observations can be concluded for the coupler:

i) Transmission of 99.99% of the power supply to the other ports

ii) Good isolation level (I = -S_{14} = 37dB).

iii) Approximately half of the input power is directed to the coupled port (with a coupling of C = 3.1 dB) and the other half is oriented to the through port (L = S_{12} = 3.11dB)

iv) High degree of directivity with a value of 34dB

v) Large bandwidth of around 1000 MHz for the S_{14} and about 900 MHz for the S_{11}

The phase shift variations of S_{12} and S_{13} parameters are depicted in Figure III.6 (b). A phase shift of approximatively 89.2° between the through and the coupled ports is noticed at the operating frequency. This value is almost equal to the ideal value of 90°. Hence, this coupler can be utilized for designing the multi-beam antenna. Indeed, by switching the power supply between the ports, the radiation pattern will be steerable.

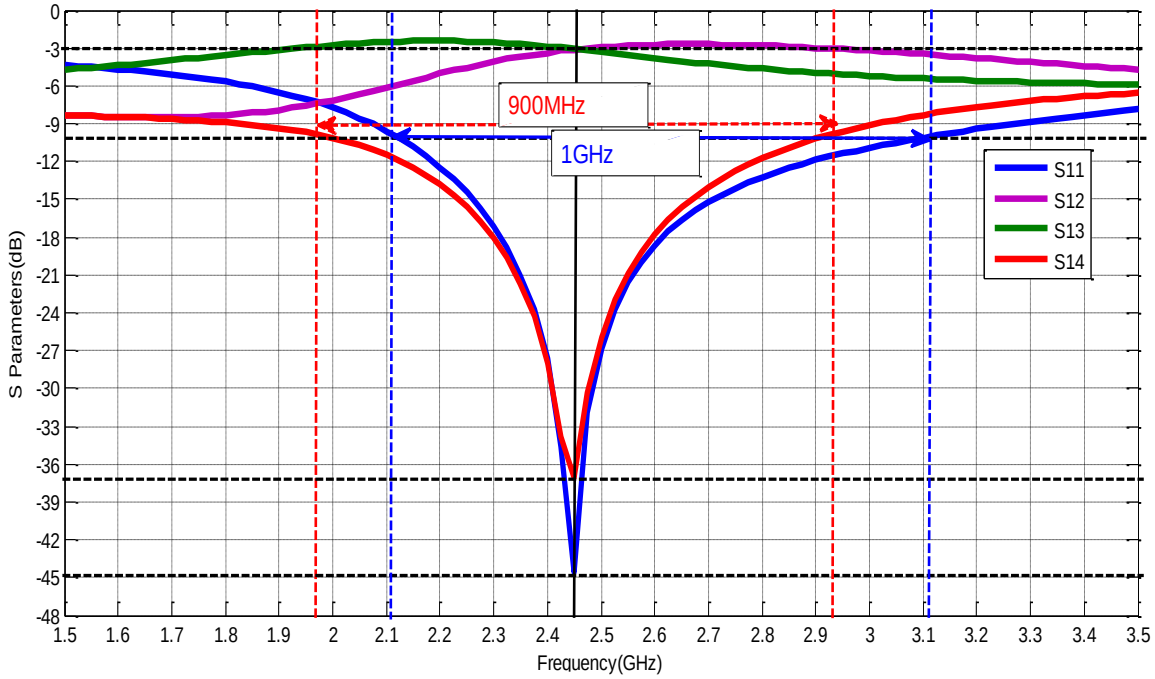

a

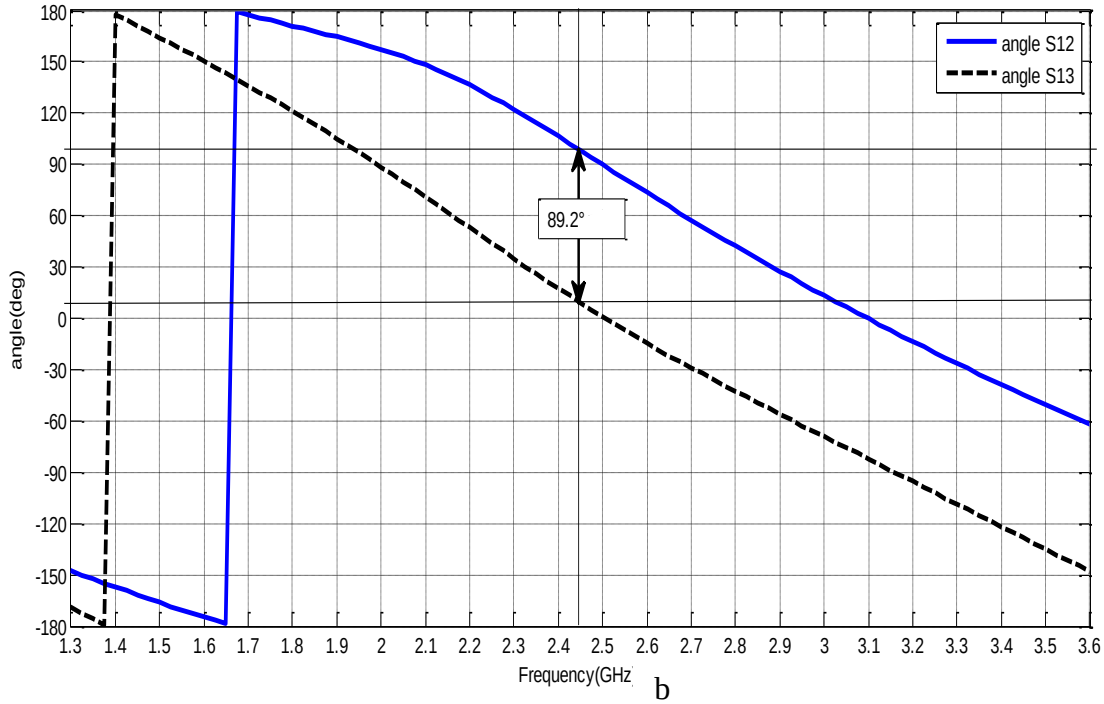

b

Figure III. 6 Magnitude of S11, S12, S13, and S14 parameters (b): phase variations of S12 and S13for the designed hybrid coupler.

4. Design, realization and measurement of the proposed beam switchable broadband 1×2 array antenna

The single-element lacks flexibility i.e sometimes we need to be able to control the antenna radiation pattern for tracking applications. A single antenna element is not adequate to fulfill such

a requirement, therefore, a phased antenna array could be a viable solution to achieve a switched beam antenna This latter could be acomplished by phased antenna fed through a beam former circuit. The simplest beam former circuit is the 90° 3dB hybrid directional coupler that divides the input power into two parts equal in amplitude, with a 90° phase shift. In this section we are going to use the designed coupler to feed a set of two miniaturized elements, this approach aims to transform the array antenna into a beam-reconfigurable system.

4.1. Concept of the switched beam antenna

In this part, we are going to reminde the basic operational principle of a switched beam antenna. Let's consider that there are two elements in the array antenna configuration separated by a distance d and supplied by a beam former circuit that provides the same amplitudes with a phase shift β between them, as presented in Figure III.7. Thanks to the introductionof the phase shift, the radiation pattern would be flexibile and provides an electrically scanned beam in a desired deriction avoiding the mechanical rotation. Thus, the radiation pattern changes its direction creating an angle θ between its maximal direction and the normal to the antenna array. The concept of this scheme is illustrated in Figure III.7.

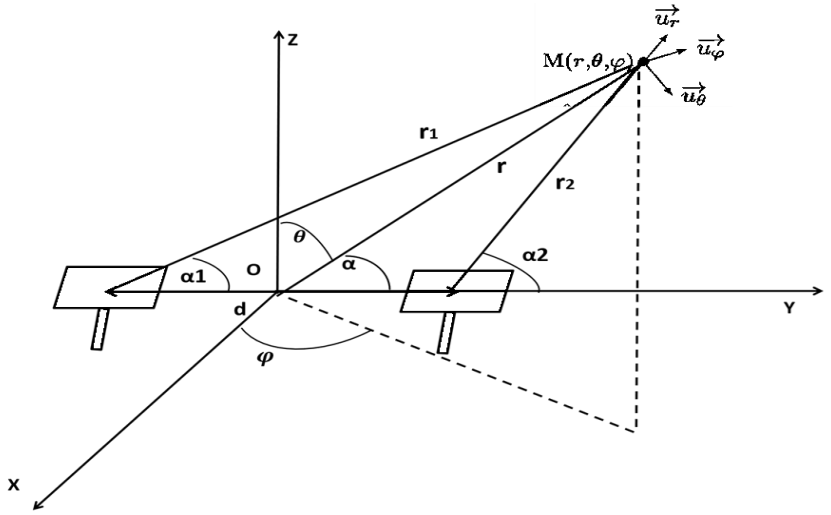

Figure III. 7 Diagram of a phased array antenna comprising two elements

As we have seen in the previous chapter, the modulus of the total field E_T radiated by the two elements is given as follow:

$$E_T = 2.E_0.(\cos(\psi)) \quad (8)$$

With $$\psi = \frac{k.d}{2}\cos(\alpha) - \frac{\beta}{2} \quad (9)$$

The maximum of the total field E_T is at $\psi = 0$

which is $\psi = \frac{k.d}{2}\cos(\alpha) - \frac{\beta}{2} = 0$ (10)

So, $\beta = k.d\cos(\alpha) = k.d\sin(\theta)$ (11)

Thus, $\sin(\theta) = \frac{\lambda.\beta}{2\pi d}$ (12)

Therefore, the direction of maximum radiation can deviate to direction θ given by this equation[21]:

$$\theta = \text{Arcsin}(\frac{\lambda.\beta}{2\pi d}) \quad (13)$$

Where:

θ = the angle between the maximum beam and the normal to the antenna array

λ = wavelength in free space, for operating frequency, fr = 2.45GHz, the value of $\lambda = 122.45mm$

β = the phase shift introduced by the beamformer circuit between the two patches (in the case of coupler as beamformer circuit β =90°).

d = the distance between radiating patch elements

Several performance parameters depend on the value of the distance d. In fact, to achieve optimal gain and directivity, minimal mutual coupling, and a radiation pattern characterized by a single main lobe without grating lobes, the distance between elements must adhere to the condition: λ/4 ≤ d ≤ λ/2 [23-24]. Thus, the optimal value chosen is d = λ/2.

According to the equation (13), the direction θ is a function of λ, β, and d. Since d is constant, The lobe's direction defined by the angle θ is controlled by the two parameters the phase shift, β, and the wavelength (λ). Subsequently, for a given operating frequency, the angle θ is controlled through the phase shift β delivered by the beam former circuit. Based on this principle, the proposed multi-beam antenna works that is discussed in the next section.

The maximum radiation pattern can be controlled by changing the phase shift β delivered by the beamformer circuit.

In the case of coupler as beamformer circuit $\beta = \pm 90°$ allows to obtain the directions of the maximum angular beams θ = ± 30°. The beams can be controlled by switching the supply power between the two ports of the integrated coupler.

4.2. Design and realization of the switched beam antenna

After validating the basic element and the hybrid directional coupler, as well as analyzing the principle of the multi-beam antenna in the preceding sections, the proposed dual-beam 1×2 array antenna has been designed and implemented using HFSS software. Figure III.8 illustrates the

topology of the proposed switched beam antenna. The front and back views of the proposed multi-beam antenna fed by a hybrid directional couple are shown in Figures III.8 (a) and (b), respectively. The prototype of the fabricated antenna is depicted in Figures III.8 (c) and (d). The suggested multi-beam antenna prototype has been fabricated on a 1.56 mm thick Rogers RT/duroid 5880 substrate with a physical area of 112×100 mm^2. The proposed antenna is designed and simulated by using of HFSS software and the prototype has been fabricated to validate the proposed design.

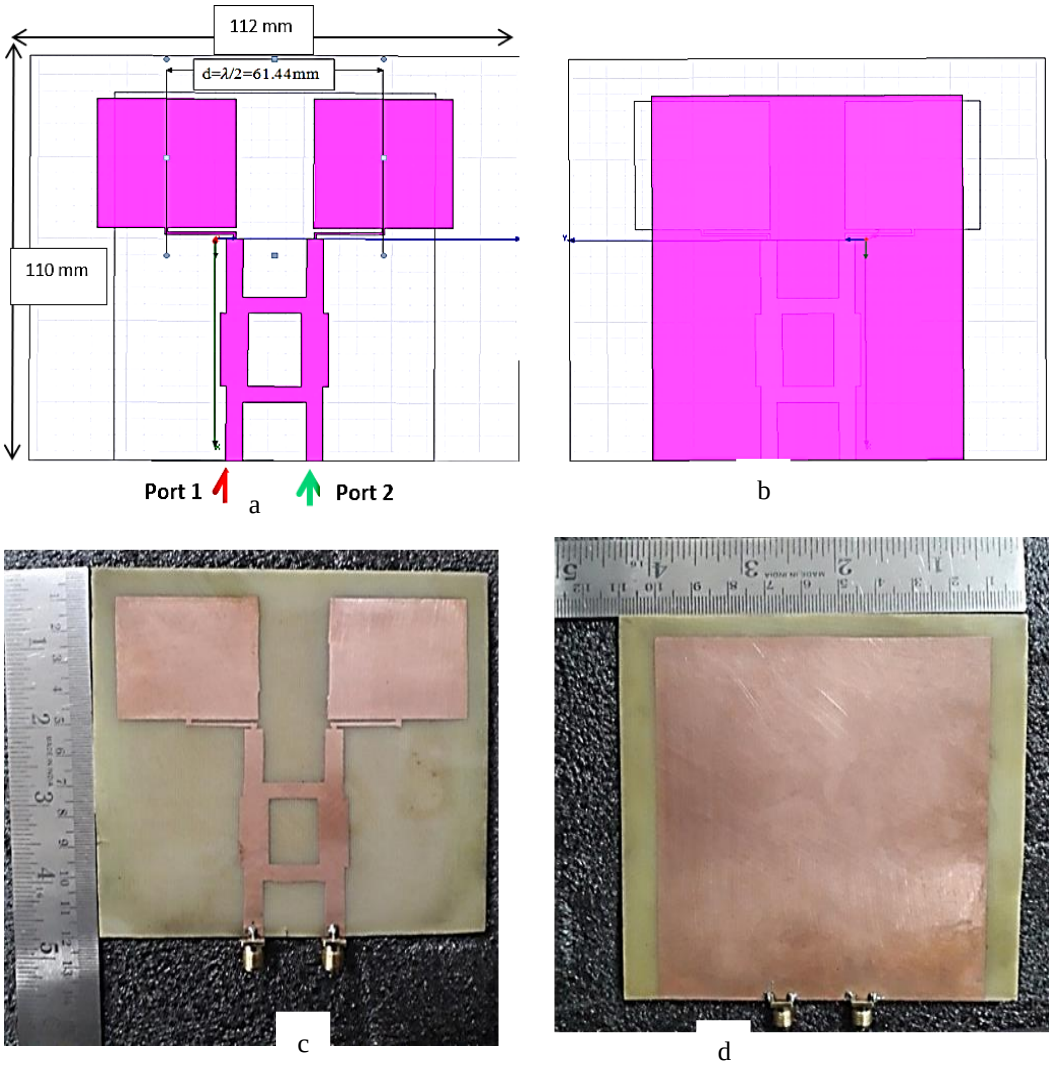

Figure III. 8 The topology of the proposed switched beam antenna: (a) front view, (b) back view, (c) front view of fabricated prototype, and (d) back view of fabricated prototype

4.3. Simulated results versus measured results

In this section, the simulations results are compared with the measurement results through two measurement steps:

(i) 1st step: port 2 is adapted to 50 Ω, and port 1 used as power port. Results are shown in Figure III.9.

(ii) 2nd step: port 1 is adapted to 50 Ω, and port 2 used as power port. Results are shown in Figure III.10.

Figures III.9 (a) and III.10 (a) show the simulation and measurement results of the reflection coefficient (S_{11}), when port 1 and port 2 are activated, respectively. It can be noted that the simulation and measured values show excellent agreement. A wide bandwidth of around 842 MHz (1.958-2.80 GHz) is achieved when port 1 is activated and 844 MHz (1.956-2.80 GHz) when port 2 is activated. At the operating frequency, the value of S_{11} is acceptable; it is equal to −18 dB when the port1 is activated and −16 dB when the port 2 is activated. The simulated and measured gains at the operating frequency (2.45 GHz) by activating port 1 and 2, respectively are illustrated in Figures III.9 (b) and III.10 (b). When port 1 is ON, the simulation results provide a peak gain of 8.84 dB while the measured value reaches 8.5 dB. In case of port 2 is ON, the simulated gain is 8.86 dB and the measured one is 8.46 dB. Figures III.9 (c) and 10 (c) depict the simulated and measured radiation efficiencies at 2.45 GHz in both scenarios.

At 2.45 GHz, when port 1 is activated, the peak radiation efficiency equals to 98.64 % for simulation and about 95 % for measurement. Similarly, when port 2 is activated, the peak efficiency equals is 99.52 % for simulation and about 95.9 % for measurement. These obtained values indicate that the suggested antenna is highly efficient for the intended application band. The directions of the main beam in these two scenarios are represented in Figures III.9 (d) and 10 (d). When port 1 is activated, the beam is directed to the right at approximately 30° from the normal to the antenna plane. Conversely, when port 2 is activated, the beam is directed to the left at approximately -30° from the normal to the antenna plane. The directions of the main beam obtained in simulations are compared to the measured data.

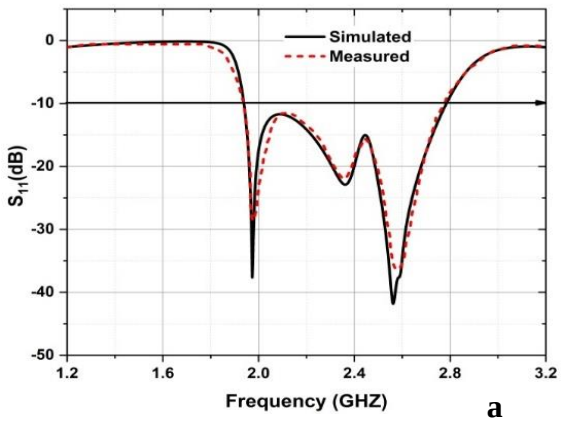

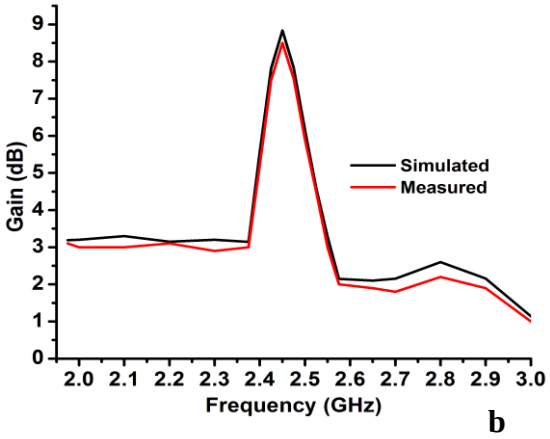

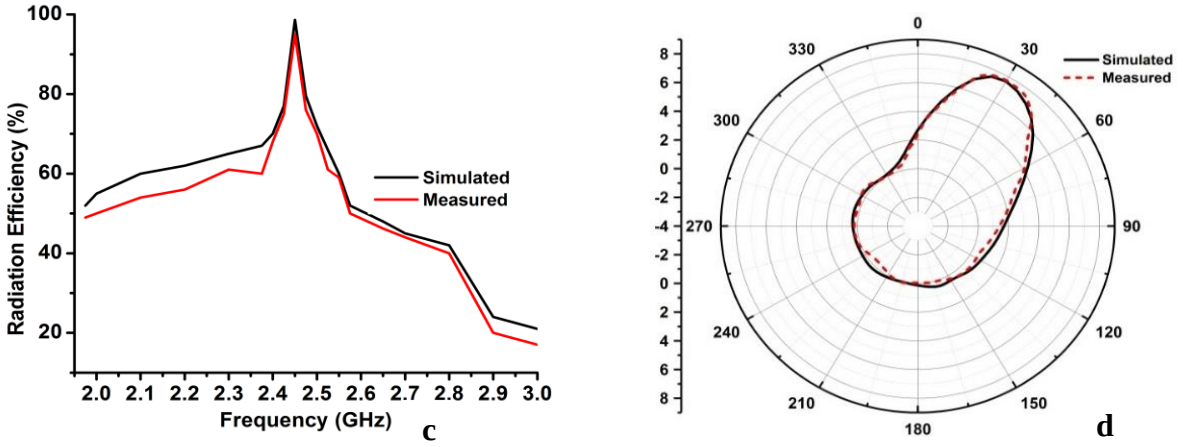

Figure III. 9 Simulated and measured results of the proposed antenna for input port 1 (a): S11Vs. frequency, (b): Gain versus frequency, (c): Radiation efficiency versus frequency, (d): Beam direction

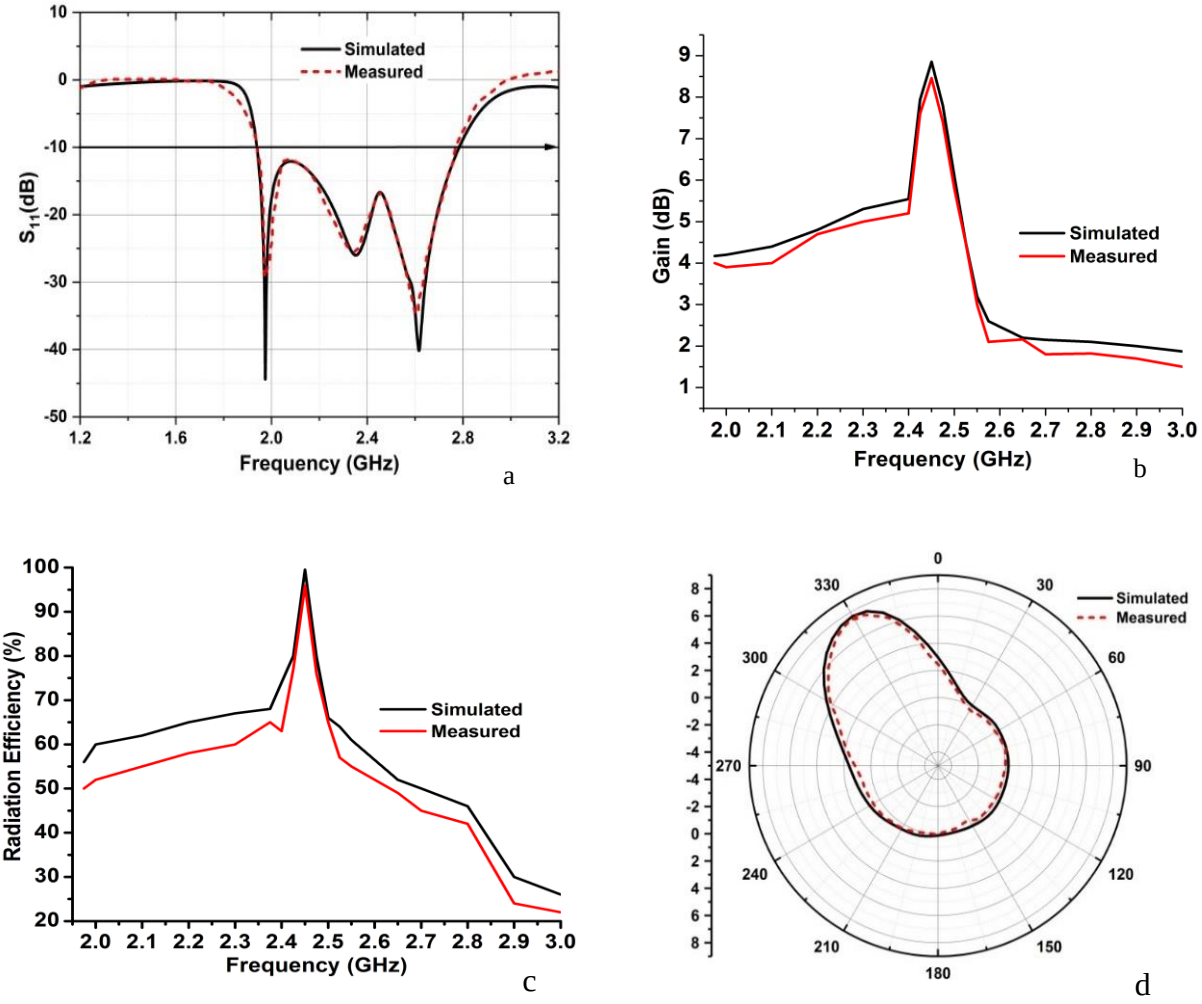

Figure III. 10 Simulated and measured results of the proposed antenna for input port 2 (a): S11 vs. frequency, (b): Gain versus frequency, (c): Radiation efficiency versus frequency, (d): Beam direction, and (e): Radiation pattern.

4.4. Performance comparison analysis

A comparison between the performance of the designed switched beam array antenna and some other antennas for RFID applications in ISM band is summarized in Table III.4. It is evident that the proposed switched beam antenna exhibits optimal size, good gain, high efficiency, broad bandwidth, and beam switching capability.

Table III. 4 Performance comparison of the proposed antenna with other works.

References	Operating Frequency (GHz)	Size (mm2)	Peak gain (dB)	Radiation Efficiency (%)	Bandwidth (MHz)	Beam switching capability
[5]	2.45	80×95	4.66	42.62	88	No
[11]	2.4-2.5	90×65	5	-	115	No
[12]	2.45	96×275	7.95	46	95	No
[13]	2.45	225×225	7.5	-	62	No
[14]	2.45	232.7×78.10	8.36	70	110	No
This work	**2.45**	**110×112**	**8.86**	**99.52**	**844**	**Yes**

5. Hybrid Coupler Integrated 1×4 Printed Array Antenna

5.1. Design and simulation results of the miniaturized 1×2 array antenna

The prime focus of making an array antenna is to enhance the gain, and directivity of the antenna. In this section, we present and discuss a miniaturized 1×2 array antenna fed by a T power divider that can divide the input power into two equal parts in phase at its output ports.

A T-junction power splitter is a microwave circuit made of 3 T-branch transmission lines (see figure III.11). It can be used as a power divider or a power combiner. In this section, it will be used as a 3dB power divider that splits the power feed into two equal- in-phase output signals.

The design of proposed the microstrip T-network power splitter is presented in figure III.11. It has an input impedance $Z_0 = 50\Omega$ (Its length is L_f and its width is W_f) and output impedances $Z_1 = Z_2 = 100\ \Omega$ (Its length is L_T and width is W_T)

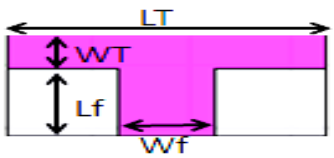

Figure III. 11 design of T power divider

The analytical equation that allows the switching between impedance and its width of each arm was presented in the previous chapter.

A parametric study on the lengths L_f and L_T are performed to obtain the desired values S_{12} =S_{13} =-3dB in phase. The reached parameters of the T power divider are: $W_T = 2.78mm$, $W_f = 4.48mm$, $L_T = 16.11mm$, $L_f = 5.4mm$

The simulation results in terms of scattering parameters S_{11}, S_{12} and S_{13} versus frequency are depicted in Figures III.12. Figure III.12 (a) presents magnitudes of the S-parameters and (b) their phases. As it can be seen, for the aimed frequency 2.45GHz, the reflection coefficient (S_{11}) is -11dB, while the coupling coefficients (S_{12} and S_{13}) are both -3.36dB. Furthermore, the phases of S_{12} (-49.86°) and S_{13} (-49.88°) remain nearly identical across all frequencies.

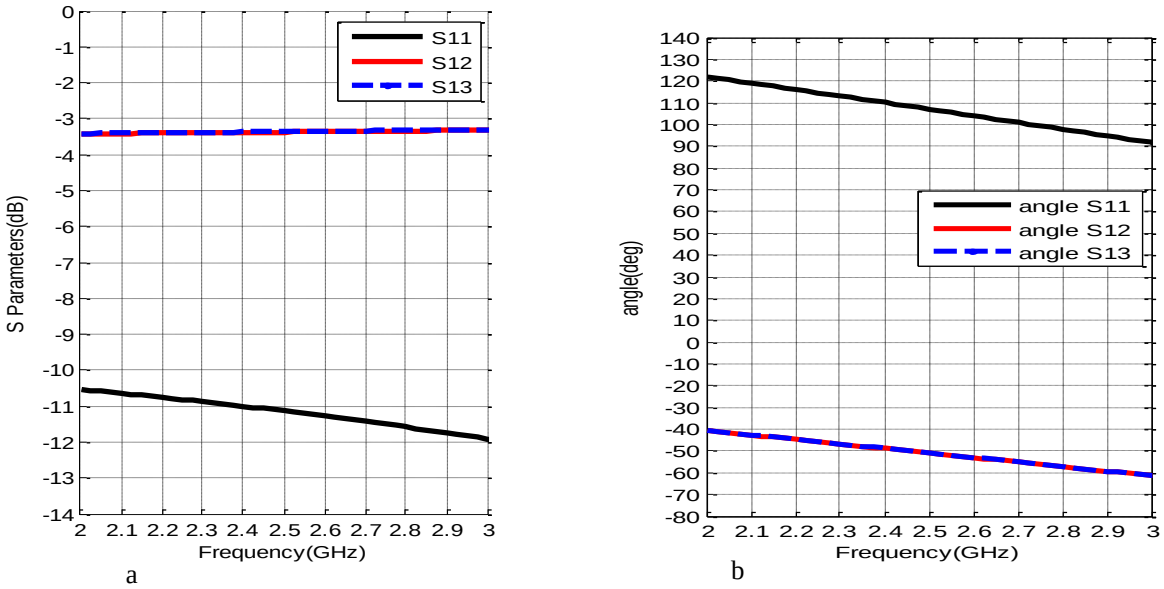

Figure III. 12 Scattering parameters S11, S12 and S13. (a): magnitude versus frequency (b): angles in degrees versus frequency.

Figure III.13 shows the suggested miniaturized 1×2 antenna array, consisting of two identical miniaturized elements powered by T-shaped network power splitter. The dimensions of the suggested miniaturized structure are summarized in Table III.5 .

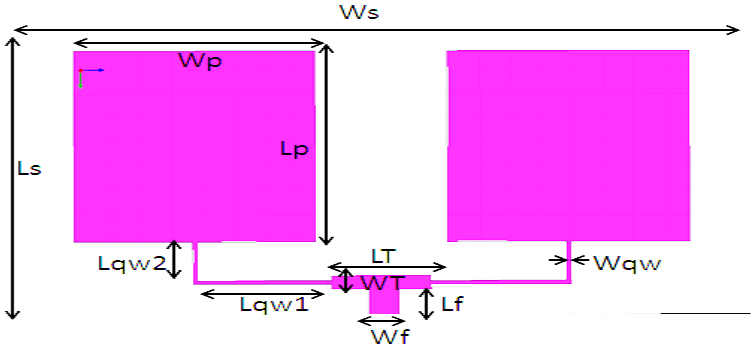

Figure III. 13 Proposed miniaturized 1×2 array antenna.

Table III. 5 parameters of the proposed miniaturized 1×2 array antenna

Parameters	Ls	Ws	Lp	Wp	Lqw1	Lqw2	Wqw	Lf	Wf	LT	WT
Value (mm)	66	120	39.42	39.28	21.13	4	0.74	5.4	4.48	2.78	16.11

The simulation results obtained by HFSS software for the proposed miniaturized 1×2 array antenna in terms of S_{11} parameter, VSWR, efficiency, gain, directivity, principal E and H plane radiation patterns, and the maximum beam direction are presented in Figure III.14.

- It is illustrated in igure 14 (a) that the S_{11} parameter reaches to 27.17 dB at the resonant frequency 2.45GHz, and an impedance bandwidth of about 50 MHz.
- Figure III.14 (b) presents the VSWR's variations versus frequency, its value is equal to 1.09 at the resonant frequency which indicates perfect impedance matching, hence the proposed structure is very well matched.
- Figure III.14 (c) depicts the radiation efficiency versus frequency. it reaches 98.15% at the operating frequency. This implies that our miniaturized array antenna radiates 98.15% of its supplied power. So, it is almost an ideal antenna.
- Figure III.14 (d) shows plot of gain and directivity versus frequency. The peak gain of the antenna is about 9.42 dB at 2.45GHz indicating an improvement in gain of 2.31 dB compared to the basic antenna. The peak directivity equals to 9.52 dB showing an increase of 2.33dB compared to the basic antenna. Hence, the array antenna is more directional than the basic element,
- Figure III.14 (e) displays the radiation patterns in two principal planes (E and H planes) for the proposed 1×2 array antenna at the operating frequency. The radiation pattern in H-plane appears different as compared to the basic element.
- Figure III.14 (f) shows the maximum beam direction. There is revealing a single fixed beam oriented in the direction perpendicular to the array antenna plane.

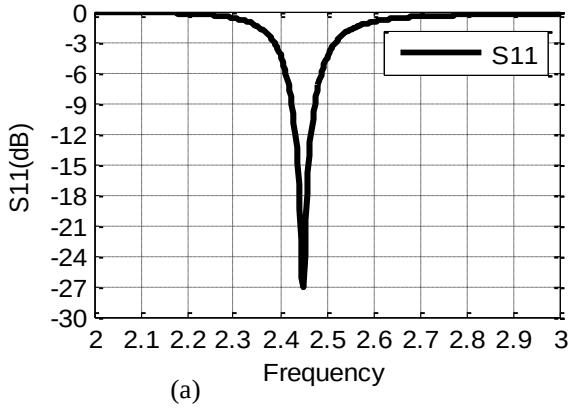

(a)

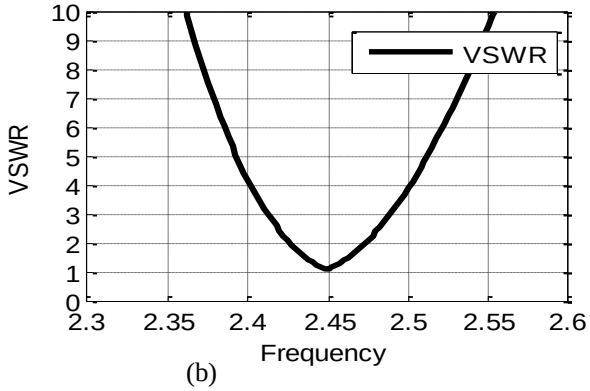

(b)

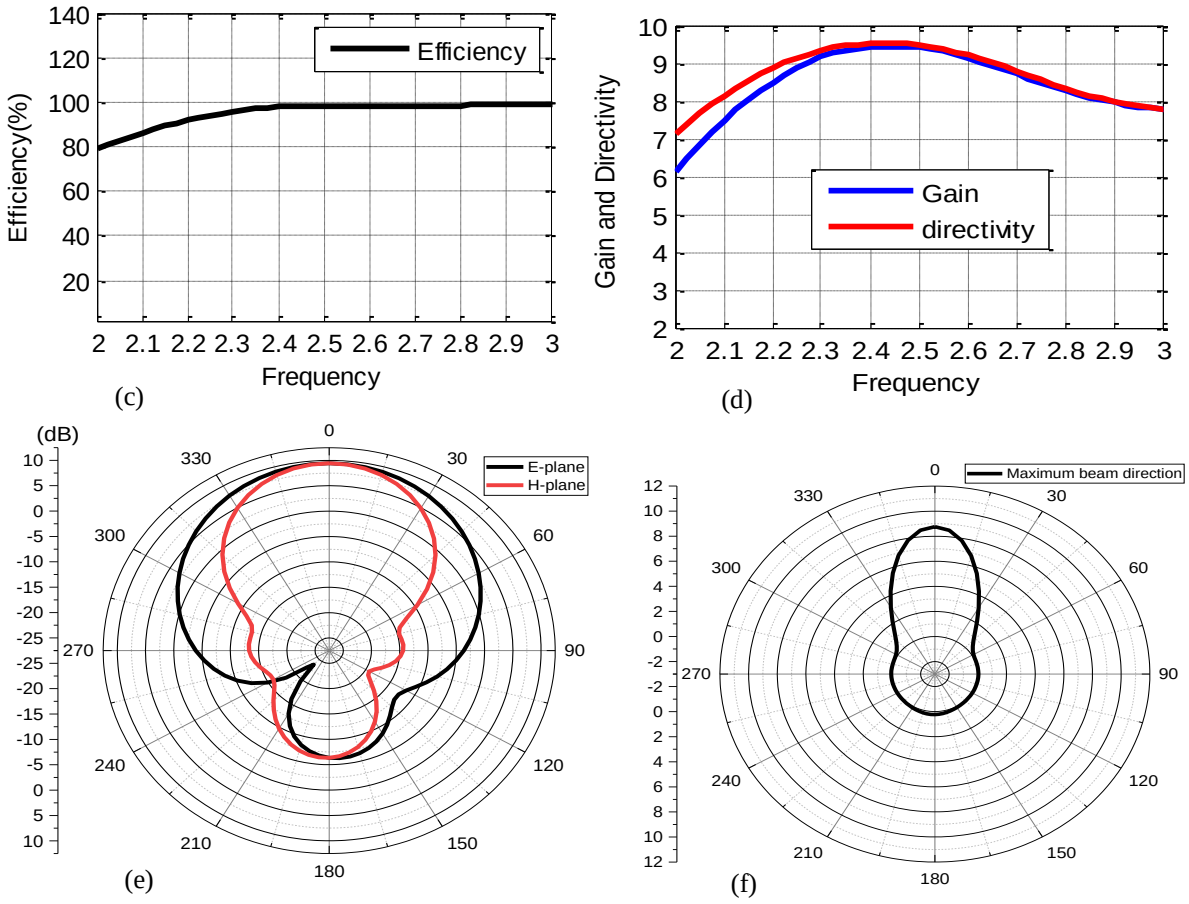

Figure III. 14 Characteristic parameters of the 1×2 array antenna fed by T power divider (a): S11, (b): VSWR, (c): Efficiency, (d): Gain and Directivity, (e): E and H plane radiation patterns, (f): maximum beam direction

Table III. 6 Summary of simulation results of proposed the miniaturized 1×2 array antenna

Parameters	S11	VSWR	Bandwidth	Gain	Directivity	Efficiency
Value	-27dB	1.095	50 MHz	9.42dB	9.51dB	98.15%

A comparison between the 1×2 array antenna with others published works has been analyzed. As shown in Table III.7, the proposed antenna stands out as the smallest one with good gain and high efficiency.

Table III. 7 Comparison of the proposed 1×2-array antenna with other works

References	Array	Frequency (GHz)	Substrate	Size (mm^2)	Peak gain (dB)	Efficiency (%)
[5]	1×2	2.45	Rogers TR5880	114×135	9.65	99
[7]	1×2	2.40	Rogers TR5880	83×110.5	9.22	-
This work	**1×2**	**2.45**	**Rogers TR5880**	**66×120**	**9.42**	**98.5**

5.2. Geometry and simulation of the hybrid coupler fed 1x4 array antenna

Although the designed 1x2 array antenna discussed in the previous section has a high gain and high efficiency, it suffers from the narrow bandwidth and inflexibility particularly concerning beamforming capabilities. In this section, these limitations are addressed and resolved with optimized performance. Indeed, a hybrid coupler is used to feed two pieces of the miniaturized 1x2 array antenna (Adhering to the condition $\lambda/4 \leq d \leq \lambda/2$ [23-24], the optimal value of $d = \lambda / 2$ is employed to ensure a minimal mutual coupling between elements and grating lobes are avoided as well). This 3 dB hybrid coupler can divide the input power in two equal quantities at their two outputs ports, while making a phase shift of +-90° between them. Thanks to the phase shift, the array antenna became flexible (can radiate in two different directions +30° & -30°) having a broadband, high gain and high radiation efficiency.

The layout of the designed and fabricated proposed broadband array antenna is shown in Figure III.15.

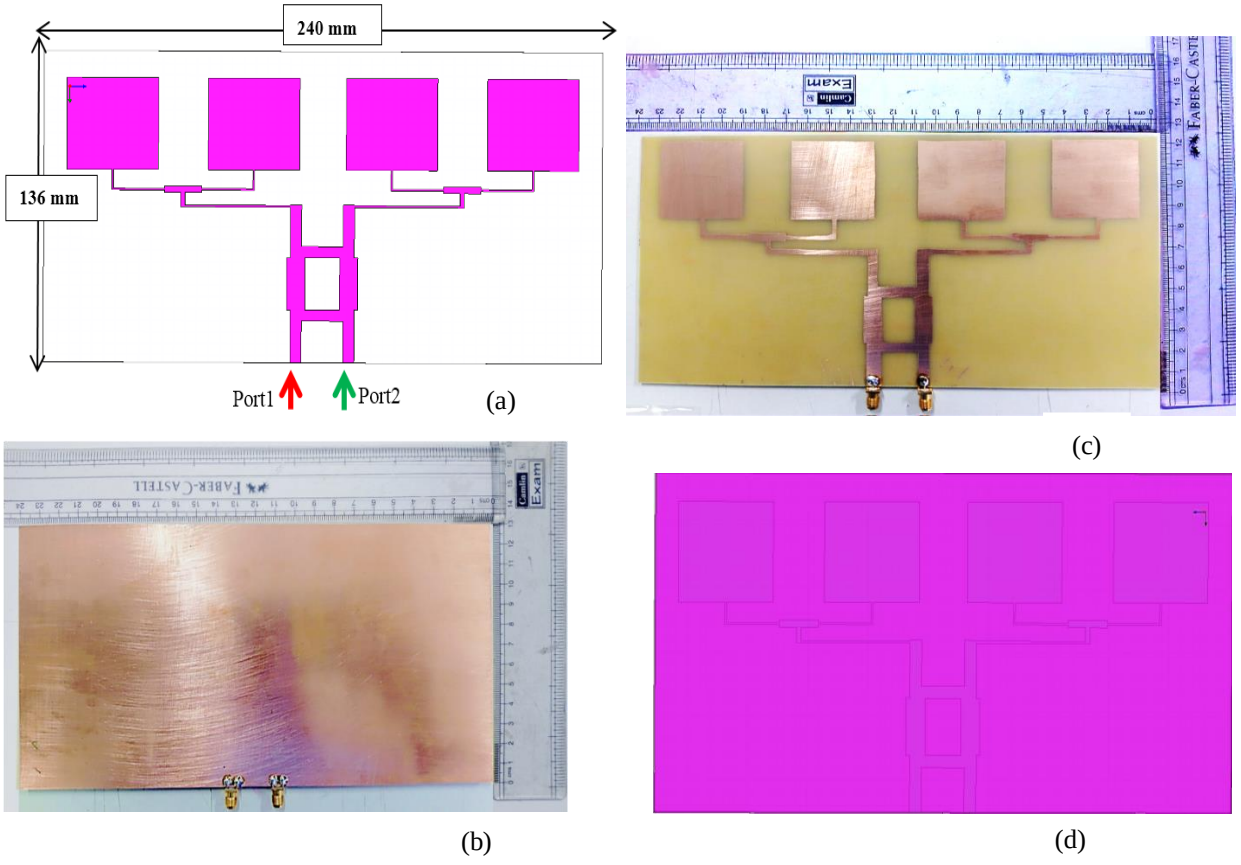

Figure III. 15 Design and fabricated prototype of the proposed 3dB hybrid coupler feeding 1x4 array antenna, (a) and (b): front view, (c) and (d): back view.

5.2.1. Simulation versus measurement results

Initially the design and simulation results of the proposed broadband antenna are conducted by using the HFSS. Then, the simulation results are validated by measurements. Both results are in good agreement as shown in figures III.15,16 and table III.8.

There are two studied scenarios: when port1 is fed and then when port 2 is fed.

a) Results when port 1 is activated:

Figures III.**15 (a)** displays the variations of voltage standing wave ratio (VSWR) when port1 of hybrid coupler feed is fed. It can be noted that there is a good agreement between the results of simulation and measures. The reported result signifies a wide bandwidth of about 1.25GHz (1.725-2.96 GHz). Moreover, the VSWR of 1.023 and 1.22 are attained at the operating frequency by HFSS, and measurment, respectively.

Figure III.15 **(b)** illustrates the directivity versus frequency obtained by simulation and measurment. It is noted that there is an agreement between both results. At the operating frequency is 2.45GHz, the gain reaches its maximum value of 11.54 dB by simulation and 11.38dB by measurment.

Figure III.15 (c) shows the simulated and measured gain as fonction of frequency. It is noted that there is an agreement between both results. At the operating frequency 2.45GHz, the gain reaches its maximum value of about 11.27 dB as obtained by simulation and 11.18dB by mesurment.

Figures III.15 (d) and (e) show the maximum beam direction in 2D and 3D radiation patterns obtained at the operation frequency. According to the results, the main beam is oriented towards 30° right direction at a plane normal to the axis of the antenna. Both simulation and measurement show the same direction of the maximum radiated beam.

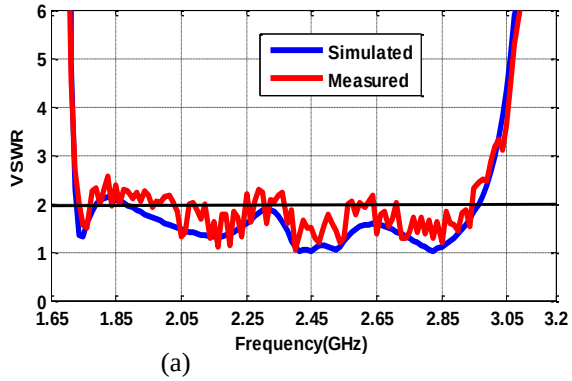

(a)

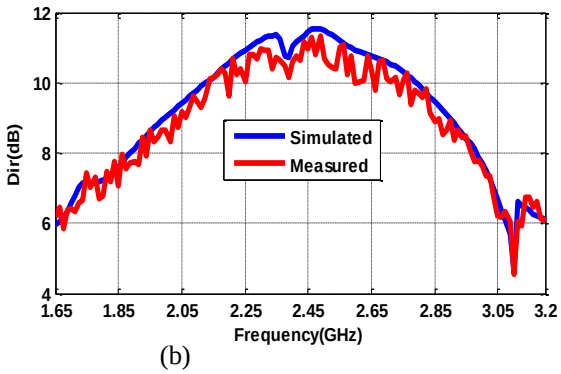

(b)

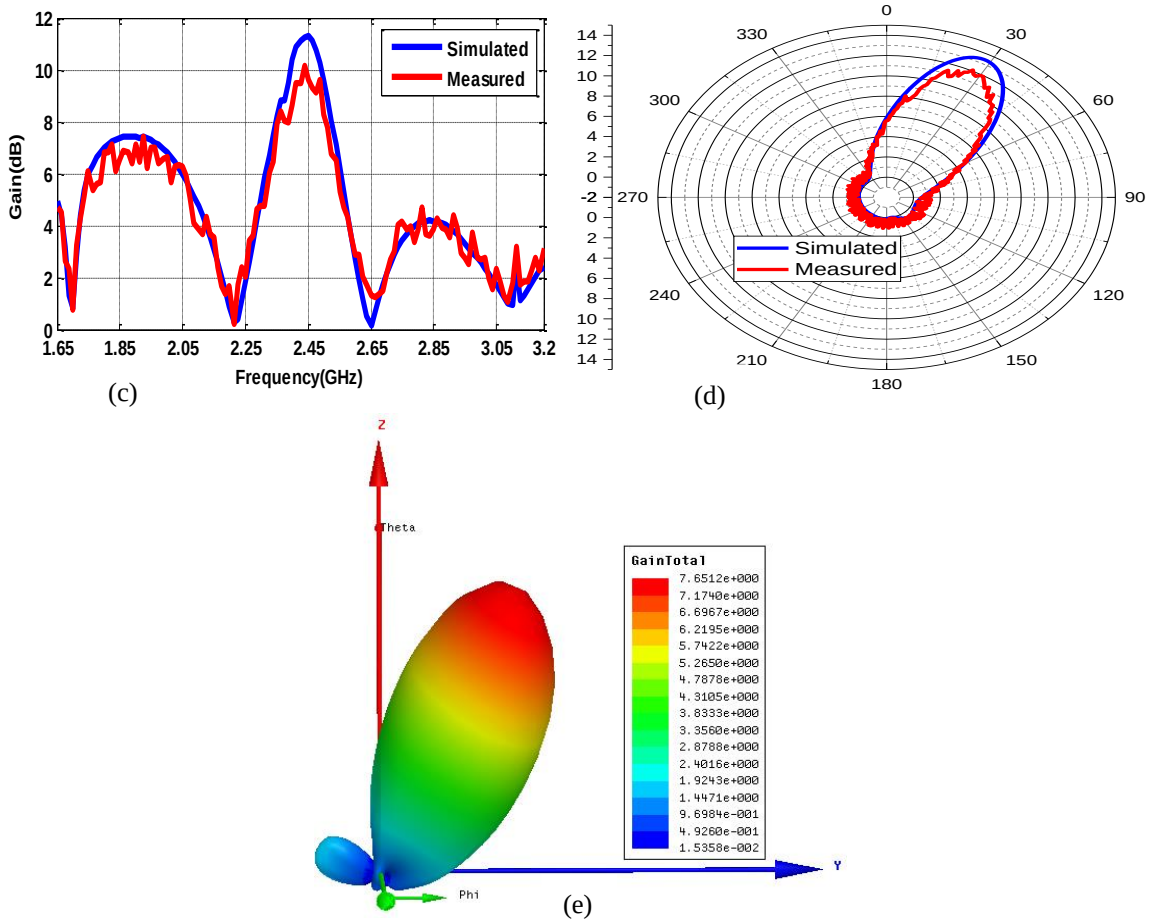

Figure III. 16 Simulated and measured results of the proposed antenna when input port 1 is powered (a): VSWR (b): Directivity, (c): Gain, (d): Maximum beam direction in 2D radiation pattern, (e): Maximum beam direction in 3D radiation pattern.

b) Results when port 2 is activated:

In this section, the results are reported by both simulation and measurements to investigate the characteristic parameters by exciting port 2 of the coupler.

The result of voltage standing wave ratio (VSWR) is depicted in **Figure III.16 (a),** when port 2 is activated. It can be noted that there is close agreement between the results obtained by the simulator HFSS and by measurment. The findings suggest a wide bandwidth of about 1.25GHz (1.725-2.96 GHz). At the operating frequency, the value of VSWR is equal to 1.48 by HFSS, then 1.38 by measurment, showing a good impedance matching.

Figure III.16 (b) shows the obtained simulated and measured directivity versus frequency. The maximum peak directivity obtained at the resonant frequency 2.45 GHz is 11.46 dB by simulation while 11.36 dB by measurment.

Figure III.16 (c) shows the obtained simulated and measured gain versus frequency . It is observed that there is an agreement between both results. At the operating frequency 2.45GHz, the gain reaches its maximum value equals about 11.21dB by HFSS and 11.16dB by measurment.

Figure III.16 (d) and (e) show the maximum beam direction in 2D and 3D radiation patterns at the operating frequency. The maximum beam is focused at -30° direction with respect to a plane normal to the axis of the multibeam patch antenna. Both simulation and measurement results indicate the same direction (-30°) of the main beam for the proposed array antenna.

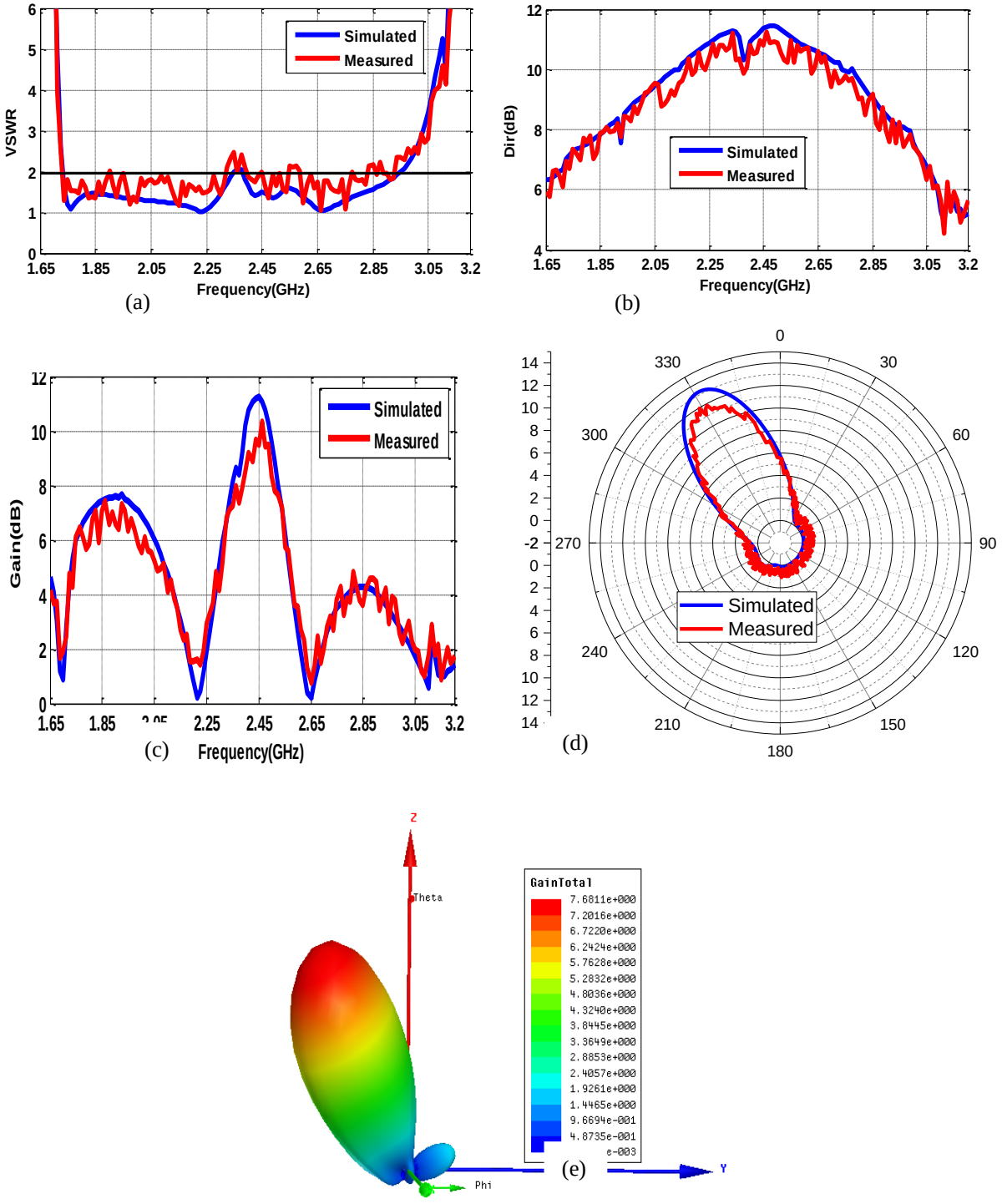

Figure III. 17 Simulated and measured results of the proposed antenna when input port 2 is powered (a): VSWR (b): Directivity, (c): Gain, (d): Maximum beam direction in 2D radiation pattern, (e): Maximum beam direction in 3D radiation pattern.

Table III. 8 Summary of simulated versus measured results of proposed switched directional antenna.

	Results	bandwidth	VSWR	Gain	Dirictivity	Maximum beam direction
When port 1 is fed	Simulated	1.25GHz (1.725-2.96 GHz)	1.023	11.27 dB	11.54 dB	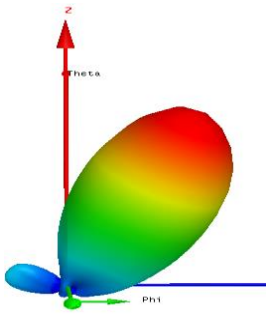
	Measured		1.22	11.18 dB	11.38dB	
When port 2 is fed	Simulated	1.25GHz (1.725-2.96 GHz)	1.48	11.21dB	11.46 dB	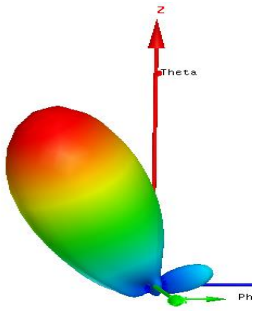
	Measured		1.38	11.16dB	11.36 dB	

5.2.2. Comparative analysis with some other published works

The performance of the proposed beam-switching, high gain broadband printed array antenna has been evaluated and compared with some other works as illustrated in Table III.9. It is clear that the proposed antenna has the widest bandwidth, the highest gain, and the highest efficiency, in addition to its capability of beam switching that justifies a high coverture.

Table III. 9 Performance comparison of the proposed dual-beam array antenna with previous works.

References	Operating Frequency (GHz)	Size (mm2)	Peak gain (dB)	Radiation Efficiency (%)	Bandwidth (GHz)	Beam switching capability
[5]	2.45	80×95	4.66	42.62	0.088	No
[11]	2.4-2.5	90×65	5	-	0.115	No
[12]	2.45	96×275	7.95	46	0.095	No
[13]	2.45	225×225	7.5	-	0.062	No
[14]	2.45	232.7×78.10	8.36	70	0.110	No
[25]	2.45	110×112	8.86	99.52	0.844	Yes
This work	**2.45**	**136x240**	**11.23**	**99.4**	**1.25**	**Yes**

6. Conclusion

In this chapter a dual-beam switched planar array antenna based on hybrid coupler was designed for ISM band RFID reader applications at 2.45 GHz. A novel concept of a pleated quarter-wavelength impedance transformer (PQWIT) has been implemented for impedance matching and area miniaturization of the patch element. The miniaturized patch is considered as radiating elements for designing the proposed beam switchable 1×2, 1x4 phased array antennas feed by a hybrid coupler. All the simulation studies of the basic patch element, hybrid coupler, and proposed switchable 1×2, 1x4 array antennas are performed using HFSS software. The obtained simulation results for the proposed 1x2 dual-beam switchable antenna are verified through the measurement of the fabricated prototype. for the simulation results obtained for the proposed 1x4 dual-beam switchable antenna are verified through measurments as well . The suggested array antennas offer a high gain, high directivity, high radiation efficiency, a broadband impedance bandwidth and a large coverture due to its multi-beam features that makes it preferable to detect the objects in motion. This antenna is dedicated to RIFD reader that operates in the ISM band.

References

1. Paret, D., RFID at Ultra and Super High Frequencies Theory and Application, 2nd Edition, Wiley, United Kingdom, 2009.
2. PARET, Dominique. RFID en ultra et super hautes fréquences: UHF-SHF: Théorie et mise en oeuvre. Dunod, 2008, ISBN 972 2 10 049347 0.
3. B. Aghoutane, S. Das, H El Faylali, B.T.P. Madhav, M El Ghzaoui, Ali El Alami, Analysis, design and fabrication of a square slot loaded (SLL) milimeter wave patch antenna array for 5G applications, Journal of Circuits, Systems, and Computers, Vol. 30, No.5, 2150086 (2021)
4. S. Lakrit, H. Ammor, S.Matah, J. Terhzaz, and A. Tribak, Study and design of single and double layer square patch antennas for UWB applications, Journal of Circuits, Systems and Computers, Vol. 28, 1950233, 2019.
5. TabakhIkram, Mohammed Jorio, and Najiba El Amrani El Idrissi. "1x2 RFID reader array antenna for narrowband indoor positioning applications" Journal of Engineering Science and Technology Review 12.6 (2019): 167-172.
6. Ikram. T, El Idrissi. N. E. A., Jorio, M., &Slimani, A. (2017, April). A high gain 1* 2 array RFID reader MPA for indoor localization applications. In 2017 International Conference on Wireless Technologies, Embedded and Intelligent Systems (WITS) (pp. 1-6). IEEE.
7. El Alami. A., Ghazaoui,.Y., Das. S., Bennani S. D., & El Ghzaoui. M. (2019). Design and simulation of RFID array antenna 2x1 for detection system of objects or living things in motion. Procedia Computer Science, 151, 1010-1015.
8. PRZESMYCKI, Rafal, BUGAJ, Marek, et NOWOSIELSKI, Leszek. Broadband microstrip antenna for 5g wireless systems operating at 28 ghz. Electronics, 2021, vol. 10, no 1, p. 1.
9. Bendali.A., El Fellahi.A., Srifi. M. N., Bri. S., &Habibi. M. (2018, November). A Novel Adaptive Array Antenna for a RFID Applications. In 2018 International Symposium on Advanced Electrical and Communication Technologies (ISAECT) (pp. 1-5). IEEE.
10. El Alami.A., Das. S., Madhav. B. T. P., & Bennani. S. D. (2019). Design, optimization and realization of high gain RFID array antenna 4× 1 for detection system of objects in motion. Journal of Instrumentation, 14(05), P05002.
11. LU, KueiJih, NGUYEN, Tuan, TRAN, Nghi, et al. Parasitic spirals for enhancing bandwidth of a simultaneous transmit and receive patch antenna. Microsystem Technologies, 2021, vol. 27, no 9, p. 3333-3338..
12. I. Tabakh, S. Das, M. Jorio, N. El Amrani El Idrissi, S. Mohapatra, D. Barad "Defected Ground Structure (DGS) Incorporated RFID Reader Antenna Array for Indoor Positioning Systems at 2.45 GHz."International journal of microwave and optical technology, Vol.15, No.6, pp. 517-524, 2020.
13. Abu, M., Masrom, N., Hussin, E. E., Othman, A. R., Yatim, N. M., Johar, F. M., & Munawar, R. F. (2012, December). 2.45 GHz RFID reader array antenna with hexagonal geometry arrangement. In 2012 IEEE Asia-Pacific Conference on Applied Electromagnetics (APACE) (pp. 338-341). IEEE.
14. Ouazzani, O., S. D. Bennani, and M. Jorio. "Design and simulation of 2*1 and 4*1 array antenna for detection system of objects or living things in motion." 2017 International Conference on Wireless Technologies, Embedded and Intelligent Systems (WITS). 19-20 April, 2017, pp. 1-5.

15. Billal Aslam, Muhammad Kashif, Yasar Amin, Hannu Tenhunen, “Low-profile magnetically coupled dual resonance patch antenna for UHF RFID applications”, AEU - International Journal of Electronics and Communications, Volume 133, 2021, 153672
16. Sudhir Bhaskar, Amit Kumar Singh, “Meandered cross-shaped slot circularly polarised antenna for handheld UHF RFID reader”, AEU - International Journal of Electronics and Communications, Volume 100, February 2019, Pages 106-113
17. J.N.Lin, N.N.Wang, T.Y.Du, “A Near-Field focused planar microstrip array for 2.4 GHz RFID readers”, Proceedings of ISAP,Okinawa, Japan, pp. 758-759,October 24-28, 2016.
18. Tanmay Kumar Das, Biswajit Dwivedy, Santanu Kumar Behera, “Design of a meandered line microstrip antenna with a slotted ground plane for RFID applications”, AEU - International Journal of Electronics and Communications, Volume 118, May 2020, 153130
19. Pozar, David M. Microwave engineering. New York: John Wiley & Sons, 2011.
20. Helszajn, J., & McKay, M. (2018). 0°, 90°, and 180° Passive Power Dividers. Microwave Polarizers, Power Dividers, Phase Shifters, Circulators, and Switches, 301. UK: Wiley-IEEE Press.
21. Huang, Yi, and Kevin Boyle. Antennas: from theory to practice. UK: John Wiley & Sons, 2008.
22. Ahmed Fatthi Alsager, “Design and Analysis of Microstrip Patch Antenna Arrays”,Universitym College of Boras School of Engineering, SE501 90 BORÅ.
23. PICON, Odile, CIRIO, Laurent, RIPOLL, Christian, et al. Les antennes: Théorie, conception et applications. Dunod Paris, ISBN 978- 2-10-054245-1, 2009.
24. SLIMANI, A., BENNANI, S. D., ALAMI, A. Effect of inter-elements distance and phase shift excitation on radiation performance of linear, planar and circular arrays antennas□. In : 2017 International Conference on Wireless Technologies, Embedded and Intelligent Systems (WITS). IEEE, 2017. p. 1-7.
25. Abdelaaziz El Ansari et al., Design and Realization of a broadband multi-beam 1 × 2 array antenna based on 2 × 2 Butler Matrix for 2.45 GHz RFID Reader Applications, Journal of Circuits, Systems, and Computers, doi: 10.1142/S0218126622503054.

Chapter IV: A Four-Beams Array antenna Based on a New Beamformer Circuit For ISM Band Aplications

1.Introduction

In wireless communication systems, the antenna is an essential component for data transmission and reception. Over the past decade, the most widely used antennas have been conventional antennas that radiate energy in one direction [1-5] making them limited in terms of radiation area coverage. Currently, the most sought-after antennas are those that are flexible and capable of radiating energy in various directions. For certain applications, such as object tracking, precise control of the antenna's radiation pattern is essential. Radiation paterns control can be achieved by using a multibeam antenna [6-7].

A multibeam antenna is a reconfigurable antenna that radiates energy in many directions to increase area coverage. It can be used for satellites, radars or base stations (BTS) applications to replace the sector antenna. To achieve a multi-beam antenna, a switched network beamformer must feed an array antenna. This beamformer circuit could be either Lens-based beamformer (e.g Rotman [8-9], Bootlace[9-10] or Luneburg [11-12] lens), or beamformer-based Hybrid couplers(e.g Blass Matrix [13], Nolen Matrix [14] or Matrix Butler [15-25]. The Matrix Butler which, thanks to its parallel power supply, is becoming the most popular beam-forming circuit. However, it suffers from the weakness of crossovers, particularly in microstrip technology. A crossover occurs when two microstip transmission lines cross. This intersection increases signal interference, degrades the SNR (signal-to-noise ratio), causes circuit malfunction and leads to unpredictable device behavior. Many researchers have suggested solutions to this Weakness, such as two 0 dB coupler based on a Butler matrix [16-17], a hybrid 0 dB coupler based on a Butler matrix [18], a pleated configuration based on a Butler matrix [19], a double-layer substrate based on a Butler matrix [20] and SIW (substrate-integrated waveguide) technology based on a Butler matrix [21].

Thus, in this chapter, we'll suggest a new beamformer circuit, that provides four beams in four different directions without using crossovers. The suggested beamformer could replace the Butler matrix 4x4 thanks to its small size, simple design, easy fabrication and incredible results.

Moroever, in this chapter we will propose another solution to this weak point of the Butler matrix to compensate for its crossover vulnerability. The proposed solution is an ultra-wideband, reconfigurable microstrip crossover. Thanks to the incredible results that presents and its flexibilty, the proposed crossover could be used not only for the Butler matrix for beamforming purposes,

but is also dedecated to phased array antennas, reconfigurable antennas, MIMO antenna, reconfigurable filters…etc to control the power fed into the desired port(s).

After this introduction, the following sections of this chapter will be as follows: section 2 explains the concept of the switched-beam antenna. Section 3 shows the vulnerability of the Butler matrix. Section 4 exhibits the proposed 4x4 beamformer. Section 5 presents the four-beams antenna based on the proposed 4x4 beamformer. Section 6 exihibtes the ultra-wideband reconfigurable microstrip crossover, and the last section concludes this chapter.

2. Switched-beam antenna concept

Typpically, a phased array antenna lacks flexibility i.e we sometimes need to be able to control the antenna radiation pattern for tracking devices. An array antenna is therefore not enough to meet this requirement. Thus, a multibeams antenna could be a good solution. This could be acomplished by a phased antenna fed via a beamformer circuit as shown in figure IV.1. A multibeam antenna is a smart and agile antenna in terms of radiation pattern. In this section, we'll review the basic operating principle of a switched beam antenna.

Consider a beam-former circuit feeding a phased array antenna with the same amplitudes and a phase gradient β between them. Thanks to the introduced β phase shift, the radiation pattern would be flexibile and provides an electrically scanned beam in a desired direction avoidingthe mechanical rotation. Thus, the radiation pattern changes direction, creating an angle θ (see equation 1) between its maximum direction and the normal to the antenna array [22]. The concept of this diagram is illustrated in Figure IV.1.

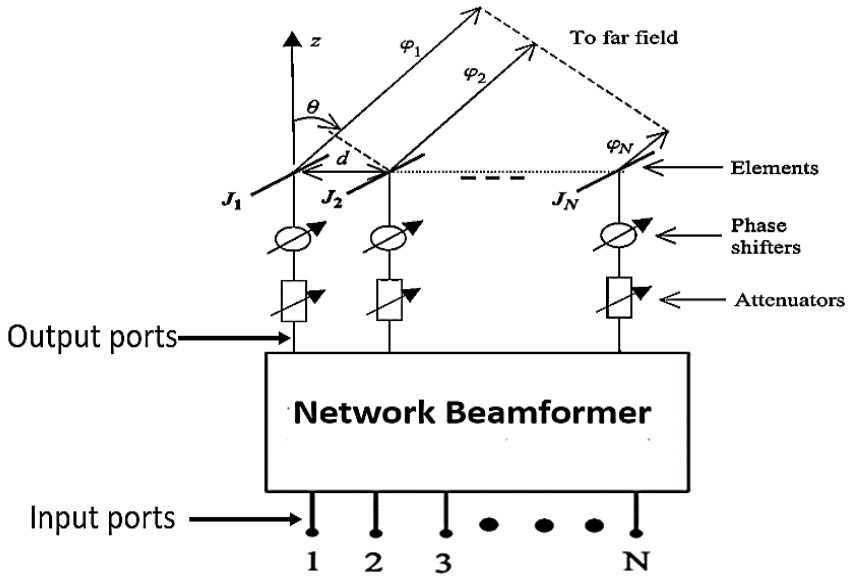

Figure IV. 1 Structure of a switched multi-beam antenna.

$$\theta = \text{Arcsin}(\frac{\lambda.\beta}{2\pi d}) \qquad (1)$$

Where:

θ : is the angle between the maximum beam and the normal to the antenna array.

d = the distance inters elements.

λ = wavelength in free space.

In practice, the maximum beam direction is usually excited by an input signal of the beamformer circuit.

3. The 4x4 Butler Matrix and its vulnerability

3.1. Presentation of the 4x4 Butler Matrix

The Butler matrix is a beamformer based on hybrid couplers that provides a parallel feed to the array antenna. It can cause an array antenna to radiate in many directions. In fact, many configurations in the Butler matrix are possible such as: 2x2 [22], 4x4[16], or 8x8 [25]. The 2x2 Butler matrix contains a hybrid coupler feeding an array antenna to provide two beams in two different direction (-30° & +30°) [22-23]. The 4x4 Butler matrix contains four hybrid directional couplers, two crossovers and two phase shifters (see figure IV.2). It was used to feed an array antenna to obtain four beams in four different directions (-45°, -15°, +15° & +45°) [16-21] in order to increase area coverage.

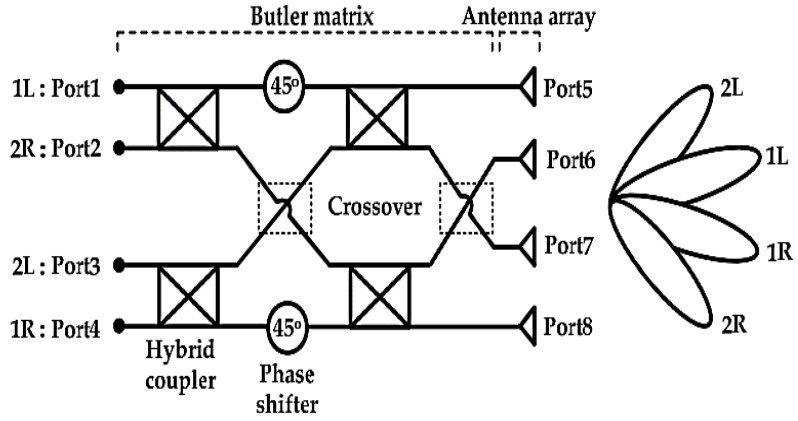

Figure IV. 2 Structure of switched four beams array antenna feed by the 4x4 Butler matrix.

The transmission coefficients matrix of a 4x4 Butler matrix based on 3dB 90° hybrid coupler is:

$$MB_{4x4} = \frac{1}{2}\begin{bmatrix} e^{-j45^\circ} & e^{-j135^\circ} & e^{-j90^\circ} & e^{-j180^\circ} \\ e^{-j90^\circ} & e^{j0^\circ} & e^{-j225^\circ} & e^{-j135^\circ} \\ e^{-j135^\circ} & e^{-j225^\circ} & e^{j0^\circ} & e^{-j90^\circ} \\ e^{-j180^\circ} & e^{-j90^\circ} & e^{-j135^\circ} & e^{-j45^\circ} \end{bmatrix} \qquad (2)$$

Therefore, the phase gradient β at the four output ports of the 4x4 Butler matrix corresponding to its four input ports 1,2,3 and 4 are +45°, -135°, +135°, -45° respectively. Thanks to the phase gradient, using equation 1, the maximum beam could be oriented into 4 directions: 15°, -45°. +45°, -15° respectively.

To further increase area coverage, multiple beams are needed. The 8x8 Butler matrix provides 8 beams in 8 different directions (-52.5°, -37.5°, -22.5°, -7.5°,+7.5°, +22.5°, -+37.5° and +52.5°). It contains 12 couplers, 8 phase shifters and 16 crossovers [24]. As a result, the number of crossovers increases with the number of beams required. The vulnerability of the Butler matrix lies in the crossovers problem, especially in the PCB technology. In the next section, we'll discuss this weakness of the Butler matix.

3.2. The vulnerability of Butler's matrix

Although The Butler matrix increases the radiation area coverure, it suffers from the problem of the crossovers weak spot of crossovers, especially in Microstrip technology. A Microstrip crossover is a combination of two superimposed microstrip transmission lines (see figure IV.3). One of the key challenges associated with this crossover in Microstrip technology is signal interference and crosstalk especially in MMIC (Microwave Monolithic Integrated Circuits). Such interference can degrade SNR (signal-to-noise ratio), cause circuit malfunctioning and lead to unpredictable device behavior. This problem has attracted many researchers from all over the world to propose solutions for maintaining signal purity. Many researchers have proposed new configurations of the Butler 4x4 matrix to replace this type of crossing, such as Butler matrix based on two 0 dB couplers [16-17], Butler matrix besed one 0dB hybrid coupler [18], Butler matrix based pleated configuration [19], Butler matrix based double layer substrate [20] and Butler matrix based SIW (substrate integrated waveguide) technology [21] as shown in figure IV.4. All these configurations were used to avoid crossovers and maintain the desired radiation directions: 15°, -45°. +45°, -15°.

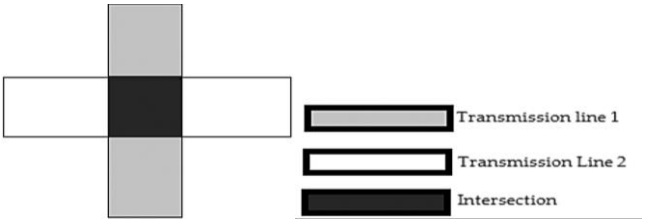

Figure IV. 3 Microstrip crossover

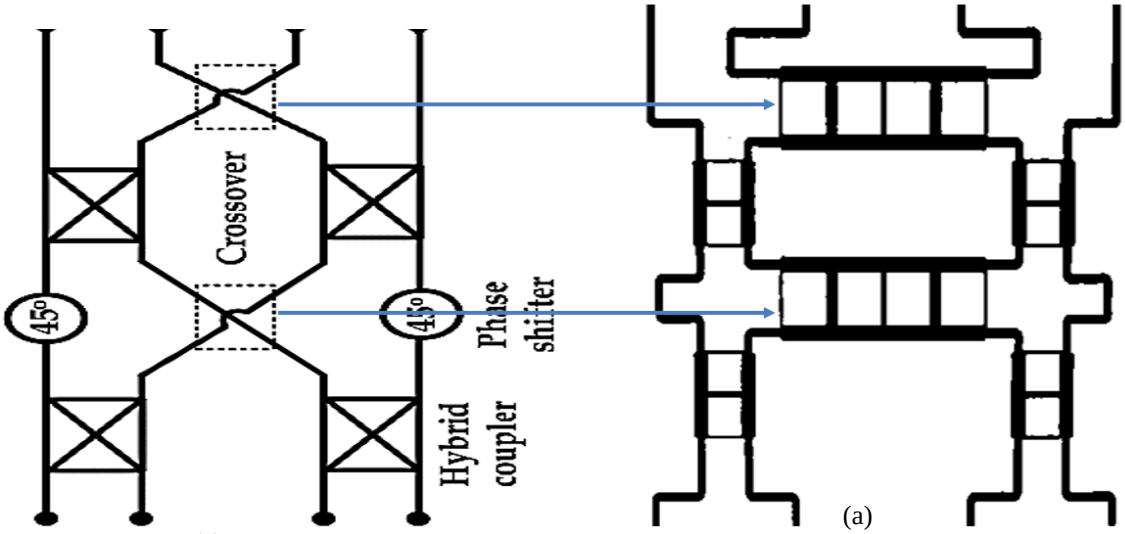

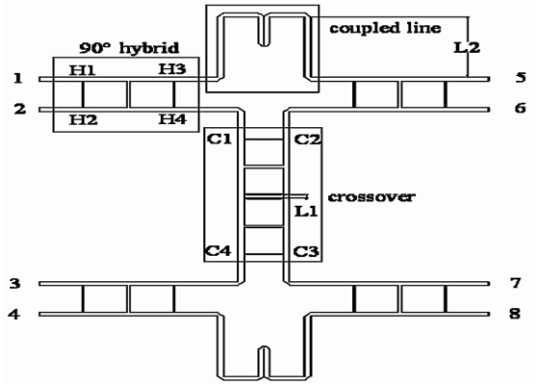

(c)

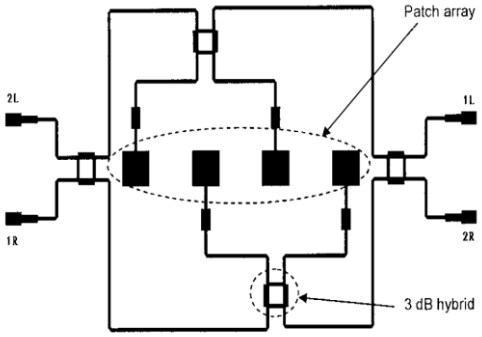

(d)

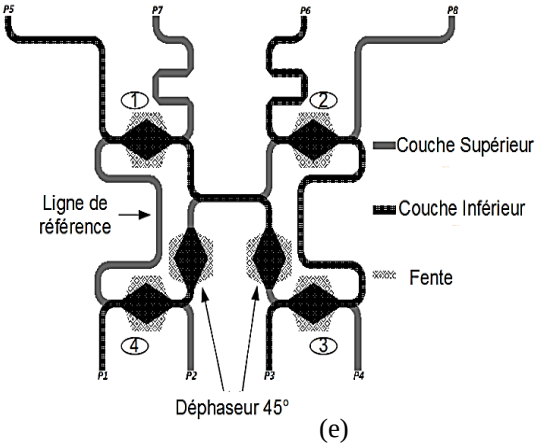

(e)

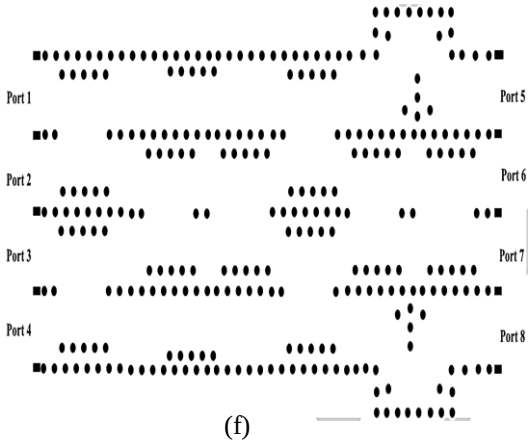

(f)

Figure IV. 4 Different configurations have been used to avoid crossings in the 4x4 Butler Matrix PCB circuit, (a): 4x4 Butler matrix with crossover problem, (b): Butler matrix based on two 0 dB couplers, (c): Butler matrix besed one 0dB hybrid coupler, (d): Butler matrix based pleated configuration, (d): Butler matrix based double layer substrate, (a): Butler matrix based SIW.

All these configurations are too complicated and have been used to avoid crossings and to obtain the desired directions: 15°, -45°. +45°, -15° for beamforming purposes. So, in the next section,

we'll suggest a **new 4x4 beamformer circuit** that has simple design and fabrication and provides the desired directions: 15°, -45°. +45°, -15° without using crossovers.

4. Design process for the new 4x4 Beamformer

The main componant of the Butler matrix is the hybrid coupler. The most widely used is the 3 dB hybrid coupler, that provides a ±90° phase shift at their output ports [7]. In the praviouse section, we presented the problem from which the Butler matrix suffers, which is crossover. So, In this section we will propose a new beamformer circuit without using crossovers. The proposed 4x4 beamformer is shown in figure IV.5. It has 4 input ports, 4 output ports and provides phase shifts of 45°,-135°,135°,-45° when one of the input ports: port1, port2, port3, or port4 is activated respectivelly. Thanks to these phase shifts, the proposed structure could feed an array antenna to obtain multibeam antenna that radiats energy in four derictions 15°, -45°. +45° and -15°.

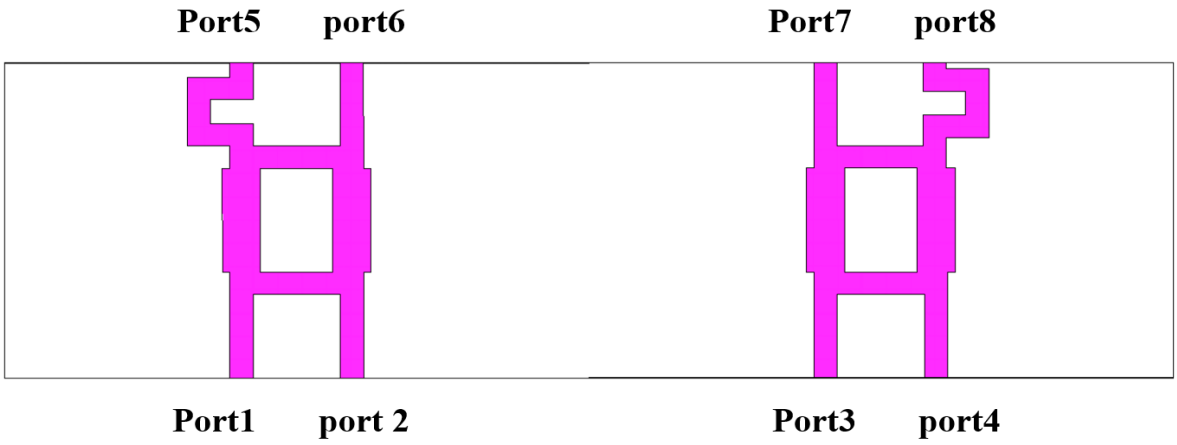

Figure IV. 5 Structure of the proposed 3dB beamformer circuit

This beamformer is based on two 3dB hybrid couplers which provide phase shift 45°/-135° and 135°/-45°, these two coulpers are hosted from the 3dB 90°/-90° hybrid couplers using a delay line as shown in figure IV.5.

4.1. The proposed 3dB 90°/-90° hybrid couplers

The 3dB ±90° hybrid coupler is a symmetrical microwave component that splits the input power into two equal quanties (-3 dB) with a phase shift equals to 90 or -90° between them when one of the inputs port (port 1 or port 4) is excited repectivley. The structure of the proposed 3dB ±90° hybrid coupler is shown in figure IV.6. This sructure is desigend at the operation frequency 2.45GHz according to the equations provided in reference [7].

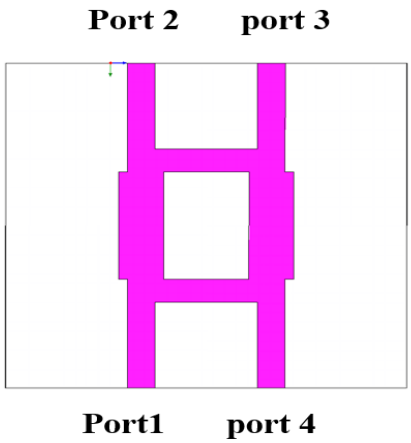

Figure IV. 6 Designed 3 dB 90°/-90° hybrid couplers

Figures IV.7 exhibit the simulation resultes in terms of scattring parmetters obtained by HFSS EM simulator. Figure IV.7 (a) shows their magnitudes in dB versus frequency. It can be seen that, at the operating frequency, the trasmirssion coefficients are close to the ideal value -3dB, which mean; that the power supply is divided into two equal quantities. Moreover, the reflexion (S_{11} or S_{44}) and isolation (S_{14} or S_{41}) coefficients are less than -37dB, which mean that the input power is almost entirely transmitted to the output ports 2 and 3.

Figure IV.7 (b) shows the angles of the transmission coefficients versus frequency when input port 1 is powered, and then when input port 4 is powered. According to this figure, it is clear that the phase shift between the output port is 89.77° when port1 is powered. When port 4 is powered, the phase shift is -89.77**°.**

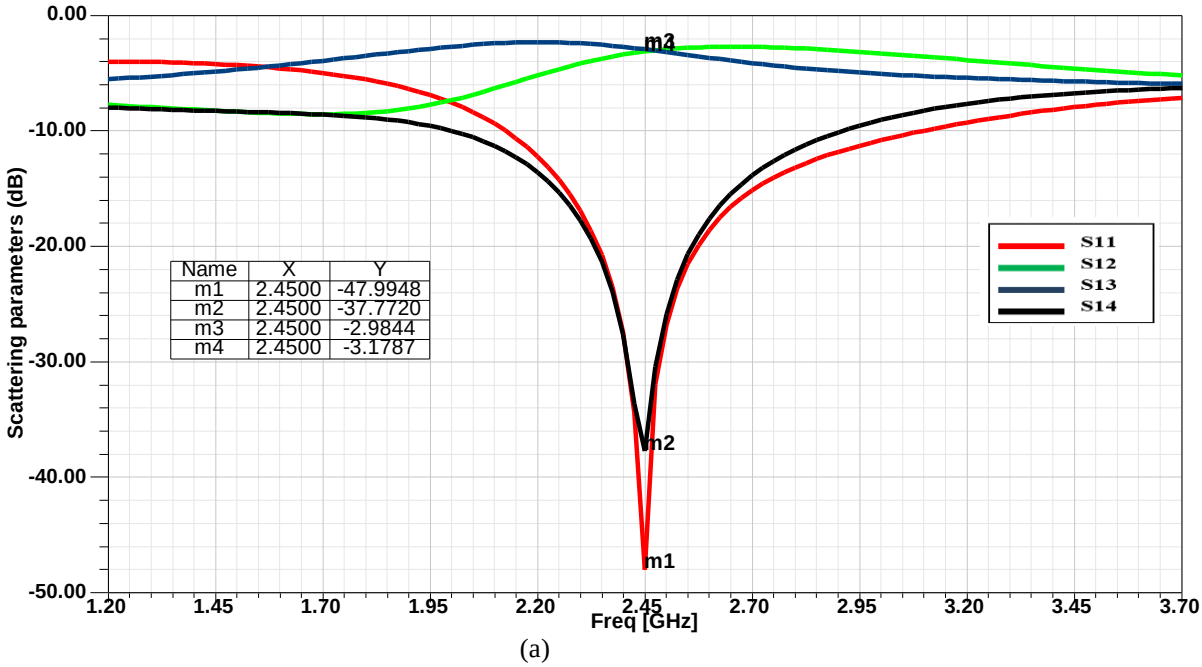

(a)

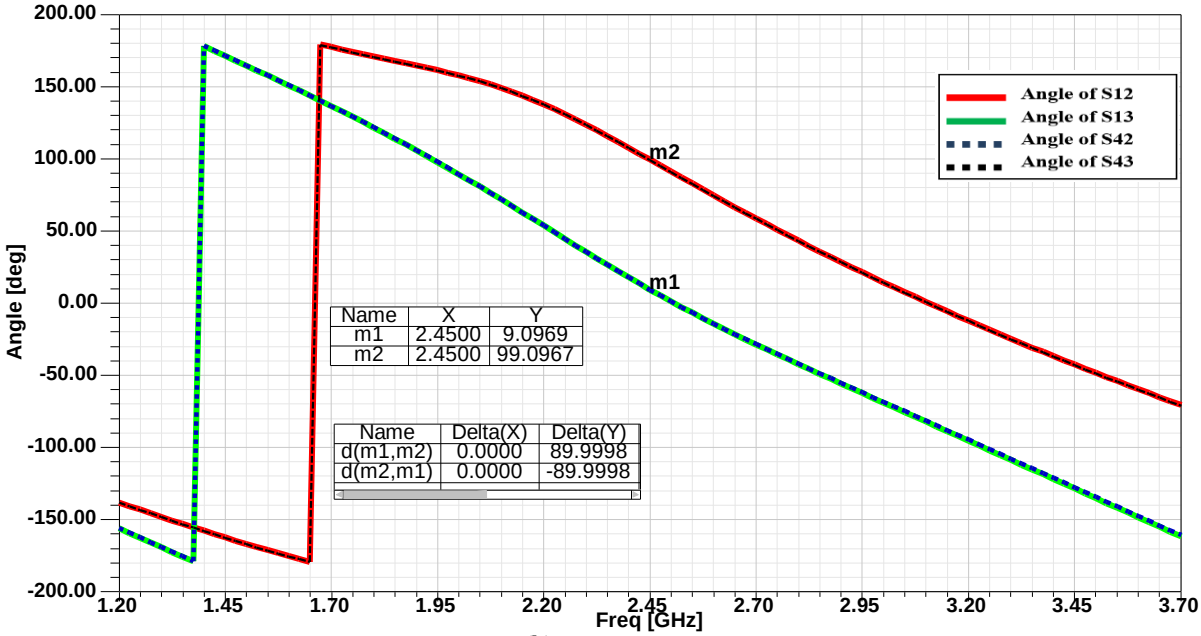

(b)

Figure IV. 7 Simulation results for the 3dB ±90° proposed hybrid coupler; (a) magnitude of the scatring parameters versus frequency; (b): angles of the transmission coefficients versus frequency.

Table IV. 1 Summary of the simulation results obtained for the proposed 3 dB 90° hybrid coupler at 2.45 GHz operating.

Scatring prameters	S_{12} or S_{42}	S_{13} or S_{43}	Phase shift $\beta =$ anglePort3 − anglePort2
When port 1 is fed	-3.17dB/**9.07°**	-2.98dB/**99.09°**	**89.99°**
When port 4 is fed	-2.98dB/**98.85°**	-3.17dB/**9.09°**	**-89.99°**

4.2. The proposed 3dB hybrid couplers 45°/-135° and 135°/-45°

In this section, we will improve the previousn 3dB ±90° hybrid coupler so that it offers a phase shift of 45° / -135° then 135 / -45 instead of ± 90° when input port 1 or port 4 is powered fed respectivelly.

Typpically, a microstrip line operates within a defined range of wavelength and frequencies, guiding electromagnetic waves. This wavelength is the distance between two consecutive peaks of the guided wave, constituting a complete 360° phase cycle. To introduce a phase delay (θ) between two microstrip lines, we need to incorporate an additional delay line (ΔL) to effectively adjust their relative positions. such as: $\Delta L/\lambda g = \theta /360$.

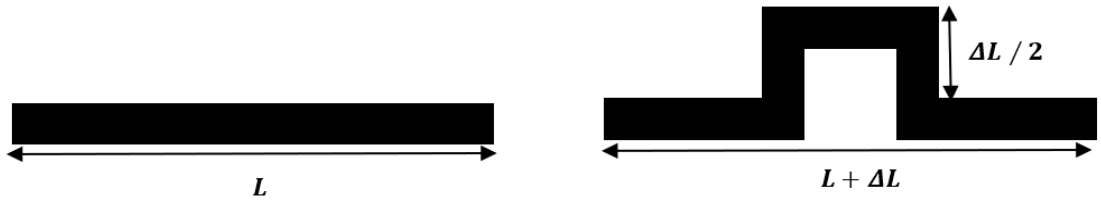

Figure IV. 8 phase delay line

Using the phase-delay line concept, the 3 dB 90°/-90° hybrid coupler will be improved by introducing additional delay elements to achieve 45°/-135° and 135°/-45° hybrid couplers. This improvement involves integrating delay lines that introduce a $\beta = \pm 45°$ phase shift at the outputs of the straight branch lines of the 3dB ±90° hybrid coupler.

The improved couplers are shown in figure IV.9 (a) and (b). (a): present the 3 dB hybrid coupler that provides a phase shift of 45° when the port is excited and -135° when port4 is excited. while (b): shows the 3 dB hybrid couplers that provides a phase shift of 135° when the port1 is excited and -45° when port4 is energized.

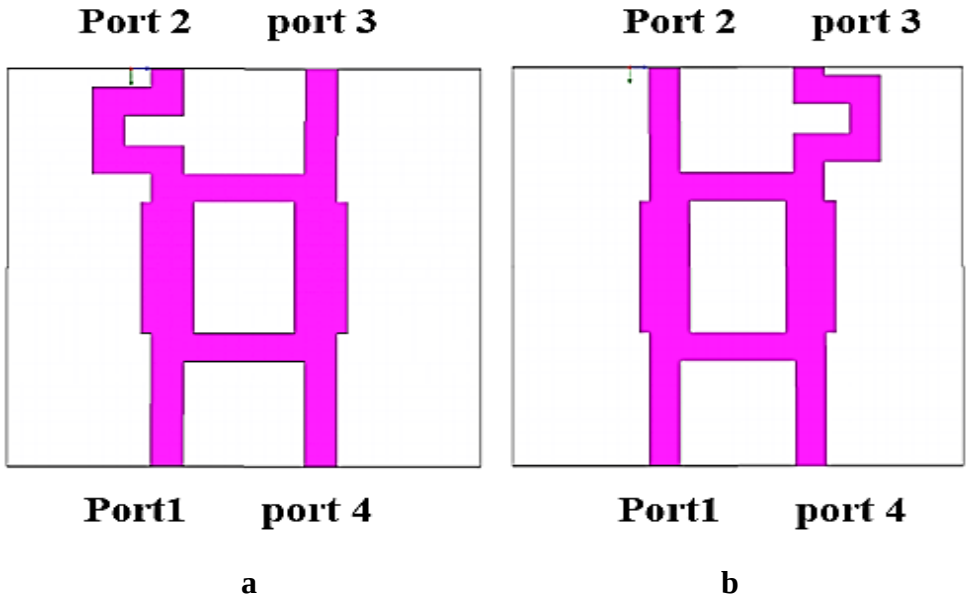

Figure IV. 9 Enhanced 3 dB hybrid couplers: a: 45°/-135°; b:135°/-45°.

4.2.1 Simulation results of the the proposed 3dB hybrid coupler 45°/-135°;

Figures IV.10 exhibit the simulation resultes in terms of scattring parmetters obtained by HFSS EM simulator. Figure IV.10 (a) their magnitudes in dB versus frequency, while figure IV.10 (b) shows angles of the transmission coefficients versus frequency when input port1 is fed, and then when input port4 is fed. It can be seen that at the operating frequency, the trasmirssion coeficients are close to the ideal value -3dB which indicate that the power supply is divided into two equal

quantities. Moreover the reflexion coefficient (S_{11} or S_{44}) and isolation (S_{14} or S_{41}) are less than -20 dB, showing that the input power is almost transmitted to the output ports 2 and 3. Furthermore, it is clear that the phase shift between the output ports is **44.97°** when port1 is powered. While when port4 is powered the phase shift is **-134.26°.**

Table IV.2 summarizes the simulation results obtained when port 1 is powered and when port 4 is powered.

Table IV. 2 Summary of the obtained simulation for the proposed 45°/-135° 3 dB hybrid coupler at 2.45 GHz the operating frequency.

Scatring prameters	S_{12} or S_{42}	S_{13} or S_{43}	Phase shift $\beta = anglePort3 - anglePort2$
When port 1 is fed	-3.24dB/**9.79°**	-3.24dB/**54.76°**	**44.97°**
When port 4 is fed	-3.24dB/**96.74°**	-3.24dB/**-37.52°**	**-134.26°**

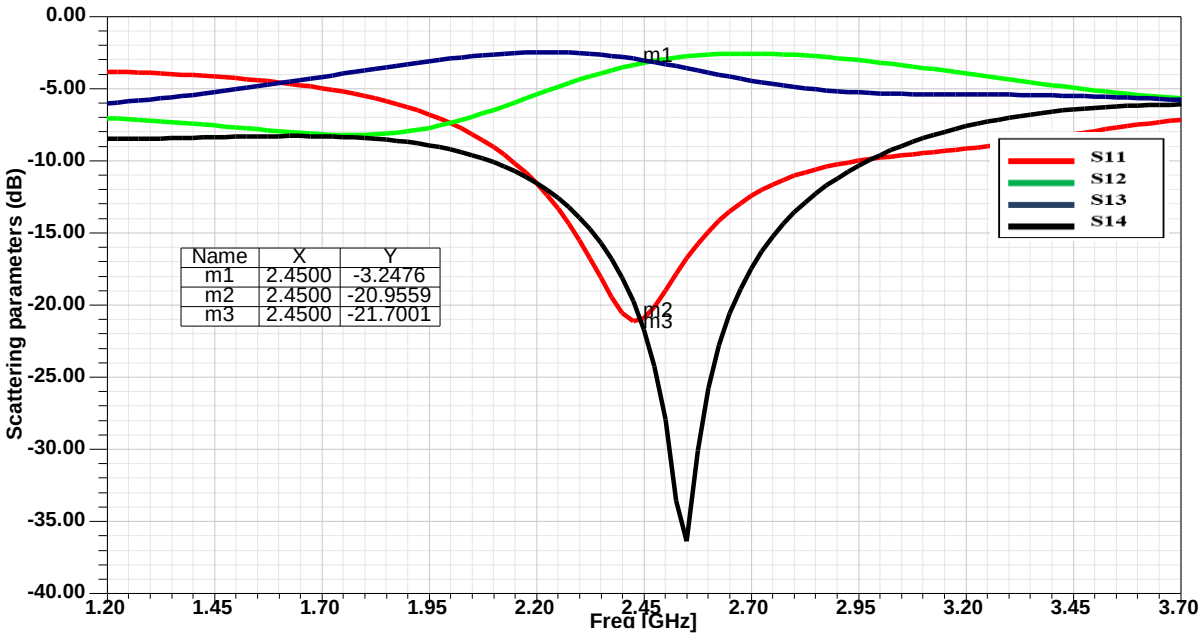

(a)

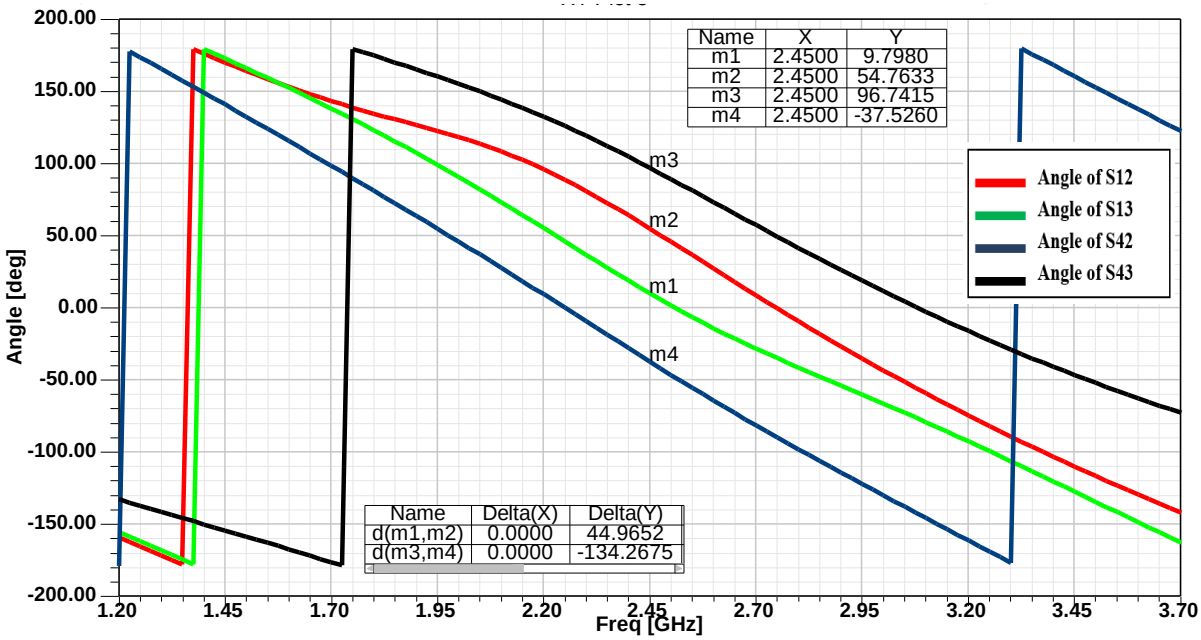

(b)

Figure IV. 10 Simulation results of the proposed 3dB hybrid coupler; (a): module of the scattering parameters versus frequency; (b): angles of the transmission coefficients versus frequency.

4.2.2 Simulation results of the proposed 3dB hybrid coupler 135°/-45°

Figures IV.11 presents the simulation resultes obtained in terms of scattring parmetters. Figure IV.11 (a) shows their modules in dB versus frequency, while figure IV.11 (b) shows angles of the transmission coefficients versus frequency when the port1 is powered then when the port4 is powered. According to this figure, it is clear that at the operating frequency the transmission coefficients are equals to approximately -3.09dB which mean that the power supply is divided into two equal quantities. Moreover, the reflection coefficient (S_{11} or S_{44}) and isolation coefficient (S_{14} or S_{41}) are less than -20 dB which means that input power is almost transmitted to output ports 2 and 3. Also, it can be seen that the phase shift between output ports is **133.5°** when port 1 is powered. While when port 4 is powered, the phase shift is **-45.31°.**

The table IV.3 summarises the simulation results obtained when port 1 is powered and when port 4 is powered.

Table IV. 3 Summary of the simulation for the proposed 135°/-45°3 dB hybrid coupler at 2.45GHz operating frequency.

Scattring prameters	S_{12} or S_{42}	S_{13} or S_{43}	Phase shift $\beta = anglePort3 - anglePort2$
When port 1 is fed	-3.09dB/**-36.67°**	-3.09dB/**97.25°**	**133.5°**
When port 4 is fed	-3.24dB/**54.21°**	-3.24dB/**8.9°**	**-45.31°**

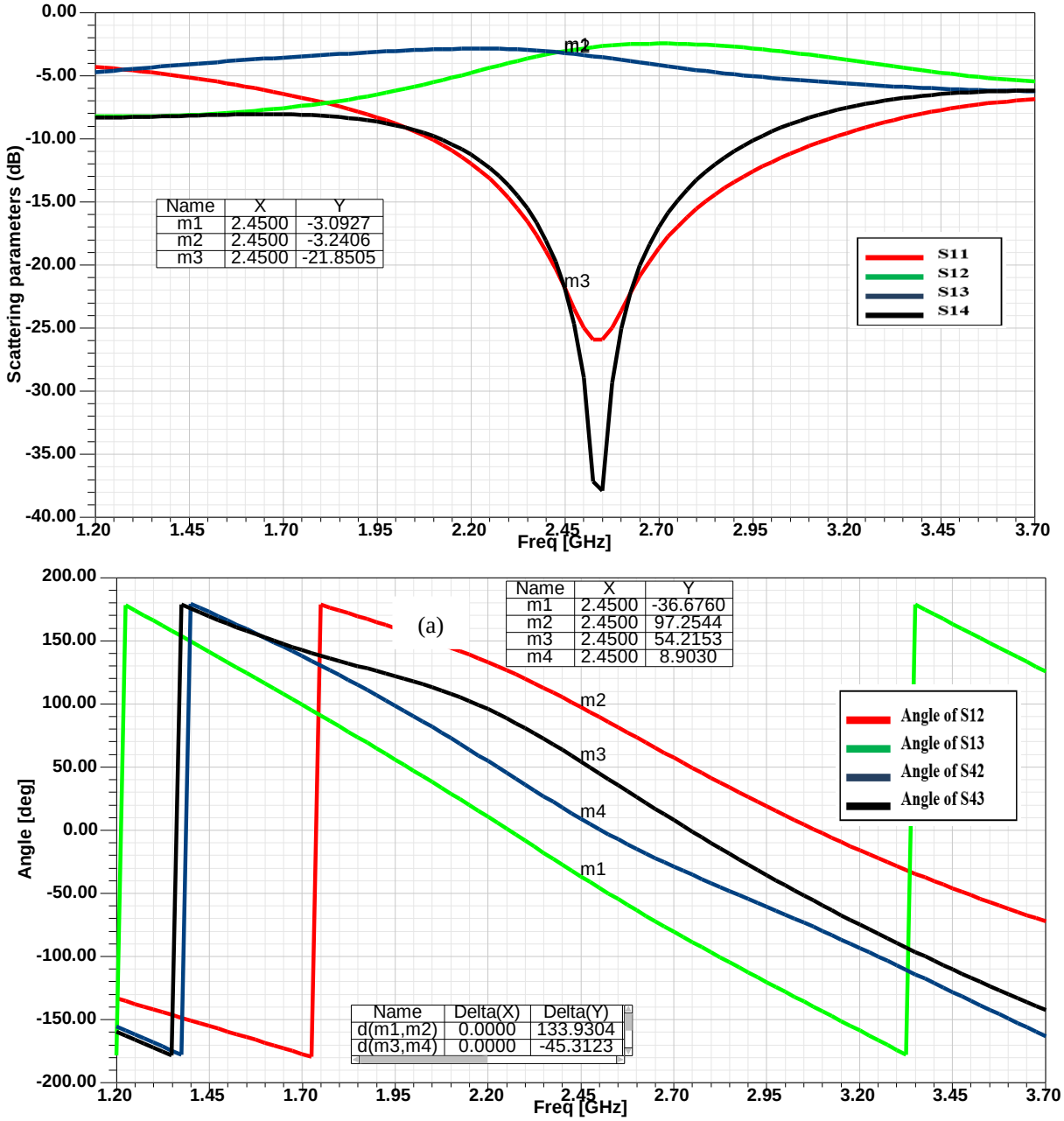

(b)

Figure IV. 11 Simulation results of the proposed 3dB 135°/-45° hybrid coupler; (a): module of the scattering parameters versus frequency; (b): angles of the transmission coefficients versus frequency.

5. Four-beams antenna based the proposed 4x4 beamformer circuit

5.1. Design

In this section, we will use the proposed 4x4 beamformer circuit to feed a four-element array antenna to obtain a multibeam antenna that provides four beams in four different directions for beamfoming purposes. The layout of the designed and fabricated proposed multibeam array antenna are illustrated in Figure IV.12; (a),(b) exhibit their front view, while (c), (d) show their

back view. The proposed antenna is designed and simulated utilizing with the HFSS simulator using the RT/duroid 5880 substrate (relative permitivity = 2.2, loss tangent = 0.0009) with a totale size of **130 x 240 x 1.56 mm^3**. This sructure has four input ports, one of them must be activated to obtain a beam in the desired direction. Prot1 provides a beam in oriented to 18°, prot2 provides a beam in oriented to -43°, prot3 provides a beam in oriented to 43° and prot4 provides a beam in oriented to -18°.

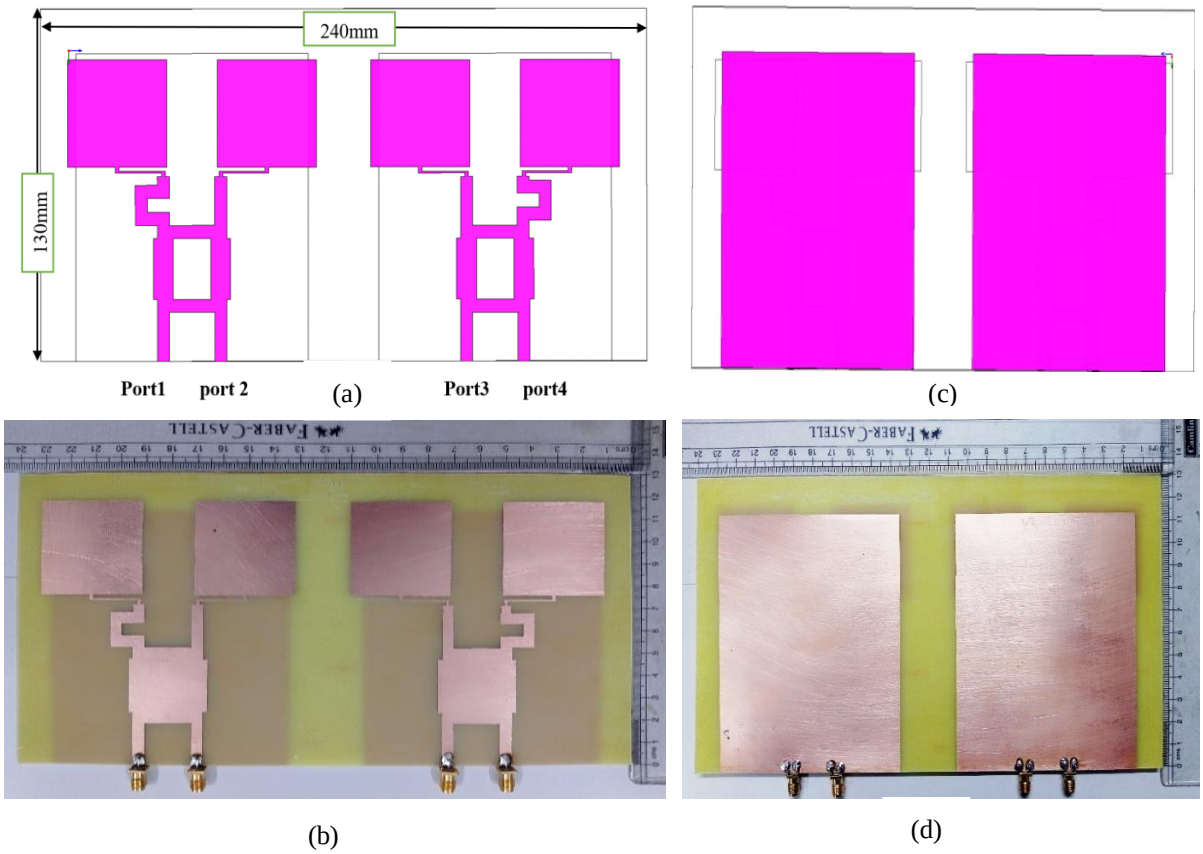

Figure IV. 12 Design and fabricated prototype of the proposed 4x4 beamformer feeding an array antenna, (a) and (b): front view, (c) and (d): back view.

5.2. Simulation versus measurements results of the Proposed Four-Beams antenna

Initially the design of the proposed four beams array antenna was done by HFSS solver and the obtained result was validated by mesurments. The simulation versus measurements results of in terms of reflection coefficient, gain , radiation efficieny, maximum beam diretion in 2D and 3D radiation patterns are shown in figures IV.13, 14, 15, 16 and 17 respectively. These results are obtained according to four feeding scenarios i.e when one of the input ports (port1 , port2, port3, port4) is activated. According to these figures both simulated and measured results exhibit almost the same results.

Figure IV.13 plots the reflection coefficients associated with port1, port2, port3 and port4. It can be seen that there is a brodband impedance bandwidth such as : by simulation equals about 1.2 GHz (from 2.1 to 3.2 GHz), while by measurements the impedance bandwidth equals about 1 GHz (from 2.1 to 3 GHz). In addition, at the operating frequency 2.45 GHz all reflection coefficients are less than -20dB.

Figure IV.14 exhibits the gain in dB associated with Port 1, Port 2, Port 3 and port4. From this figure, it is clear that, at the operating frequency, their corresponding simulated peak gain is 8.57dB, 8.01 dB, 7.78 dB, 8.42 dB respectively, while their measured peak gain is 7.87dB, 7.821 dB, 7.58 dB, 7.22 dB respectively.

Figure IV.15 illustrates the radiation efficiency associated with Port 1, Port 2, Port 3 and port4. In From this figure, it is clear that, at the operating frequency, their corresponding maximum radiation efficiency is 97%, 94%, 75% and 87% respectively, while their measured maximum radiation efficiency is 92%, 78%, 65% and 81% respectively.

Figures IV.16 and 17 present the maximum beam direction in 2D and 3D radiation patterns associated with port 1, port 2, port 3 and port 4. It can be seen that their simulated and measured maximum beam is oriented at 18°, -43°, 43°, -18° respectively.

A summary of the simulation versus measured results obtained for port 1, port 2, port 3 and port 4 is presented in the table IV.4.

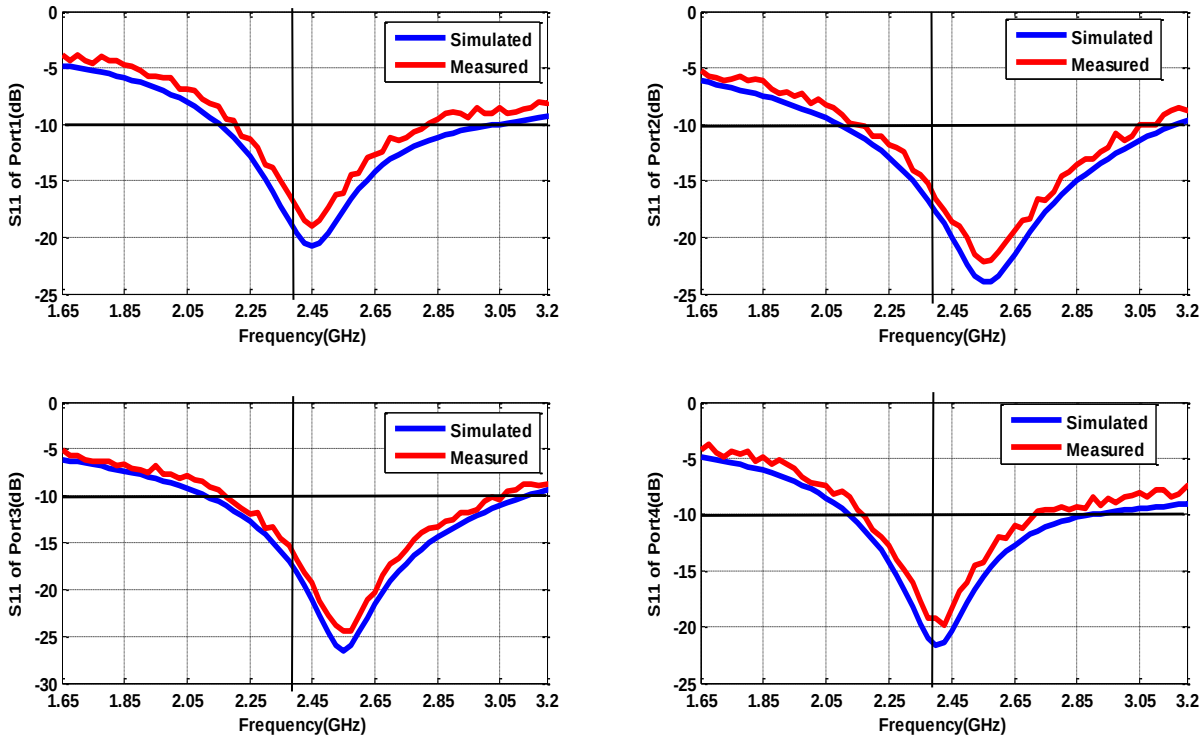

Figure IV. 13 Simulated versus measured Réflexion coefficient associated with Port 1, Port 2, Port 3, port 4

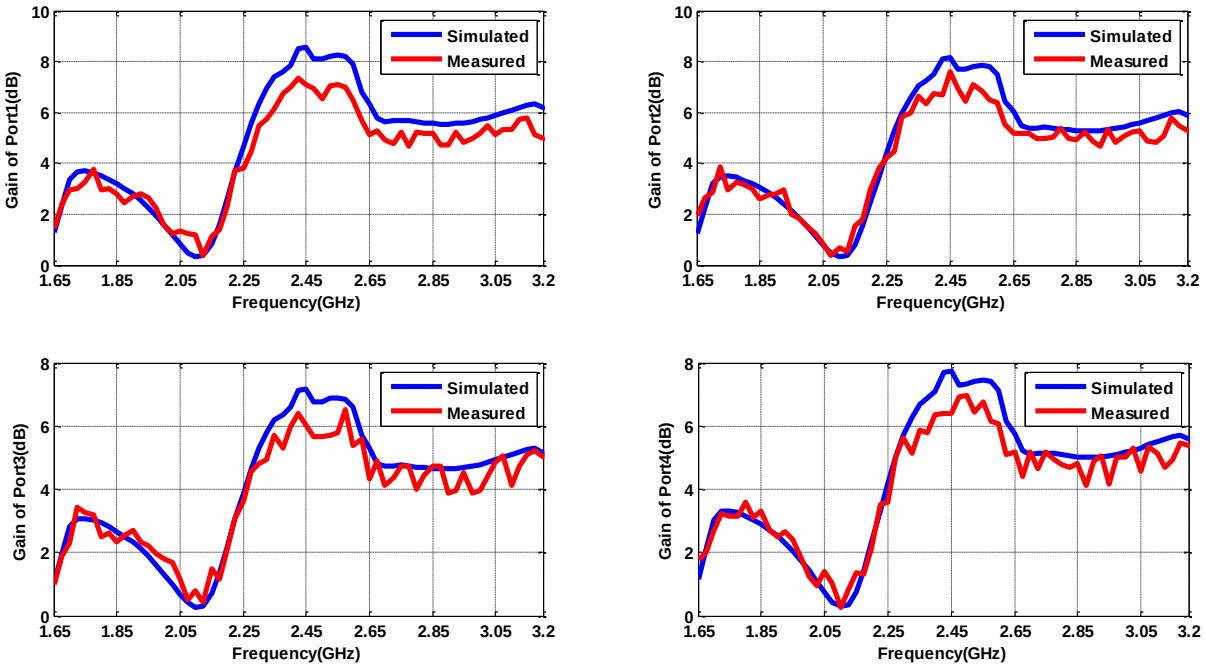

Figure IV. 14 Gain in dB associated with Port 1, Port 2, Port 3 and port 4.

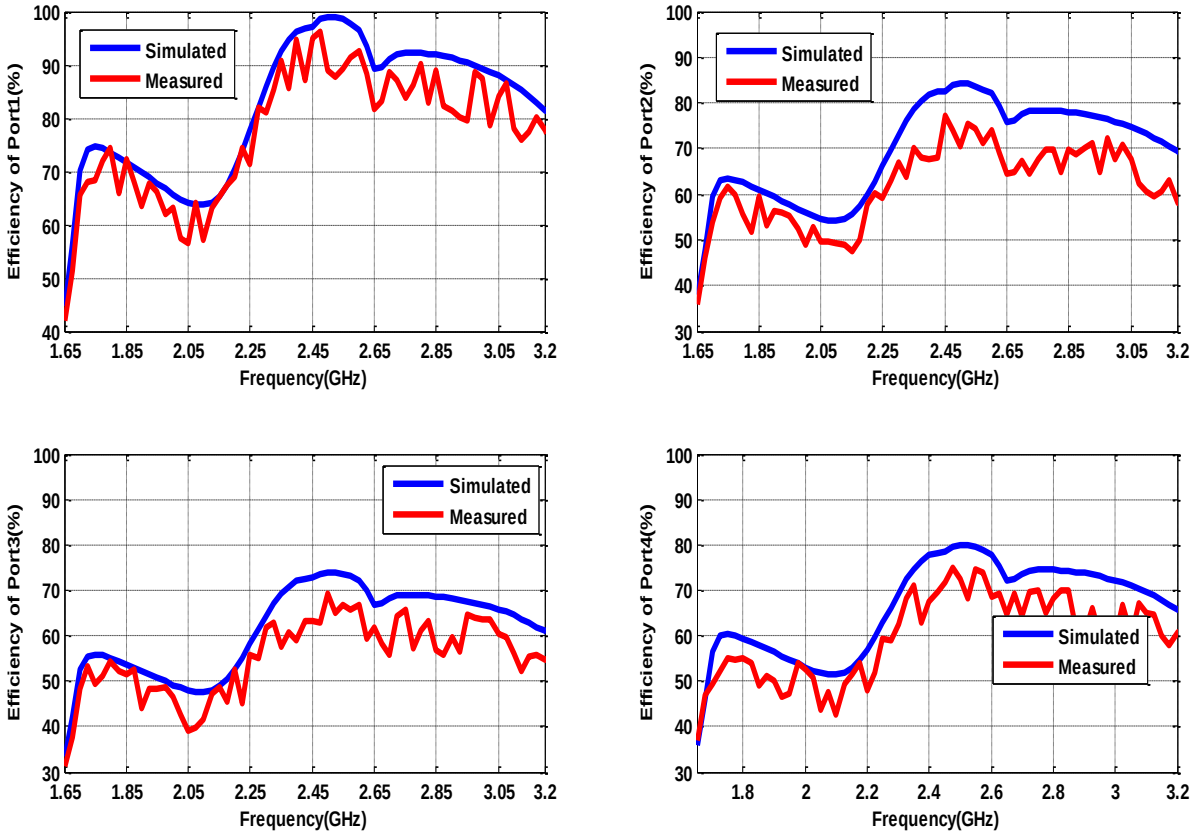

Figure IV. 15 Radiation efficiency associated with Port 1, Port 2, Port 3 and port 4.

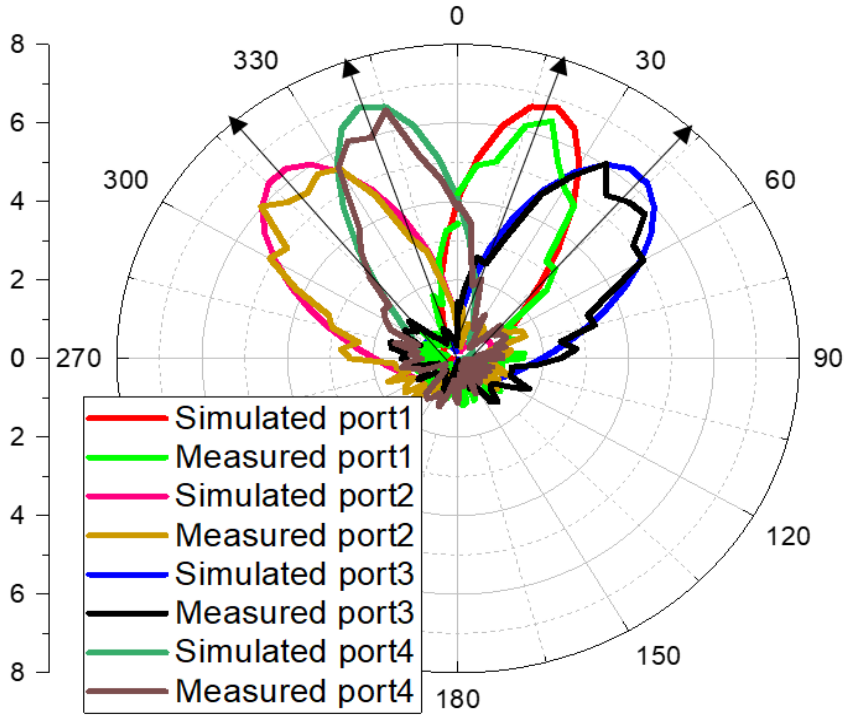

Figure IV. 16 Maximum beam direction in 2D radiation pattern associated with port 1, port 2, port 3 and port4.

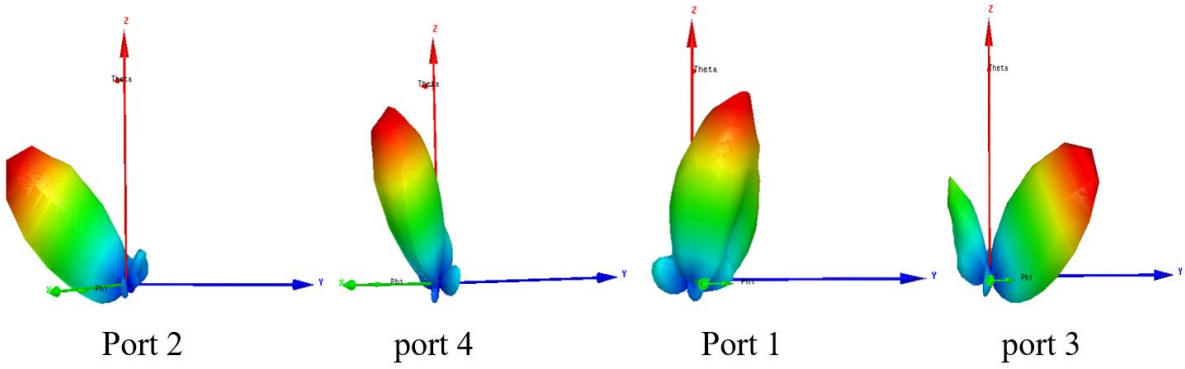

Figure IV. 17 Maximum beam direction in 3D radiation patterns for Port 1, Port 2, Port 3 and port 4.

Table IV. 4 Summary of simulation versus measurements results obtained from the proposed four beam antenna associated with Port1, Port 2, and Port 3 and port 4

	10 dB Impedance Bandwidth	Peak gain (dB)	Peak radiation efficiency (%)	Maximum beam direction
Simulation at Port 1	2.15GHz-3.07GHz	8.57	97	18°
Measurement at Port 1	2.12GHz-3.3GHz	8.57	92	
Simulation at Port 2	2.13GHz-2.97GHz	8.01	94	-43°

Measurement at Port 2	2.103GHz-2.73GHz	8.01	78	
Simulation at Port 3	2.11GHz-3.15GHz	7.78	85	43°
Measurement at Port 3	2.03GHz-2.95GHz	7.78	65	
Simulation at Port 4	2.16GHz-3.21GHz	8.42	87	-18°
Measurement at Port 4	2.14GHz-2.81GHz	8.42	81	

6. Reconfigurable ultra-wideband, microstrip crossover for ISM band applications

A Microstrip crossover is a combination of two superimposed microstrip transmission lines (see figure IV.3 above). One of the main challenges associated with this crossover in microstrip technology is signal interference and crosstalk, especially in MMIC (Microwave Monolithic Integrated Circuits). These interferences can degrade the SNR (signal-to-noise ratio), cause circuit malfunction and lead to unpredictable device behavior. These problems have prompted many researchers to propose solutions to maintain signal purity. The most pupular soltion used is the 0dB hybrid coupler [16-18]. In the following, we will design a 0 dB hybride coupler, then we will suggest a new solution of the microstrip crossover problem. After that, a comparison between these two solutions will be carried out. Then, a comparison will be made between the proposed reconfigurable crossover and others published crossovers.

6.1. The 0 dB hybrid coupler-based Crossover

A 0 dB hybrid coupler is a microwave component contains of two similar cascaded 3dB 90° hybrid couplers. The first one divides the incoming power feed from the input port1 into two equal quantities, the second one collects the devided signals and combines them to obtain the original signals at the output port 4 (opposite of the fed port) as shown in figure IV.18.

The 0 dB coupler was used as crossover to avoid any transmission power through other ports (2 and 3) as shown in figure IV.19. It was used to overcome the crossover problem in the Butler matix(see Figure IV.4 (b) and (c) above.

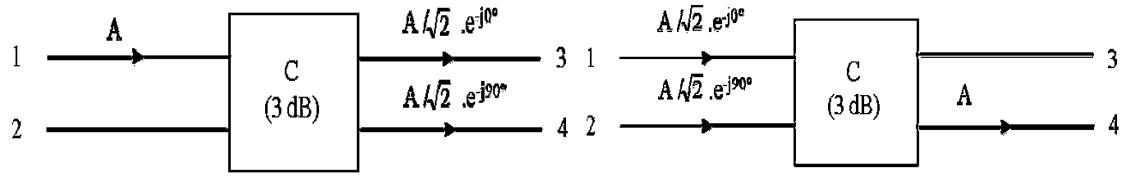

Figure IV. 18 Two cascaded 3dB hybrid.

The designed crossover is shown in figure IV.19 , and is based on two 3dB 90° couplers that we presented in the previous section 4. A parmetric study was carried out on the distance between the two couplers in order to obtain a good results i.e the output signal must be equals to 0dB.

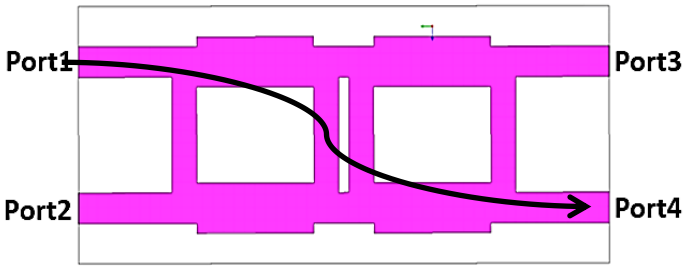

Figure IV. 19 The designed 0dB hybrid coupler

The obtained resutls in terms of scattring parameters are shown in figure IV.20. Figure IV.20 (a) shows the magnitude of S_{11}, S_{12}, S_{13}, S_{14}. In this figure, at the operating frequency 2.45 GHz, it is clear that the transmitted coefficient S_{14} is equals to -0.19 dB along a narrow band of 35Mhz (from 2.30GHz to 2.65GHz). While the other coeficients S_{11}, S_{12}, S_{13} are less than -20dB along this band, meaning that almost all the input power is transmitted to the port 4 along a narrow bandwdith equals to 35 Mhz.

figure IV.20 (b) exhibits the angles of S_{11}, S_{12}, S_{13}, S_{14}. According to this figure, at the operating frequency 2.45 GHz, the phase shift between the feed port1 and the output port4 equals to -88.88°.

(a)

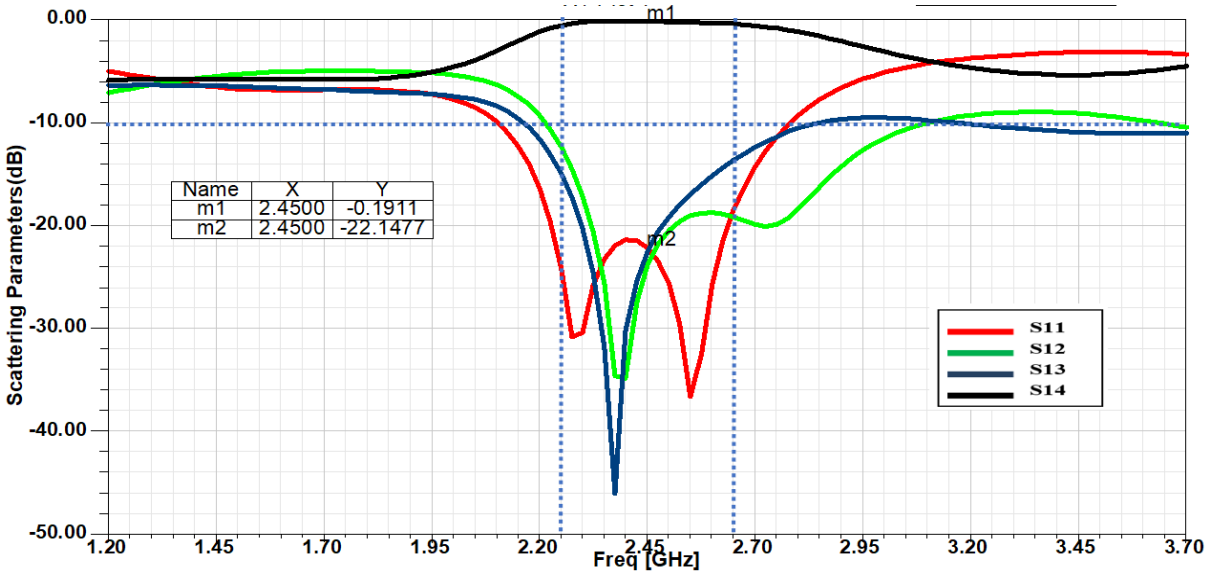

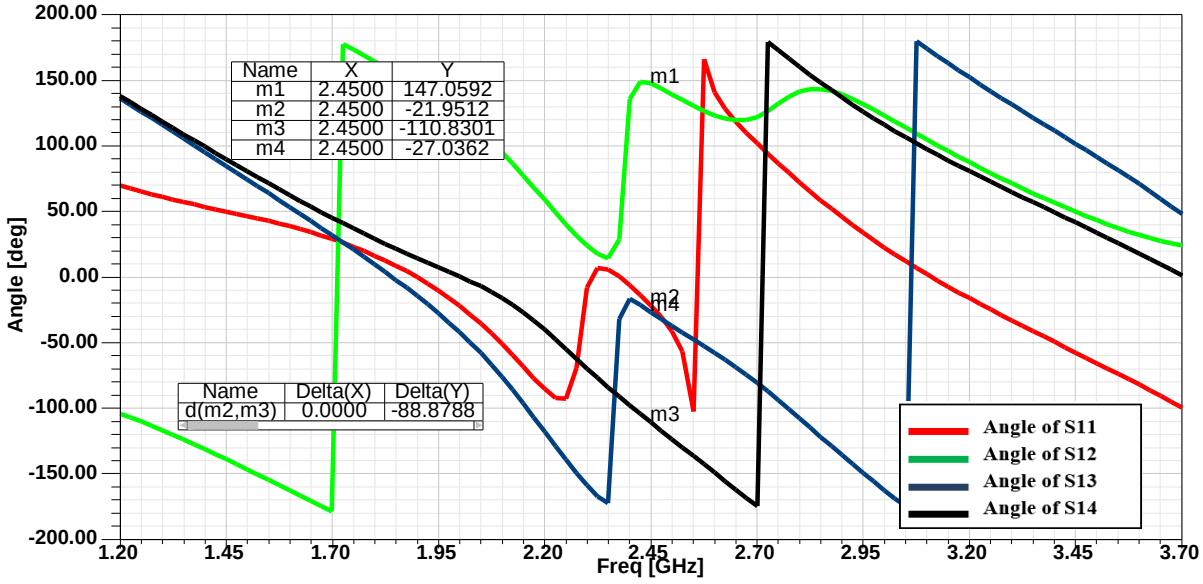

(b)

Figure IV. 20 Simulation results of designed 0dB coupler in terms of scattring parameters, (a): their magnitudes, (b): their angles.

6.2. The proposed Reconfigurable Crossover

The design of the proposed reconfigurable planar crossover went through four steps. It is a symetrical four-port structure : two input ports and two output ports. However, its design will not be presented here. Due to the novelty of the concept and its innovative aspect, a patent application has been submitted to the OMPIC (Office Marocain de la Propriété Industrielle et Commerciale) and is currently being examined.

Simulation results of the proposed crossover in terms of scattering parameters are shown in figure IV.21. The results are obtained when the input signal is at the input port 1 and the output signals is at its opposite port 4. Figure IV.21 (a) shows the magnitude in dB of S_{11}, S_{12}, S_{13}, S_{14}. In this figure, it is clear that the transmitted coefficient S_{14} is equals to -0.4 dB and that this value is constant along the ultra-wideband frequency of 8GHz, i.e. there is no frequency limitation. Moroever, the other coeficients S_{11}, S_{12}, S_{13} are less than -18.5 dB along this ultra large band frequency, meaning that all input power is tottally transmitted to the desired prot4. Figure IV.21 (b) shows the angles of S_{11}, S_{12}, S_{13}, S_{14}. According to this figure, at the operating frequency 2.45 GHz, their angles are -93°, -76°, -78°, 175° respectively. In addition, the phase shift between the feed port1 and the output port4 is approximately -236°.

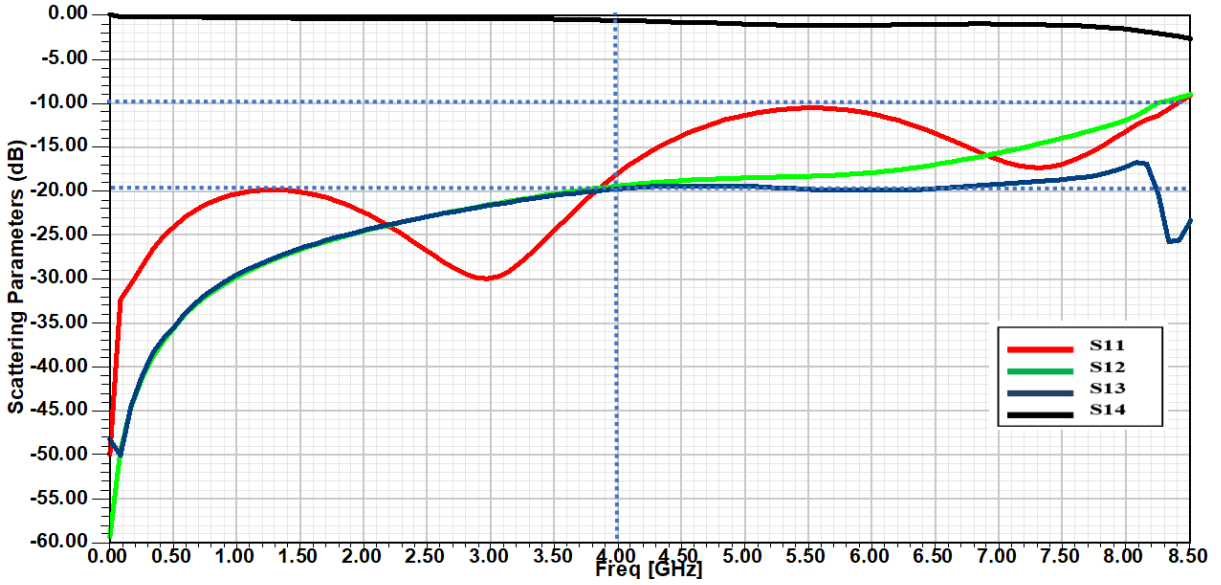

(a)

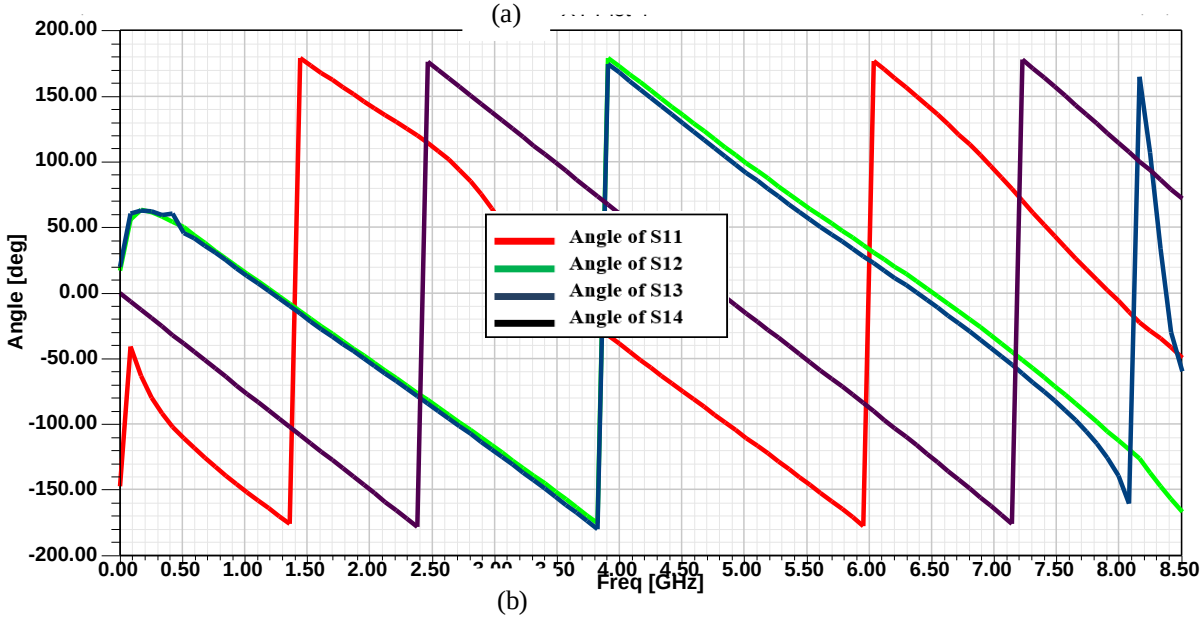

(b)

Figure IV. 21 Simulation results of the proposed crossover in terms of scattering parameters, (a): their magnitudes, (b): their angles

6.2.2 Preformance Comparison

The table IV.5 shows a comparison between the proposed crossover and the 0 dB coupler based crossover. According to this table, the proposed crossover has an ulta-wide bandwidth (no frequency limitation) with reduced size in addition to its reconfigurable capability through the use of diode.

Table IV. 5 The diode-based crossover versus the 0dB coupler-based crossover.

Crossovers	Size (mm^2)	Bandwidth
0 dB coupler based crossover	40x101.64	Narrow bandwidth equals to 35Mhz: from 2.30GHz to 2.65GHz
proposed crossover	36x30.34	**Ultra large band** equals to 8 GHz (from 1Hz to 8GHz)

Table IV.6 presents a comparative analysis between the proposed crossover and those presented in high-impact publications in this field. Acoording to this table, all the crossovers in previous works have narrow bandwidth, while the proposed crossover has an ulta wide bandwidth with no frequency limitation, and maintains signal purity. Moroever , it is small , easy to design and manufacture, in addition to its capabilty of flexibility and reconfigurability .

Thanks to its flexiblity, reconfigurability and excellent results that presents, the proposed crossover could be used not only for Butler matrix for beamforming purposes, but also for phased array antennas, reconfigurable antennas, MIMO antennas, reconfigurable filters…etc to control the power feed throughout the desired port(s).

Table IV. 6 The proposed diode-based crossover versus others published crossovers

References	Substrate permittivity	Size: λg × λg (mm2)	Operating Bandwidth	Isolation in dB	Flexibility and Reconfigurability
[29]	10.2	0.25 × 0.25	Single Narrow band	<20	No
[30]	3.38	0.24 × 0.33	Single Narrow band	<20	No
[31]	2.65	0.45 × 0.28	Single Narrow band	<20	No
[32]	2.2	0.58 × 0.58	Dual Narrow band	>10/>10	No
[33]	3.55	1.00 × 0.78	Dal Narrow band	>25/>25	No
[34]	10.2	0.63 × 0.63	Single Narrow band	<17	No
[35]	4.4	0.50 × 0.50	Dual Narrow band	>12/>33	No
Proposed Crossover	**2.2**	**0.36 × 0.34**	**Ultra-Wide-Band of 8 GHz (from 1Hz to 8GHz)**	**>18.5**	**Yes**

7. Conclusion

To summarize, a microstrip multibeam antenna based on a new 4x4 beamformer has been presented in this chapter. This beamformer is used to avoid crossover, which is a major problem in microstrip technology. The obtained results proved that the proposed multibeam antenna has a good gain, high radiation efficiency and the ability to radiate energy in four different directions 18°, -43°, 43°, -18° by switching its four input ports. A new solution to the microstrip lines crossover problem has, therefore, been proposed. The proposed microstrip crossover is flexible, reconfigurable and has an ultra-wide operating bandwidth of around 8 GHz (from 1Hz to 8GHz). Thanks to its incredible results that exhibits, it is dedicated to work in microwave bands (ISM, L, S and C bands…) as a splitter for all microwave components e.g amplifiers, mixers, reconfigurable filters, Butler matrix for beamforming purposes, Mutlibeam antenna, phased array antennas, reconfigurable antennas, MIMO antenna…etc to control the power feed throughout the desired port(s) by swiching of its diodes PIN.

Although, in this chapter, we have we chalanged limitations of flexiblity. The patch antennas still shortcoming against linear polarization. So, in the next chapter we are going to chalange the problem of linear ploarization and make it circular polarization in the Teraherz .

References

1. El Alami, A., Das, S., Madhav, B. T. P., & Bennani, S. D. (2019). Design, optimization and realization of high gain RFID array antenna 4× 1 for detection system of objects in motion. Journal of Instrumentation, 14(05), P05002.
2. Ansari, A. E., Das, S., Islam, T., Asha, S., El Idrissi, N. E. A., & Madhav, B. T. P. (2024). A High-Gain Directional 1x8 Planar Antenna Array for 2.4 GHz RFID Reader Applications. Journal of Circuits, Systems and Computers.
3. Tabakh, I., Das, S., Jorio, M., El Idrissi, N. E. A., Mohapatra, S., & Barad, D. (2020). Defected ground structure (DGS) incorporated RFID reader antenna array for indoor positioning systems at 2.45 GHz. International journal of microwave and optical technology, 15(6), 517-524.
4. El Arrouch, T., El Idrissi, N. E. A., & El Ansari, A. (2022, October). Microstrip Patch Antenna using a Parasitic Mushroom for 5GApplication at 28GHz. In 2022 9th International Conference on Wireless Networks and Mobile Communications (WINCOM) (pp. 1-6). IEEE.
5. El Ansari, A., Das, S., El Idrissi, N. E. A., El-Arrouch, T., & Bendali, A. (2022). Slot incorporated high gain Printed RFID Reader Array antenna for 2.4 GHz ISM band applications. In E3S Web of Conferences (Vol. 351, p. 01056). EDP Sciences.
6. Li, W. R., Chu, C. Y., Lin, K. H., & Chang, S. F. (2004). Switched-beam antenna based on modified Butler matrix with low sidelobe level. Electronics Letters, 40(5), 1.
7. Ansari, A. E., Das, S., Tabakh, I., Madhav, B. T. P., Bendali, A., & Idrissi, N. E. A. E. (2022). Design and Realization of a broadband multi-beam 1× 2 array antenna based on 2× 2 Butler Matrix for 2.45 GHz RFID Reader Applications. Journal of Circuits, Systems and Computers, 31(17), 2250305.
8. A. Eid, J. G. D. Hester, and M. M. Tentzeris, “Rotman Lens-Based Wide Angular Coverage and High-Gain Semipassive Architecture for Ultralong Range mm-Wave RFIDs,” IEEE Antennas Wirel. Propag. Lett., vol. 19, no. 11, pp. 1943–1947, 2020, doi: 10.1109/LAWP.2020.3002924.
9. SINGHAL, P. K., KUSHWAH, Ravi Pratap Singh, et SHARMA, P. C. Design of Rotman type bootlace lens for wide area scanning. In : 2009 6th International Conference on Electrical Engineering/Electronics, Computer, Telecommunications and Information Technology. IEEE, 2009. p. 762-765.
10. KUSHWAH, Ravi Pratap Singh, SINGHAL, Pramod Kumar, et SHARMA, P. C. Design of symmetric bootlace lens with gain analysis at UHF band. Progress In Electromagnetics Research Letters, 2009, vol. 6, p. 83-89.
11. XUE, L. et FUSCO, V. F. Printed holey plate Luneburg lens. Microwave and Optical Technology Letters, 2008, vol. 50, no 2, p. 378-380.
12. Pfeiffer, C., & Grbic, A. (2010). A printed, broadband Luneburg lens antenna. IEEE Transactions on Antennas and Propagation, 58(9), 3055-3059.
13. CHEN, Peng, HONG, Wei, KUAI, Zhenqi, et al. A double layer substrate integrated waveguide Blass matrix for beamforming applications. IEEE Microwave and Wireless Components Letters, 2009, vol. 19, no 6, p. 374-376.
14. FONSECA, Nelson JG. Printed S-Band 4$\times $4 Nolen Matrix for Multiple Beam Antenna Applications. IEEE transactions on antennas and propagation, 2009, vol. 57, no 6, p. 1673-1678.

15. Jizat, NoorlindawatyMd, et al. "5G beam-steering 2×2 butler matrix with slotted waveguide antenna array." Telkomnika 17.4 (2019): 1656-1662.

16. Tseng, C. H., Chen, C. J., & Chu, T. H. (2008). A low-cost 60-GHz switched-beam patch antenna array with Butler matrix network. IEEE Antennas and Wireless Propagation Letters, 7, 432-435.

17. Nachouane, H., Najid, A., Tribak, A., &Riouch, F. (2016). Beamforming Antenna Array Combining Pattern and Polarization Diversity for Cognitive Radio Applications. Wireless Personal Communications, 91(2), 957-973.

18. He, J., Wang, B. Z., He, Q. Q., Xing, Y. X., & Yin, Z. L. (2007). Wideband X-band microstrip Butler matrix. Progress In Electromagnetics Research, 74, 131-140.

19. Dall'Omo, C., Monediere, T., Jecko, B., Lamour, F., Wolk, I., & Elkael, M. (2003). Design and realization of a 4× 4 microstrip Butler matrix without any crossing in millimeter waves. Microwave and Optical Technology Letters, 38(6), 462-465.

20. Kim, S., Yoon, S., Lee, Y., & Shin, H. (2019). A miniaturized Butler matrix based switched beamforming antenna system in a two-layer hybrid stackup substrate for 5G applications. Electronics, 8(11), 1232.

21. Yang, Q. L., Ban, Y. L., Lian, J. W., Yu, Z. F., & Wu, B. (2016). SIW butler matrix with modified hybrid coupler for slot antenna array. IEEE Access, 4, 9561-9569.

22. El Ansari, A., Das, S., El-Arrouch, T., & El Idrissi, N. E. A. (2022, October). A Hybrid Coupler Integrated 1× 4 Printed Array Antenna with Broadband and High Performance For Beamforming RFID Reader. In 2022 9th International Conference on Wireless Networks and Mobile Communications (WINCOM) (pp. 1-6). IEEE.

23. EL ANSARI, Abdelaaziz, JAYAPRAKASAN, V., DURAISAMY, K., et al. A Wideband Microstrip 1 x 2 Array Antenna Fed by Coupler for Beam Steering Terahertz (THz) Band Applications. Journal of Nano-and Electronic Physics, 2023, vol. 15, no 3.

24. DUYEN, Bui Thi, PHUONG THAO, Hoang Thi, MINH THUY, Le, et al. Design of a beam steering antenna array using 8x8 butter matrix for indoor positioning system. Electromagnetics, 2020, vol. 40, no 7, p. 500-514.

25. OJAROUDI PARCHIN, Naser, JAHANBAKHSH BASHERLOU, Haleh, AL-YASIR, Yasir IA, et al. Reconfigurable antennas: Switching techniques—A survey. Electronics, 2020, vol. 9, no 2, p. 336.

26. ITOH, Kenji, SAKAI, Naoki, et NOGUCHI, Keisuke. Highly efficient high-power rectenna with the diode on antenna (DoA) topology. IEICE Transactions on Electronics, 2022, vol. 105, no 10, p. 483-491.

27. Clemente, A.; Dussopt, L.; Sauleau, R.; Potier, P.; Pouliguen, P. 1-bit reconfigurable unit cell based on PIN diodes for transmit-array applications in x-band. IEEE Trans. Antennas Propag. 2012, 60, 2260–2269

28. Slimani, A., Das, S., El Alami, A., Madhav, B. T., D Bennani, S., & Jorio, M. (2021). Phase shift switching of a miniaturized ultra-wideband hybrid coupler for 5G technology. Microwave and Optical Technology Letters, 63(2), 437-442.

29. Xin, N.L.; Cuiping, Y.; Yuanan, L.; Shulan, L.; Fan, W.; Ming, S. A Novel Compact Planar Crossover with Simple Design Procedure. In Proceedings of the Asia-Pacific Microwave Conference, Yokohama, Japan,7–10 December 2010; pp. 1633–1636.

30. Guo, Q.Y.; Zhang, X.Y.; Gao, L. Novel Compact Planar Crossover With Bandpass Response Based on Cross-Shaped Resonator. IEEE Trans. Compon. Packag. Manuf. Technol. 2017, PP, 1–9.

31. Feng, W.; Zhang, T.; Che, W. Compact Single-band Planar Crossover Based on Coupled Lines. In Proceedings of the 46th European Microwave Conference, London, UK, 4–6 October 2016.

32. Lee, Z.-W.; Pang, Y.-H. Compact planar dual-band crossover using two-section branch-line coupler. Electron. Lett. 2012, 48, 1348–1349.

33. Shao, J.; Ren, H.; Arigong, B.; Li, C.; Zhang, H. A fully symmetrical crossover and its dual-frequency application. IEEE Trans. Microw. Theory Tech. 2012, 60, 2410–2416.

34. Henin, B.; Abbosh, A. Design of compact planar crossover using Sierpinski carpet microstrip patch. IET Microw. Antennas Propag. 2015, 7, 54–60.

35. Menon, S. K. (2017). Microstrip patch antenna assisted compact dual band planar crossover. Electronics, 6(4), 74.

Chapter V: A Circularly Polarized Graphene based Wideband 1×2 Array Antenna for Terahertz Spectrum Applications

1. Introduction

The terahertz spectrum (0.1 to 10 THz) has tremendous potential applications in numerous fields including both outdoor and indoor communications. Moreover, it promises significant applications in many areas precisely in Manufacturing, agriculture, materials characterization, spectroscopic imaging and security [1]. Due to the availability of unallocated enormous bandwidth, the terahertz band supports a significant high-speed communication by implementing effective terahertz antennas [2-3], which is impossible to reach in the microwave band that is totally allocated and congested with specified applications. However, there are several factors including high atmospheric attenuation as well as the free space path loss which meanwhile limits the use of the entire THz spectrum effectively. In this regard, high gain and highly directive antennas are supremely required to overcome these problems and to permit efficient transmission of data over the long distance. Over the last few decades, the dominance of printed circuit technology has been clearly evident and as a result of this, microstrip patch antennas (MPAs) are highly preferred for successful establishment of wireless communication systems from RF up to THz frequency bands. Further, MPA has various advantages such as compactness, low weight, low cost, and can be easily fabricated, installed and conformed to any curved surface. However, some limitations such as low gain, low directivity, narrow bandwidth, linear polarization etc. are also associated with it. Therefore, many scientists and researchers have reported a few techniques to make up these deficiencies of microstrip antenna by modifying the patch and ground structures [4-6], multilayer substrate [7-8], metamaterials [9-10], electromagnetic band gap (EBG) [11-12], and MEMS-based [13] antenna structures etc. The photoconductive antennas play a vital role for generation and detection of terahertz (THz) radiations, but they have the main drawback of low output power due to impedance mismatching. To resolve this issue, microstrip patch antennas are alternatively preferred to support applications in different spectrums of terahertz frequency regime. In the literature, researchers have adopted and explored many new design methodologies for designing various geometries of printed terahertz antennas which includes a Yagi antenna with graphene patch [14], simple rectangular patch antenna with graphene conducting material [15-17], graphene

nano ribbon based patch [18], waveguide integrated patch antenna [19], patch antenna loaded with 1D, 2D, and 3D photonic crystals [20], patch antenna with U-shaped slot [21], patch with defected ground and PBG substrate [22, 23], two-layered array antenna [24], metamaterial loaded antenna [25], rectangular MPA on a polyimide substrate [26], RMPA with combinations of PBG and frequency selective surface (FSS) [27], graphene based ring shaped patch on SiO2 substrate [28], 2×2 MIMO [29], semi-circular moon shaped radiator [30], octagonal shorted annular ring 1×2 array antenna [31], 2×2 loop antenna array antenna [32], fractal MIMO antenna [33], rhombus shaped patch radiator [34], novel coronavirus shaped patch [35] etc.

Although these techniques have successfully managed to design terahertz antennas with acceptable characteristics parameters, these structures are restricted against polarization i.e., the antennas are arbitrary orientated and linearly polarized. Nowadays, the most demandable antennas are the antennas having a circular polarization (CP) due to their ability to transmit electromagnetic waves in any direction. A CP antenna is highly required to establish an efficient communication system link as it transmits in all planes. From an antenna, the circularly polarized waves can be generated by exciting two orthogonal modes with a 90° phase shift difference between them. Two orthogonal modes can be excited by using dual feeds and single feed methods. The best way to apply the dual feeds is to excite the radiating elements at two adjacent edges using either a 90° power divider or 90° hybrid coupler [36]. Some suggestions are reported in the literature using the dual feeds [37-39]. However, the dual feed arrangements have some complexities such as the symmetry, bulky size and maximum cross polarization level. These complexities can be significantly reduced using a single feed along the diagonal of the radiating element, starting at the point of the left corner for LHCP (Left Hand Circular Polarization) or at the point of the right corner for RHCP (Right Hand Circular Polarization). Moreover, using the single feed, a nearly CP wave can be achieved by cutting the thin rectangular slots at the centers of the patch or by cutting two opposite corners of the patch. Several single feed configurations are reported in the literature [40-41]. In this context of single feed, few works are proposed to achieve circular polarization by cutting meandered cross-shaped slots [42] or only cross-shaped slots [43]. The above-mentioned design methodologies [36-43] for achieving circular polarization are referred for microwave and mm-wave application bands. In a likewise manner, there are high demands for circularly polarized THz antennas for supporting numerous applications at different terahertz frequency spectrum as recommended and reported in [44-48]. It includes S-shaped and Z-shaped slots loaded CP antenna structure [44], rectangular dielectric resonator CP antenna [45], E-shaped transparent antenna [46], an optical transparent antenna perturbed with E and I-shaped slots [47] etc.

In this work, based on the literature studies, the authors are motivated with an aim to design an array antenna to offer high gain, wide bandwidth and circular polarization (CP) characteristics by maintaining its compact size. The proposed array configuration has been adopted to achieve CP characteristics using a single feed technique. The corner truncated optimized patches are modified by adding flower slots and a circular slot in order to get an ideal circular polarization with enhanced performance. Finally, these two patch elements are fed together by a T power divider which results in an increase in impedance bandwidth, 3dB axial ratio bandwidth, gain, and efficiency. This array antenna is dedicated to operate for wireless communications in the Terahertz (THz) band, especially at around 2.45 THz. Consequently, it can be utilized for high-speed data transmission, material characterization, terahertz spectroscopy and terahertz imaging, etc. applications.

After this introduction part, the rest of the chapter is arranged as follows: In section 2, the design methodology for the proposed single radiating element is discussed. Section 3 is dedicated to design and simulation results of the single fed circularly polarized array antenna. After that, an extensive performance comparison analysis with state of the art is analyzed in section 4. Then, finally the chapter is concluded in section 5.

2. Basic Radiating Element Design Methodology

The basic element is considered as a rectangular shaped patch antenna (RSPA). The radiating patch and the feed line are realized above the substrate, then the ground plane is integrated below the substrate. The proposed basic element is fed by a folded impedance matching transformer to get a minimized antenna size. The intended shape of the single element antenna has been reached after following seven optimization steps through the incorporation of truncated corners, flower-shaped slots and a circular slot. These seven steps are used in order to obtain resonating frequency at 2.45 THz with an improved return loss and axial ratio. This proposed design is conducted on Rogers' substrate (RT/duroid 5880) with the total dimensions of $50\times51\times1.56$ μm^3. Graphene is used as conducting material due to its impressive electrical, thermal, and mechanical properties.

2.1 Effect of Truncated Corners

Initially the basic radiating element is shown in Figure V.1 (a). Its length (L) and width (W) are almost the same (dimensions are included in Table V.1). First of all, in Case 1, the proper impedance matching has been assured by a quarter wave impedance transformer in folded shape in order to achieve minimum antenna size as displayed in Figure V.1(a). Its reflection coefficient versus frequency is shown in Figure V.2 (a) that shows a resonance peak at 2.62 THz with a S_{11}

of about −5.5 dB. Moreover, its axial ratio variations are shown in Figure V.2 (b), according to the curve, it has values tending to maximum limit (much above 3 dB) which confirms that the design in Case1 has a linear polarization. In order to make the basic element a circularly polarized, 90° phase differed two orthogonal resonant modes of equal magnitudes should be generated. In the next steps, we are going to introduce some improvement design steps that can help to generate these orthogonal modes.

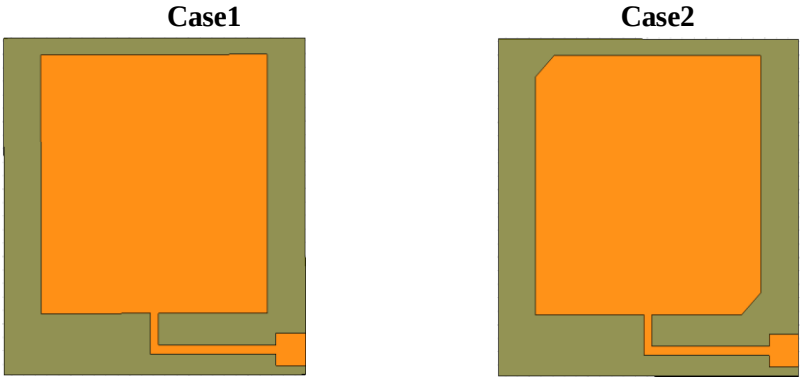

Figure V. 1 (a) The basic element fed by a folded quarter wave impedance transformer. (b) The basic element with two truncated corners

The first stage for improving the performance of the structure presented as Case1 is to truncate two corners at two opposite sides as shown in Case 2 of Figure V.1 (b). These two truncated corners perturb the patch along its diagonal axes, and make an asymmetric structure. Consequently, it leads the basic element near to the circular polarization and offers significant impedance matching and shifting of resonance to a lower value. Figure V.2 (a-b) shows its reflection coefficient S_{11} versus frequency as well as its axial ratio versus frequency for Case 2. The reflection coefficient is improved to −11 dB at 2.52 THz and also, the axial ratio is down to 9 dB at 2.54 THz.

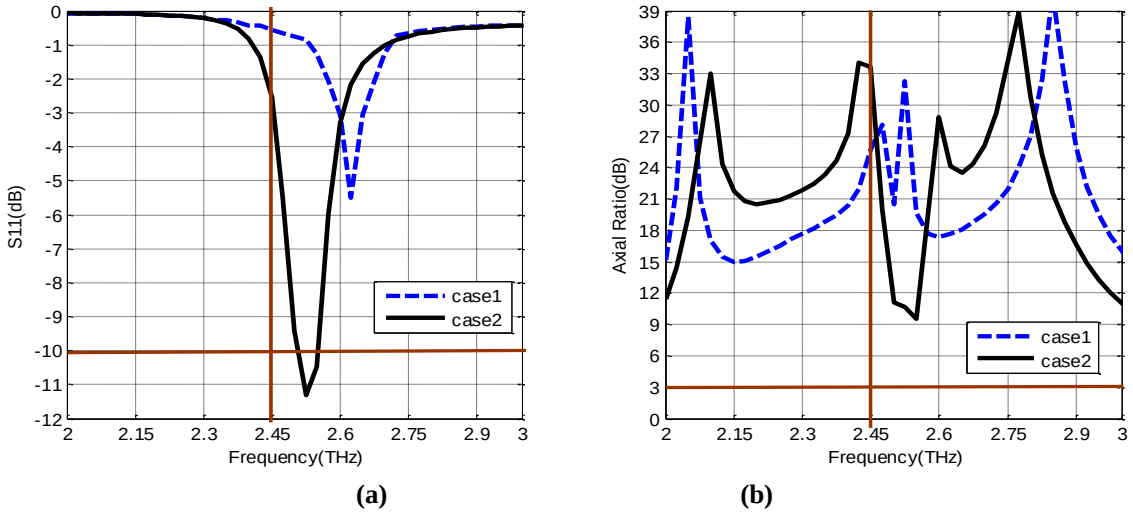

Figure V. 2 Simulation results of case 1 versus case 2. (a): S11 versus frequency (b): The axial ratio versus

frequency

2.2 Effect of Flower Slots

In Case 2, the values in terms of S_{11} (=−11 dB) and AR (=9 dB) aren't enough to obtain a wideband antenna with good circularly polarized waves. In the third step (Case 3), objective is to resonate the basic element at the desired frequency (2.45 THz) with improved performance. The first flower-shaped slot is introduced within the patch as displayed in Case 3 of Figure V.3. As seen, the resonant frequency is further moved to a lower value, but the minimum value of the AR is not reached to 3 dB at the desired frequency of 2.45 THz [see Figure V.4(b)]. In order to achieve it, the next step is executed in which a second flower slot is added in the opposite quarter (see Figure V.3, Case 4). As shown in Case 4 of Figure V.4, the resonance is further lowered and decreased to 3 dB value as per AR vs frequency plot. After that, a 3rd flower slot is added in the 3rd quarter as depicted in Case 5 of Figure V.3. Now, with respect to both S_{11} and AR, the resonant frequency is achieved at the same value but not at the desired value of 2.45 THz as shown in Figure V.4 [Case 5]. In this context, the 4th flower slot is added (see Figure V.3, Case 6). In this case, the resonant frequency at 2.45 THz is obtained for both AR and S_{11} plots. The antenna shows S_{11} = −19 dB, and AR=1.3 dB at 2.45 THz with an improved −10 dB IBW and 3 dB axial ratio BW as compared to the preceding design cases.

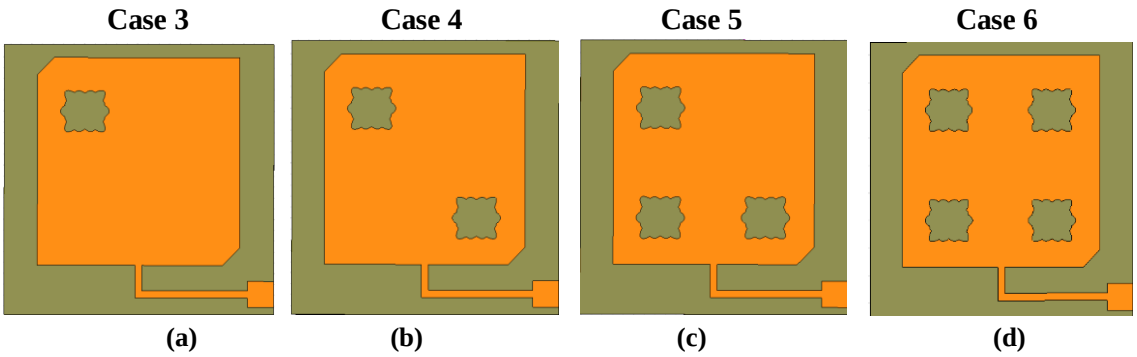

Figure V. 3 Flower shaped slots loaded design cases (a) one flower slot (b) two (c) three (d) four flower slots

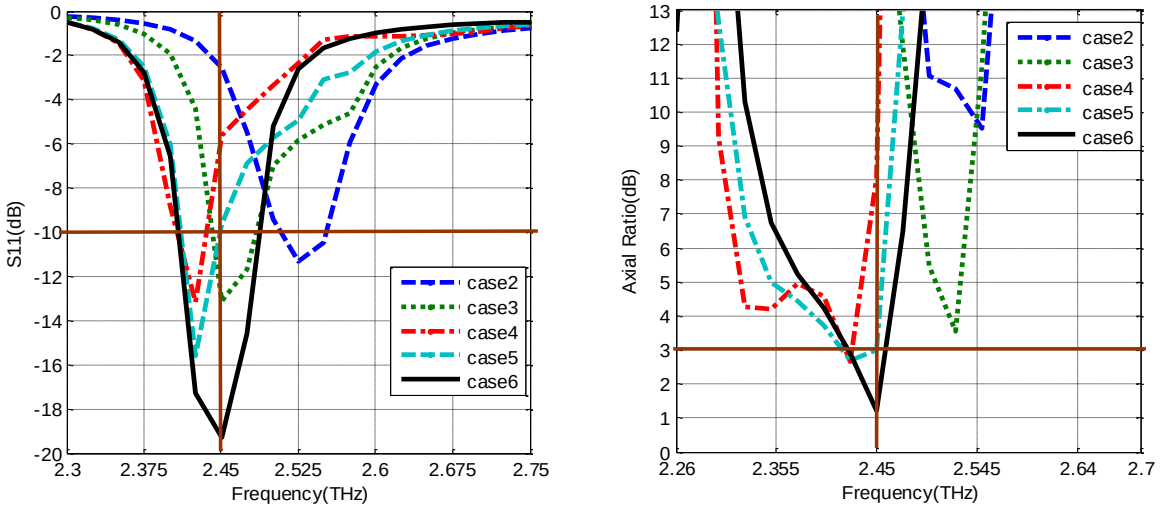

(a) **(b)**

Figure V. 4 Simulation results of Case 2, 3, 4, 5, and 6. (a): S11 versus frequency (b): Axial ratio versus frequency

2.3 Effect of Circular Slot

In addition to the previous six improvement steps, in this section we present the last improvement step designated as Case 7. In this case, a circular slot is added to the patch antenna as depicted in Figure V.5. The optimal radius of this circular slot is obtained after parametric sweep. This slot is used for the enhancement of bandwidth in terms of both reflection coefficient S_{11} and axial ratio as well as for decreasing their minimum values. Also, the gain and the radiation efficiency in this case are slightly enhanced due to the presence of an optimized circular slot. The design parameters of the optimized basic antenna are tabulated in Table V.1.

Case 7

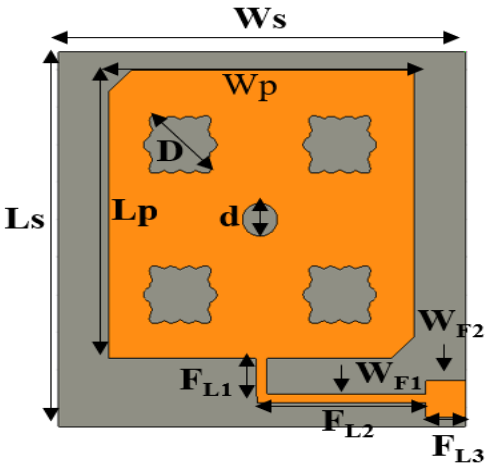

Figure V. 5 Proposed Flower- shaped and circular slots-based CP antenna

Table V. 1 The final geometrical parameters of the basic antenna

Parameters	L_S	W_S	L_P	W_P	F_{L1}	F_{L2}	F_{L3}	W_{F1}	W_{F2}	D	d
Value (µm)	50	51	38.42	38.22	10	21.43	5	1.35	4.84	10.4	4.5

The results of simulation study for basic element (comparison of Case 7 against Case 6) are exhibited in Figure V.6. As shown, the performance parameters achieved in Case 7 are improved compared to Case 6. The reflection coefficient is improved to −24 dB with a little bit increment in impedance bandwidth at−10 dB reference level. However, prominently, the 3 dB axial ratio bandwidth is increased from 35 GHz to 165 GHz along with little bit improvements in the peak gain and radiation efficiency as well.

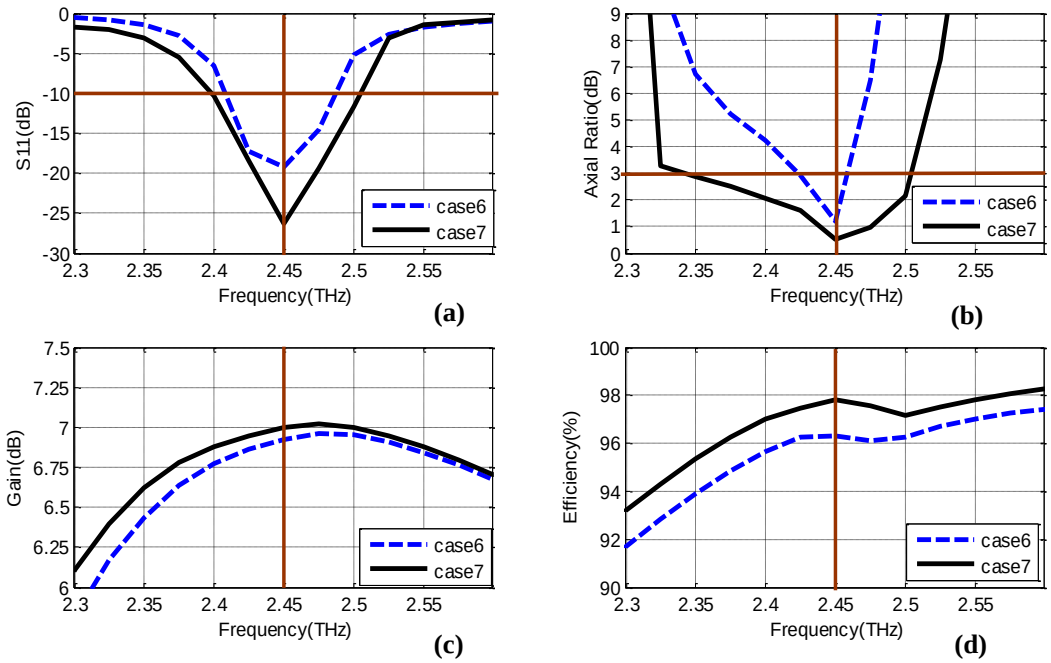

Figure V. 6 Simulation results of the proposed single fed circularly polarized basic element antenna. (a): reflection coefficient bandwidth. (b): Axial ratio bandwidth. (c): Gain. (d): Radiation efficiency

The surface current distribution of the optimized basic element with phases 0°, 90°, 180° and 270° at 2.45 THz are shown in Figure V.7. The current vectors tip direction changes clockwise which means that the basic element has a right-hand circular polarization (RHCP). These flower slots as well as the circular slot helped to perturb the surface current distribution in the patch. Therefore, two orthogonal degenerate modes of some resonance frequency having equal amplitude have been excited.

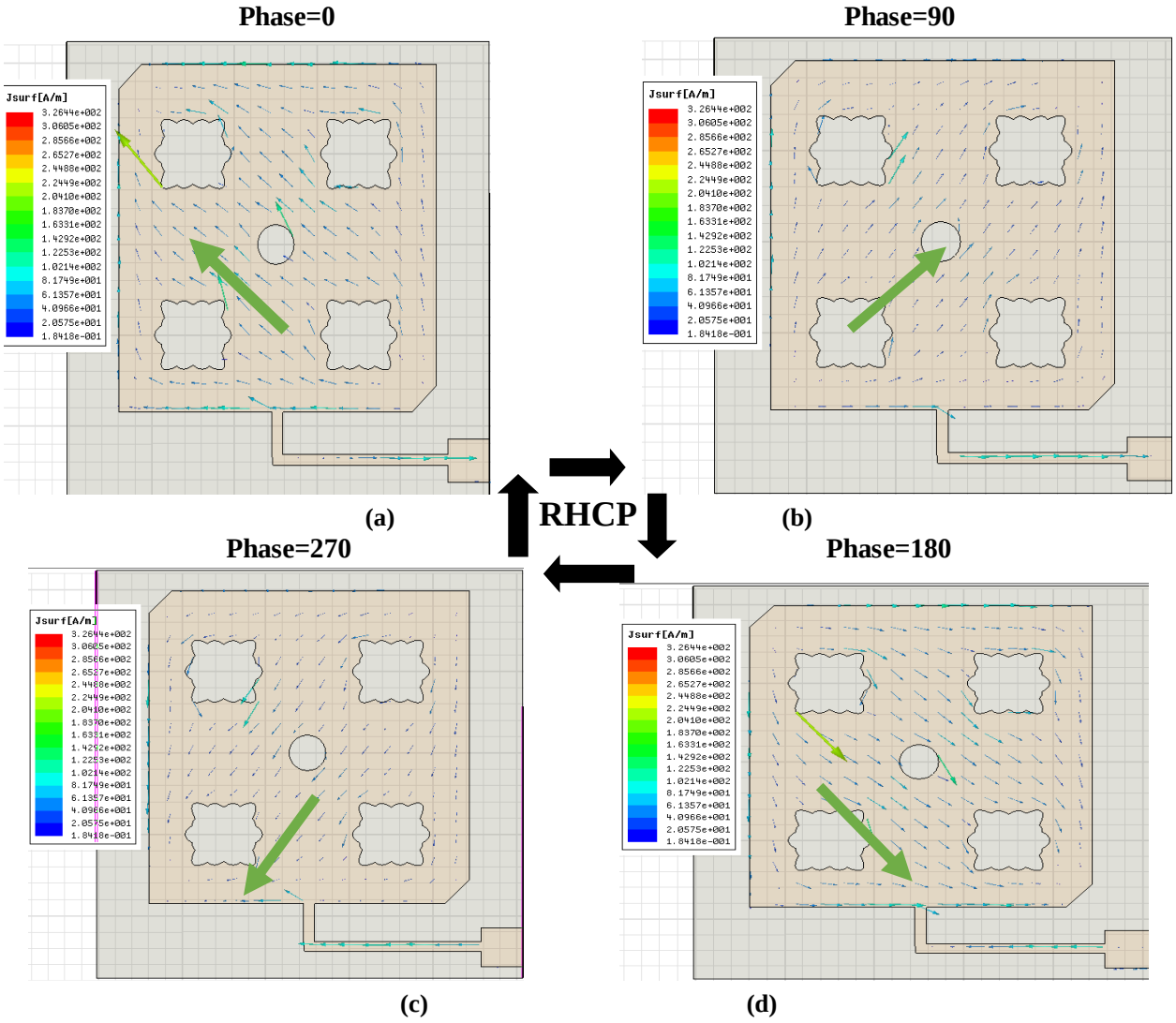

Figure V. 7 surface current distribution 2.45 THz with the phase of (a) 0° (b) 90° (c) 180° (d) 270°

2.4 Parametric variations Analysis

The effect of variation in the radius of the incorporated circular slot has been examined through simulation tool. It can be visualized that the addition of a circular slot within the patch structure is a very crucial design step. The variations in its radius (r) control the bandwidth of the antenna very significantly. The variations in S_{11} (dB) and Axial Ratio (dB) as a function of radius (r) is depicted in Figure V.8 (a-b), respectively. It can be noticed that maximum IBW and 3-dB ARBW are

achieved for the proposed dimension of r = 2.75 µm as indicated by black solid line. The bandwidth performance is getting worse with further increase or decrease in its dimensions. So, r = 2.75 µm is considered as the optimal radius of the circular slot during the design process.

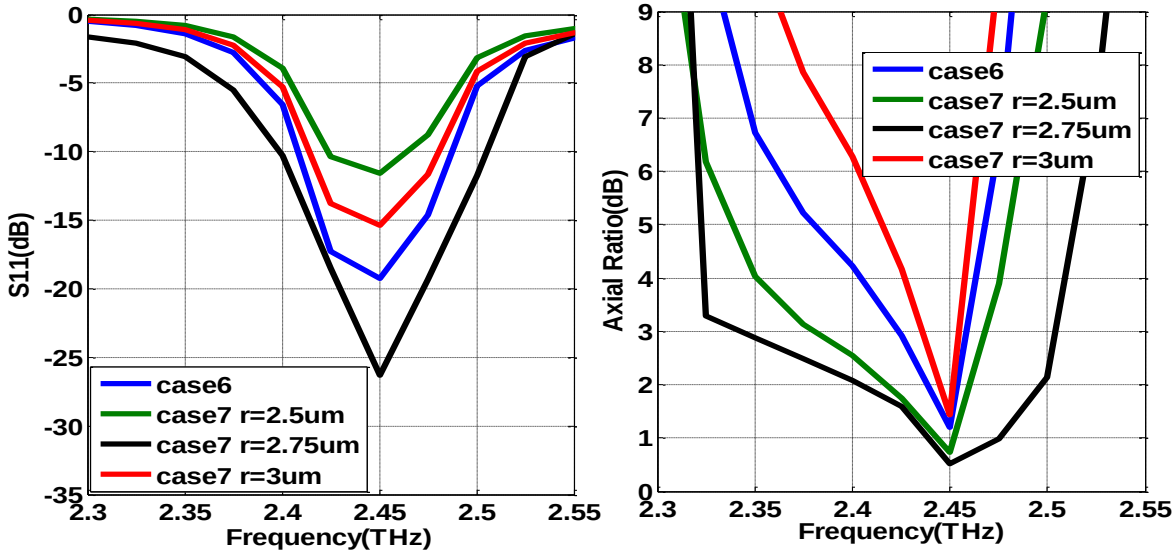

(a) **(b)**

Figure V. 8 Variations in operating bandwidth as a function of circular slot radius 'r' (a) S11 (dB) (b) Axial Ratio (dB).

3. Proposed 1×2 Array Antenna

In this section, the design and simulation results of the proposed graphene based single fed circularly polarized 1×2 array antenna are discussed. For the excitation of the array, a simple T-power divider is used to feed two identical radiating elements to get well adopted impedance matching as shown in Figure V.9. The performance of this array is analyzed to justify improvements in gain, radiation efficiency, axial ratio bandwidth and the reflection coefficient bandwidth. The intended array design is executed on the rogers' RT/duroid 5880 substrate with the overall size of 53.5×102×1.56 μm^3.

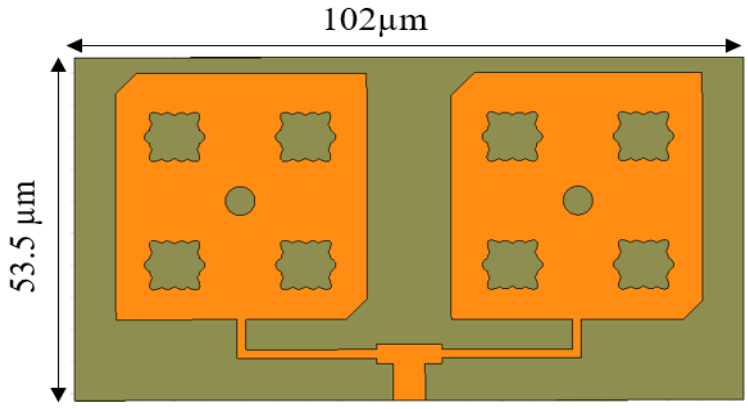

Figure V. 9 Proposed single fed circular polarized 1×2 array antenna

The simulation studies of the proposed single fed circularly polarized array antenna have been performed by HFSS EM solver. Figure V.10 (a) shows the reflection coefficient versus frequency which shows bandwidth of the array antenna is well improved and equals 210 GHz (from 2.345 THz to 2.555 THz). The axial ratio versus frequency is shown in Figure V.10 (b). The 3 dB axial ratio bandwidth is also significantly enhanced and it equals 205 GHz (2.345−2.55 THz). The gain versus frequency is illustrated in Figure V.10 (c), according to this figure, it is clearly noticed that the peak gain is increased to 8.65 dB at 2.45 THz. The radiation efficiency versus frequency is depicted in Figure V.10 (d); the peak radiation efficiency is increased to 99.97% at 2.45 THz. The E and H plane radiation patterns of the proposed array antenna are presented indicating both co-pol and cross pol components. The patterns are displayed in Figure V.11(a-b). The radiation patterns resemble almost omnidirectional in shape and the cross-pol levels are adequately down in comparison to co-pol in both the planes.

In addition, the circular polarization is evaluated using the surface current distribution at the 2.45 THz as shown in Figure V.12. The circular polarization is achieved by excitation of two orthogonal modes with 90° phase shift difference. This is accomplished by the single feed, corners truncated, flower slots and circular slot inserted on the patch element. In surface current distributions, figures with 0°, 90°, 180°, and 270° phases are plotted. Thus, it is clear that the direction of the vector current tips rotates in clockwise direction, which proves the RHCP (Right Hand Circular Polarization) of the antenna in boresight direction.

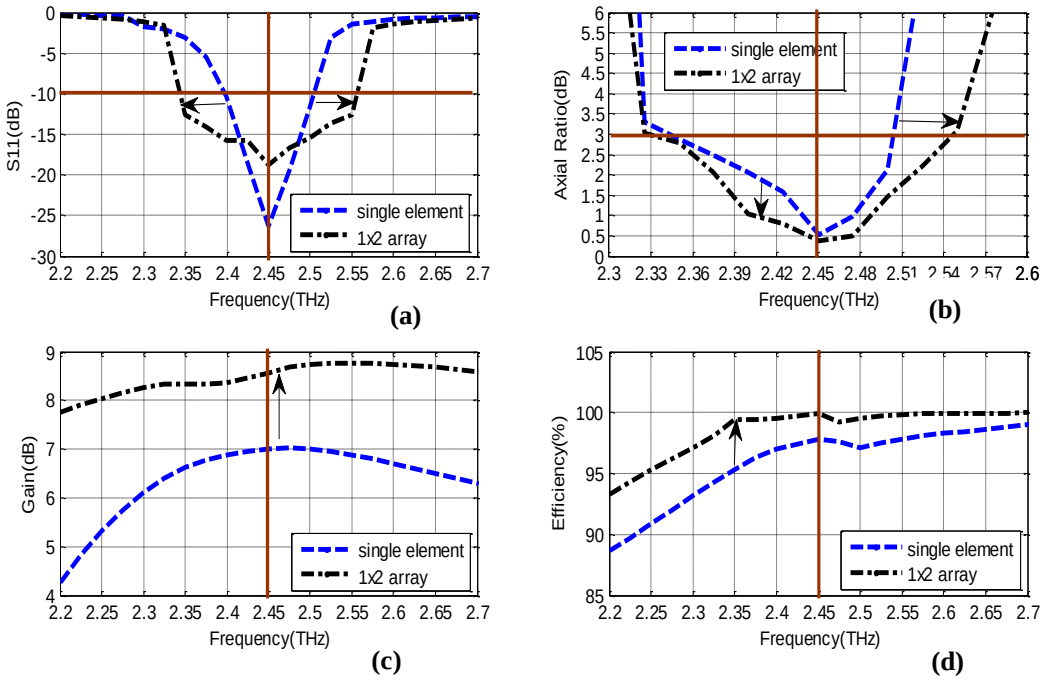

Figure V. 10 Simulation results of the proposed single fed circularly polarized 1×2 array antenna. (a): S11 (dB) (b): Axial ratio bandwidth. (c): Gain (d): Radiation efficiency versus frequency

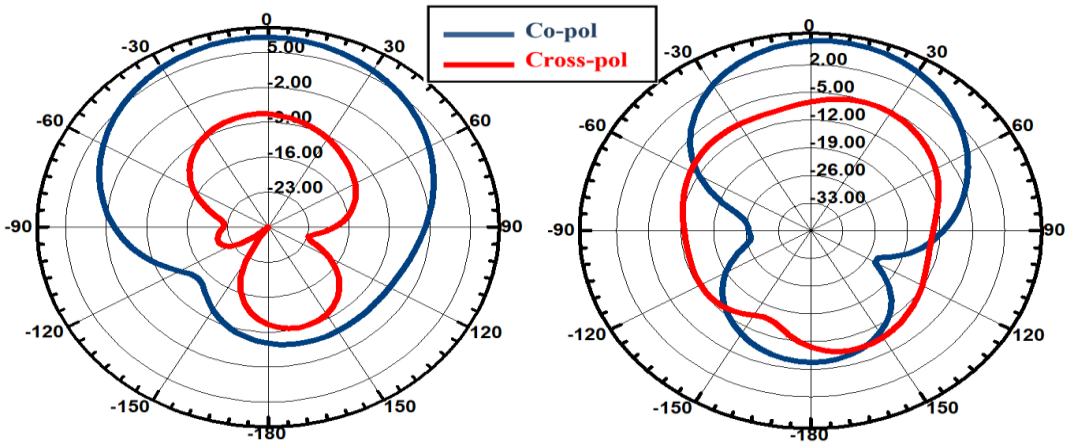

(a) (b)

Figure V. 11 Radiation patterns representing Co-pol and Cross-pol at 2.45 THz (a) E plane (b) H-plane

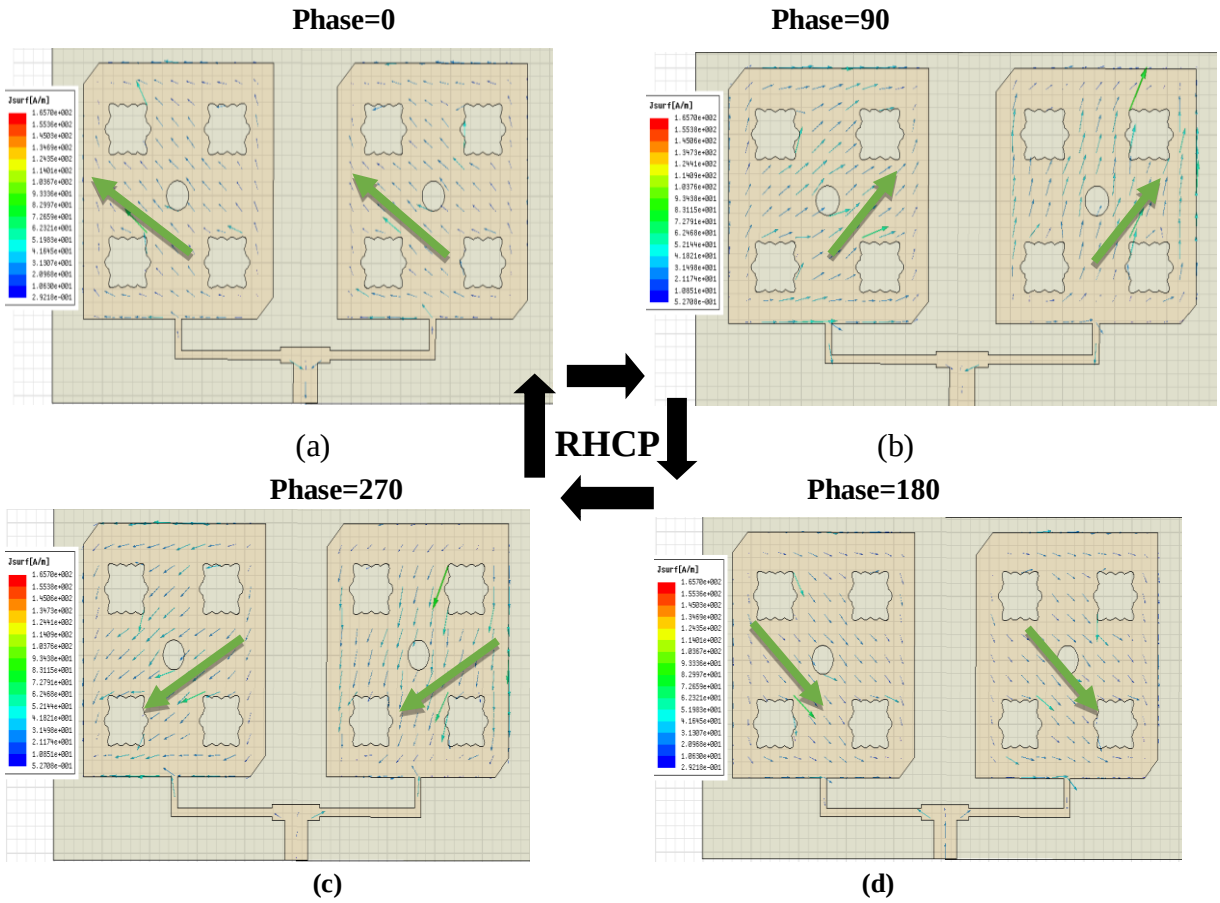

Figure V. 12 surface current distribution of the proposed 1×2 array antenna at 2.45 THz with phases of :(a) 0° (b) 90° (c) 180° (d) 270°.

4. Performance comparison with other terahertz antennas and Discussion

The performance of the suggested circularly polarized high gain, highly efficient terahertz array antenna is compared with few previously referred terahertz antennas [14-35, 44-47] in terms of antenna size, operating band, impedance bandwidth, axial ratio bandwidth, gain, and polarization. The literature review of other reported antennas is presented with an extensive discussion on their design methodologies and reported results. The performance comparison is summarized and presented in Table V.2. In the Table, the referred antenna structures are single element, array, and MIMO antennas of different configurations. The reported antennas [14-35] do not possess the capability to radiate with circular polarization. But the circularly polarized (CP) antenna is highly required to establish an efficient communication system link as it transmits in all planes. Hence, many researchers have carried out research on this issue and a few terahertz antenna designs with CP characteristics are referred to in [44-47]. This works as the motivation of this proposed work; the authors of this chapter got encouragement to work on a new design and propose a terahertz antenna with standard performance parameters such as wide bandwidth, wideband circular polarization, high gain, and high radiation efficiency with miniaturized antenna size. As compared with other existing linearly polarized (LP) THz antenna designs [14-35], the proposed array antenna is most miniaturized. It offers much broader operating bandwidth as compared to references [14-27, 29-32]. The proposed array antenna provides highest gain as compared to all other references except ref. [30]. But it offers much wider impedance bandwidth with compact size compared to ref. [30]. Some other linearly polarized antennas [28, 33-35] report wider bandwidth in comparison to the proposed antenna but as a whole the proposed array configuration is advantageous in terms of smaller size, better gain, and shows circular polarization with wider 3 dB AR bandwidth.

On the other hand, except ref. [44], the impedance bandwidth (210 GHz) of the proposed array is not higher than other referred CP THz antennas [45-47]. However, it is evident that 3 dB AR BW of the proposed antenna is 205 GHz (2.345-2.55 THz), which is broadest as compared with other Terahertz CP antennas and this confirms better circular polarization performance over maximum range of frequencies. Finally, the proposed design holds most miniaturized size ($0.84\lambda_0 \times 0.44\lambda_0$) and also shows highest gain value of 8.65 dB in comparison to other referred CP antennas [44-47]. So, the suggested array antenna could be promising for high-speed data transmission, material characterization, terahertz spectroscopy and terahertz imaging applications in terahertz regime due to its attractive size and superior performance.

Table V. 2 Performance comparison of the proposed array antenna with other previous references

Ref.	Antenna Size $\lambda_0 x \lambda_0$ (μm^2)	Operating Band (THz)	−10 dB Impedance Bandwidth	3 dB Axial Ratio (AR) Bandwidth (BW) (GHz)	Maximum Gain (dB)	Circular Polarization Capability
[30]	1.58×1.4	0.616-0.64	4%	NA	9.45	No
[31]	1.13×0.56	0.303-0.320	5.4%	NA	4.4	No
[32]	1.26×1.26	0.335-0.360	7.2%	NA	7.7	No
[33]	0.71×0.35	0.35-0.75	11%	NA	5.49	No
[34]	0.55×0.55	0.445-0.714	48%	NA	5.7	No
[35]	0.44× 0.44	0.3627- 0.5918	52%	NA	4.0	No
[44]	1.2× 0.46	0.258-0.355	35%	9.3%	5.6	Yes
[45]	-	3.3688-3.7232	10%	2%	8.0	Yes
[46]	1.1×0.55	0.98-1.225	22%	8.8%	2.59	Yes
[47]	1.1×0.55	0.98-1.23	23%	8.7%	2.61	Yes
Proposed	**0.84×0.44**	**2.345-2.555**	**8.57%**	**9.4%**	**8.65**	**Yes (RHCP)**

NA= Not Applicable; RHCP= Right hand circular polarization

5. Conclusion

In this chapter, an effort has been made to design a new 1×2 array antenna with a circular polarization using a single feed technique for terahertz band applications. The intended geometry of the single antenna element has been obtained through the execution of six development stages. The design methodology includes connection of folded feed line, corner truncation of the patch, and the inclusion of four flower shaped slots placed in each quadrant of the patch along with the presence of a circular shaped slot. The modified single element patch antenna shows transformed polarization from linear to circular with enhanced 3 dB AR bandwidth performance. Finally, a 1×2 array is configured comprising of two single element patches, which are fed together by a T power divider. The suggested circularly polarized terahertz array antenna measures a compact geometry with an overall size of 102×53.5×1.56 in micrometer scale. Furthermore, it offers IBW of 210 GHz (2.345 to 2.555 THz), 3 dB ARBW of 205 GHz (2.345 to 2.55 THz), maximum gain and radiation efficiency of 8.65 dB and 99.8%, respectively. This suggested circularly polarized microstrip 1×2 array antenna is dedicated to work for wireless communications in the Terahertz (THz) spectral band precisely at around 2.45 THz. Therefore, it can be utilized for high-speed data transmission, material characterization, terahertz spectroscopy and terahertz imaging, etc. applications.

References

1. Shamim, S.M., Das, S., Hossain, M.A. *et al.* Investigations on Graphene-Based Ultra-Wideband (UWB) Microstrip Patch Antennas for Terahertz (THz) Applications. *Plasmonics.* **16**, 1623–1631 (2021). https://doi.org/10.1007/s11468-021-01423-8

2. Eddine Lamri, Isam, Ahmad, Sarosh, Nakmouche, Mohammed Farouk, Ghaffar, Adnan, Fawzy, Diaa E., Allam, A.M.M.A., Ali, Esraa Mousa, Dalarsson, Mariana and Alibakhshikenari, Mohammad. "Design and development of a graphene-based reconfigurable patch antenna array for THz applications" *Frequenz*, vol. 77, no. 3-4, 2023, pp. 219-228. https://doi.org/10.1515/freq-2022-0051

3. Sharma, Amit, Tiwari, Pratik and Vishwakarma, Dinesh Kumar. "Frequency re-configurable metal-graphene hybrid MIMO patch antenna for terahertz communication" *Frequenz*, vol. 76, no. 7-8, 2022, pp. 381-389. https://doi.org/10.1515/freq-2021-0174

4. Fatima Kiouach, Bilal Aghoutane, Sudipta Das, Tanvir Islam, Mohammed El Ghzaoui and BTP Madhav, A dual operating (27/38 GHz) high performance 2 × 4 MIMO antenna array for 5G new radio applications, *Phys. Scr.* **98** 115504, 2023.

5. K Vasu Babu, Das Sudipta, Gorre Naga Jyothi Sree, Abdulkarem H M Almawgani, Tanvir Islam and Adam R H Alhawari, Deep Learning Assisted Fractal Slotted Substrate MIMO Antenna with Characteristic Mode Analysis (CMA) for Sub-6GHz n78 5G NR Applications: Design, Optimization and Experimental Validation, *Phys. Scr.* 98 115526, 2023.

6. Ansari, A. E., Das, S., Islam, T., Asha, S., El Idrissi, N. E. A., & Madhav, B. T. P. (2024). A High-Gain Directional 1x8 Planar Antenna Array for 2.4 GHz RFID Reader Applications. Journal of Circuits, Systems and Computers.

7. Yu X, Liang M, Shemelya C, et al. 3-D Printed Parts for a Multilayer Phased Array Antenna System. IEEE Antennas Wirel Propag Lett. 2018;17(11):2150-2154.

8. Lamminen A, Saïly J, Ala-Laurinaho J, Cos J De, Ermolov V. Patch Antenna and Antenna Array on Multilayer High-Frequency PCB for D-Band. IEEE Open J Antennas Propag. 2020;1(1):396-403. doi:10.1109/OJAP.2020.3004533

9. Saktioto, Soerbakti Y, Syahputra RF, et al. Improvement of low-profile microstrip antenna performance by hexagonal-shaped SRR structure with DNG metamaterial characteristic as UWB application. Alexandria Eng J. 2022;61(6):4241-4252. doi: 10.1016/j.aej.2021.09.048

10. Althuwayb AA, Alibakhshikenari M, Virdee BS, et al. Design technique to mitigate unwanted coupling in densely packed radiating elements of an antenna array for electronic devices and wireless communication systems operating in the millimeter-wave band. AEU - Int J Electron Commun. 2023; 159:154464. doi: 10.1016/j.aeue.2022.154464

11. Dellaoui S, Kaabal A, El Halaoui M, Asselman A, Ahyoud S, Rmili L. High Gain Array Antenna Using Electromagnetic Band Gap Structures for 5G Applications. Prog Electromagn Res C. 2022;118(February):83-97. doi:10.2528/PIERC21111503

12. Kumar G, Singh D, Kumar R. A planar CPW fed UWB antenna with dual rectangular notch band characteristics incorporating U-slot, SRRs, and EBGs. Int J RF Microw Comput Eng. 2021;31(7). doi:10.1002/mmce.22676

13. Saha R, Maity S, Bhunia CT. Design and characterization of a tunable patch antenna loaded with capacitive MEMS switch using CSRRs structure on the patch. Alexandria Eng J. 2016;55(3):2621-2630. doi: 10.1016/j.aej.2016.05.002
14. Zarrabi FB, Seyedsharbaty MM, Ahmed Z, Arezoomand AS, Heydari S (2017) Wide band yagi antenna for terahertz application with graphene control. Optik (Stuttg) 140:866–872. https://doi.org/ 10.1016/j.ijleo.2017.05.009
15. Sharma A, Singh G (2009) Rectangular microstirp patch antenna design at THz frequency for short distance wireless communication systems. J Infrared Millimeter Terahertz Waves 30(1):1–7. https:// doi.org/10.1007/s10762-008-9416-z
16. R.H. Mahmud, Terahertz microstrip patch antennas for the surveillance applications, Kurdistan Journal of Applied Research (KJAR), Vol.5, pp. 17-27, 2020, DOI:10.24017/science.2020.1.2
17. Goyal, Rahul, and Dinesh Kumar Vishwakarma. "Design of a graphene-based patch antenna on glass substrate for high-speed terahertz communications." Microwave and Optical Technology Letters 60, 7 (2018): 1594-1600.
18. S. Anand, D. Sriram Kumara, R. J. Wub, M. Chavali, "Graphene nanoribbon-based terahertz antenna on polyimide substrate", Optik 125 (2014) 5546–5549
19. K. R. Jha and S. K. Sharma, "Waveguide integrated Microstrip patch antenna at THz frequency," in 2014 IEEE Antennas and Propagation Society International Symposium (APSURSI), pp. 1851-1852, 2014.
20. Kushwaha, Ritesh Kumar, and P. Karuppanan. "Investigation and design of microstrip patch antenna employed on PCs substrates in THz regime." Australian Journal of Electrical and Electronics Engineering 18.2 (2021): 118-125.
21. Q. Rubani, S.H.Gupta, S.Pani, A. Kumar, Design and analysis of a terahertz antenna for wireless body area networks, Optik, Vol. 179, 2019, 684-690.
22. Shahid Ullah, Cunjun Ruan, Tanveer Ul Haq & Xingyun Zhang (2019): High performance THz patch antenna using photonic band gap and defected ground structure, Journal of Electromagnetic Waves and Applications, 33.15 (2019): 1943-1954. DOI: 10.1080/09205071.2019.1654929
23. Paul LC, Islam M. Proposal of wide bandwidth and very miniaturized having dimension of μm range slotted patch THz microstrip antenna using PBG substrate and DGS. 20th Int Conf Comput Inf Technol ICCIT. 2017: 1–6.
24. Azarbar, A.; Masouleh, M.S.; Behbahani, A.K. A new terahertz microstrip rectangular patch array antenna. Int. J. Electromagn. Applications 2014, 4, 25–29.
25. Sirmaci, Y.D., Akin, C.K., Sabah, C.: Fishnet based metamaterial loaded THz patch antenna. Opt. Quantum Electron. 48(2), 168 (2016)
26. Dhillon, A.S., Mittal, D., Sidhu, E.: THz rectangular microstrip patch antenna employing polyimide substrate for video rate imaging and homeland defence applications. Optik 144, 634–641 (2017)
27. Nejati, A., Sadeghzadeh, R.A., Geran, F.: Effect of photonic crystal and frequency selective surface implementation on gain enhancement in the microstrip patch antenna at terahertz frequency. Phys. B 449, 113–120 (2014)
28. Nickpay, M.R., Danaie, M., Shahzadi, A.: Wideband rectangular double-ring nanoribbon graphene-based antenna for terahertz communications. IETE J. Res. (2019).

29. TayfunOkan, High efficiency unslotted ultra-wideband microstrip antenna for sub-terahertz short range wireless communication systems, Optik, Volume 242, 2021, 166859
30. Ahmad, Inzamam, Sadiq Ullah, Shakir Ullah, Usman Habib, Sarosh Ahmad, Adnan Ghaffar, Mohammad Alibakh shikenari, Salahuddin Khan, and Ernesto Limiti. 2021. "Design and Analysis of a Photonic Crystal Based Planar Antenna for THz Applications" Electronics 10, no. 16: 1941. https://doi.org/10.3390/electronics10161941
31. H. Zhu, X. Li, Z. Qi and J. Xiao, "A 320 GHz Octagonal Shorted Annular Ring On-Chip Antenna Array," in IEEE Access, vol. 8, pp. 84282-84289, 2020, doi: 10.1109/ACCESS.2020.2991868.
32. X.-D. Deng, Y. Li, W.Wu, and Y.-Z. Xiong, ``340-GHz SIW cavity-backed magnetic rectangular slot loop antennas and arrays in silicon technology," IEEE Trans. Antennas Propag., vol. 63, no. 12, pp. 5272_5279, Dec. 2015.
33. K.V. Babu, S. Das, G.N.J. Sree, B.T.P. Madhav, S.K.K. Patel, J. Parmar, Design and optimization of micro-sized wideband fractal MIMO antenna based on characteristic analysis of graphene for terahertz applications. Opt. Quantum. Electron. 54(5), p1-20 (2022)
34. Krishna, C.M., Das, S., Nella, A. et al. A Micro-Sized Rhombus-Shaped THz Antenna for High-Speed Short-Range Wireless Communication Applications. Plasmonics 16, 2167–2177 (2021). https://doi.org/10.1007/s11468-021-01472-z
35. Kiani, S., Rezaei, P. & Fakhr, M. On-chip coronavirus shape antenna for wide band applications in terahertz band. J Opt (2023). https://doi.org/10.1007/s12596-022-01048-y
36. Shamim, S.M., Das, S., Hossain, M.A., Madhav, B.T.P.: Investigations on graphene-based ultra-wideband (UWB) microstrip patch antennas for terahertz (THz) applications. Plasmonics **16**, 1623–1631 (2021). https://doi.org/10.1007/s11468-021-01423-8
37. Wen L, Gao S, Luo Q, Hu W, Sanz-Izquierdo B. Design of a Wideband Dual-Feed Circularly Polarized Antenna for Different Axial Ratio Requirements. IEEE Antennas Wirel Propag Lett. 2021;20(1):88-92. doi:10.1109/LAWP.2020.3041362
38. Ahmad N, Aslam J, Nawaz H, Shahid H, Shoaib N. Dual circularly polarized series-fed patch antenna array integrated with beam switching network. Int J Numer Model Electron Networks, Devices Fields. 2021;34(5):1-19. doi:10.1002/jnm.2885
39. Tran HH, Nguyen-Trong N, Park HC. A compact dual circularly polarized antenna with wideband operation and high isolation. IEEE Access. 2020; 8:182959-182965. doi:10.1109/ACCESS.2020.3022845
40. Almorabeti S, Rifi M, Terchoune H, Tizyi H, Afyf A, Latrach M. 2X2 circular polarized antenna array for RF energy harvesting system to a UAV. Int J Microw Opt Technol. 2018;13(6):508-516.
41. Tran HH, Hussain N, Le TT. Low-profile wideband circularly polarized MIMO antenna with polarization diversity for WLAN applications. AEU - Int J Electron Commun. 2019; 108:172-180. doi: 10.1016/j.aeue.2019.06.028
42. Bhaskar S, Singh AK. Meandered cross-shaped slot circularly polarised antenna for handheld UHF RFID reader. AEU - Int J Electron Commun. 2019; 100:106-113. doi: 10.1016/j.aeue.2018.12.024
43. Nasimuddin, Chen ZN, Qing X. Slotted microstrip antennas for circular polarization with compact size. IEEE Antennas Propag Mag. 2013;55(2):124-137. doi:10.1109/MAP.2013.6529322

44. S. Ullah, C. Ruan, M.S. Sadiq, T.U. Haq, W. He, Microstrip system on-chip circular polarized (CP) slotted antenna for THz communication application, J. Electromagn. Waves Appl. 34 (8) (2020) 1029–1038
45. Vishwanath, Varshney, G. & Sahana, B.C. Tunable Terahertz Circularly Polarized Dielectric Resonator Antenna with the Higher Order Modes. Silicon 14, 6279–6289 (2022). https://doi.org/10.1007/s12633-021-01398-5
46. M. S. U. Chowdhury, M. A. Rahman, M. A. Hossain and A. T. Mobashsher, "A Transparent Conductive Material Based Circularly Polarized Nano-antenna for THz Applications," *2020 IEEE Region 10 Symposium (TE*NSYMP), 2020, pp. 754-757, doi: 10.1109/TENSYMP50017.2020.9230696.
47. Muhammad Asad Rahman Md. Sarwar Uddin Chowdhury Md. Azad Hossain Ahmed Toaha Mobashsher, "Numerical Analysis of a ITO Based Circularly Polarized Optically Transparent THz Antenna Employing Characteristic Mode Analysis," Progress In Electromagnetics Research C, Vol. 117, 1-16, 2021.

General Conclusion and Perspective

Conclusion:

Although planar antennas have some advantages such as: affordability, compactness, lightness, easy fabrication and easy integration with PCB (Printed Circuit Boards). They are still limited in size, low gain, low directivity, narrow bandwidth, no flexibility, no circular polarization, no directional radiation pattern. Therefore, in this thesis we challenged all these limitations of patch antennas for ISM band and TeraHertz band [0.1 THz to 10 THz] applications.

First, we began to solve the problems of low gain, low directivity and lack of directional radiation pattern in the ISM band by feeding an 8-element array antenna through an advanced 8-output power divider. A quarter-wave impedance transformer provided impedance matching between the patches and the power divider. The result was a high gain antenna with a directional radian pattern.

We then tackled the problems of size, narrow bandwidth and lack of flexibility. The 50% reduction in size compared to other sizes in the literature was achieved by introducing a pleated quarter wave impedance transformer between the feed (supply) line and the radiating element. To solve the problem of narrow bandwidth and lack of flexibility, a hybrid directional coupler was used to feed two identical miniaturize*d* elements. The result is a flexible, a broadband, miniaturized dual-beam antenna. This antenna radiates in two different directions -30°&+30° with good performance.

Next, in order to increase the radiation coverture area, a four beams antenna was proposed using a new beamformer circuit to feed a four-element an array antenna of four elements. This beamformer circuit was proposed to avoid the weak spot of microstrip crossovers that from which the Butler matrix suffers from. As The obtained results obtained is a multibeam antenna able that to radiates energy in four directions: -45°, -15°, 15° and 45° with good performance is achieved.

Then, a new solution to the weak spot of the microstrip crossover was achieved using diode. The proposed crossover is reconfigurable and has an ultra-wide bandwidth of 8 Ghz. It could be used not only in the Butler matrix, but is also dedicated for phased array antennas, reconfigurable antennas, MIMO antenna, reconfigurable filters…etc to control the power feed in the desired port(s) by swiching between diodes.

Finally, the linear polarization problem from which the patch antenna suffers is solved in the THZ band by proposing a single feed circularly polarized antenna using the Graphene as conductor. This CP antenna was used to build a CP array antenna of two elements. As results, an RHCP array antenna is achieved with good performance.

Perspectives :

Nowadays, research on planar antennas is moving towards the TheraHerz band [0.1THz-10 THz] using graphene as conductor. This band has a enormous application potential in many fields, including outdoor and indoor communications. Moreover, it promises significant applications in many areas including manufacturing, agriculture, materials characterization, spectroscopic imaging and security. Due to the availability of enormous unallocated bandwidth, the terahertz band supports a significant high-speed communication by implementing efficient terahertz antennas, which is impossible to achieve in the fully allocated microwave band and crowded by specified applications.

So, As perspectives in this thesis, we suggest to follow research in this band and improve the performance of Graphen-based planar antenna by introducing Metasurface or EBG (Electromagnetic Band Gap) srucrtures. We also suggest to propose new stuctures for dual circular polarization antenna (LHCP & RHCP), MIMO antenna, rectantennas and multibeams antennas based on graphen and improving their performance in this band.

Publications indexées (Scopus, WOS) :

➔ *Cinq articles de journaux :*

1. **Ansari, A. E.**, Das, S., Islam, T., Asha, S., El Idrissi, N. E. A., & Madhav, B. T. P. (2024). A High-Gain Directional 1x8 Planar Antenna Array for 2.4 GHz RFID Reader Applications. Journal of Circuits, Systems and Computers.
2. **EL ANSARI, Abdelaaziz**, JAYAPRAKASAN, V., DURAISAMY, K., et al. A Wideband Microstrip 1 x 2 Array Antenna Fed by Coupler for Beam Steering Terahertz (THz) Band Applications. Journal of Nano-and Electronic Physics, 2023, vol. 15, no 3.
3. **Ansari, A**., Islam, T., Rama Rao, S. V., Saravanan, A., Das, S., & Idrissi, N. A. (2023). "A Broadband Microstrip 1 x 8 Magic-T Power Divider for ISM Band Array Antenna Applications," J. Nano- Electron. Phys, Vol. 15, No. 3, 03003, **2023**.
4. **Ansari, A. E**., Das, S., Tabakh, I., Madhav, B. T. P., Bendali, A., & Idrissi, N. E. A. E. (**2022**). Design and Realization of a broadband multi-beam 1× 2 array antenna based on 2× 2 Butler Matrix for 2.45 GHz RFID Reader Applications. Journal of Circuits, Systems and Computers, 31(17), 2250305.
5. El-Arrouch, T., Das, S., Islam, T., Sorathiya, V., Madhav, B. T. P., **El Ansari, A.**, & El Idrissi, N. E. A. (2024). Slots and stubs incorporated annular ring-shaped compact microstrip antenna with circular polarization characteristics for wireless UWB communication systems. Physica Scripta, 99(6), 065519.

➔ *Quatre Articles de conférences*

1. **El Ansari, A**., Das, S., El-Arrouch, T., & El Idrissi, N. E. A. (**2022**, October). A Hybrid Coupler-Integrated 1× 4 Printed Array Antenna with Broadband and High Performance For Beamforming RFID Reader. In 2022 9th International Conference on Wireless Networks and Mobile Communications (WINCOM) (pp. 1-6). IEEE.
2. **El Ansari, A**., Das, S., El Idrissi, N. E. A., El-Arrouch, T., & Bendali, A. (**2022**). Slot incorporated high gain Printed RFID Reader Array antenna for 2.4 GHz ISM band applications. In E3S Web of Conferences (Vol. 351, p. 01056). EDP Sciences
3. El Arrouch, T., El Idrissi, N. E. A., & **El Ansari, A**. (2022, October). Microstrip Patch Antenna using a Parasitic Mushroom for 5GApplication at 28GHz. In 2022 9th International Conference on Wireless Networks and Mobile Communications (WINCOM) (pp. 1-6). IEEE.
4. Yakkou, H., Chillali, A., Elyamani, N. E. E., **El Ansari, A**., & Taoussi, A. (2023, November). Effect of the Integration of Information and Communication Technology on the Motivation and Learning

of Electricity Lessons for High School Students in Morocco. In The International Conference on Artificial Intelligence and Smart Environment (pp. 306-310). Cham: Springer Nature Switzerland.

Communications orale Internationales :

Titre	Nom de la Manifestation	Auteurs	Date d'organisation	Type de communication	Ville
Slot incorporated high gain Printed RFID Reader Array antenna for 2.4 GHz ISM band applications	WITS2022	**Abdelaaziz El Ansari** Sudipta Das, Najiba El Amrani El Idrissi Tarik El-Arrouch, Abdelhak Bendali	Mars 2022	Orale	Tanger (Maroc)
A Hybrid Coupler Integrated 1×4 Printed Array Antenna with Broadband and High Performance for Beamforming RFID Reader	WINCOM22	**Abdelaaziz El Ansari** Sudipta Das, Najiba El Amrani El Idrissi EL ARROUCH Tarik Abdelhak Bendali	October 2022	Orale	Rabat (Maroc)
Microstrip Patch Antenna Using a Parasitic Mushroom for 5GApplication	WINCOM22	EL ARROUCH Tarik **Abdelaaziz El Ansari** Najiba El Amrani El Idrissi	October 2022	Orale	Rabat (Maroc)
A Wideband Dual-Beam Phased Array Antenna Based on Hybrid Coupler for ISM Band Utilizations Around 2.45 GHz	International Conference on Big Data and Artificial Intelligence Applications (ICBDAIA'23, Second Edition)	**Abdelaaziz El Ansari** Najiba El Amrani El Idrissi Hassan yakkou	3rd - 4th November, 2023	Orale	Laayoune (Maroc)
Miniaturized 1x2 array antenna using a bent quarter wave impedance transformer for RFID Reader 2.45 GHz utilizations	International Conference on Big Data and Artificial Intelligence Applications (ICBDAIA'23, Second Edition)	**Abdelaaziz El Ansari** Najiba El Amrani El Idrissi Hassan yakkou	3rd - 4th November, 2023	Orale	Laayoune (Maroc)
Effect of the Integration of Information and Communication Technology on the Motivation and Learning of Electricity Lessons for High School Students in Morocco	5th International Conference on Artificial Intelligence and Smart Environment, ICAISE 2023	Hassan Yakkou, Abdelhakim Chillali, Nacer Eddine Elkadri Elyamani, **Abdelaaziz El Ansari** Aziz Taoussi	November 2023	Orale	Errachidia (Maroc)

Communications orale nationales :

Titre	Nom de la Manifestation	Auteurs	Date d'organisation	Type de communication	Ville
Conception d'un réseau d'antenne 1x8 directive et de gain élevé pour un lecteur RFID	RNJC-SI22	**Abdelaaziz El Ansari** Tarik El-Arrouch , Najiba El Amrani El Idrissi	Mai 2022	Orale	Fès (Maroc)
Design, Optimization, and Miniaturization of Patch Antenna for ISM band Applications	6ème Rencontre Nationale des Jeunes Chercheurs en Sciences de l'Ingénieur (RNJC-SI'23)	**Abdelaaziz El Ansari** Tarik El-Arrouch, Najiba El Amrani El Idrissi	13-14 Décembre 2023	Orale	Fes (Maroc)
Design and Realization of a Broadband Switched Beam Antenna for ISM Band Applications	6ème Rencontre Nationale des Jeunes Chercheurs en Sciences de l'Ingénieur (RNJC-SI'23)	**Abdelaaziz El Ansari** Tarik El-Arrouch, Najiba El Amrani El Idrissi	13-14 Décembre 2023	Orale	Fes (Maroc)
Broadband Circularly polarized MIMO antenna with circular stub ground plane and circular slot for 5G UWB Applications	6ème Rencontre Nationale des Jeunes Chercheurs en Sciences de l'Ingénieur (RNJC-SI'23	Tarik EL-ARROUCH, Sudipta Das, Najiba El Amrani El Idrissi **EL Ansari abdelaaziz**	13-14 Décembre 2023	Orale	Fes (Maroc)